Volatile apocarotenoid biosynthesis and carotenoid catabolism in *Arabidopsis thaliana*

John Yates Rivers

December 2017

A thesis submitted for the degree of Doctor of Philosophy of The Australian National University

Declaration of original work:

I certify this thesis is my own work and does not contain any results that have been generated by persons other than myself, except where due reference and acknowledgement have been made. Results presented in this thesis have not been used for the award of any other degree or diploma at any other university.

John Rivers

12th December 2017

Word Count: 52,811

Acknowledgements

I would like to thank my supervisor Barry Pogson for allowing me to undertake doctoral research in his laboratory. We have had a long association, stretching back to when he was my mentor during my undergraduate years. I have learnt a lot from him over these years about how good research is first done then communicated. I have always respected the passion he has for science and the commitment he brings to the task of mentoring all his students, including myself. I am particularly grateful for the space he granted me to pursue extracurricular activities which, whilst increasingly relevant for a modern scientific and professional career, were outside the scope of a traditional research doctorate.

I am also very grateful for the support of the rest of my official supervisory panel. In no particular order, they are Chris Cazzonelli, Thy Truong and Ryan McQuinn. I thank Chris for the straightforward nature he brought to our dealings, and will always admire the enthusiasm he has for the research field we worked in. Thanks also to Thy, for always being on hand for help and advice, and for going that 'extra mile' when called upon. And finally, I am also thankful to Ryan: not only was his advice consistently useful, his work ethic and attention to detail have been an inspiration to me.

Thank you also to Phil Marriott, and his (then) PhD student Yong Foo Wong, of Monash University. I approached them to instigate a collaboration, resulting in Chapter Three of this thesis, and I could not have asked for more friendly, accommodating, and enthusiastic collaborators.

I am also indebted to my wider support group of friends and colleagues in the Pogson Lab, our Plant Energy Biology Centre of Excellence, the Research School of Biology, and the university in general. These co-workers, friends, and mentors are incredible, stimulating, and inspiring. They include, but are not limited to: Sophie Holland, Diep Ganguly, Estee Tee, Xin Hou, Jacinta Watkins, Aaron Smith, Bethany Stone, Su Yin Phua, Kai Xun Chan, Peter Crisp, Arun Yadav, Andrew Bowerman, Pip Wilson, Norman Warthmann, Justin Borevitz, Spencer Whitney, Tony Millar, Susan Howitt and Denise Higgins.

Finally, I would like to thank my family and friends, especially my mother, Olive, and our close family friend Foster. They have borne the 'human cost' of my decision to pursue

research: a distracted, depressed (and depressing) friend and son. Thank you all for bearing with me.

This research was supported by an Australian Government Research Training Program (RTP) Scholarship, and by a Grains Research and Development Corporation (GRDC) Grains Industry Research Scholarship (GRS10687). I am very grateful for the support of both these programs.

Dedication

To my late father, Samson Rivers, the man who first instilled in me an admiration for scholarship and a commitment to excellence and integrity in all I do. Thank you.

And to my mother, Olive Rivers. I can only say thanks, and hope that I give my own children half the patience, care, and love that you have given me.

John Yates Rivers

12th December 2017

Abstract

Carotenoids are essential for plant photosynthesis. But, the story doesn't end there: volatile apocarotenoids, carotenoid oxidative cleavage products, are important plant fragrances and semiochemicals, and some are believed to be so-called 'apocarotenoid signals' (ACS), regulating plant processes. From *in vitro* experiments, apocarotenoids are known to be formed either by carotenoid cleavage dioxygenases (CCDs) or non-enzymatic oxidation. But, *in planta* mechanisms are in many cases unclear. Are there volatile apocarotenoids yet to be discovered? Are volatile apocarotenoids formed *via* CCD or non-enzymatic processes *in planta*? And are some volatile apocarotenoids ACSs?

To study volatile apocarotenoid metabolism *in planta*, a solid phase microextraction (SPME) gas chromatography mass spectrometry (GC/MS) protocol for analysing volatile apocarotenoids was developed. I also detoured to examine a new MS ionisation technology, cold electron ionisation (cold-EI). This technology improves molecular mass determination *via* GC/MS. The ability of cold-EI to enhance GC/MS plant volatile identification (*via* provision of molecular mass data) was evaluated.

SPME-GC/MS was then applied to analyse volatile apocarotenoid profiles from the model plant *Arabidopsis thaliana*. Col-0 (wild-type) and *ccd*-loss-of-function single and double mutants were analysed, as were the *Arabidopsis ccr2* mutant and corresponding *ccr2*-background *ccd* mutants. *ccr2* accumulates linear carotenoids not typically observed in *Arabidopsis*, and I've found it also emits exotic volatile apocarotenoids. A more-targeted study of volatile apocarotenoids and CCD1 and CCD4 activity during senescence was also performed.

This thesis discusses aspects of analytical method development, specifically optimisation and applications of SPME sampling and cold-EI technology. Using untargeted SPME-GC/MS volatile metabolomics, a remarkable breadth of known and putative volatile apocarotenoids was uncovered in *Arabidopsis*. Evidence suggests CCDs barely contribute to volatile apocarotenoid production, most likely producing non-volatile apocarotenoids instead. Volatile apocarotenoids seem to be formed mainly *via* carotenoid non-enzymatic oxidation. My results suggest carotenoid turnover in photosynthetic tissues is important: volatile apocarotenoid production often increases markedly when CCD function is lost. Despite previous studies' results, no new evidences were found for CCD-derived ACS contributing to either the *ccr2* phenotype or senescence retardation.

Table of Contents

Glossary of abbreviations and commonly-used terms

ABA	Abscisic Acid
ACS	Apocarotenoid Signal
Arabidopsis	*Arabidopsis thaliana*
CCD	Carotenoid Cleavage Dioxygenase
CD	Chromatogram Deconvolution
DAD	Diode Array Detector
DGAT3	*DIACYLGLYCEROL ACYLTRANSFERASE3*
DNA	Deoxyribonucleic Acid
cold-EI	cold Electron Ionisation
EI	Electron Ionisation
GC	Gas Chromatography
GC/MS	Gas Chromatography Mass Spectrometry (Spectrometer)
HCA	Hierarchical Clustering Analysis
HPLC	High-Performance Liquid Chromatography
HS	Headspace
LHCPII	LIGHT-HARVESTING COMPLEX PROTEIN II

$M^{+\bullet}$	Molecular ion
MM	Molecular Mass
MS	Mass Spectrometry (Spectrometer)
m/z	mass-to-charge ratio
PCA	Principal Component Analysis
PCR	Polymerase Chain Reaction
qPCR	real-time Quantitative Polymerase Chain Reaction
PG	Plastoglobule
RNA	Ribonucleic Acid
RES	Reactive Electrophile Species
ROS	Reactive Oxygen Species
SGR1	*STAYGREEN1*
SL	Strigolactone
SPME	Solid-Phase Microextraction
T-DNA	Transfer DNA
WRKY53	*WRKY DNA-BINDING PROTEIN 53*

Publications directly related to this thesis:

Hou, X.*, Rivers, J.*, León, P., McQuinn, R.P. and Pogson, B.J. (2016) Synthesis and Function of Apocarotenoid Signals in Plants. *Trends in Plant Science*.

* Authors contributed equally to this work

Other academic publications by the doctoral candidate:

Rivers, J., Warthmann, N., Pogson, B.J., Borevitz, J.O. (2015) Genomic breeding for food, environment and livelihoods. *Food Security*.

Rivers, J., Smith, A.B., Higgins, D., Mills, R., Maier, A.G., Howitt, S.M. (2017) Asking and answering questions: partners, peer learning, and participation. *International Journal for Students as Partners*.

Chapter One: Apocarotenoid biosynthesis in *Arabidopsis thaliana*

1.1 Carotenoids: the precursors to apocarotenoids

Carotenoids are lipid-soluble isoprenoid compounds, based on a C_{40} polyene backbone with varying degrees of double bond conjugation (Hirschberg 2001, Maresca *et al.* 2008). In nature, carotenoids are synthesised by all photosynthetic organisms (i.e. cyanobacteria, algae and higher plants), as well as some non-photosynthetic organisms such as fungi and bacteria (Nisar *et al.* 2015, Ruiz-Sola and Rodriguez-Concepcion 2012). Carotenoids and apocarotenoids are the basis for many plant pigments and flower and fruit aromas, and aid in attracting pollinators and seed dispersing organisms. Chloroplast-associated carotenoids also stabilise membranes and act as structural and accessory pigments in photosystems (PS) and light-harvesting antennae, thereby protecting the photosynthetic apparatus from photooxidative damage (Nisar, *et al.* 2015). In etiolated seedlings, carotenoids are required to form prolamellar bodies (PLB), the lattice of tubular membranes that define etioplasts and accelerate photomorphogenesis upon illumination (Park *et al.* 2002, Rodriguez-Villalon *et al.* 2009a). Carotenoids are also precursors of the phytohormones ABA (abscisic acid) and SL (strigolactones); see reviews (Nambara and Marion-Poll 2005, Trivedi *et al.* 2016, Xie *et al.* 2010). They are also important to human health, being precursors of retinal (vitamin A) (Fraser and Bramley 2004), acting as antioxidants (Fiedor and Burda 2014), being linked to reducing age-related macular degeneration and the risk of certain cancers (Nishino *et al.* 2000, Snodderly 1995).

The core carotenoid biosynthetic pathway is shared with nearly all plant species (Nisar, *et al.* 2015). Briefly, the pathway commences with PHYTOENE SYNTHASE (PSY) condensation of two geranylgeranyl pyrophosphate (GGPP) molecules to create the first carotenoid, the carotene 15-*cis*-phytoene (note that carotenoids lacking oxygen atoms are also referred to as carotenes, whilst oxygenated carotenoids are termed xanthophylls). In photosynthetic organisms, subsequent isomerisations and desaturations (by PHYTOENE DESATURASE, PDS, ZETA-CAROTENE ISOMERASE, Z-ISO, ZETA-CAROTENE DESATURASE, ZDS and CAROTENOID ISOMERASE, CRTISO, Figure 1.1) yield, progressively, 9,15-di-*cis*-phytofluene, 9,15,9'-tri-*cis*-ζ-carotene, 9,9'-di-*cis*-ζ-carotene, 7,9,9'-tri-*cis*-neurosporene, 7,9,9',7'-tetra-*cis*-lycopene and *trans*-lycopene. Given these carotenes lack ring moieties, they are referred to here as 'linear carotenes'. It is important

to note that, whilst these linear carotene stereoisomers are the main isomers, required by the pathway enzymes, many other stereoisomers are known to accumulate (Li *et al.* 2007).

Cyclisation of *trans*-lycopene (and only *trans*-lycopene) occurs *via* either BETA-CYCLASE, βLCY or EPSILON CYCLASE, εLCY, to create β-carotene (two β rings) or α-carotene (one ε and one β ring). Subsequent hydroxylation of the α and β rings occurs (*via* EPSILON HYDROXYLASE AND BETA HYDROXYLASE, εOH and βOH) to yield lutein (from α-carotene) and zeaxanthin (from β-carotene). Further epoxidation of zeaxanthin (*via* ZEAXANTHIN EPOXIDASE, ZEP) is also commonplace, leading sequentially to antheraxanthin and violaxanthin. Violaxanthin is then isomerised to 9-*cis*-violaxanthin and may also be converted (*via* NEOXANTHIN SYNTHASE, NSY) to 9-*cis*-neoxanthin. More exotic pathway steps and carotenoids are also known, although these are not believed to occur in my model species, *Arabidopsis* (Walter and Strack 2011).

1.2 Apocarotenoids: important plant signalling compounds

Carotenoids can be further catabolised to produce apocarotenoids. Some apocarotenoids appear to help fine-tune carotenoid levels, plant development and environmental responses, in part *via* retrograde (plastid-to-nucleus) signalling altering nuclear gene expression (Chan *et al.* 2016, Hou *et al.* 2016, Pogson *et al.* 2008). Thus, the discovery and characterisation of novel apocarotenoids *in planta* provides new opportunities for plant development research.

Apocarotenoids are produced *via* enzymatic and non-enzymatic oxidative cleavage of carotenoids along the polyene backbone. The apocarotenoid products of cleavage are dictated by the precursor carotenoids. Cleavage of linear carotenes yields apocarotenoids such as farnesylacetone (theoretically from either phytoene or phytofluene), geranylacetone (phytofluene, ζ-carotene or neurosporene), and pseudoionone, 6-methyl-5-hepten-2-one (6MHO) and citral (neurosporene and lycopene). Analogous cleavage of cyclic carotenes α-carotene and β-carotene can lead to α and β cyclocitrals and ionones (Figure 1.2). Apocarotenoids produced from carotenes are relatively hydrophobic and this, combined with their low molecular mass, means they are volatile and semi-volatile

components of plant aroma and fragrance. They will be collectively referred to as 'volatile apocarotenoids' in this thesis.

Cleavage of the xanthophylls can also occur e.g. 9,10-cleavage of lutein to 3-hydroxy-α-ionone. These compounds are more hydrophilic and are not believed to be volatiles; glycosylation of xanthophyll-derived apocarotenoids, forming apocarotenoid glycosides, has also been reported (Lätari *et al.* 2015), and further precludes their being volatiles. Xanthophyll-derived apocarotenoids (and their glycoside derivatives) will be referred to as non-volatile apocarotenoids in this thesis.

One should also note that the 'reciprocal' products of carotenoid cleavage are also apocarotenoids (given their molecular mass they are non-volatile). Some of these larger molecular mass apocarotenoids are biosynthetic precursors to important plant signalling compounds and may also be important in their own right (Walter *et al.* 2010).

Carotenoid cleavage can be catalysed by CAROTENOID CLEAVAGE DIOYXGENASES (CCD) enzymes, or non-enzymatic oxidation (Figure 1.2). To date, β-carotene cleavage by singlet oxygen is the only documented example of non-enzymatic carotenoid cleavage (Ramel *et al.* 2012a, Ramel *et al.* 2012b), but analogous cleavage reactions appear quite plausible.

1.2.1 *In planta* biosynthesis of apocarotenoids

The CCDs are an evolutionarily-conserved family of non-heme, iron-dependent enzymes that catalyse carotenoid oxidative cleavage (Harrison and Bugg 2014). CCDs typically act by incorporating oxygen atoms between adjacent carbon atoms along the conjugated carotenoid backbone (McQuinn *et al.* 2015). In *Arabidopsis thaliana* there are nine CCDs categorised according to their enzymatic specificities, and they determine CCD nomenclature in other species. Five CCD members are in the nine-*cis*-epoxy carotenoid dioxygenase subfamily (NCED2, NCED3, NCED5, NCED6, NCED9); and participate in ABA synthesis (Tan *et al.* 2003). NCEDs have been extensively reviewed (Nambara and Marion-Poll 2005, Trivedi, *et al.* 2016) and are not discussed further herein. CCD1, CCD4 and CCD7 have broad substrate specificity, whilst CCD8 may be specific for SL synthesis (Figure 1.1) (Alder *et al.* 2012b). One additional CCD subfamily, dubbed 'CCD2' (not to be confused with NCED2), has also been identified in *Crocus sativus*; it produces saffron flavour and fragrance apocarotenoids (Frusciante *et al.* 2014).

The roles and specificities of CCDs have long been debated. Understanding of CCDs comes mostly from *in vitro* enzymatic assays, and "*in bacterio*" heterologous expression

analysis using *Escherichia coli* engineered to accumulate particular carotenoids (Cunningham and Gantt 1998). Studies of CCD1 enzymes from many species indicate they possess the broadest substrate specificity. CCD1s cleave various linear, monocyclic and bicyclic carotenoids, regardless of their stereochemistry, and in various positions along the carbon backbone (Figure 1.1 and Figure 1.2) (Ilg *et al.* 2014, Vogel *et al.* 2008). Both carotene and xanthophyll cleavage has been recorded, albeit in CCDs of different species (Floss *et al.* 2008, Ilg, *et al.* 2014, Simkin *et al.* 2004a, Vogel, et al. 2008). CCD1s are localised to the cytoplasm (Auldridge *et al.* 2006), although they may also associate with the outer chloroplast membrane (Simkin, et al. 2004a), and seem to have roles in fruit and flower volatile production (Baldermann *et al.* 2010, Mathieu *et al.* 2005, Simkin *et al.* 2004b). In some species however, CCD1 gene duplication has occurred, leading to functional specialisation e.g. the differing substrate specificities of CCD1a and CCD1b in *Solanum lycopersicum* (Ilg, et al. 2014).

Medicago truncatula CCD1 is known to act cooperatively with CCD7 to synthesise the apocarotenoids mycorradicin and blumenol. Mycorradicin is the yellow pigment that accumulates to high levels in roots of many plant species upon colonisation with arbuscular mycorrhiza (AM) (Fester *et al.* 2002a), and is produced from cleavage of root carotenoids (Fester *et al.* 2002b, Klingner *et al.* 1995). Its production appears associated with that of various C_{13} apocarotenoids, primarily the cyclohexenone blumenol and blumenol's glycoside derivatives, which also accumulate upon AM colonisation (Maier *et al.* 1995), given cleavage of C_{40} carotenoids to produce C_{14} mycorradicin naturally yields two C_{13} apocarotenoids. RNAi silencing of *CCD1* expression in *Medicago* roots led to accumulation of the C_{27} apocarotenoids 3-hydroxy-α-10'-apocarotenal, and other C_{27} apocarotenoids (Floss, *et al.* 2008). CCD7 is believed to cleave the initial carotenoid substrate in a two-step pathway to produce mycorradicin and blumenol (Floss, *et al.* 2008).

CCD4 enzymes generally cleave carotenoids (especially β-carotene) at the 9,10-double bond when tested *in vitro* and *in bacterio* (Huang *et al.* 2009b). However, the substrate specificity of CCD4 is still unclear. Recent work suggests zeaxanthin and β,β-epoxyxanthophylls are also substrates for CCD4-mediated 9,10-cleavage in *Arabidopsis* leaves, yielding apocarotenoid glycosides (Lätari, *et al.* 2015), and that CCD4 may also cleave lutein (Rottet *et al.* 2016). Other species' CCD4 enzymes appear specific for 7,8-cleavage: Satsuma mandarin (*Citrus unshiu*) CCD4 enzymes cleave β-cryptoxanthin and zeaxanthin asymmetrically at 7,8/7',8' positions to yield β-citraurin and apo-8'-β-

carotenal (Ma *et al.* 2013). CCD4 may also metabolise ζ-carotenes (Avendaño-Vázquez *et al.* 2014), although recent *in vitro* reaction of a truncated AtCCD4 protein with ζ-carotene isomers did not yield cleavage (Bruno *et al.* 2016).

Many CCD4 enzymes seem to have a role in carotenoid catabolism, particularly in carotenoid-sink tissues such as flowers (Rubio *et al.* 2008), fruits (Brandi *et al.* 2011), seeds (Gonzalez-Jorge *et al.* 2013) and roots (Campbell *et al.* 2010). Similarly to CCD1, CCD4 genes exist as duplicates in many species, and often differ in substrate selectivity, tissue localisation and regulation of expression (Ahrazem *et al.* 2010, Lashbrooke *et al.* 2013, Ohmiya *et al.* 2006, Rubio-Moraga *et al.* 2014). In some species however, CCD4 duplicates share such high identity in their amino acid and promoter sequences that they may simply be allelic variants, such as *Cs*CCD4a and *Cs*CCD4b from *C. sativus* (Ahrazem, *et al.* 2010, Rubio-Moraga, *et al.* 2014).

CCD7's primary role is to catalyse the first step in SL biosynthesis, namely 9',10'-cleavage of 9-*cis*-β-carotene to give 9-*cis*-β-apo-10'-carotenal (Figure 1.1 and Figure 1.3) (Alder, et al. 2012b, Booker *et al.* 2004). As mentioned above however, *Medicago* CCD7 also catalyses the initial 9,10-cleavage required for mycorradicin synthesis (Figure 1.1) (Floss, et al. 2008, Vogel *et al.* 2010b). *In bacterio* assays suggest CCD7 also cleaves lycopene and ζ-carotene at the 9,10 bonds, albeit slowly (Booker, *et al.* 2004, Schwartz *et al.* 2004). A recent *in vitro* study also demonstrated cleavage of 9-*cis*-configured ζ-carotene, neurosporene and lycopene (Bruno, *et al.* 2016). Whilst the biological significance of these latter findings is still unclear, CCD7 substrate selectivity seems broader than previously believed.

CCD8 follows CCD7 in SL biosynthesis, catalysing an unusual oxidative cleavage and intramolecular cyclisation of 9-*cis*-apo-10'-carotenal to yield the SL precursor, carlactone (Figure 1.1 and Figure 1.2) (Alder, *et al.* 2012b). Interestingly, CCD8 also cleaves *trans*-apo-10'-carotenal to yield apo-13-carotenone, which was originally postulated to be the SL precursor. Although the biological relevance of this reaction is unclear as it is ten-fold slower than carlactone formation (Alder, *et al.* 2012b), phylogenetic studies in maize, rice and sorghum also suggest a subset of CCD8 enzymes may synthesise non-SL-pathway apocarotenoids (Vallabhaneni *et al.* 2010).

As mentioned above, non-enzymatic carotenoid cleavage (by singlet oxygen) has been documented (Ramel, *et al.* 2012b, Ramel *et al.* 2013). Singlet oxygen appears able to cleave β-carotene at many positions along the polyene backbone, yielding a range of

apocarotenoid products (Ramel, *et al.* 2012a). To date, research into non-enzymatic carotenoid cleavage *in planta* has been limited.

In addition to the typical double-bond cleavages, there are examples of more complex carotenoid cleavage/re-arrangement reactions yielding apocarotenoids with exotic structures. Enzymatic and non-enzymatic examples of such reactions are known: CCD8 cleavage of 9-*cis*-10'-β-apocarotenal to carlactone and singlet oxygen cleavage of β-carotene to dihydroactinidiolide (DHA) being previously reported (Alder, *et al.* 2012b, Ramel, *et al.* 2012b).

Moreover, biologically-active apocarotenoids often require additional enzymatic transformations prior to and/or following cleavage. Carotenoid isomerisation is often crucial; ABA and SL biosynthesis both require 9-*cis* substrates (Alder, *et al.* 2012b, Schwartz *et al.* 2003). Little is known about the mechanism of these isomerisations. In rice D27 catalyses the *trans*-9-*cis* conversion needed for subsequent CCD7 cleavage and SL synthesis (Figure 1.1). Orthologues of D27 exist in other plants and are the only known isomerase involved in apocarotenoid metabolism (Alder, *et al.* 2012b, Lin *et al.* 2009).

1.2.2 Apocarotenoid signals play regulatory roles *in planta*

Many apocarotenoids are also believed to have biological signalling roles (i.e. ACSs). The structures of apocarotenoids point to their potential signalling roles: most apocarotenoids contain an α,β-unsaturated carbonyl moiety, and are thus classed as reactive electrophilic species (RES), which can easily react with the nucleophilic moieties of biological molecules (Farmer and Mueller 2013). RES react with thiols on transcription factors, altering gene expression (Levonen *et al.* 2004), for example, and apocarotenoids also mediate apoptosis (Liu *et al.* 2008) and retinoid signalling (Eroglu *et al.* 2012) in mammals *via* RES mechanisms. The relationships between apocarotenoid structure and signalling activity however, remain unclear (Linnewiel *et al.* 2009) in most instances.

Enzymatic (CCD)-derived plant ACS can be considered to include the phytohormones ABA and SL, as well as blumenol (the synthesis of which was described above). Blumenol derivatives are responsible for systemic suppression of additional AM-colonisation following initial colonisation (Vierheilig *et al.* 2000); more-detailed descriptions of AM-induced apocarotenoids and their roles are found elsewhere (Akiyama 2007).

One uncharacterized ACS, dubbed 'ACS1', alters leaf development and chloroplast biogenesis (Avendaño-Vázquez, *et al.* 2014). The *Arabidopsis chloroplast biogenesis 5*

(*clb5*) mutation in ζ-carotene desaturase (ZDS) accumulates linear carotenes upstream of ZDS (Figure 1.1). *clb5* exhibits needle-like and translucent leaves and reduced expression of nuclear- and plastid-encoded genes required for chloroplast biogenesis. Genetic and biochemical analyses demonstrated the *clb5* leaf and transcriptional phenotypes were due to cleavage of phytofluene and/or ζ–carotene isomers to produce ACS1 (Figure 1.1): when phytoene/ζ-carotene biosynthesis or CCD4-mediated cleavage was inhibited, leaf development and gene expression patterns were reverted to wild-type (Avendaño-Vázquez, *et al.* 2014). As mentioned above however, *in vitro* reaction of *cis*-ζ-carotene isomers with CCD4 has led to ambiguous results (Bruno, *et al.* 2016, Huang, *et al.* 2009b). This does not preclude phytofluene or *cis*-ζ-carotene cleavage *in planta,* and may reflect the difficulties in drawing *in planta* conclusions from *in vitro* data.

Two additional CCD4-derived ACS have been speculated. RNAi knockdown of CCD4 in potato (*Solanum tuberosum*), in addition to increasing carotenoid levels, elongated tubers and increased stolon-like growth (Campbell, *et al.* 2010). Similar phenotypes are seen under heat stress (Jefferies and Mackerron 1987). Campbell *et al*. speculated the CCD4 apocarotenoid product might therefore be an important regulator of heat stress responses; based on *in vitro* data, it appears derived from 9,10-asymmetric cleavage of all-*trans*-β-carotene (Bruno *et al.* 2015, Campbell, *et al.* 2010). Notably, the saffron CCD4 homologue *CsCCD4a* is also induced by heat (Rubio, *et al.* 2008).

A putative CCD4-derived ACS has also been mooted to contribute to retardation of thylakoid membrane degradation in senescing leaves (Rottet, *et al.* 2016). Rottet *et al*. (2016) observed that senescent *Arabidopsis* leaves overexpressing *CCD4* had decreased carotenoids (as expected) but also exhibited elevated levels of galacto- and phospholipids. These lipids are major components of thylakoid membranes, (Dueñas *et al.* 2017, Kelly *et al.* 2016, Kobayashi *et al.* 2016), suggesting to the authors that *CCD4*-OX leaves had higher levels of intact thylakoid membranes during senescence as a result of a CCD4-derived ACS retarding thylakoid membrane degradation and possibly other aspects of senescence as well.

Linear carotenes in tomato fruit may yield another apocarotenoid signal, dubbed ACS2. *SlPSY1* transcription, eliminated in the *yellow-flesh* mutant r^{2997}, is partially recovered in the double mutant r^{2997}/*tangerine* (t^{3002}; Figure 1.1). *PSY1* transcription recovery seems linked to accumulation of tetra-*cis*-lycopene and various neurosporene isomers present in the t^{3002} tomato, which lacks a functional carotenoid isomerase (CRTISO). Either of these two linear carotenes might be precursors of ACS2. Consistent with this theory, expression

of *PSY1* is rescued in the loss-of-function *PSY*/*ZISO* double mutant r^{2997}/z^{2803}that lacks the aforementioned linear carotenes (Figure 1.1) (Kachanovsky *et al.* 2012). ACS2 may also be present in *Arabidopsis.* The *Arabidopsis* homologue of *tangerine*, *CAROTENOID CHLOROPLAST REGULATORY2* (*ccr2*), is an ethylmethanesulfonate (EMS)-induced loss-of-function CRTISO mutant that similarly accumulates linear carotenes and has a distinctive yellowing phenotype in newly-emerged leaves (Hou 2015), and reduced lutein and *εLCY* transcription (Cuttriss *et al.* 2007, Park, *et al.* 2002). The yellow leaf phenotype is also observed in the rice *tangerine* homologue, *zebra2* (Chai *et al.* 2011, Han *et al.* 2012). Recent work by others in my laboratory similarly suggest a linear carotene-derived ACS may be responsible for these phenotypes (Hou 2015).

Given the carotene isomerisation step catalysed by CRTISO can also be catalysed by light, it should be noted that *ccr2* tissue only exhibits detectable levels of linear carotenes, and the *ccr2* phenotype, under shorter-photoperiod days (i.e. ≤ 10 h light, longer dark photoperiods). Fruit linear carotene accumulation in *crtiso* mutants (Galpaz *et al.* 2013, Isaacson *et al.* 2002) is not photoperiod-dependent; the crystalline nature of carotenoid accumulation in fruit chromoplasts appears to prevent photoisomerisation.

ACS3 a third putative ACS, is believed to be derived from the β,β-branch of the carotenoid pathway, regulates periodic root branching and lateral root (LR) capacity in *Arabidopsis* in conjunction with the oscillatory LR-clock gene expression network (Van Norman *et al.* 2014). Treatment of *Arabidopsis* seedlings with the carotenoid cleavage inhibitor D15 reduced LR capacity, similarly to that seen upon carotenoid biosynthesis inhibition (i.e. *via* Norflurazon and CPTA treatment) and in carotenogenic mutants (*clb6* and *psy*, Figure 1.1). Genetic analysis suggests that the reduced LR-capacity was unrelated to ABA or SL signalling, demonstrating the existence of the putative ACS3. Analysis of the *lut* mutants revealed ACS3 was not derived from the ε,β-carotenoid pathway branch, indicating ACS3 is derived from a β,β-carotenoid (Van Norman, *et al.* 2014).

Non-enzymatically-generated apocarotenoids can also be signals (Estavillo *et al.* 2012). Singlet oxygen ($^1O_2$) quenching by β-carotene in photosystem II forms various β-apocarotenoids *via* an unknown mechanism, presumably involving oxidative cleavage (González-Pérez *et al.* 2011, Havaux 2013). β-cyclocitral and DHA concentrations were elevated in *Arabidopsis* within minutes of high-light treatment, as was β-ionone concentration (Ramel, *et al.* 2012b). *Arabidopsis* exposed to physiologically-relevant concentrations of β-cyclocitral increased the expression of stress response,

environmental-interaction and $^1O_2$ marker genes, and reduced that of development, growth and cellular biogenesis genes. These changes increased tolerance to photooxidative stress (Ramel, *et al.* 2012b). DHA also triggered gene expression patterns correlating with enhanced photooxidative stress-tolerance (Shumbe *et al.* 2014). Crucially, β-ionone elicited only moderate induction of one $^1O_2$ gene marker (Ramel, *et al.* 2012b), suggesting β-cyclocitral and DHA have special signalling roles. Further findings have been made regarding β-carotene signalling pathways (Alboresi *et al.* 2011, Kim *et al.* 2012, Lv *et al.* 2015, Ramel, *et al.* 2012b, Wagner *et al.* 2004).

1.2.3 Subcellular compartmentalisation regulates apocarotenoid production

The varying subcellular localisation of carotenoids further complicates our understanding of apocarotenoid production *via* CCDs (these enzymes also have specific localisations), and non-enzymatic paths. Most CCDs are plastid-localised, allowing access to carotenoid substrates (Figure 1.3). Within the plastid, suborganellar compartments such as plastoglobules (PGs) may function as sites of apocarotenoid production using carotenoid intermediates under specific developmental conditions. Proteomic analysis has identified several enzymes of the carotenoid biosynthetic pathway inside PG including ZDS, lycopene β-cyclase (Lundquist *et al.* 2012, Ytterberg *et al.* 2006) and CCD4 (Huang, *et al.* 2009b), and chromoplastic PGs accumulate high levels of carotenoids (Frusciante, *et al.* 2014). Recent studies suggest that the stability of CCD4 in PG may be regulated by phosphorylation-mediated environmental stimuli (Lundquist, *et al.* 2012), pointing to a mechanism by which environmental cues could induce more or less ACS biosynthesis. ACS1 has been speculated to be synthesised in PGs (Hou, *et al.* 2016).

In contrast to other CCDs, CCD1 is cytosol-localised (Auldridge, *et al.* 2006). How does CCD1 access carotenoid substrates? Simkin *et al*. (2004a) found tomato CCD1 enzymes are associated with chloroplast outer chloroplast membrane where carotenoid cleavage might occur. A similar mechanism has been proposed for CsCCD2, which is also cytosolic (Frusciante, *et al.* 2014). However, many researchers have found CCD1 mRNA expression and carotenoid levels do not correlate (Ibdah *et al.* 2006, Ilg *et al.* 2010, Lashbrooke, *et al.* 2013). This would suggest CCD1-mediated cleavage is controlled by other factors or other levels of regulation might operate including translational or post-translational regulation. Thus, the significance of cytosolic CCD enzymes associating with outer chloroplast membranes will require future analyses.

Organellar processes may also control CCD1 substrate access. Hemifused-membranes at plastid-endoplasmic reticulum (ER) contact sites may also allow interorganellar enzymatic activity (Mehrshahi *et al.* 2014). Another interesting hypothesis suggests stromules are involved in apocarotenoid transport (Fester, *et al.* 2002a); stromules and CCDs are affected by similar environmental cues and stromules are also thought important for subcellular organelle communication (Kwok and Hanson 2004, Noctor and Foyer 2016).

Additional possibilities are that CCD1 enzymes might only cleave apocarotenoids generated by other CCDs capable to diffuse outside of the plastid. MtCCD7 produces the C_{27} apocarotenoid substrate/s for MtCCD1 in mycorrhizal roots, for example (Floss, *et al.* 2008). In other instances, perhaps CCD1 might cleave carotenoid substrates leaked into the cytosol in some particular conditions such as plastid degradation during fruit ripening. The observed increases in CCD1 expression in the fruits of many species, and the concurrent increases in fruit volatile emission, support this hypothesis (García-Limones *et al.* 2008, Ibdah, *et al.* 2006, Kato *et al.* 2006, Mathieu, *et al.* 2005, Yahyaa *et al.* 2015). The broad substrate specificity of fruit-specific CCD1 enzymes, such as SlCCD1b, also support the notion of CCD1 'indiscriminately' cleaving leaked carotenoids (Ilg, *et al.* 2014). Carotenoid release from plastids might also happen during insect attack, as suggested by Vogel *et al.* (2008) with carotenoids then cleaved to produce insect-repellent compounds. Carotenoids released from damaged plastids could then be cleaved to produce insect-repellent compounds. This theory concurs with the observation that CCD1 overexpression can reduce crucifer beetle attack (Wei *et al.* 2011). A similar mechanism may also help mitigate pathogen attack since many apocarotenoids seem to possess antimicrobial and antifungal properties (Utama *et al.* 2002). Considering these uncertainties, it seems existing results need to be complemented by *in planta* measurements of apocarotenoids.

1.3 Research Questions and Thesis Outline

Apocarotenoids are an exciting class of compounds whose biochemistry and functions are still largely unexplored. In this thesis I will focus on volatile apocarotenoids, both on practical grounds and given the emerging wealth of literature pointing to volatile apocarotenoids (Ramel, *et al.* 2012b, Shumbe, *et al.* 2014) as important plant signalling compounds. I have listed two main questions that will be addressed in my thesis:

1. Are there unidentified volatile apocarotenoids produced *in planta*, in *Arabidopsis*?
2. Are volatile apocarotenoids produced by specific CCDs in *Arabidopsis*?

To address these questions a new high-sensitivity, *in planta*, method for analysing volatile apocarotenoids was developed: solid-phase microextraction gas-chromatography mass spectrometry (SPME-GC/MS). This is described in Chapter Two of my thesis. Following this (in Chapter Three), a new GC/MS ionisation technology, cold electron ionisation (cold-EI), was evaluated for its ability to aid in the identification of volatile apocarotenoids from GC/MS spectra.

The above research questions concerning volatile apocarotenoid biology were then investigated by profiling volatile apocarotenoids in three biological contexts, the tissues of *Arabidopsis ccd* loss-of-function mutants in both Col-0 and *ccr2* backgrounds, and in tissue of Col-0, *ccd1*, *ccd4* and *ccd1;4* plants following dark-induced senescence.

The *ccd* loss-of-function mutants were essential to this study as they allowed selective observation of plant apocarotenoid profile in the absence of one or more CCDs, thus allowing inferences about the roles of the absent CCD(s). Mutants in three of the four *Arabidopsis* CCD enzymes (CCD1, CCD7 and CCD8) were previously characterised by Auldridge *et al*. (2006), whilst an AtCCD4 mutant was reported by Gonzalez-Jorge *et al*. (2013). The *ccd1* and *ccd4* mutants have been associated with increased seed carotenoid level (Auldridge, *et al.* 2006); indeed, *ccd4* mutants were originally reported as part of a genome-wide association study (GWAS) identifying loci associated with elevated seed carotenoids (Gonzalez-Jorge, *et al.* 2013, Gonzalez-Jorge *et al.* 2016). Additionally, overexpression of *CCD1* has led to elevated β-ionone emissions from whole *Arabidopsis* plants (Wei, *et al.* 2011). Various changes to volatile apocarotenoid profile may be observable in these mutants.

The carotenoid and apocarotenoid compositions of *ccd7 (Booker, et al. 2004)* and *ccd8* (also known as *MORE AXILLARY GROWTH (MAX)* mutants *max3* and *max4* respectively) have been less well-studied given greater interest in their SL-deficiency phenotype. The *in vitro* and *in bacterio* results described above however suggest they may have additional roles in apocarotenoid biosynthesis, warranting their study.

Despite the discrete roles for CCDs envisioned given the literature to date, I generated *ccd* double mutants and proceeded to examine their volatile apocarotenoid profiles as well, to partially account for the possibility of redundancy in CCD activity. For this study, I chose to focus on crosses between *ccd1*, *ccd4*, and *ccd7* mutants, given the greater

wealth of evidence suggesting these are involved in production of volatile apocarotenoids (Adami *et al.* 2013, Bruno, *et al.* 2016, Huang, *et al.* 2009b, Ilg, *et al.* 2014, Wei, *et al.* 2011). The study of Col-0 background *ccd1*, *ccd4*, *ccd7*, *ccd8*, *ccd1;4*, *ccd1;7* and *ccd4;7* mutants is described in Chapter Four.

I then performed essentially the same study but in *ccr2* background plants grown under an 8 h light photoperiod (Chapter Five). I anticipated linear carotene accumulation and cleavage would be more pronounced, increasing the likelihood of observing trace linear carotene-derived volatile apocarotenoids, and helping validate that certain apocarotenoids, such as 6MHO, citrals and geranylacetones, are indeed derived from linear carotene cleavage in *Arabidopsis* (as opposed to production *via* some non-carotenoid route).

Additionally, I hoped that by addressing the above two questions, this study would identify linear carotene-derived volatile apocarotenoids as ACS2 and ACS1 candidates. The putative ACS2 signal was further studied by examining *ccd x ccr2* single and double mutants (referred to collectively as *ccd x ccr2* mutants) for reversion of the aforementioned *ccr2* phenotypes: a phenotypic reversion in a particular *ccd x ccr2* mutants, accompanied by loss/decrease of a particular apocarotenoid, would provide strong evidence for that metabolite acting as ACS2, and would point to that CCD(s) producing ACS2.

Finally, volatile apocarotenoid profiles were also studied during dark-induced senescence (Chapter Six). As mentioned above, there is strong evidence of CCD4 activity, and concurrent carotenoid catabolism, during senescence, making the volatile apocarotenoid profile in senescent tissues of interest. As was done to search for the ACS2 signal in Chapter Five, I searched for the putative senescence-retarding ACS, and tested for its biological effects, using this experimental system; the absence of the CCD4-derived ACS was expected to *accelerate* senescence.

In addition to volatile apocarotenoid measurements, I examined the expression of *CCD* genes in three experimental systems to gain further insight into the CCDs that might be responsible for the observed apocarotenoid profiles, and to test for compensatory increases in expression (and, by inference, enzyme abundance) of the remaining CCDs when specific CCDs are lost. Although reported subcellular localisation of the CCDs (Auldridge, *et al.* 2006, Hou, *et al.* 2016, Rottet, *et al.* 2016) would tend to suggest CCDs cannot compensate for one another, this possibility has not been previously tested for in *ccd* loss-of-function mutants. Carotenoid measurements were also made *via* high-

performance liquid chromatography (HPLC), to gain a deeper understanding of carotenoid catabolism, particularly to help conclude whether volatile apocarotenoid changes are accompanied by increased carotenoid levels (decreased catabolism) or a diversion of carotenoid catabolism toward non-volatile apocarotenoid production (manifesting as reduced volatile apocarotenoid and unchanged carotenoid abundances).

1.3.1 Thesis Chapter Outline

- Chapter Two: Development of high-sensitivity SPME-GC/MS for volatile apocarotenoid analysis, Results and Discussion
- Chapter Three: Evaluation of cold electron-ionisation as a tool for GC/MS identification of volatile apocarotenoids, Results and Discussion
- Chapter Four: Studying CCD activity *in planta* using SPME-GC/MS
- Chapter Five: Linear carotene metabolism in the *Arabidopsis ccr2* mutant and the ACS2 signal
- Chapter Six: CCD4 and CCD1 function and volatile apocarotenoid abundance during leaf senescence
- Chapter Seven: General discussion and conclusions regarding apocarotenoid biosynthesis in *Arabidopsis thaliana*
- Chapter Eight: Materials and Methods

1.4 Figures

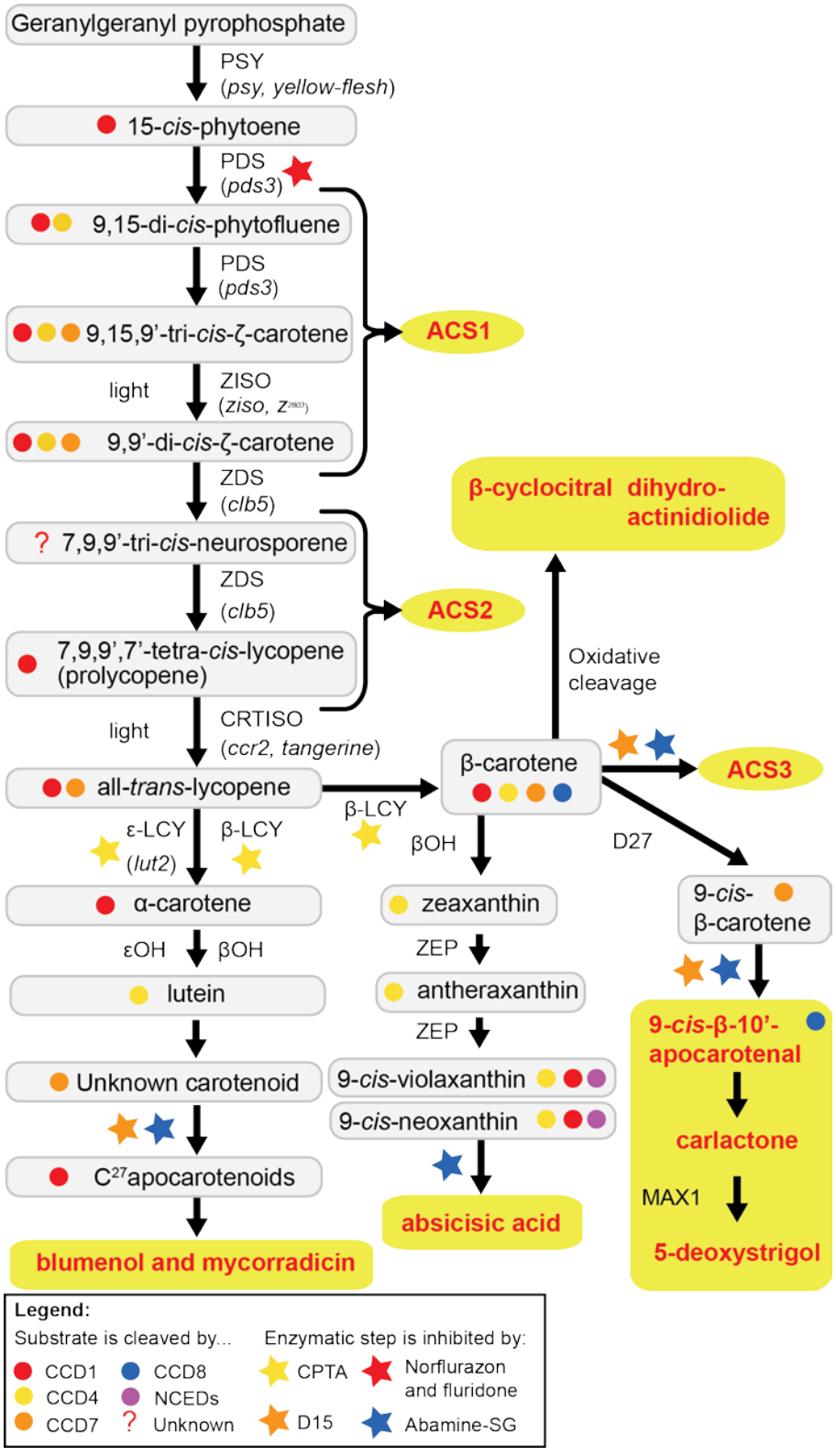

Figure 1.1: Carotenoid and apocarotenoid biosynthesis

The major Arabidopsis carotenoids and biosynthetic enzymes are depicted here, as well as the names of pathway mutants mentioned in the text. In addition, selected apocarotenoid signals (ACS) are also depicted (highlighted in yellow). Given

the importance of chemical inhibitors in the study of apocarotenoid biosynthesis, the enzymatic targets of norflurazon, fluridone, CPTA, D15 and abamine-SG have also been annotated.

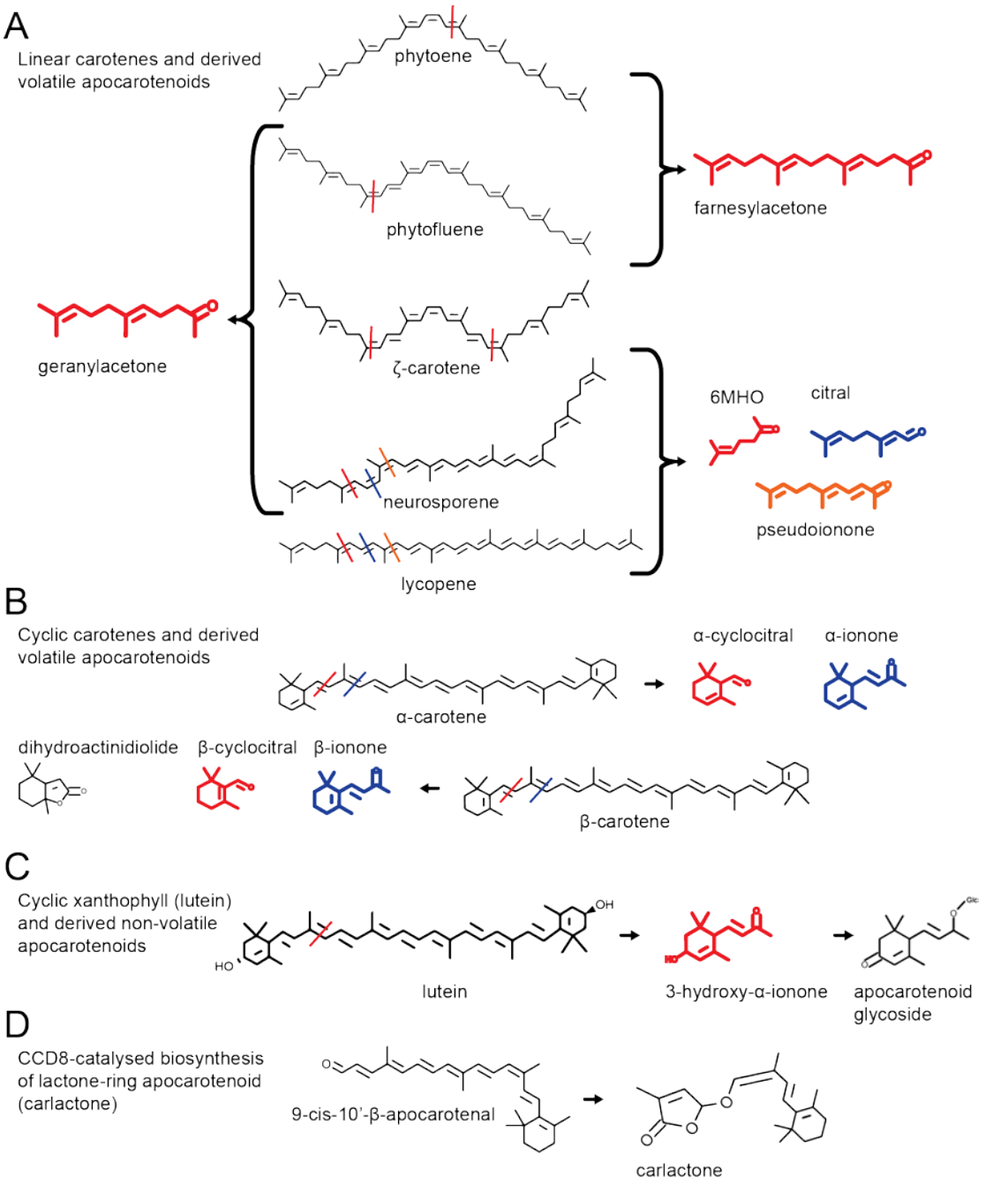

Figure 1.2: Examples of apocarotenoid biosynthesis from carotenoid cleavage

Examples of carotenoids and derived apocarotenoid products for A) linear carotenes, B) cyclic carotenes and C) cyclic xanthophylls. An example of non-standard cleavage activity, producing a lactone apocarotenoid (carlactone) is provided in D) Apocarotenoid products have been colour-coded to identify positions of polyene-backbone cleavage. Further details of reactions are provided in the text.

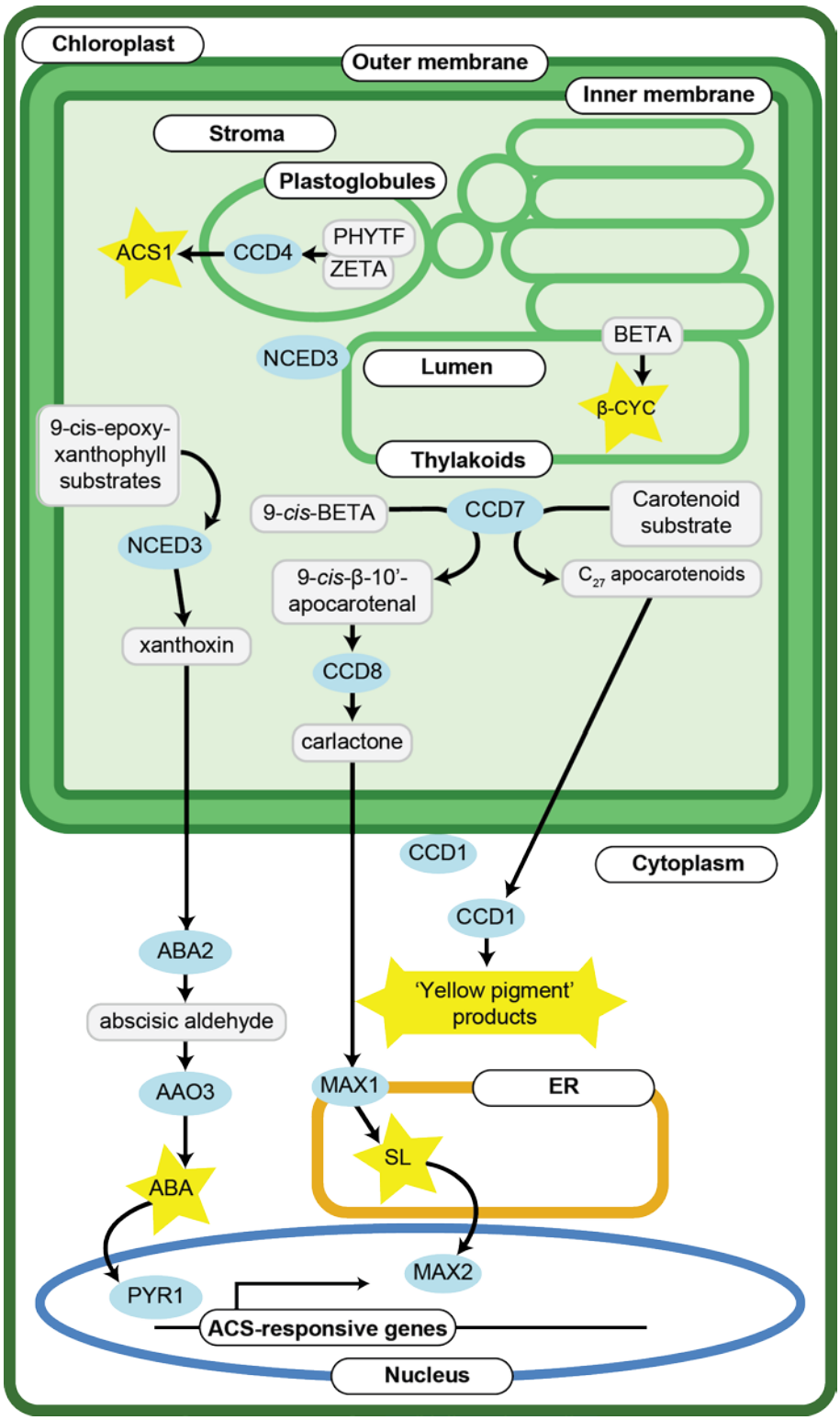

Figure 1.3: Subcellular localisations of ACS biosynthesis

Apocarotenoid signal generation and perception take place across several subcellular compartments. In this scheme, the biosynthesis of some known (ABA, SL, 'Yellow Pigment' products, β-cyclocitral) and novel (ACS1) ACSs are placed in the context of a plant cell, and the various chloroplastic compartments. The carotenoid precursors are typically found in chloroplast membranes, such as PSII-associated β-carotene. The 9-*cis*-epoxyxanthophyll ABA precursors are believed to be inner membrane-embedded, given the necessary carotenogenic enzymes are also localised here. ζ-carotene and phytofluene, putative ACS1 precursors, are believed to accumulate in the plastoglobules. It is not known where the

precursors for strigolactones (9-*cis*-β-carotene) and the yellow-pigment products (unknown) are localised. These substrates are cleaved by CCD and NCED enzymes, save for β-carotene, which is cleaved by singlet-oxygen to yield β-cyclocitral. CCD4 is localised to the plastoglobules, consistent with its putative role in ACS1 generation. CCD7 and CCD8 are localised to the stroma, as are the NCEDs involved in ABA biosynthesis (although transient association with the stroma-facing thylakoid membrane has also been observed). Subsequent modification of ACS precursors may occur in the cytoplasm or other organelles, as depicted for ABA, SL and yellow pigment products. Unknown mechanisms must export these precursors from the chloroplast. Notably, elaboration of carlactone to strigolactones may occur in the endoplasmic reticulum, based on localisation predictions for MAX1, a strigolactone biosynthetic enzyme downstream of CCD8. CCD1, localised to the cytosol (but also known to associate with the cytoplasm-facing outer chloroplast membrane), further cleaves C_{27}-apocarotenoid substrates to yield the yellow pigment products. Completed ACSs may then interact with receptors, such as PYR/PYL/RCARs (denoted here as PYR) and MAX2, to effect a biological response. It is not known how, or where, the yellow pigment products, ACS1 and β-cyclocitral exert their effects. Abbreviations: AAO3, *Arabidopsis* aldehyde oxidase 3; ABA, abscisic acid; ABA2, short-chain dehydrogenase/reductase ABA2; BETA, β-carotene; β-CYC, β-cyclocitral; ER, endoplasmic reticulum; MAX1, more axillary growth 1; MAX2, more axillary growth 2; PHYTF, phytofluene; PYR1, pyrabactin resistance 1; ZETA, ζ-carotene.

Chapter Two: Development of high-sensitivity SPME-GC/MS for volatile apocarotenoid analysis

Chapter Two

2.1 Introduction

New roles of apocarotenoids in plants continue to emerge, making sensitive, high-throughput methods to better survey, discover and quantify volatile apocarotenoids in planta crucial. Volatile apocarotenoids are typically analysed by gas chromatography-mass spectrometry (GC/MS). Following use of a sampling method to extract apocarotenoid and non-apocarotenoid volatiles, the analytes are separated *via* GC before being ionised *via* impact by electron beams of a fixed voltage, generated by a mass spectrometer ion source filament (referred to as 'electron ionisation' or EI). This yields characteristic mass-to-charge (m/z) ion fragments, collectively known as a mass spectrum, which can be used to identify analyte peaks.

Analyses of apocarotenoids and other volatiles commonly utilise analyte introduction onto a GC/MS instrument following organic extraction and LI, static HS sampling *via* gas-tight syringe, or dynamic HS purge-and-trap or thermal desorption methods (Baldermann, *et al.* 2010, Lerch and Gil 2008, Ramel, *et al.* 2012b, Rowan 2011). But, these methods have various disadvantages, including laborious sample preparation (organic extraction for LI and static HS), expensive, specialist apparatus (static and dynamic HS) and, potentially, low sensitivity and/or poor reproducibility. Pfannkoch and Whitecavage, for example, have compared sampling techniques targeting other volatiles (2000).

One sampling method could combine simplicity, precision and sensitivity: headspace solid-phase micro-extraction, or HS-SPME (Huang, *et al.* 2009b). SPME involves sampling volatile analytes with a special sorbent fibre (Risticevic *et al.* 2010). Samples are typically incubated at elevated temperatures to help release VOCs from the solid or liquid sample matrix (e.g. plant tissue), making solvent extraction obsolete. Then, the sorbent fibre is exposed to the sample headspace, adsorbing VOCs over a given extraction time. VOC analytes are then desorbed onto the GC column upon fibre insertion into the heated GC inlet.

SPME-GC/MS has been used for analysis of various classes of volatile compounds such as aldehydes (Matsui *et al.* 2012), alcohols (Xiao *et al.* 2014), lipids (Cavalli *et al.* 2003), haloketones (Serrano *et al.* 2015) and phenols (George *et al.* 2015). It has been used to analyse water samples (Serrano, *et al.* 2015), foodstuffs (Butkhup *et al.* 2011) and plant tissues (Matsui, *et al.* 2012). Indeed, Rohloff and Bones (2005) detected some

apocarotenoids, whilst screening volatile secondary metabolites from *Arabidopsis* tissues and whole plants, *via* SPME-GC/MS with a three-hour extraction time at ambient temperature using a 65 µm polydimethylsiloxane/divinylbenzene (PDMS/DVB) SPME fibre. SPME-GC/MS has also been used to analyse apocarotenoids from *in vitro* and *in bacterio* assays of carotenoid catabolism (Bruno, *et al.* 2015, Bruno, *et al.* 2016, Huang, *et al.* 2009b, Ilg *et al.* 2009, Ilg, *et al.* 2014). But, no efforts have been made to optimise SPME-GC/MS parameters for apocarotenoid analysis *in planta*. The previous SPME analyses of apocarotenoids employed generic SPME protocols, using one fibre type (either 65 µm PDMS/DVB or 100 µm PDMS) alongside a short extraction time of between 15 and 30 min (the Rohloff and Bones study being an exception). No studies have tried incubating samples at elevated temperatures prior to SPME, nor have other SPME fibre types been trialled (in addition to PDMS and PDMS/DVB, 75 µm PMDS/Carboxen and 50/30 µm DVB/Carboxen on PDMS fibres are commercially available). Thus, it is not known whether changing these SPME parameters might improve sensitivity and reproducibility of apocarotenoid measurements. Moreover, no attempt has been made to use SPME to quantify apocarotenoids. An optimised, quantitative, SPME method however, should give better apocarotenoid analytical performance than either LI-GC/MS of organic extracts or static HS-GC/MS, as seen for other VOC classes (Cavalli, *et al.* 2003).

2.2 Results and Discussion:

2.2.1 SPME Parameter optimisation

We started by optimising SPME parameters against median MS detector response and reproducibility (relative standard deviation, RSD) for a mixture of apocarotenoid standards: 6-methyl-hepten-2-one (6MHO), α-cyclocitral, β-cyclocitral, β-cyclocitrol, citral, DHA, farnesylacetone, geranylacetone, β-ionol, β-ionone and pseudoionone. The following standards were stereoisomeric mixtures: citral (*cis/trans* isomers), farnesylacetone (four isomers, numbered 1-4; I designated farnesylacetone-4 as *trans*-farnesylacetone given it has the closest Kovat's Retention Index (RI) to that in the National Institute of Standards and Technology (NIST) GC/MS library (version 14; NIST 2014)), geranylacetone (*cis/trans*) and pseudoionone (designated as *trans*-pseudoionone and 3-*trans*-5-*cis*-pseudoionone, based on NIST library spectral match (NIST 2014)). A representative GC/MS chromatogram depicting elution of all volatile standards is

provided in (Figure 2.1). A general-purpose poly di-methyl siloxane/divinylbenzene/carboxen (50/30 µM DVB/CAR on PDMS) SPME fibre was used for initial analyses. The analyte concentration for method development was set at 10 ppb (µg/L). The SPME fibre reconditioning time, following desorption of sample onto the GC column, was required to avoid carry-over between samples, and was set at 10 min.

Sample incubation temperature and time, as well as SPME extraction time and desorption time were sequentially optimised. Starting with sample incubation temperature, I trialled different values and identified optimal values (Table 2.1). I then fixed this parameter and trialled different values for the next parameter i.e. incubation, extraction and desorption times. One should note that the fluctuations in raw peak area response between optimisation steps is a result of SPME fibre batch-variation. The general conclusions of parameter optimisation are, however, consistent between batches.

Median MS response increased alongside incubation temperature for the four temperatures trialled (40, 50, 60 and 70 °C), reflecting increasing volatilisation of the analytes. The highest temperature, 70 °C, was selected, as this gave the highest response whilst maintaining a reasonable RSD. Higher temperatures were not tested as the potential for analyte degradation was considered too high.

Interestingly, median response declined as the incubation time was increased from 5 to 10, 20 and 30 min. A 5 min incubation time, yielding an RSD of 0.041 was selected. Increasing extraction time from 10 to 20 and 30 min increased median response, but a further increase to 40 min did not yield further increases, suggesting optimal analyte adsorption is reached with an extraction around 30 min long. The 40 min condition was selected as the median RSD was the lowest (0.029) and the median MS response was only slightly lower than under the 30 min condition.

Finally, as desorption time was increased (from 20 to 30 and 40 min) median compound response also increased, although response decreased slightly on increasing desorption time from 10 to 20 min. Whilst the results suggest desorption times greater than 40 min may further increase MS response by allowing more analyte to desorb from the SPME fibre, the 40 min setting was selected as it appeared further increases might increase RSD, which reached a minimum of 0.026 at 30 min desorption time. The 40 min desorption time was also preferred to minimise the duration of each SPME run.

2.2.2Different SPME fibres suit different applications

Polymer-based, fused-silica fibres are available with various fibre chemistries and coating thicknesses (µm), potentially allowing SPME users to tweak selectivity according to analyte volatility, polarity and/or MM. I thus tested whether other common SPME fibres might improve apocarotenoid analysis. Using the optimised parameters, I trialled 100 µm PDMS (recommended for volatiles, MW 60-275), 65 µm PDMS/DVB (volatiles, amines and nitro-aromatics, MW 50-300), and 75 µm PDMS/CAR (gases and low-MW compounds, MW 30-225) fibres, reasoning that parameters developed for PDMS/DVB/CAR (volatiles and semi-volatiles, MW 40-275) would also suit fibres with the component coatings (Supelco 2016). Whilst these coatings have different chemical selectivity, little data has been published about their selectivity toward plant volatiles (Kusano *et al.* 2013). Therefore, I examined whether one of the fibre types might give better overall performance for the standards or, failing that, whether one fibre type is especially suited to analysing a particular subset of apocarotenoids.

Assessment of SPME fibre performance was based on MSD peak area and reproducibility against the full apocarotenoid standard set (Table 2.2). PDMS/DVB gave the best median peak area (16.6×10^5) and lowest median RSD (0.06). PDMS/DVB/CAR performance was marginally poorer (14.64×10^5). PDMS/CAR had comparatively poor performance, with the lowest median peak area (12.63×10^5) and highest median RSD (0.19) metrics.

PDMS and, to a lesser extent PDMS/DVB, gave better responses for higher MW and/or RI compounds, such as pseudoionones and farnesylacetones, whilst having low responses for low MW/RI apocarotenoids (Table 2.2). Conversely PDMS/CAR recorded the best responses for the majority of low-mid MW/RI apocarotenoids, but had poor responses for the farnesylacetones.

The RSD results for most fibre-compound combinations were within the generally accepted RSD range (≤ 20%), with the exception of PDMS/CAR measurements, which were more variable (up to 54%). PDMS/DVB and PDMS/DVB/CAR demonstrated reproducibility for all apocarotenoids, although the latter gave the best RSDs for the high-RI pseudoionones and farnesylacetones.

Ultimately, PDMS, DVB and CAR coatings have complementary affinities for apocarotenoids of different RI. The different affinities might be more-appropriately attributed to differences in compound volatility, but I did not explore this given the lack of volatility data for some compounds. As suggested for other compound classes,

PDMS/CAR is suited best for low MW/RI compounds, and PDMS best for higher-RI, semi-volatile compounds (Risticevic, *et al.* 2010).

The PDMS/DVB/CAR fibre was identified as the optimal fibre for overall apocarotenoid analysis, with only minor MW/RI-dependent biases compared to the other fibres. Its broad selectivity was imperative, given the uncertainty about what known or putative apocarotenoids are generated in specific plant tissues. One must note however, that the presence of plant matrix might reduce extraction efficiency of the various fibres to different extents, given non-apocarotenoid volatiles might out-compete apocarotenoids for active sites on a given fibre. This was investigated in Section 2.2.5.

2.2.3 SPME analytical performance is superior to other common analytical methods

The analytical performance of the optimized SPME method was compared to established LI and static HS-GC/MS methods (Feng *et al.* 2017, Ramel, *et al.* 2012b). I constructed calibration curves for the three analytical methods to compare LOQs, LODs and precision (R^2 correlation coefficients of the calibration curves) between methods. Furthermore, I trialled normalising SPME apocarotenoid measurements to an isotope-labelled internal standard: 13,13,13-D_3-β-ionone (Table 2.3).

SPME easily had the best sensitivity of the three methods. LOQs and LODs were tens of thousands and hundreds of times lower using SPME compared to static HS and LI respectively. Moreover, farnesylacetone-2 and *trans*-farnesylacetone, the two farnesylacetones less abundant in the standard stereoisomer mixture, were not even detected by static HS.

There was no significant change in precision between the three methods, although static HS had the highest median R^2 value (0.999), followed by SPME (0.996). Inspecting the R^2 values by compound revealed static HS and LI precision deteriorated for higher-RI compounds whilst SPME maintained high precision.

Normalisation of SPME measurements to β-ionone-D_3 improved precision for most compounds, although it decreased the R^2 value for 3-*trans*-5-*cis*-pseudoionone and farnesylacetones 2 and 3. This is likely due to differences in volatilisation rates and fibre-affinity between the internal standard and analytes. I expect *in planta* analysis using internal standards with characteristics closer to that of the farnesylacetones (e.g.

compound structure and volatility i.e. vapour pressure) would give better results (isotope-labelled farnesylacetone would be ideal).

The difference in higher-MW/RI compound sensitivity between static HS and SPME is particularly intriguing. Perhaps this is due to the lower volatility of compounds like pseudoionone and farnesylacetone. The equilibria in the sample vial for such compounds (based on partition coefficient, K) favours the sample matrix meaning there is little gas-phase analyte for static HS to sample (Restek 2000). SPME is different, as the fibre continuously adsorbs analytes from the gas-phase, concentrating analytes on the fibre and simultaneously promoting further volatilisation of analytes from the sample.

2.2.4 SPME volatile apocarotenoid analysis does not produce isomerisation, oxidation or time-dependent artefacts

We then checked whether SPME produced analytical artefacts. Processes such as apocarotenoid stereoisomerisation and/or oxidation might occur during sample incubation at elevated temperatures, or due to prolonged exposure to ambient oxygen/light, given carotenoids are susceptible (Melendez-Martinez *et al.* 2013). To test for thermal stereoisomerisation I examined whether incubation temperature had an effect upon citral, geranylacetone, pseudoionone, or farnesylacetone isomer composition (Figure 2.1). For each compound the stereoisomer composition remained constant when incubated at 40, 50, 60 or 70 ^{o}C (70 ^{o}C being the method parameter). Photo-stereoisomerisation under laboratory light exposure is also minimal, with consistent stereoisomer ratios for the above compounds between samples across given GC/MS sequences (Figure 2.2).

Artefactual apocarotenoid oxidation was assessed using β-ionone as a model. The β-ionone standard used in this study contains small levels of the oxidation product 5,6-epoxy-β-ionone. Similarly to the stereoisomerisation study, no significant differences were observed in relative proportions of β-ionone and its 5,6-epoxide when incubation temperature was varied (Figure 2.3A). The potential for oxidation *via* ambient light/oxygen exposure was examined. Amber vials were used to limit light exposure, while oxygen exposure was reduced by purging vials with nitrogen prior to sealing. These conditions did not change the proportion of β-ionone to 5,6-epoxy-β-ionone (Figure 2.3B). Furthermore, no other oxidation products of β-ionone were observable in the GC/MS chromatograms. The differing proportions of 5,6-epoxy-β-ionone in the β-ionone solution between the two experiments is due to different reagent batches being used.

Finally, I explored the possibility that the time a sample spends queued, prior to analysis, may affect the quantities of apocarotenoids detected. This was expected to be relevant for fresh, biological samples, which might continue to metabolise over the duration of a typical SPME-GC/MS sequence (e.g. 10-20 h). Time-dependent variation intrinsic to SPME-GC/MS had been ruled out by the photoisomerisation results (Figure 2.2). Five replicate 500 mg aliquots of *Arabidopsis* leaf were queued for analysis at varying points over a 20 h time-course. Total apocarotenoid peak area and the areas of two volatile apocarotenoids known to accumulate in *Arabidopsis* leaves, β-ionone and β-cyclocitral (Rohloff and Bones 2005), were monitored and observed not to show time-dependent trends in abundance, indicating enzymatic/non-enzymatic factors should not confound the analyses of apocarotenoid abundances over the timeframe of the SPME-GC/MS analysis (0-20 h after tissue harvest). Nevertheless, SPME-GC/MS analytical sequences were limited to around 15 h in practice so as to further minimise this potentially confounding factor.

2.2.5 Matrix effects must be accounted for

The final method development consideration was potential plant tissue matrix effects that might interfere with apocarotenoid analysis. Such interferences arise in SPME-GC/MS from non-volatile leaf materials preventing SPME extraction of analytes, high-abundance volatiles preventing adsorption of target analytes, or co-eluting compounds interfering with MS ionisation, yielding ion enhancement or suppression. The latter matrix effect has been well-reviewed (Duncan 2012).

To explore matrix effects, I examined recovery rates for apocarotenoid standards when spiked at 10 ppb into vials with 500 mg of *Arabidopsis* leaf tissue versus empty vials (Table 2.4). I also adjusted for endogenous apocarotenoid levels measured in un-spiked leaves, as well as other interferences measured in blank vials. Apocarotenoid recovery rates were recorded for the PDMS/DVB/CAR fibre and compared to the rates obtained with the PDMS, PDMS/DVB and PDMS/CAR fibres, allowing examination of matrix effects caused by non-apocarotenoid plant volatiles interfering with binding of apocarotenoids to the SPME fibre. I observed significant matrix effects for all four fibres tested (Table 2.4). Recovery rates ranged from moderate (~60-75%) to poor (<10%). Only 6MHO recovery *via* PDMS/DVB/CAR and PDMS/CAR was above 80% (99% and 84%, respectively). PDMS/CAR yielded the best, albeit still poor, median recovery (15%). PDMS had the poorest median recovery (5.9%).

Our results suggest either leaf tissue prevents apocarotenoids from fully volatilising, or other plant volatiles are interfering with SPME absorption and/or MS ionisation of specific compounds. Each factor is likely involved. The former factor is consistent with increased suppression of higher-MW, less-volatile apocarotenoids: farnesylacetone has a much lower vapour pressure compared to other apocarotenoids and showed consistently low recovery. Poor standard recovery using PDMS also suggests *Arabidopsis* leaves emit many volatiles with high affinities toward PDMS that interfere with apocarotenoid analysis. Such compounds would include terpenes and other non-polar hydrocarbons (Rohloff and Bones 2005) known to have affinity for this coating (Supelco 2016). These findings notwithstanding, I retained the PDMS/DVB/CAR fibre type, given its broad chemical compatibility, a potentially-crucial factor for the discovery of novel apocarotenoids.

Given the overall poor standard recoveries, I opted for re-calibration of the SPME-GC/MS method *via* standard additions to plant tissue (Duncan 2012). For *in planta*, standard addition calibration curves, I spiked *Arabidopsis* leaf tissues (500 mg) with varying calibration concentrations of apocarotenoid standards (Table 2.5) and the 10 ppb β-ionone-D_3 internal standard. Endogenous apocarotenoid levels in unspiked leaves were subtracted from peak areas of spiked tissues.

In planta apocarotenoid standard addition calibrations were still precise. Only two compounds yielded R^2 correlation coefficients below 0.90, β-ionone and *trans*-farnesylacetone. The reduced precision of β-ionone quantification is perhaps due to its high endogenous abundance. Given the heterogeneous nature of the leaf samples, β-ionone 'background' was hard to calculate, confounding precise quantification of the spiked standard. The difficulty in quantifying *trans*-farnesylacetone is harder to explain given this compound is believed to be undetectable in Col-0 *Arabidopsis* leaves. Variable abundance of co-eluting interferences may explain the decreased precision. Regardless, all calibration curve R^2 correlation coefficients were considered robust enough for absolute quantification.

In planta calibration curves confirmed the sensitivity of the SPME-GC/MS method, maintaining gas-phase headspace LOQs and LODs in the sub-ppb range. Converting this to endogenous tissue concentration, I estimate the method provides median LOQ for tested apocarotenoids of 31 pg/g fresh weight of *Arabidopsis* leaf tissue and a median LOD of 9 pg/g, making it as or more sensitive than previously reported quantitative techniques (LI and dynamic HS, respectively: Gallon *et al.* 2013, Simkin, *et al.* 2004b).

Given the factors that may contribute to matrix effects, I anticipate *in planta* standard addition calibration curves should be generated for different matrices e.g. different plant tissues, plant species. But, once established, SPME-GC/MS should provide precise, accurate and sensitive apocarotenoid quantification in various applications. One could improve precision and accuracy by using internal standards specific to target apocarotenoids e.g. isotope-labelled standards.

I should note I did not directly compare *in planta* apocarotenoid concentrations determined *via* SPME-GC/MS with that obtained *via* a solvent extraction-analysis protocol. Thus, despite accounting for matrix effects arising from the presence of plant matrix in the sample vial, it is unclear whether there are *in planta* processes that further preclude the complete release of apocarotenoid volatiles from within plant tissues. This could be an issue for leaves in particular, given the role of stomata in regulating normal gas exchange. I view this possibility as unlikely however. Over the course of SPME sample incubation and extraction (45 min), the sample is maintained at 70 ^{o}C. any residual restriction of volatile apocarotenoid release during this process would be expected to be minimal, given that stomata are known to open at elevated temperatures and, in any case, the elevated temperatures would also be expected to perturb with the osmotic mechanisms required for stomatal closing. Nevertheless, further studies comparing SPME and solvent extraction techniques on duplicate plant tissue samples would be required to conclusively rule out the possibility of stomatal regulation perturbing analysis of volatile apocarotenoids *via* this SPME-GC/MS method.

2.2.6 SPME-GC/MS survey of plant tissues reveals interesting apocarotenoid distributions and novel, putative apocarotenoids

Applying my *in planta* apocarotenoid standard addition curves (Table 2.5), I quantified volatiles from *Arabidopsis,* tomato and rose tissue to 1) validate my method by detecting known apocarotenoids in these tissues and 2) demonstrate SPME's sensitivity by identification of new, putative, apocarotenoids.

From *Arabidopsis* (Col-0), I examined leaves, whole inflorescence tissue (internodes and nodes of primary and secondary inflorescences), developing and anthesis inflorescence buds (separately), mature, green, siliques, dry seeds, and fresh root tissue (Table 2.6). I also examined tomato ('Roma') leaves, sepals, anthesis flowers and red, ripe, fruit (Table 2.7; see Methods and Materials for details of harvested tissues). Fully-opened rose flowers were also analysed (Table 2.8).

Many of the observed apocarotenoids were identified using authentic standards and/or by mass spectral and Kovat's RI matching. The spectral matches for compounds that could not be identified with standards are depicted in Figure 2.5 and Figure 2.6. Observed and expected Kovat's RIs are also listed in Table 2.6**,** Table 2.7 and Table 2.8. Putative novel apocarotenoid compounds were identified based on assessment of their chemical structure. Furthermore, their endogenous concentrations (ng/g tissue, fresh weight) were determined using calibration data for compounds with similar structures and RIs (see Appendix for compound structures and identification documentation).

2.2.6.1 SPME-GC/MS survey is consistent with known plant carotenoid biochemistry

Arabidopsis and tomato apocarotenoid SPME survey results were consistent with existing apocarotenoid literature. Many apocarotenoids were accurately quantified using the calibration curves. Some apocarotenoids with calculated endogenous concentrations falling below the *in planta* standard addition LOQs were denoted 't' for "trace levels' when I was nonetheless confident, based on mass spectral (≥80% confidence) and RI matching, that they were genuine observations.

Out of the seven quantifiable, known, apocarotenoids reported for leaves and inflorescences herein, all except for *trans*-citral and DHA previously detected in *Arabidopsis* leaves and inflorescences by Rohloff and Bones (2005). DHA, has also been previously observed in *Arabidopsis* leaf organic extract (Ramel, *et al.* 2012b). Rohloff and Bones (2005) may not have detected this compound using their 3 h-extraction SPME method, given the detrimental effect prolonged extraction time has on detection of higher-volatility chemicals (Rohloff 2004); *trans*-citral may have been similarly overlooked. Curiously, Rohloff and Bones (Rohloff and Bones 2005) also reported observing *cis*-geranylacetone across leaves, inflorescences and flowers, whereas this study did not detect *cis*-geranylacetone. Differences in *Arabidopsis* growth conditions and SPME parameters may have affected apocarotenoid distribution. No literature data was available to validate the volatile profiles of the other *Arabidopsis* tissues, which in any case had only traces of various apocarotenoids (with the exception of seeds, which had high levels of DHA).

Interestingly, my observations, and those made previously (Rohloff and Bones 2005), of linear carotene-derived volatile apocarotenoids indicates cleavage of linear carotenes

occurs in *Arabidopsis* tissues, despite these substrate carotenoids not accumulating to detectable levels in normal *Arabidopsis* tissues (Van Norman, *et al.* 2014).

Tomato apocarotenoids were also consistent with those found in previous studies. In fruit, I recorded quantifiable levels of 6MHO, *cis* and *trans*-citral, *trans*-geranylacetone and *trans*-farnesylacetone. I also observed trace levels of β-cyclocitral, α-ionone, *cis*-geranylacetone, β-ionone, pseudoionone isomers (3-*trans*-*5*-*cis* and all-*trans*), DHA and other farnesylacetone isomers. All quantifiable compounds were previously identified in an untargeted analysis of tomato fruit volatiles *via* Super Q column dynamic HS sampling (Vogel *et al.* 2010a). All compounds save for *trans*-farnesylacetone were also detected in another untargeted SPME analysis of tomato fruit (Tikunov *et al.* 2005). Of the trace compounds, only DHA and α-ionone had not been observed before, perhaps owing to differences in sampling protocol or tomato cultivar. All known apocarotenoids detected in previous studies of tomato fruit were accounted for.

Whilst no literature was available for comparison of leaf, sepal and flower apocarotenoids, the observed apocarotenoids were also consistent with expectations. Tomato leaves (including sepals) had a similar profile to *Arabidopsis* leaves, with quantifiable levels of β-cyclocitral, β-ionone and DHA. *Cis*-geranylacetone (leaves) and α-ionone (leaves and sepals) were also abundant in tomato. Farnesylacetone-1 was also abundant in sepals.

α-ionone was the only volatile apocarotenoid quantifiable in tomato flowers. This is consistent with the shift in flower carotenoid biosynthesis toward the α,β-xanthophyll lutein (Galpaz *et al.* 2006). α-carotene, the precursor of lutein, is presumably cleaved to produce α-ionone. Cleavage products of lutein (e.g. 4-hydroxy ionones) were not observed; expected, given they are not believed to be volatile. The one confirmed apocarotenoid found in rose (Table 2.8), 6MHO, has also been previously observed, (Joichi *et al.* 2013)

The quantitative measurements of tomato fruit apocarotenoids in this study are also consistent with those in the literature. Although the quantitative tomato fruit apocarotenoid data by Vogel *et al.* (2010a) are not directly comparable given they describe apocarotenoid emission rate, not total tissue apocarotenoid content, trends are consistent between studies, with high levels of 6MHO and citrals and lower and trace levels of β-ionone, geranylacetones and pseudoionones. β-cyclocitral was detected at moderate levels by Vogel *et al.* (2010a) but only at traces in this study. This difference may be due to variation in cultivar or growth condition; Vogel *et al.* (2010a) observed

high seasonal variability in β-cyclocitral levels. Interestingly, very little farnesylacetone emission was observed by Vogel *et al.* (2010a) whilst this was the most abundant apocarotenoid I observed in tomato fruit. This is again attributable to the differences in sampling protocols between the two studies. Under ambient conditions, farnesylacetone is not highly volatile, leading to the low emission levels detected with the ambient-temperature, dynamic-sampling method employed by Vogel *et al.* (Tieman *et al.* 2006). By elevating sample temperature prior to and during sampling, this study reveals a much-higher farnesylacetone concentration within fruit. Minor inconsistencies notwithstanding, it appears the SPME protocol reported here provides apocarotenoid measurements consistent with the literature.

2.2.7.1 SPME-GC/MS survey reveals novel putative apocarotenoids

In addition to previously observed apocarotenoids, I identified many GC/MS peaks that may correspond to putative apocarotenoids. In *Arabidopsis* leaves, 5,6-epoxy-β-ionone and β-homocitral were quantifiable (2.3 and 3 ng/g FW respectively), with traces in various other tissues. Hexahydrofarnesylacetone, was also abundant in leaves (11 ng/g), with similarly high levels in flowers and seeds (55 and 166 ng/g respectively). Traces of a potentially-related compound, hexahydropseudoionone, was also observed in leaves and other tissues. Two more novel compounds were abundant in flowers, *cis*-citrol acetate (676 ng/g) and 7,8-dihydro-β-ionone (30 ng/g), whilst 6-methyl-3,5-heptadiene-2-one was abundant in seeds (181 ng/g). Traces of 3,4-dehydro-β-ionone were also observed in seeds. Finally, trace levels of β-ionol were found in inflorescences and developing buds.

As in *Arabidopsis*, tomato leaves had quantifiable levels of 5,6-epoxy-β-ionone (2.6 ng/g) and hexahydrofarnesylacetone (11 ng/g), which were also abundant in sepal leaves (12 and 120 ng/g respectively). In addition, geranylacetone alcohol and *cis*-citrol were also highly-abundant (22 and 59 ng/g, respectively) in leaves; 7,8-dihydro-β-ionone (0.92 ng/g) was also present. α-cyclocitral, β-cyclocitrol, β-homocitral, β-ionol and *trans*-citrol, were also present as traces in leaves. Most of these compounds were also present as traces in other tomato tissues. Two putative apocarotenoids, 7,8-dihydro-β-ionone and (±)-theaspirane were present and abundant in rose flowers (10 and 34 ng/g respectively).

Of these novel, putative apocarotenoids, α-cyclocitral and 5,6-epoxy-β-ionone appear most-obviously apocarotenoid-derived. Although α-cyclocitral has not been previously documented, it seems derived from the 7,8-cleavage of α-carotene, just as β-carotene yields β-cyclocitral. β-cyclocitral forms non-enzymatically following β-carotene singlet oxidation (Ramel, *et al.* 2012b). Whilst this process is photoprotective, as are the

signalling effects of β-cyclocitral (Ramel, *et al.* 2012b), it is not known whether α-carotene shares similar biosynthetic origins and/or signalling properties.

Similarly, whilst 5,6-epoxy-β-ionone has not been reported before, β-carotene-5,6-epoxide accumulates in plants under reactive oxygen species (ROS) stress (Ashikawa *et al.* 1987, Bradbury *et al.* 2012) and is a plausible precursor of 5,6-epoxy-β-ionone. This compound may thus also be a ROS stress marker. Moreover, there are only traces of 5,6-epoxy-β-ionone in *Arabidopsis* reproductive tissues and tomato fruits and flowers, and it is absent in *Arabidopsis* roots. This distribution further suggests this compound forms predominately in photosynthetic tissues that generate high ROS levels.

β-homocitral possesses a β-ring, suggesting it may also be derived from a β-ring carotenoid. But, its structure, with an extra methylene moiety compared to β-cyclocitral, indicates it cannot be produced directly from carotenoid cleavage. Its biosynthetic origin is unclear.

The large variety of putatively apocarotenoid-derived alcohols (i.e. citrols, geranylacetone alcohol, β-cyclocitrol, β-ionol) in tomato is noteworthy. It is not hard to imagine these compounds being derived from reduction of citrals, geranylacetone, β-cyclocitral and β-ionone respectively; these compounds have been documented in tomato and other fruits before (Eggink *et al.* 2012, Sánchez *et al.* 2012, Tikunov, *et al.* 2005). Moreover, tomato leaves have quantifiable levels of *cis*-citrol and trace *cis*-citral, whilst fruits have the opposite, further suggesting conversion of citral to citrol. Enzymes that convert aldehydes to alcohols are known (Oberschall *et al.* 2000), and such enzymes may act upon apocarotenoids. Aldehydes and ketones are reactive electrophile species (RES) and are known to affect gene expression in plants (Alméras *et al.* 2003); reduction may be one method of controlling apocarotenoid RES activity. Citrol acetate, observed in *Arabidopsis* flowers, may also result from citral reduction, with subsequent esterification.

Other putative apocarotenoids also appear to result from conversions of known apocarotenoids. 7,8-dihydro-β-ionone, hexahydrofarnesylacetone and hexahydropseudoionone seem derived from saturation of β-ionone, farnesylacetone, and either geranylacetone or pseudoionone, respectively (we note that whilst hexahydrofarnesylacetone was previously reported (Rohloff and Bones 2005), it remains unclear whether it is apocarotenoid-derived or not, thus I discuss it here). An alternative biosynthesis of 7,8-dihydro-β-ionone is also possible, involving cyclisation and 9,10-cleavage of carotenes preceding lycopene; *Capsicum annuum* lycopene cyclase, for example, cyclises neurosporene into the plausible 7,8-dihydro-β-ionone carotenoid

precursor (Takaichi *et al.* 1996). The significance of 7,8-dihydro-β-ionone and the other putative apocarotenoid saturation-derivatives is unclear, although 7,8-dihydro-β-ionone is known to attract certain insects when applied exogenously to *Arabidopsis* (Cáceres *et al.* 2016). Analogously to the apocarotenoid saturations proposed above, 6-methyl-3,5-heptadiene-2-one and 3,4-dehydro-β-ionone may be derived from desaturation of 6MHO and β-ionone respectively.

(±)-Theaspirane, which I found in rose flowers, and has also been found in quince fruit (Winterhalter and Schreier 1988), tea (Renold *et al.* 1974) and fermented beverages (Scholtes *et al.* 2015), is believed to be apocarotenoid-derived and is known to undergo interconversions between α and β-ionone derivatives (Scholtes, *et al.* 2015, Winterhalter and Schreier 1988).

2.2.9 Analysis of total apocarotenoid levels

There was considerable variation in total apocarotenoid levels between the tested tissues. *Arabidopsis* apocarotenoid concentrations ranged from highs of 1020 ng/g in anthesis flowers and 450 ng/g in seeds, to 85 and 14 ng/g in leaves and inflorescences respectively. Only traces of apocarotenoids were observable in developing buds, siliques and roots. Tomato apocarotenoid levels were highest in sepals (354 ng/g), with 188 ng/g in leaves, 40 ng/g in flowers and 36 ng/g in fruit. Given the lack of literature references for apocarotenoids from many of the sampled tissues, however, there is uncertainty whether apocarotenoids levels are truly low in certain tissues or whether aspects of specific samples (e.g. waxes on siliques and seed, residual soil/water on roots) might prevent volatilisation of analytes, confounding SPME analysis.

To address this, I examined the abundance of various non-apocarotenoid compounds inadvertently extracted and detected *via* SPME-GC/MS from the various tissues. Many compounds, including aldehydes, alcohols, aromatics and glucosinolate-derivatives, were detected across all or most of the tissue types in both species (Supplementary Table 2.1 and Supplementary Table 2.2). Crucially, compounds had abundances largely within the same order of magnitude for tissues from a given species. This indicates there is no issue with SPME volatile extraction from any particular tissue, and suggests there is a genuine paucity of apocarotenoids in *Arabidopsis* developing buds, siliques and roots.

To further validate calculated apocarotenoid quantities, total apocarotenoid measurements from various *Arabidopsis* and tomato tissues were compared against corresponding total carotenoid measurements obtained from the literature. I obtained

measurements of *Arabidopsis* and tomato leaf carotenoids from various studies (Enfissi *et al.* 2017, Fraser *et al.* 1994, Kim and DellaPenna 2006, Pogson *et al.* 1996, Stigliani *et al.* 2011, Van Norman, *et al.* 2014); many measurements of carotenoids in tomato fruit were also readily available (Enfissi, *et al.* 2017, Fraser, *et al.* 1994, Stigliani, *et al.* 2011, Vogel, *et al.* 2010a). Carotenoid measurements were also obtained for *Arabidopsis* roots (Van Norman, *et al.* 2014) and dry seeds (Auldridge, *et al.* 2006), and tomato flowers (Fraser, *et al.* 1994). The ratio of apocarotenoid to carotenoid levels in different tissues were examined against expectations for carotenoid source versus sink tissues (Cazzonelli and Pogson 2010). Leaf tissues, for example, are known to have high carotenoid turnover (Beisel *et al.* 2010, Lätari, *et al.* 2015) and would be expected to have a high apocarotenoid/carotenoid ratio; carotenoid storage tissues should have a lower ratio.

The apocarotenoid/carotenoid (ng/g:µg/g FW) ratios were as expected (Supplementary Table 2.3). For both *Arabidopsis* and tomato, leaves registered relatively high ratios between 0.2 and 0.48. Notably, the average ratio in both species was 0.32. *Arabidopsis* roots and tomato flowers and fruit, in contrast, had low ratios between 0.05 and 0.17. This concurs with the known role of tomato flowers and fruit as carotenoid storage organs. The low apocarotenoid/carotenoid ratio in *Arabidopsis* roots is consistent with the low rate of carotenoid cleavage observed by Lätari *et al*. (2015). The magnitude of ratios also suggests low proportions of the carotenoid pool are subject to cleavage at any point in time, a finding similar to that for cleavage of nine-*cis*-epoxy-carotenoids for ABA production (Tian *et al.* 2004); it appears low proportions of the carotenoid pool are subject to cleavage to form apocarotenoids at any given point in time.

Strikingly however, *Arabidopsis* seed had an apocarotenoid/carotenoid ratio of 22, suggesting a relatively high rate of carotenoid cleavage. The ratio is elevated due to the inclusion of two putative apocarotenoids in the total apocarotenoid measure (6-methyl-3,5-heptadiene-2-one and hexahydrofarnesylacetone), but levels of DHA, the sole, known, apocarotenoid quantifiable in seeds still yields an apocarotenoid/carotenoid ratio of 5. It is unclear why there should be such a high level of apocarotenoids relative to carotenoids in seeds but, given the high levels of DHA, a mediator of oxidative stress response in *Arabidopsis* (Shumbe, *et al.* 2014), apocarotenoids may be part of processes to protecting seeds from oxidative damage.

2.2.10 Summary

The work in this chapter has led to the optimisation of an SPME-GC/MS protocol for sampling of apocarotenoids from plant tissues. The demonstrably superior sensitivity relative to other mainstream GC/MS sampling techniques allowed me to detect a multitude of putative apocarotenoids of potential biological interest. The quantitative data obtained was validated against literature data, confirming the information collected by SPME-GC/MS is consistent with what is already known, quantitatively, about apocarotenoid and carotenoid metabolism.

2.3 Figures and Tables

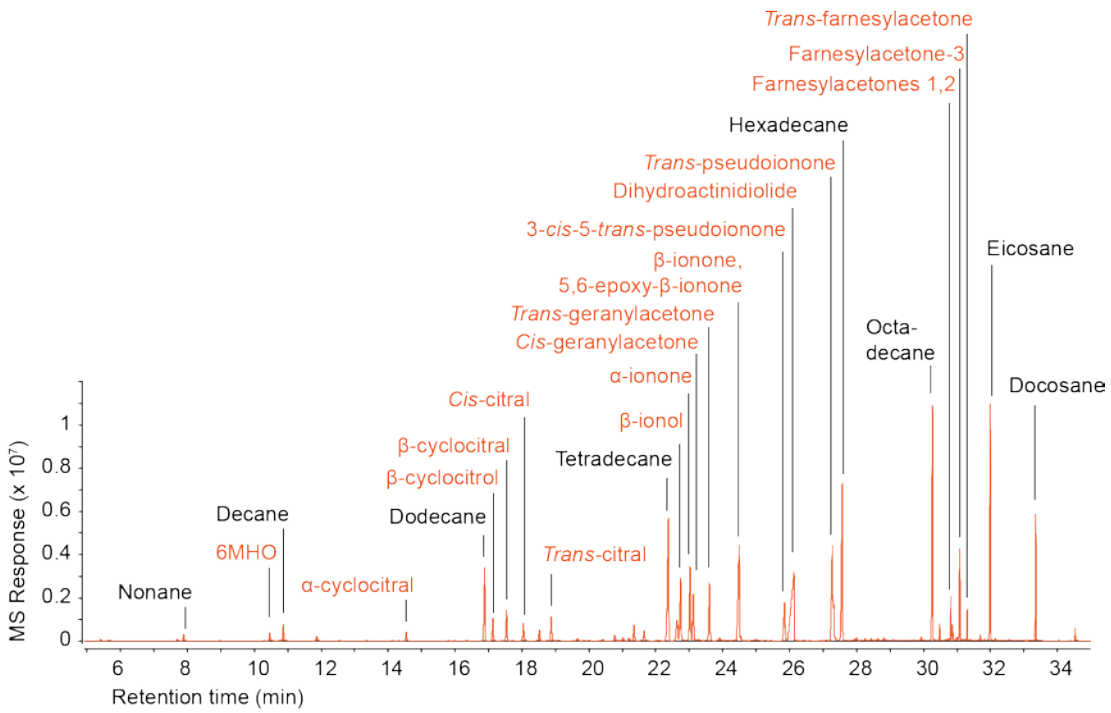

Figure 2.1: GC/MS TIC chromatogram of volatile apocarotenoid standards.

Volatile apocarotenoids have been labelled in orange on the GC/MS total ion chromatogram (TIC) above. For reference, the alkane peaks (used to calculate Kovat's Retention Indices) have also been labelled (in black).

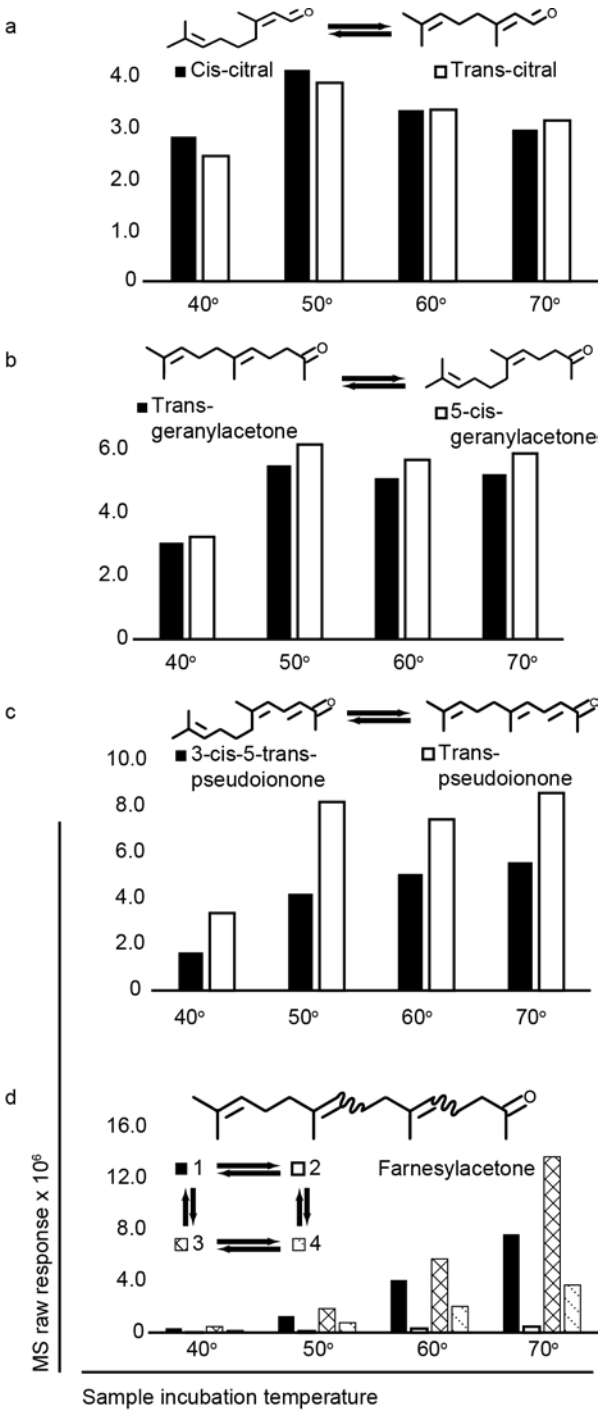

Figure 2.2: Thermal stability of apocarotenoid stereoisomers.

We incubated apocarotenoid standard solutions at different temperatures prior to SPME-GC/MS analysis. None of the apocarotenoid standards, a) citral, b) geranylacetone, c) pseudoionone and d) farnesylacetone, differed significantly in stereoisomeric composition under the temperatures tested (Chi-squared test of dependence; χ^2 = 0.0058, 0.00060, 0.019 and 0.021, DF = 3, 3, 3 and 9, p = 0.999, 1, 0.999 and 1 respectively, *n* = 3).

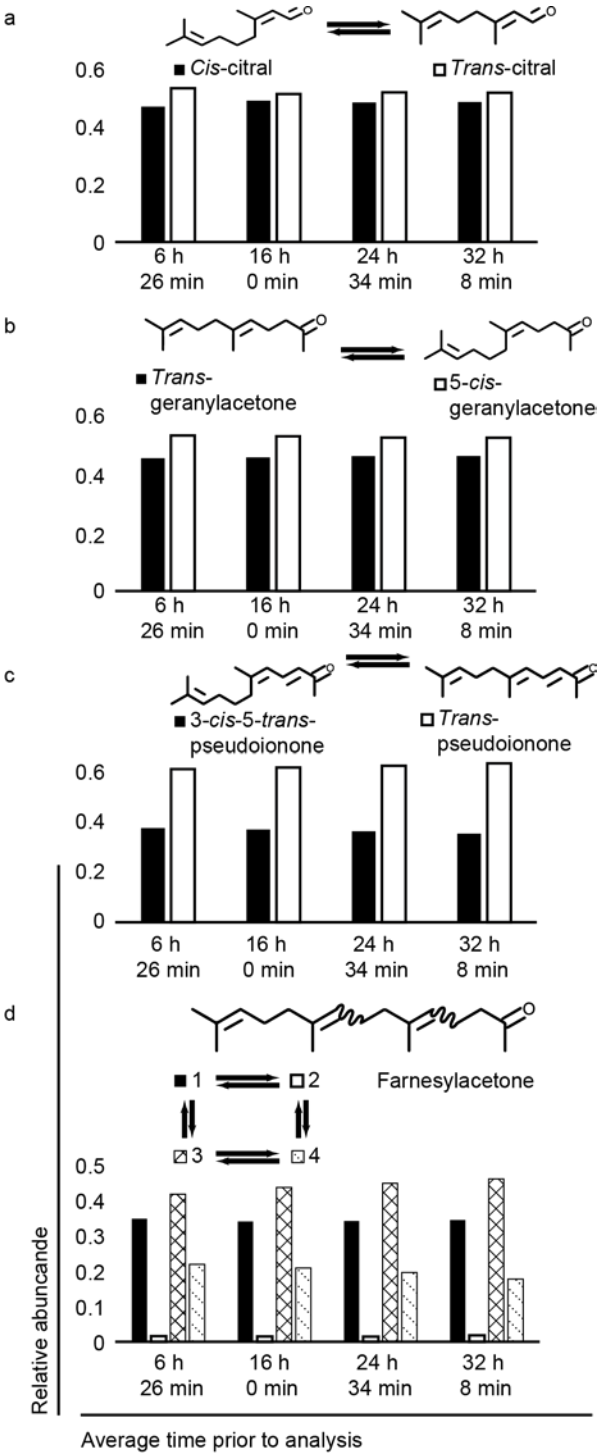

Figure 2.3: Stability of apocarotenoids to photo-stereoisomerisation.

We queued apocarotenoid standards for varying durations prior to SPME-GC/MS analysis in clear glass vials exposed to ambient light/oxygen. None of the apocarotenoid standards, a) citral, b) geranylacetone, c) pseudoionone and d) farnesylacetone differed significantly in stereoisomeric composition when time prior to analysis was varied (χ^2-squared test of dependence; χ^2 = 0.000925, 0.00015, 0.00126 and 0.00764, DF = 3, 3, 3 and 9, respectively; p = 1 in all cases; *n* = 3).

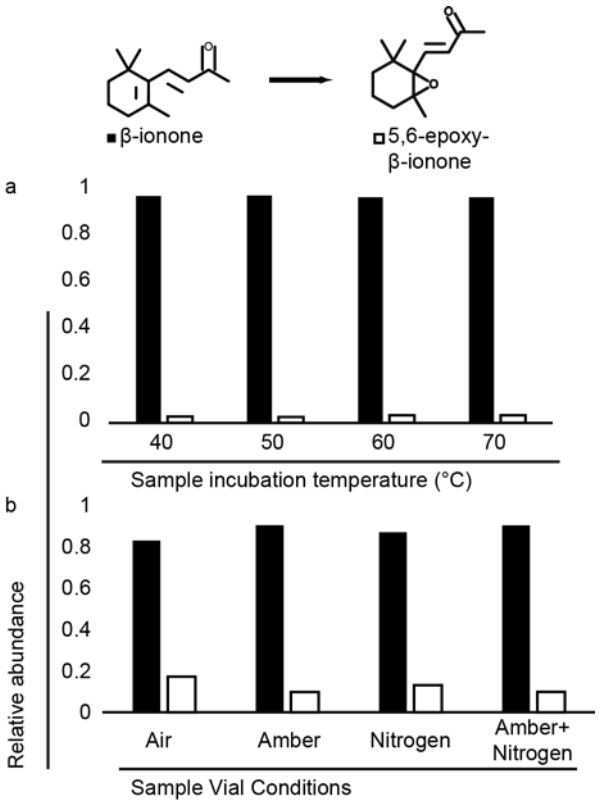

Figure 2.4: Oxidative stability of β-ionone during SPME.

We tested the stability of β-ionone standard against oxidative conversion to 5,6-epoxy-β-ionone (traces of which are present in the commercial standard) by first testing whether different SPME incubation temperatures change 5,6-epoxy-β-ionone levels (a). I then tested for changed epoxidation levels under different vial conditions (b): amber vials (low light storage), N_2-purged vials (low oxygen) and N_2-purged amber vials (low light and oxygen). Neither incubation temperature nor sample vial conditions significantly affected proportions of β-ionone to 5,6-epoxy-β-ionone (χ^2-squared test of dependence; $\chi^2 = 0.0015$ and 0.0034, DF = 3 and 3, p = 0.999 and 0.999 respectively, $n = 3$).

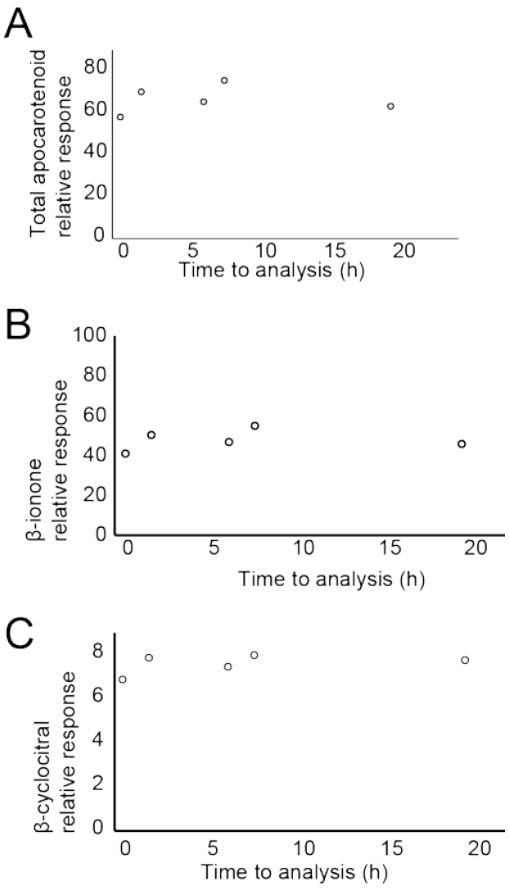

Figure 2.5: Apocarotenoid levels detected following varying lengths of time prior to analysis

Arabidopsis leaf samples were excised, sealed in sample vials and kept at room temperature for varying lengths of time prior to SPME-GC/MS analysis. GC/MS total ion chromatogram apocarotenoid peak area (normalised to D_3-β-ionone internal standard) was compared across samples (a). D_3-β-ionone-normalised levels for β-ionone (b) β-cyclocitral (c) were also examined.

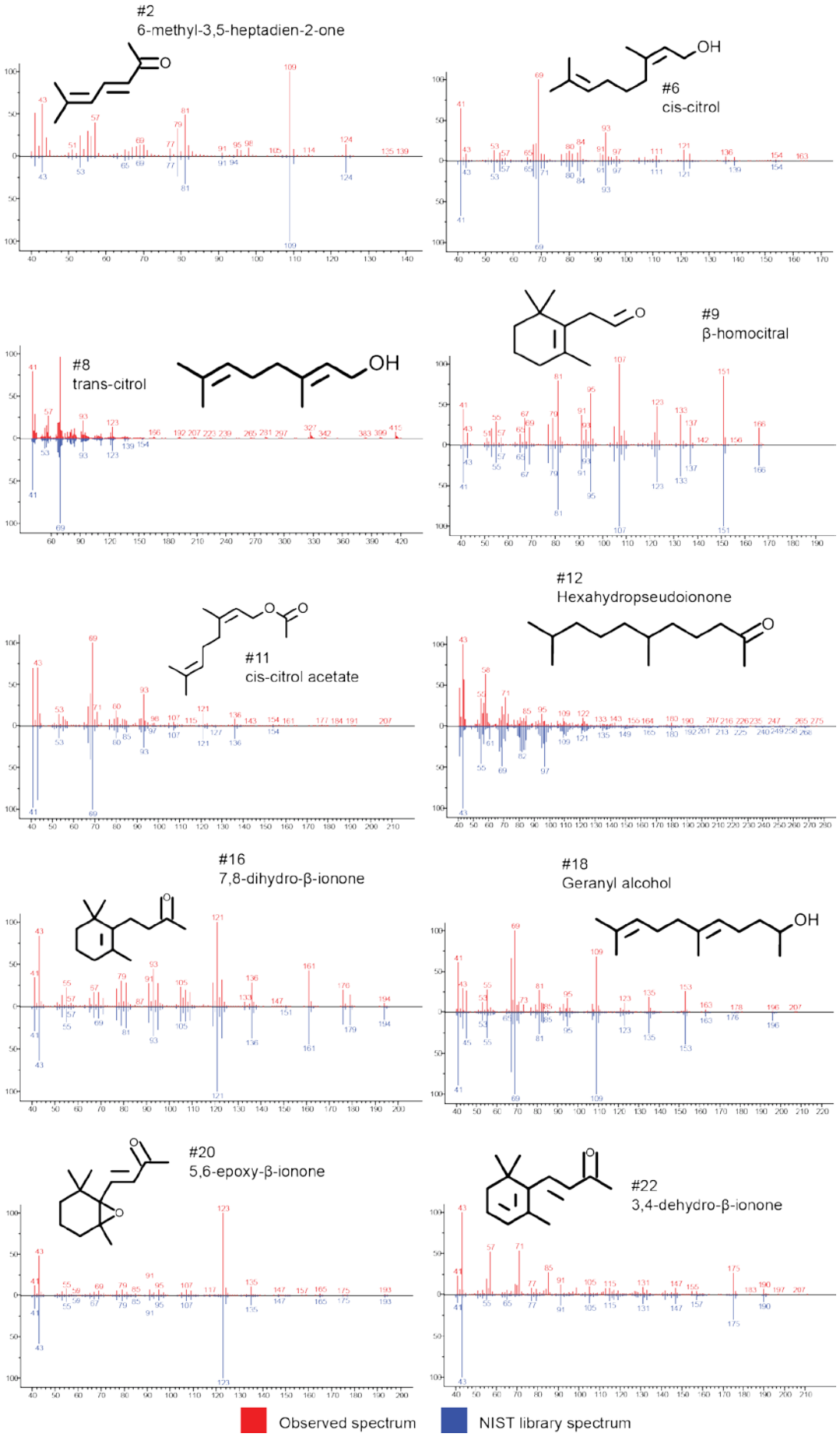
#2
6-methyl-3,5-heptadien-2-one
#6
cis-citrol
#8
trans-citrol
#9
β-homocitral
#11
cis-citrol acetate
#12
Hexahydropseudoionone
#16
7,8-dihydro-β-ionone
#18
Geranyl alcohol
#20
5,6-epoxy-β-ionone
#22
3,4-dehydro-β-ionone
Observed spectrum
NIST library spectrum

Figure 2.6: Comparisons between spectra acquired from *Arabidopsis* and tomato surveys and NIST library spectra.

Here I describe spectra for the putative novel apocarotenoids I observed in *Arabidopsis* and tomato that 1) could not be verified using authentic standards and 2) have not been previously reported in the *Arabidopsis* and tomato volatile literature. The acquired spectra (red) were compared to NIST library spectra (blue).

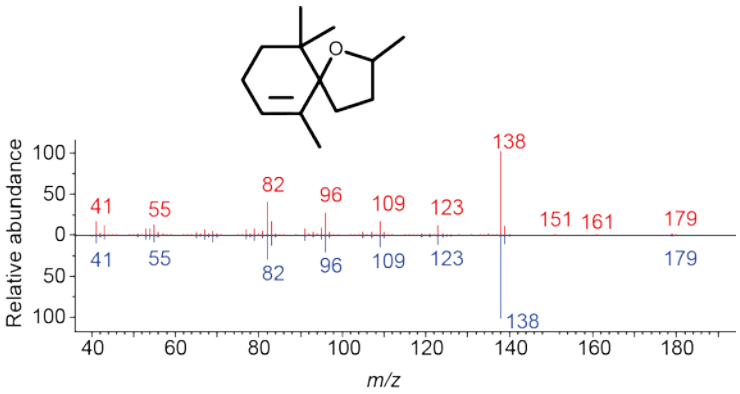

Figure 2.7: Mass spectrum of (±)-theaspirane.

The putative mass spectrum of (±)-theaspirane acquired from *R. damascena* by SPME-GC/MS (red) was compared with that in the NIST library (blue).

Table 2.1: Optimisation of SPME parameters for apocarotenoid analysis.

Parameter	Value	Median MS response	Median MS signal RSD
Incubation Temperature (°C)	40	2.73 x 106	0.656
	50	4.14 x 106	0.051
	60	5.09 x 106	0.081
	70	5.40 x 106	0.070
Incubation Time (min)	5	5.04 x 106	0.041
	10	4.77 x 106	0.026
	20	4.47 x 106	0.029
	30	3.78 x 106	0.080
Extraction Time (min)	10	5.62 x 106	0.040
	20	6.21 x 106	0.042
	30	6.51 x 106	0.043
	40	6.25 x 106	0.029
Desorption Time (min)	10	2.68 x 106	0.055
	20	2.62 x 106	0.027
	30	2.87 x 106	0.026
	40	2.91 x 106	0.033

n = 3 for all observed values

Table 2.2: Comparison of SPME fibre performance against apocarotenoids standards.

#		MW (g/mol)	Kovat's RI	Compound Response (x 10^5)				Compound MS Signal RSD			
				PDMS/ DVB/ CAR	PDMS	PDMS/ DVB	PDMS/ CAR	PDMS/ DVB/ CAR	PDMS	PDMS/ DVB	PDMS/ CAR
1	6-methyl-5-hepten-2-one	126.2	986	3.72	1.69	1.96	6.66	0.078	0.079	0.074	0.043
3	α-cyclocitral	152.2	1122	2.95	2.23	2.42	4.19	0.105	0.077	0.070	0.093
4	β-cyclocitrol	154.3	1209	5.24	4.39	5.82	5.04	0.084	0.066	0.075	0.228
5	β-cyclocitral	152.2	1224	7.82	6.77	8.31	12.63	0.119	0.070	0.065	0.092
7	*Cis*-citral	152.2	1242	7.00	3.19	4.12	4.86	0.149	0.072	0.017	0.020
10	*Trans*-citral	152.2	1273	14.64	7.29	11.00	16.12	0.158	0.078	0.068	0.177
13	β-ionol	194.3	1413	13.97	12.56	21.22	14.53	0.070	0.075	0.051	0.190
14	α-ionone	192.3	1424	34.30	37.72	41.14	60.72	0.099	0.058	0.061	0.092
15	*Cis*-geranylacetone	194.3	1448	20.74	13.90	11.91	21.03	0.116	0.242	0.098	0.542
17	*Trans*-geranylacetone	194.3	1452	30.77	27.98	29.77	27.11	0.112	0.062	0.062	0.215
19	β-ionone	192.3	1480	74.90	97.19	112.85	149.23	0.102	0.085	0.060	0.090
21	3-*trans*-5-*cis*-pseudoionone	192.3	1590	39.63	58.15	127.86	16.25	0.049	0.072	0.073	0.224
23	Dihydroactinidiolide	180.2	1540	80.20	66.32	105.87	125.86	0.048	0.059	0.054	0.033
24	*Trans*-pseudoionone	192.3	1533	20.58	19.78	23.22	6.16	0.066	0.068	0.055	0.313
26	Farnesylacetone-1	262.4	1864	10.23	19.14	16.60	2.55	0.015	0.058	0.050	0.231
28	Farnesylacetone-3	262.4	1893	29.05	66.00	56.67	8.08	0.012	0.059	0.043	0.226
29	*Trans*-Farnesylacetone	262.4	1920	6.58	15.42	13.53	1.28	0.026	0.066	0.047	0.257
	Median			14.64	15.42	16.60	12.63	0.08	0.07	0.06	0.19

Compound responses for each fibre are coded along a colour gradient (blue = lowest response, red = highest response).

Instances in which a compound response's RSD is above 20% are flagged in red.

Compounds are numbered as in the Appendix.

n = *3.*for all observed values

Table 2.3: Comparisons of SPME-GC/MS sampling against LI and static HS.

			Calibration Curve correlation coefficient (R^2)				Limit of Quantification (ppb i.e. µg/L)			Limit of Detection (ppb i.e. µg/L)		
#	Compound	RI	LI	Static HS	SPME	SPME (int.std.)	LI	Static HS	SPME	LI	Static HS	SPME
1	6-methyl-5-hepten-2-one	928	0.994	0.999	0.981	0.983	0.91 ± 0.0308	3.27 ± 0.006	0.207 ± 0.0259	0.273 ± 0.0092	0.981 ± 0.002	0.062 ± 0.0078
3	α-cyclocitral	1116	0.999	0.999	0.977	0.980	12.227 ± 0.201	0.155 ± 0.008	0.303 ± 0.0087	3.668 ± 0.06	0.516 ± 0.028	0.018 ± 0.0026
4	β-cyclocitrol	1209	0.999	0.999	0.987	0.998	1.28 ± 0.1779	0.46 ± 0.181	0.01 ± 0.0013	0.384 ± 0.0534	0.138 ± 0.054	0.003 ± 0.0004
5	β-cyclocitral	1212	0.997	0.999	0.980	0.984	23.969 ± 1.869	0.29 ± 0.072	0.056 ± 0.0026	7.191 ± 0.561	0.966 ± 0.24	0.017 ± 0.0008
7	*Cis*-citral	1242	0.997	0.999	0.987	0.995	11.133 ± 0.3526	1.867 ± 0.538	0.045 ± 0.0028	3.34 ± 0.1058	0.56 ± 0.161	0.014 ± 0.0008
10	*Trans*-citral	1270	0.994	0.999	0.990	0.997	3.74 ± 0.1386	9.324 ± 1.98	0.034 ± 0.002	1.122 ± 0.0416	2.797 ± 0.594	0.01 ± 0.0006
13	β-ionol	1413	0.999	0.996	0.999	0.999	16.523 ± 1.508	2.398 ± 0.551	0.028 ± 0.0031	4.957 ± 0.452	7.992 ± 1.836	0.008 ± 0.0009
14	α-ionone	1426	0.997	0.999	0.995	0.996	3.244 ± 0.2812	14.295 ± 5.399	0.042 ± 0.0041	0.973 ± 0.0843	4.288 ± 1.62	0.013 ± 0.0012
15	*Cis*-geranylacetone	1429	0.995	0.997	0.991	0.997	3.004 ± 0.3508	3.271 ± 1.264	0.021 ± 0.0015	0.901 ± 0.1052	0.981 ± 0.379	0.006 ± 0.0004
17	*Trans*-geranylacetone	1452	0.994	0.998	0.993	0.996	0.816 ± 0.0014	0.635 ± 0.075	0.011 ± 0.0012	0.246 ± 0.0004	0.191 ± 0.022	0.003 ± 0.0004
19	β-ionone	1487	0.994	0.995	0.996	0.997	0.791 ± 0.0511	0.235 ± 0.01	0.005 ± 0.002	0.237 ± 0.0153	0.07 ± 0.005	0.002 ± 0.0001
21	3-*trans*-5-*cis*-pseudoionone	1533	0.993	0.989	0.999	0.975	17.819 ± 0.0925	5 ± 1.181	0.091 ± 0.0189	5.346 ± 0.0278	1.5 ± 0.354	0.027 ± 0.0108
23	Dihydro-actinidiolide	1547	0.999	0.999	0.999	0.994	2.875 ± 0.893	0.343 ± 0.06	0.008 ± 0.0001	0.862 ± 0.268	1.144 ± 0.201	0.002 ± 0.00003
24	*Trans*-pseudoionone	1588	0.993	0.978	0.999	0.999	4.895 ± 0.0646	12.724 ± 4.943	0.056 ± 0.0081	1.469 ± 0.0194	3.817 ± 1.483	0.017 ± 0.0024
26	Farnesylacetone-1	1864	0.996	0.990	0.999	0.999	1.849 ± 0.2652	43.486 ± 9.767	0.071 ± 0.0001	0.555 ± 0.0796	13.046 ± 2.93	0.021 ± 0.00003
27	Farnesylacetone-2	1883	0.978	n.d	0.998	0.994	42.397 ± 5.4107	n.d	1.993 ± 0.2283	12.719 ± 1.6232	n.d	0.598 ± 0.0685

28	Farnesylacetone-3	1893	0.992	0.990	0.999	0.998	10.533 ± 0.1715	12.854 ± 1.123	0.024 ± 0.0042	3.16 ± 0.0515	3.856 ± 0.337	0.007 ± 0.0013
29	*Trans*-Farnesylacetone	1921	0.972	n.d	0.997	0.998	22.691 ± 1.097	n.d	0.256 ± 0.0293	6.807 ± 0.3291	n.d	0.077 ± 0.0119
	Median value		0.995	0.999	0.996	0.997	1565	3.27	0.04	728	0.98	0.013

Values are ± standard error; n.d = not detected

Table 2.4: SPME-GC/MS matrix effects for fresh *Arabidopsis* leaf tissue.

Compound	Molecular Weight	Kovat's RI	Recovery Rate (Matrix Effect, %)			
			PDMS/DVB/ CAR	PDMS	PDMS/DVB	PDMS/CAR
6MHO	126.2	986	99 ± 8.6	37 ± 6.1	65 ± 4.8	84 ± 5.3
α-cyclocitral	152.2	1122	68 ± 3.6	33 ± 3.4	53 ± 2.7	59 ± 9.4
β-cyclocitrol	154.3	1209	19 ± 1.4	8.1 ± 1.4	17 ± 0.2	15 ± 2.3
β-cyclocitral	152.2	1224	65 ± 12	27 ± 4.7	37 ± 3.2	27 ± 15
Cis-citral	152.2	1242	9.6 ± 1.2	1.5 ± 0.2	4.2 ± 0.4	6.3 ± 0.8
Trans-citral	152.2	1273	12 ± 1.7	1.4 ± 0.2	4.3 ± 0.6	8.4 ± 1.4
β-ionol	194.3	1413	9.6 ± 0.7	5.5 ± 1	13 ± 1.3	5.7 ± 1.1
α-ionone	192.3	1424	39 ± 4	14 ± 1.2	25 ± 1.7	36 ± 2.3
Cis-geranylacetone	194.3	1448	54 ± 8.6	23 ± 0.5	57 ± 2.8	35 ± 13.7
Trans-geranylacetone	194.3	1452	61 ± 12	23 ± 3.3	47 ± 3.2	29 ± 8.4
β-ionone	192.3	1480	75 ± 12	20 ± 6.9	25 ± 7.5	34 ± 12
Trans-pseudoionone	192.3	1533	5.7 ± 0.7	4.7 ± 0.4	9.9 ± 1.7	8.1 ± 2.1
Dihydroactinidiolide	180.2	1540	4.6 ± 0.3	2.2 ± 0.2	3.9 ± 0.8	6.2 ± 1.6
5-cis-pseudoionone	192.3	1590	3.6 ± 0.3	5.9 ± 0.3	8.2 ± 2.1	17 ± 9.7
Farnesylacetone-1	262.4	1864	1.9 ± 0.4	4.4 ± 0.2	4.8 ± 0.5	4.2 ± 1.6
Farnesylacetone-3	262.4	1893	2.1 ± 0.4	4.7 ± 0.2	5 ± 0.5	3 ± 1.5
Trans-Farnesylacetone	262.4	1920	2.7 ± 0.4	5.7 ± 0.2	5.3 ± 0.8	4.2 ± 2.2
Median			12.0	5.9	13.0	15.0

Recovery rates greater than 80% are shaded.

Recovery rates are ± standard error.

n = 3.

Table 2.5: In planta analytical performance of SPME-GC/MS standard addition calibration with D3-β-ionone internal standard.

#	Compound	Calibration curve correlation coefficient (R^2)	LOQ (ppb i.e. µg/L)	LOD (ppb i.e. µg/L)	*In planta* LOQ (ng/g FW)	*In planta* LOD (ng/g FW)	*In planta* $\log_{10}$-transformed calibration curve equations	Scaling factors (for stereoisomeric standards)
1	6-methyl-5-hepten-2-one	0.995	1.578 ± 0.241	0.473 ± 0.072	0.063 ± 0.0097	0.019 ± 0.0029	y = 0.8262 x - 1.7082	
3	α-cyclocitral	0.995	0.766 ± 0.081	0.23 ± 0.024	0.031 ± 0.0033	0.009 ± 0.001	y = 0.8391 x - 1.7385	
4	β-cyclocitrol	0.999	4.046 ± 0.94	1.214 ± 0.282	0.163 ± 0.0378	0.049 ± 0.0113	y = 1.0599 x - 2.4017	
5	β-cyclocitral	0.949	0.202 ± 0.027	0.061 ± 0.008	0.008 ± 0.0011	0.002 ± 0.0003	y = 0.6374 x - 1.07724	
7	*Cis*-citral	0.979	2.447 ± 0.002	0.734 ± 0.001	0.098 ± 0.0001	0.03 ± 0.0000	y = 0.9293 x - 2.4222	0.481
10	*Trans*-citral	0.990	1.142 ± 0.304	0.343 ± 0.091	0.046 ± 0.0122	0.014 ± 0.0037	y = 0.9721 x - 1.9717	0.519
13	β-ionol	0.974	0.629 ± 0.125	0.189 ± 0.037	0.025 ± 0.005	0.008 ± 0.0015	y = 0.8785 x - 1.9285	
14	α-ionone	0.995	0.102 ± 0.015	0.031 ± 0.004	0.004 ± 0.0006	0.001 ± 0.0002	y = 0.8183 x - 0.8517	
15	*Cis*-geranylacetone	0.994	0.364 ± 0.031	0.109 ± 0.009	0.015 ± 0.0013	0.004 ± 0.0004	y = 0.8103 x - 1.0146	0.535
17	*Trans*-geranylacetone	0.989	0.206 ± 0.027	0.062 ± 0.008	0.008 ± 0.0011	0.002 ± 0.0003	y = 0.7419 x - 0.727	0.465
19	β-ionone	0.879	0.068 ± 0.008	0.02 ± 0.002	0.003 ± 0.0003	0.001 ± 0.0001	y = 0.653 x - 0.1278	
21	3-*trans*-5-*cis*-pseudoionone	0.990	2.473 ± 0.077	0.742 ± 0.023	0.1 ± 0.0031	0.03 ± 0.0009	y = 1.1733 x - 1.6585	0.370
23	Dihydroactinidiolide	0.955	0.321 ± 0.036	0.096 ± 0.011	0.013 ± 0.0015	0.004 ± 0.0004	y = 0.844 x - 1.1739	
24	*Trans*-pseudoionone	0.989	1.887 ± 0.235	0.566 ± 0.07	0.076 ± 0.0094	0.023 ± 0.0028	y = 1.1378 x - 1.8824	0.630
26	Farnesylacetone-1	0.973	1.602 ± 0.284	0.481 ± 0.085	0.064 ± 0.0114	0.019 ± 0.0034	y = 1.0567 x - 2.329	0.343
28	Farnesylacetone-3	0.958	0.745 ± 0.296	0.224 ± 0.089	0.03 ± 0.0119	0.009 ± 0.0036	y = 1.0183 x - 1.8126	0.441
29	*Trans*-farnesylacetone	0.888	12.689 ± 2.66	3.807 ± 0.798	0.511 ± 0.107	0.153 ± 0.0321	y = 1.1039 x - 2.6968	0.200
	Median Value	0.989	0.766	0.230	0.031	0.009		

Values are ± standard error; *n = 3.*

Given the stereoisomeric compositions of some standards, 'scaling factors' were applied to the concentrations obtained from the calibration curves (based on concentrations of non-stereoisomeric standards) to obtain isomer concentrations and calculate LOQs and LODs.

Table 2.6: Apocarotenoids in *Arabidopsis* tissues.

		Arabidopsis endogenous apocarotenoid concentrations (ng/g FW)									
#	Compound	Leaves	Whole inflores-cence	Developing buds	Anthesis flowers	Siliques	Seeds	Roots	Experimental RI	NIST RI	Reference
1	6-methyl-5-hepten-2-one	13 ± 2.51	n.d	n.d	n.d	n.d	n.d	t	928	938	1
2	6-methyl-3,5-heptadiene-2-one	n.d	n.d	n.d	n.d	n.d	180.742 ± 13.392	n.d	1109	1107	Novel
5	β-cyclocitral	39.477 ± 7.333	3.48 ± 0.621	t	181.243 ± 12.9	t	n.d	t	1212	1204	1
7	*Cis*-citral	n.d	n.d	n.d	n.d	n.d	n.d	t	1242	1240	Novel
9	β-homo-citral	2.965 ± 0.551	t	t	9.1 ± 4.2	t	n.d	n.d	1261	1254	Novel
10	*Trans*-citral	4.3 ± 0.62	n.d	n.d	n.d	n.d	n.d	t	1270	1270	Novel
11	*Cis*-citrol acetate	n.d	n.d	n.d	675.837 ± 202.484	n.d	n.d	n.d	1365	1364	Novel
12	Hexahydro-pseudoionone	0.423 ± 0.05	t	t	t	n.d	t	n.d	1408	1408	Novel
13	β-ionol	n.d	t	t	n.d	n.d	n.d	n.d	1413	1406	Novel
16	7,8-dihydro-β-ionone	n.d	t	t	29.98 ± 13.436	n.d	n.d	n.d	1436	1433	Novel
15	*Cis*-geranylacetone	n.d	n.d	n.d	n.d	t	n.d	t	1429	1435	1
14	α-ionone	2.712 ± 0.25	n.d	n.d	n.d	n.d	n.d	t	1426	1457	1
17	*Trans*-geranylacetone	0.125 ± 0.015	t	t	1.05 ± 0.45	t	t	t	1452	1453	Novel
19	β-ionone	23.166 ± 4.192	5.836 ± 0.82	t	77.618 ± 19.739	t	n.d	t	1487	1486	1

20	5,6-epoxy-β-ionone	2.26 ± 0.461	t	t	5.25 ± 2.31	t	t	n.d	1489	1473	Novel
21	3-*trans*-5-*cis*-pseudoionone	n.d	n.d	n.d	n.d	n.d	n.d	t	1533	1535	Novel
22	3,4-dehydro-β-ionone	n.d	t	t	n.d	n.d	t	n.d	1536	1485	Novel
23	Dihydroactinidiolide	6.443 ± 1.103	4.387 ± 0.783	t	20.99 ± 8.1	t	103.896 ± 15.501	n.d	1547	1532	2
24	*Trans*-pseudoionone	n.d	n.d	n.d	n.d	n.d	n.d	t	1588	1589	Novel
25	Hexahydrofarnesyl-acetone	10.762 ± 2.544	n.d	n.d	55.191 ± 4.058	t	166.393 ± 39.181	t	1847	1844	1
28	Farnesylacetone-3	n.d	n.d	n.d	n.d	n.d	n.d	t	1893		Novel
29	*Trans*-farnesylacetone	n.d	n.d	n.d	n.d	n.d	n.d	t	1921	1919	Novel
	Total apocarotenoids	105 ± 20	13.70 ± 2.22	t	1047 ± 268	t	451 ± 68.07	t			

t (trace) = compound concentrations below *in planta* LOQs.

n.d = not detected

Values are ± standard error

n = 3-5

Literature is referenced where the compound in question has been observed *in planta:* 1 = Rohloff and Bones (2005), 2 = Ramel *et al*. (2012b).

Table 2.7: Apocarotenoids in tomato tissues.

		Tomato endogenous apocarotenoid concentrations (ng/g FW)						
#	Compound	Leaves	Sepals	Flowers	Fruit	Experimental RI	NIST RI	Reference
1	6-methyl-5-hepten-2-one	t	t	t	10.986 ± 0.587	928	938	1
3	α-cyclocitral	t	t	t	n.d	1122	1116	Novel
4	β-cyclocitrol	t	t	t	n.d	1209		Novel
5	β-cyclocitral	7.249 ± 0.409	12.515 ± 0.947	t	t	1212	1204	2
6	*Cis*-citrol	58.845 ± 11.977	t	t	n.d	1228	1228	Novel
7	*Cis*-citral	t	t	t	3.537 ± 0.189	1242	1240	2
8	Trans-citrol	t	t	t	t	1253	1255	Novel
9	β-homo-citral	t	t	t	t	1261	1254	Novel
10	Trans-citral	t	t	t	6.664 ± 0.302	1270	1270	2
13	β-ionol	t	t	t	n.d	1413	1406	Novel
14	α-ionone	40.826 ± 3.964	46.396 ± 13.089	40.394 ± 3.424	t	1426	1457	Novel
15	*Cis*-geranylacetone	5.17 ± 0.449	t	t	t	1429	1435	3
16	7,8-dihydro-β-ionone	0.923 ± 0.665	t	t	t	1436	1433	Novel
17	*Trans*-geranylacetone	t	t	t	2.436 ± 0.181	1452	1453	3
18	Geranylacetone alcohol	22.363 ± 8.799	t	t	t	1453	1459	Novel
19	β-ionone	25.688 ± 1.655	72.712 ± 5.339	t	t	1487	1486	3
20	5,6-epoxy-β-ionone	2.604 ± 0.163	12.079 ± 0.434	t	t	1489	1473	Novel
21	3-*trans*-5-*cis*-pseudoionone	t	t	t	t	1533	1535	3
23	Dihydroactinidiolide	14.082 ± 0.887	53.042 ± 0.956	t	t	1547	1532	Novel
24	*Trans*-pseudoionone	t	t	t	t	1588	1589	3
25	Hexahydrofarnesylacetone	10.027 ± 1.489	120.379 ± 29.097	t	t	1847	1844	Novel
26	Farnesylacetone-1	t	37.346 ± 9.376	t	t	1864		4
28	Farnesylacetone-3	t	t	t	t	1893		4
29	*Trans*-farnesylacetone	t	t	t	12.769 ± 2.407	1921	1919	4
	Total	187.78 ± 30.45	354.47 ± 59.9	40.39 ± 3.424	36.39 ± 3.67			

t (trace) = compound concentrations below *in planta* LOQs.

n.d = not detected

Values are ± standard error

n = 3-5

Literature is referenced where the compound in question has been observed: 1 = Baldwin *et al*. (2000), 2 = Tikunov *et al*. (2005), 3 = Simkin *et al*. (2004a), 4 = Vogel, *et al*. (2010a).

Table 2.8: Apocarotenoids in *Rosa damascena* tissues.

#	Compound	Rose flower apocarotenoid concentration (ng/g FW)	NIST F match	NIST R match	NIST % prob.	RI	NIST RI	Literature Reference
1	6-Methyl-5-hepten-2-one	15.05 ± 4.23	694	827	42.1	928	938	1
30	(±)-Theaspirane	34.43 ± 9.69	920	949	84.1	1302	1306	1
16	7,8-Dihydro-β-ionone	10.60 ± 2.98	897	938	73.3	1436	1433	1
	Total apocarotenoids	60.08 ± 16.9						

Values are ± standard error

n = 3

Literature is referenced where the compounds in question were observed: 1 = Joichi *et al*. (2013)

Supplementary Table 2.1: Relative quantities of selected compounds detected in *Arabidopsis* tissues.

	Compound Response (1 x 10^5 units)								
Compound	Leaves	Whole Inflores-cences	Developing buds	Anthesis buds	Siliques	Seeds	Roots	RI	NIST RI
Hexanal	1 ± 0.1	1 ± 0.18	0.4 ± 0.02	0.7 ± 0.001	0.8 ± 0.04	0.7 ± 0.08	3.6 ± 0.46	800	816
Benzaldehyde	0.8 ± 0.11	1.5 ± 0.38	0.3 ± 0.03	1.6 ± 0.09	0.1 ± 0.001	3.4 ± 0.23	7.8 ± 4.59	962	965
2-Pentyl-furan	1.4 ± 0.22	1.5 ± 0.29	0.6 ± 0.03	0.6 ± 0.05	0.7 ± 0.07	0.4 ± 0.06	3 ± 1.03	933	930
Benzeneacetaldehyde	2.9 ± 0.2	1.8 ± 0.35	3.5 ± 0.53	3.8 ± 0.07	2.4 ± 0.21	6.8 ± 0.65	9.9 ± 4.08	1045	1048
Nonanal	2.6 ± 0.12	0.6 ± 0.12	0.5 ± 0.1	0.9 ± 0.01	0.2 ± 0.03	0.2 ± 0.03	1.3 ± 0.29	1104	1109
Decanal	0.3 ± 0.03	0.5 ± 0.05	0.2 ± 0.01	0.2 ± 0.01	0.1 ± 0.02	0.5 ± 0.03	0.5 ± 0.26	1206	1207
Erucin	5.5 ± 2.79	1.3 ± 0.31	6.8 ± 1.42	n.d	3.5 ± 1.22	n.d	1.7 ± 2.22	1437	1441
4-Methylpentylisothiocyanate	5.7 ± 1.13	2.3 ± 0.43	1.2 ± 0.32	n.d	8.1 ± 0.91	n.d	n.d	1164	1164
Benzenepropanenitrile	2.9 ± 0.64	0.7 ± 0.11	1.2 ± 0.28	4.4 ± 0.15	0.8 ± 0.15	n.d	n.d	1244	1244
(2-Isothiocyanatoethyl)-benzene	1.1 ± 0.21	5.9 ± 0.59	4.8 ± 0.82	n.d	4.1 ± 1.11	n.d	0.1 ± 0.15	1465	1469
1-Isothiocyanato-3-(methylthio)-propane	0.1 ± 0.03	0.1 ± 0.05	0.5 ± 0.1	n.d	0.2 ± 0.08	n.d	0.1 ± 0.12	1316	1318
1-Nonanol	n.d	0.1 ± 0.01	0.1 ± 0.02	0.1 ± 0.001	0.4 ± 0.02	0.4 ± 0.07	0.1 ± 0.02	1173	1172
Tetradecanal	n.d	0.3 ± 0.01	n.d	0.2 ± 0.01	0.3 ± 0.02	1.6 ± 0.11	0.2 ± 0.15	1613	1617

Values are ± standard error.

n = 3-5

n.d = not detected.

Supplementary Table 2.2: Relative quantities of selected compounds detected in tomato tissues.

	Compound Response (1 x 10^5 units)					
Compound	Leaves	Sepals	Flowers	Fruit	RI	NIST RI
Nonanal	0.42 ± 0.12	0.05 ± 0.01	0.04 ± 0.01	1.85 ± 0.19	1104	1109
Benzaldehyde	39.66 ± 8.72	1.41 ± 0.56	3.32 ± 0.57	0.29 ± 0.04	962	965
Benzeneacetaldehyde	49.83 ± 2.76	3.43 ± 0.55	74.73 ± 12.4	0.13 ± 0.01	1045	1048
Phenylethyl alcohol	8.33 ± 0.63	0.93 ± 0.11	3.69 ± 0.38	0.1 ± 0.01	1116	1118
Hexadecanoic acid methyl ester	0.14 ± 0.05	0.06 ± 0.02	0.32 ± 0.05	0.03 ± 0.001	1926	1929
Hexanal	0.22 ± 0.04	0.05 ± 0.03	n.d	0.16 ± 0.02	800	813
α-Phellandrene	10.24 ± 0.71	0.32 ± 0.09	1.94 ± 0.38	n.d	1005	1003
Caryophyllene	77.24 ± 7.18	6.37 ± 2.23	69.21 ± 9.21	n.d	1419	1422
(Z,Z,Z)-1,5,9,9-Tetramethyl-1,4,7,-cycloundecatriene	84.52 ± 8.29	7.07 ± 2.61	71.67 ± 12.56	n.d	1496	1494
Pentadecanal	2.61 ± 0.32	0.59 ± 0.03	0.67 ± 0.08	n.d	1715	1718

Values are ± standard error.

n = 3-5

n.d = not detected.

Supplementary Table 2.3: Comparison of *in planta* apocarotenoid concentrations with *in planta* carotenoid concentrations

Tissue	Total Carotenoids (µg/g)		Total apocarotenoids (ng/g FW)	Apocarotenoid/ carotenoid ratio (ng:µg, FW)	Reference
	DW	FW			
Arabidopsis					
Leaves	830*	249	85	0.34	1
	850*	255	85	0.33	2
	1010*	304	85	0.28	3
Roots	2.8*	0.84	1ǂ	0.14	3
Dry Seeds	20	20	451	22.22	4
Tomato					
Leaves	1300	390*	188	0.48	5
	2230*	668	188	0.28	6
	3180	950*	188	0.20	7
Flowers	1530*	460	40	0.09	6
Fruit	1300	390*	36	0.09	5
	690*	207	36	0.17	6
	700	210*	36	0.17	7
	2600	780*	36	0.05	8

* For direct comparison, carotenoid concentrations were converted from dry to fresh weight (or vice versa) based on an assumption of 70% water content in fresh tissues (save for dry seeds, assumed to have 0% water content).

ǂ For the purpose of calculating a volatile apocarotenoid:carotenoid ratio, total *Arabidopsis* root apocarotenoid concentration was set at 1 ng/g FW.

Reference key: 1 = Kim and DellaPenna (2006), 2 = Pogson *et al*. (1996), 3 = Van Norman, *et al*. (2014), 4 = Auldridge *et al*. (2006), 5 = Enfissi, *et al*. (2017), 6 = Fraser *et al.* (1994), 7 = Stigliani, *et al*. (2011), 8 = Vogel, *et al* (2010a).

Chapter Three: Evaluation of cold electron-ionisation as a tool for GC/MS identification of volatile apocarotenoids

Chapter Three

3.1 Introduction

In the preceding chapter, I was able to verify the identity of some observed volatile apocarotenoids using authentic standards. But, many remained identifiable only *via* mass spectral library match. Many spectral libraries have been generated for plant volatiles analysed *via* 70 electron-volt (eV). Many spectral libraries have been generated for compounds analysed on EI 70 eV GC/MS, including the National Institute of Standards and Testing (NIST) library (2014) as well as libraries specifically for plant, food and essential oil VOCs, such as vocBinBase (Skogerson et al. 2011), the Adams Library (Adams 2007) and MassFinder Terpenoids (Konig *et al.*) There are other volatile compound databases that contain only Kovat's Retention Index (RI) information (Dunkel *et al.* 2009, El-Sayed 2016), but mass spectral libraries are clearly more powerful.

Spectral match however, can still be problematic, as many compounds share similar substructures and thus similar mass spectra Hummel (Hummel *et al.* 2010, Stein 1995). It would be good to further validate spectral database matches with additional diagnostic information, such as a compound's molecular mass (MM), which can be obtained by inspecting the mass-to-charge (m/z) ratio of the molecular ion ($M^{+\bullet}$), the intact analyte molecule less one electron following EI. For many compounds however, the $M^{+\bullet}$ is lost when using standard 70 eV EI. This voltage is too powerful, leading to total $M^{+\bullet}$ fragmentation.

There are options for increasing $M^{+\bullet}$ abundance. Chemical ionisation (CI) is one alternative to EI using in GC/MS (Harrison 1992). Like EI it produces positive ions from electron impact. This process involves initial ionisation of reagent gases (e.g., methane, ammonia), which react with analyte molecules yielding $M^{+\bullet}$s, analyte-reagent ion adducts, and few fragment ions (Harrison 1992); the MM can then be noted from the $M^{+\bullet}$ *m/z* or calculated from the *m/z* of adducts (Hocart 2010). But, CI has drawbacks. The resulting mass spectra are not compatible with the majority of spectral libraries, which are generated *via* EI, and the CI process does not ionize all compounds. Moreover, CI requires changes to the MS hardware i.e. a CI ion source with reagent gas cylinder, which can be laborious.

I initiated a collaboration with the laboratory of Philip Marriott (Monash University, Australia) to apply a novel MS ionisation technology to help me identify volatiles, apocarotenoid and otherwise, detected *via* GC/MS. This new technology, Cold Electron Ionisation (Cold-EI, also referred to in the literature as supersonic molecular beam or

SMB-MS), adds high volumes and flow-rates of make-up gas (helium) to the GC analyte gas flow prior to entry into the standard 70 eV EI source (Amirav *et al.* 2001, Amirav *et al.* 2015, Dagan and Amirav 1995). This cools the gas flow, reducing analyte molecule vibrational energy. It is believed that this reduction in vibrational energy allows more $M^{+\bullet}$ to remain intact, enriching $M^{+\bullet}$ in the resulting spectrum. Yet, resulting spectra are still spectral-library compatible given, it has been proposed, that the analytes remaining in the excited vibrational states can still be ionised and fragmented *via* 70 eV EI (Amirav, *et al.* 2015).

Cold-EI GC/MS has been applied to the analysis of hydrocarbons and fuels (Fialkov *et al.* 2008). Spectra generated with 70 eV Cold-EI still matched well with the NIST library, generated using 70 eV EI (Amirav, *et al.* 2015). In some cases, Cold-EI spectral matches were of higher accuracy (despite reduced matching scores) than conventional EI spectra, presumably due to enrichment of higher m/z ions, which are more characteristic for particular compounds (Amirav, *et al.* 2015). This result was supported by computer simulations of the spectral-matching process (Alon and Amirav 2015), which revealed that whilst matching scores for the correct match decreased (due to the deviations in relative intensity from the expected 70 eV EI spectrum), enrichment of the $M^{+\bullet}$ and other high-*m/z* ions made the spectra highly diagnostic for the correct library entry. Cold-EI-derived $M^{+\bullet}$ data had been previously used in to analyse MM of diterpenic acids obtained from oleoresin of *Copaifera* trees (Wong *et al.* 2016). I sought to explore this new technology, attempting to validate some of the compounds identifications made using 70 eV EI GC/MS, and evaluating the usefulness of Cold-EI for analysis of plant volatiles, particularly apocarotenoids.

3.2 Results and Discussion:

3.2.1 Preliminary studies on the usefulness of Cold-EI for apocarotenoid studies

I commenced preliminary studies into the efficacy of Cold-EI for apocarotenoid analysis. First, I tested the apocarotenoid standard collection against two Cold-EI make-up gas flow rates, 50 and 4 ml/min. I compared the results to those obtained from routine GC/MS 70 eV EI conditions to determine if Cold-EI provided any novel insights that might help in identifying and quantifying apocarotenoids *in planta*.

Both the 50 and 4 ml/min gas flows had a net positive effect on the relative intensity of $M^{+\bullet}$ for all compounds tested (Table 3.1). Cyclic apocarotenoid $M^{+\bullet}$s were enriched from a median relative intensity of 7.8% under EI to 59% and 66% for the 4 and 50 ml/min Cold-EI conditions. The results were more-dramatic for the linear apocarotenoids, which had a median EI $M^{+\bullet}$ intensity of 0%, but which reached ~40% under the two Cold-EI conditions.

These results suggested that Cold-EI may be particularly useful for identifying apocarotenoids and apocarotenoid-derived compounds derived from the linear, *cis*-carotenes. Consider for example citral and citronellal, two compounds conceivably derived from cleavage of lycopene/neurosporene (Supplementary Figure 3.1). Whilst the 70 eV EI spectra of these compounds (and indeed their retention indices) are similar, their MMs, and thus $M^{+\bullet}$s, would differ by two, providing unambiguous identification.

3.2.2 Cold-EI GC/MS method development

To further develop Cold-EI GC/MS as a tool for plant volatile analysis I optimised the two parameters affecting Cold-EI source performance: flow rate of the make-up gas and ionisation energies. In general, increases in make-up gas flow rate should further reduce analyte thermal energy, enriching the $M^{+\bullet}$. But, this may be counteracted at high flow rates by sample dilution. Moreover, further increases in make-up flow rates did not greatly enrich $M^{+\bullet}$ abundance beyond the enrichment obtained with 4 ml/min gas flow for one study involving model hydrocarbons (Amirav, *et al.* 2015): there may be compound-class-specific responses to make-up gas flow that are of interest. The ionisation energy, typically set at 70 eV, can also be altered. Reducing EI voltage to 18 eV combined with Cold-EI led to a dramatic enhancement in the relative abundance of the $M^{+\bullet}$ for some hydrocarbons (Amirav, *et al.* 2015). If voltage is reduced too far however, sensitivity may become unacceptably low. Compound class-dependent patterns in response to eV change may also be expected, making this parameter worthy of study.

To broaden the impact of this work, I optimised Cold-EI settings not only for apocarotenoid standards but for 64 plant volatile standards, including acids, alcohols, aldehydes, alkanes, benzenoids, esters, ketones and terpenes (Figure 3.1), representing the major plant volatile biosynthetic pathways (Schwab *et al.* 2008). Naturally, many of the volatiles could be classified by multiple descriptors; benzenoid phenyl-propanol and methyl salicylate (MeSA) are also an alcohol and ester respectively, and dihydroactinidiolide (DHA), a lactone, was categorised as an ester for simplicity (the full

set of standards, with classifications, is listed below). Alternative groupings of compounds were also possible: saturated versus non-saturated, straight-chain versus branched and cyclic compounds. The effects of these chemical differences upon Cold-EI results are discussed.

This collection of volatiles was separated *via* liquid injection GC/MS over 27 min using a standard non-polar GC column (Figure 3.2). EI spectra were collected for later comparison with Cold-EI GC/MS spectra. To simplify method development, I used a subset 'optimisation mix' of 15 compounds from the full collection. Each of the aforementioned compound classes, excluding alkanes, were, roughly, equally-represented. I did this to focus on the effects of Cold-EI upon the spectra of non-alkanes; alkanes are already known to generally have highly-enriched $M^{+\bullet}$ under Cold-EI conditions (Patkin 2015b). The optimisation mixture was separated *via* GC within 12 min (Figure 3.2).

3.2.3 Increasing make-up gas flow enriches $M^{+\bullet}$s for most compounds

I began parameter optimisation by examining the extent of $M^{+\bullet}$-enrichment for the standard set under different make-up gas flow rates. Consistent with expectations, the $M^{+\bullet}$ abundance for most compounds in the optimisation mix increased as make-up gas flow increased (4, 25, 50, 75 and 100 ml/min conditions were examined). Some enhancements were particularly dramatic: hexanal and ocimene exhibited ~10-fold, and α-cyclocitral and 6-methyl-5-hepten-2-one 5-fold, $M^{+\bullet}$ enhancements respectively. Overall median $M^{+\bullet}$ abundance for the optimisation mix increased from 15% at 4 ml/min to 50% at 100 ml/min. Unexpectedly, however, 25 ml/min make-up gas was more effective than 50 ml/min (34% and 29% median abundance respectively, Table 3.2).

Three compounds yielded their highest $M^{+\bullet}$ abundances at flow rates lower than 100 ml/min, with further increases reducing $M^{+\bullet}$ abundance; 3-methyl-2-buten-1-ol, methyl jasmonate (MeJA) and MeSA. The impact of high make-up gas flow rates was particularly noticeable on MeJA; 25 and 50 ml/min conditions yielded 100% $M^{+\bullet}$ abundance but 100 ml/min flow saw $M^{+\bullet}$ drop to 64.5%. The basis for this is unclear from the chemical structures, although presumably higher flow rates somehow induce greater $M^{+\bullet}$ instability in these compounds.

Three compounds were completely impervious to Cold-EI $M^{+\bullet}$ enrichment: isovaleric acid, 1-heptanol and 2-ethyl-1-hexanol ionisation did not yield a $M^{+\bullet}$ under any make-up gas flow rates ($M^{+\bullet}$ were not observed under EI, either). The acid/alcohol protons in these

compounds appear to make the $M^{+\bullet}$s too labile for detection, despite application of Cold-EI.

Make-up gas flow rate did not greatly affect the fragments observed in the mass spectra, reflecting the fact that compounds in energy states sufficiently elevated for fragmentation still underwent 70 eV ionisation, as previously suggested (Amirav, *et al.* 2015). Major fragment ions of some spectra became more abundant alongside the $M^{+\bullet}$, presumably because these ions are also well-stabilised by decreasing vibrational energy.

Despite the apparent appeal of 100 ml/min gas flow for $M^{+\bullet}$ enrichment I compromised by using 50 ml/min. I did this mindful that 100 ml/min could impact the ionisation of other volatiles more severely than it affected 3-methyl-2-buten-1-ol, MeJA and MeSA, hindering observation of $M^{+\bullet}$s. A make-up gas flow rate of 50 ml/min, with a median $M^{+\bullet}$ abundance of 29% seemed an appropriate compromise.

3.2.4 Changes in ionisation energy qualitatively alter mass spectra but do not greatly enhance plant volatile $M^{+\bullet}$ intensity

Subsequent variation of the 70 eV ionisation energy, with both higher (100 eV) and lower (50, 30 or 16 eV) settings, did not yield any obvious trends (Table 3.2). Benzenoid compounds 1,2,4-trimethylbenzene and MeSA achieved highest $M^{+\bullet}$ abundance at 16 eV whilst, surprisingly, hexanal and ocimene yielded their highest abundances at 100 eV. The aforementioned isovaleric acid and saturated alcohols still failed to yield a measurable $M^{+\bullet}$. Overall, $M^{+\bullet}$ abundance did not improve greatly upon either increasing or decreasing ionisation energy.

But, some mass spectra changed dramatically as ionisation energy was reduced (Supplementary Figure 3.3). Lower eV settings generally led to sparser spectra with fewer fragment ions. Indeed, four compounds, 3-methyl-2-buten-1-ol, hexanal, isovaleric acid and 1-heptanol, did not yield spectra at all under the 16 eV condition, presumably because there was insufficient energy for effective ionisation. Given the limited improvement of $M^{+\bullet}$ abundance upon eV change, I retained the 70 eV condition, reasoning this would also yield Cold-EI spectra most similar to the 70 eV NIST library spectra, thus aiding compound identification.

3.2.5 Cold-EI improves $M^{+\bullet}$ abundance across all compound classes and also improves spectral matching for some compounds

The cold-EI method was then used to generate mass spectra for all standard compounds used in this study. The $M^{+\bullet}$s of almost all compounds were easily-observable *via* Cold-EI GC/MS. All compound classes showed a median increase in $M^{+\bullet}$ abundance upon Cold-EI of between 1.6 and 17-fold (Table 3.3). The overall median increase was 3.5-fold. Only isovaleric acid, saturated, higher-molar mass (MM) alcohols, and phenylmethanoate failed to yield a $M^{+\bullet}$ under either EI or Cold-EI. The acid and alcohol results are consistent with method development results. In the case of phenylmethanoate, perhaps the $M^{+\bullet}$s of methanoate esters are particularly unstable; difficulty in generating $M^{+\bullet}$ for various esters has been reported before (Urbanová *et al.* 2012).

In addition, the $M^{+\bullet}$ abundance of 2-methyl-1-butanol was virtually unchanged, whilst that of 2-methyl-3-buten-1-ol underwent a 65% reduction under Cold-EI. 2-methyl-3-buten-1-ol decline is unusual, given its isomer, 3-methyl-3-buten-1-ol had increased $M^{+\bullet}$ abundance under Cold-EI conditions. Perhaps factors unrelated to the MS ion source account for increased fragmentation of 2-methyl-3-buten-1-ol under Cold-EI conditions.

As expected, alkanes responded well to Cold-EI conditions, with an average 17-fold improvement of $M^{+\bullet}$ abundance compared to EI. The ketone collection also exhibited marked $M^{+\bullet}$ enhancement, going from an EI median $M^{+\bullet}$ relative abundance of 3 to a Cold-EI median of 30. I note that this result may be somewhat skewed given 7 out of 10 ketones were non-cyclic, and such compounds seem to respond particularly well to Cold-EI. Cyclic ketones in comparison already have abundant $M^{+\bullet}$ under EI, and correspondingly responded with a lower improvement under Cold-EI conditions. α-ionone and (+)-carvone for instance had the two most abundance EI $M^{+\bullet}$s amongst the ketones and, along with β-ionone, recorded the three lowest-fold Cold-EI improvements in $M^{+\bullet}$ abundance.

It may be that cyclic ketone molecules are more rigid and thus their $M^{+\bullet}$s have inherently less vibrational energy and greater stability. This would reduce the potential for Cold-EI-mediated $M^{+\bullet}$ enrichment. Indeed, it seems increased molecular rigidity (i.e. less molecular degrees of freedom), whether due to carbon double-bond conjugation, aromaticity or cyclisation, correlates with increased $M^{+\bullet}$ abundance under standard EI and smaller improvements with Cold-EI. Consistent with this hypothesis, the classes containing many ‘rigid’ compounds, such as terpenes, esters and benzenoids, had median

EI $M^{+\bullet}$ abundances of 22.5, 29 and 49 respectively and only improved 2.8, 2.5 and 1.6-fold under Cold-EI respectively. Small compounds, which inherently have less degrees of freedom, also responded less to Cold-EI $M^{+\bullet}$ enrichment. The alcohol standard collection, dominated by low-MM compounds, only enriched $M^{+\bullet}$ abundance 2.3-fold under Cold-EI. Conversely, alkane, aldehyde and ketone collections, with many higher-MM, non-rigid compounds, showed dramatic $M^{+\bullet}$ enrichments upon Cold-EI.

Whilst enriching for $M^{+\bullet}$s, Cold-EI also reduced the NIST library-matching scores of resultant compound spectra. It was noted that forward and reverse spectral matching scores for most compounds declined when Cold-EI spectra were queried instead of EI spectra, due to Cold-EI induced spectral skewing towards the dominant $M^{+\bullet}$ (Supplementary Figure 3.2 and Supplementary Figure 3.3). Some compounds did however improve their NIST matching scores with Cold-EI spectral queries. Cold-EI make-up gas flow may 'dilute' interfering noise, presenting a cleaner spectrum for NIST query: this would particularly improve NIST matching for low-intensity peaks, provided the make-up gas flow does not reduce MS sensitivity too much. It may also be that matching of some compounds particularly benefit from the greater abundance of the $M^{+\bullet}$ and other high *m/z* ion fragments, which are often highly diagnostic for particular compounds (Alon and Amirav 2015). The ability for the NIST algorithm to select the correct library entry as the top spectral match improved in many instances (data not shown), consistent with previous observations (Alon and Amirav 2015).

3.2.6 Cold-EI survey of plant volatiles

The above data suggests Cold-EI data might be particularly useful combined with parallel standard EI analysis of a given sample. Under this scenario, researchers would be able to combine 70 eV EI mass spectra with MM data and confirm or refute peak annotations provided by spectral matching software (e.g. NIST). In the case of unidentifiable peaks, Cold-EI would provide MM data to complement EI mass spectra and RI values, thus helping to narrow down the list of possible compound identities. This workflow is described in Figure 3.3.

I applied this workflow to Arabidopsis leaves and tomato fruit tissue as a proof-of-concept, and also to attempt to validate some of the apocarotenoids identified in previous surveys. Duplicate samples of Arabidopsis leaves and tomato fruit were prepared, and extracted *via* SPME, with one extract desorbed on a Cold-EI GC/MS instrument and the other on a conventional EI instrument.

The workflow from Figure 3.3 was applied, and the peak-annotation results are summarised in Table 3.4. From the sampling of Arabidopsis leaves, 64 peaks were isolated from the EI dataset (Table 3.5), of which 50 could be matched to the NIST library. For this study, the NIST library-match confidence threshold was decreased to 60%, to test whether even low-confidence spectral matches can be confirmed or refuted using the Cold-EI data. Of the 64 EI peaks, 53 were also detected in Cold-EI, judging from their spectral and RI similarity. Here, one should note that peak alignment was hampered by differences in column composition between the EI and Cold-EI instruments used. In future, matching GC columns should be used to make parallel Cold-EI and EI data easier to interpret.

Nevertheless, Cold-EI added considerably to the plant volatile data obtained. Of the 53 peaks detected in both EI and Cold-EI data, 43 peaks were tentatively identified by matching EI spectra to entries in the NIST library, and 40 of those peaks had Cold-EI-elucidated $M^{+\bullet}$s that validated the library match. Crucially, for ten of those peak identifications, the $M^{+\bullet}$ was not present in the EI spectrum, meaning acquisition of $M^{+\bullet}$ data and thus $M^{+\bullet}$ validation of NIST-annotation was only possible using Cold-EI GC/MS. The remaining three NIST-annotated peaks were refuted upon inspection of the Cold-EI spectrum. Examples of these spectral matching scenarios are provided in Figure 3.4. Moreover, of the 14 compounds detected across both platforms but unidentifiable *via* EI-spectrum NIST-matching, nine peaks had putative $M^{+\bullet}$s only observable under Cold-EI. Thus, Cold-EI analysis has provided information beyond that available using EI GC/MS alone.

Similar results were obtained from analysis of tomato, although fewer peaks could be matched between the EI and Cold-EI data (Table 3.6). Only 19 of the 50 peaks isolated from EI GC/MS data were found in the Cold-EI data. This may be due to the aforementioned differences in column. It should also be noted that the make-up gas flow of the Cold-EI instrument has a dilutive effect upon the peak intensities. Thus, many peaks present at trace level in the EI analysis were lost in the Cold-EI analysis. Nevertheless, of the 19 peaks detected across both platforms, 14 had EI-spectrum NIST library-matches that could be confirmed by Cold-EI. For six of these compounds $M^{+\bullet}$ information was only observable *via* Cold-EI. The $M^{+\bullet}$ of four peaks with unidentifiable spectra were also obtained exclusively by applying Cold-EI.

3.2.7 Apocarotenoid spectral identification enhanced using parallel EI and Cold-EI analysis

Considering the apocarotenoids specifically (Table 3.7), I observed that 5 out of 5 (*Arabidopsis*) and 8 out of 12 (tomato) apocarotenoids observed *via* EI-GC/MS were also detected by cold-EI-GC/MS (some compounds were not observed in the Cold-EI data due to the dilution effect discussed above). The expected $M^{+\bullet}$s were observed for all apocarotenoids detected *via* Cold-EI. In particular, one *Arabidopsis* apocarotenoid (5,6-epoxy-β-ionone) and four tomato apocarotenoids (*cis*-geranylacetone, β-ionone and *trans*-farnesylacetone, as well as 5,6-epoxy-β-ionone) did not have $M^{+\bullet}$s observable under EI conditions. Thus, the additional data provided by Cold-EI has added to confidence in some of the spectral identifications.

One should note however, that a number of compounds observed in the original apocarotenoid surveys (Chapter Two) were not observed in these EI and Cold-EI parallel analyses. This might be attributable to differences in *Arabidopsis* leaf developmental stage and tomato fruit age. An unforeseen delay to use of the Cold-EI-GC/MS instrument meant *Arabidopsis* plants in this study were harvested when they were two weeks older than the plants analysed in Chapter Two. For logistical reasons, plants were also grown in a different laboratory and thus growth conditions might have varied in other, subtle, ways. Tomato fruits were also store-bought for this study instead of being harvested from plants, and this may also have affected the observed apocarotenoid profile. Regrettably, given the current scarcity of Cold-EI-GC/MS instruments (the instrument used is the only one of its kind in Australia, and is not located at my home institution), and the high demand from other users, it was impractical to repeat these experiments.

3.2.8 Summary

In this chapter, cold-EI was investigated as a GC/MS ionisation technique, evaluating its effectiveness for plant volatile (particularly volatile apocarotenoid analysis). Cold-EI-GC/MS technology was optimised for $M^{+\bullet}$-enrichment in plant volatile spectra. This data revealed trends in $M^{+\bullet}$ enrichment of interest to mass spectrometrists and physical chemists. Of practical interest to the chemical biologist, I applied Cold-EI, in parallel with EI-GC/MS, to analyse unknown plant tissue volatiles, obtaining previously-unavailable MM data. But, data from my original (EI) SPME-GC/MS apocarotenoid surveys could only be partially-validated. This difficulty highlights two shortcomings of Cold-EI that precluded its routine use in this thesis: low sensitivity, due to Cold-EI make-up gas flow-

dependent signal-dilution, and logistical challenges, given the scarcity of Cold-EI instruments.

Nevertheless, this technology shows promise. As Cold-EI instruments become more widely available, the logistical issues will be overcome. The dilution effect could be addressed by increased concentration of volatiles, perhaps using dynamic HS techniques. Regrettably, such work was outside the scope of this work. Cold-EI-GC/MS could not be applied in subsequent routine analyses of volatile apocarotenoids in *Arabidopsis*.

3.2 Figures and Tables

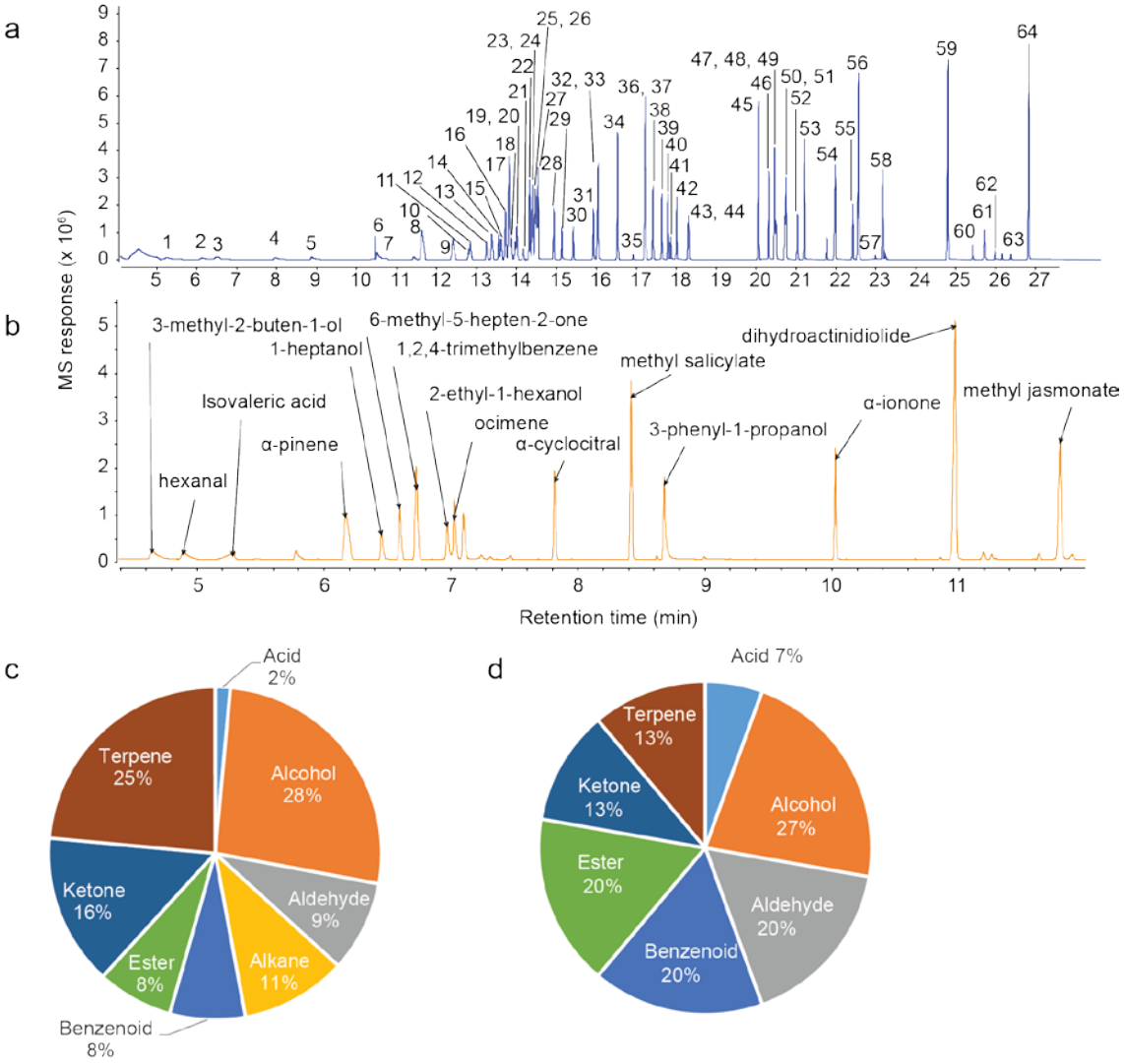

Figure 3.1: GC separation and analysis of plant volatile standard mixes

The mixture of 64 plant volatile standards could be separated *via* GC over 27 min (a), whilst the 15-compound optimisation mix could be separated within 12 min (b). Many compound classes were represented in the full plant volatile collection (c), although terpenes and alcohols dominated. The optimisation mix was better-balanced (d). Compounds in panel a are numbered as in Table 3.3.

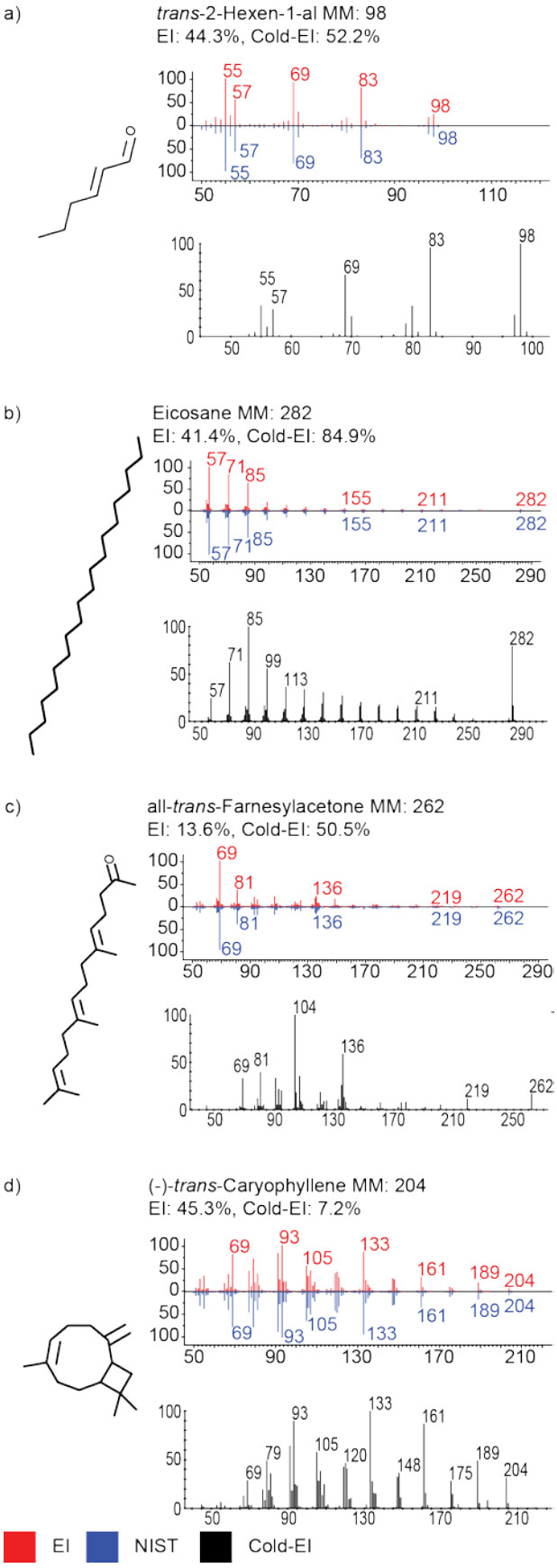

Figure 3.2: Comparison of spectral match percentage probabilities between 70 eV EI and Cold-EI GC/MS.

Standard compounds were analysed *via* both EI and Cold-EI GC/MS. The resulting EI spectra (red spectra) were matched to their NIST library entries (blue spectra) and the correct-match percentage probabilities were calculated. The EI-derived

probabilities could then be compared to those derived from Cold-EI spectra (black).The calculated probabilities for Cold-EI spectra being correctly-matched to their corresponding NIST entries were higher for*Trans*-2-hexen-1-al (a), eicosane (b) and all-*trans*-farnesylacetone (c), whilst the EI spectrum for (-)-*trans*-caryophyllene (d) yielded a higher match probability than the Cold-EI spectrum.

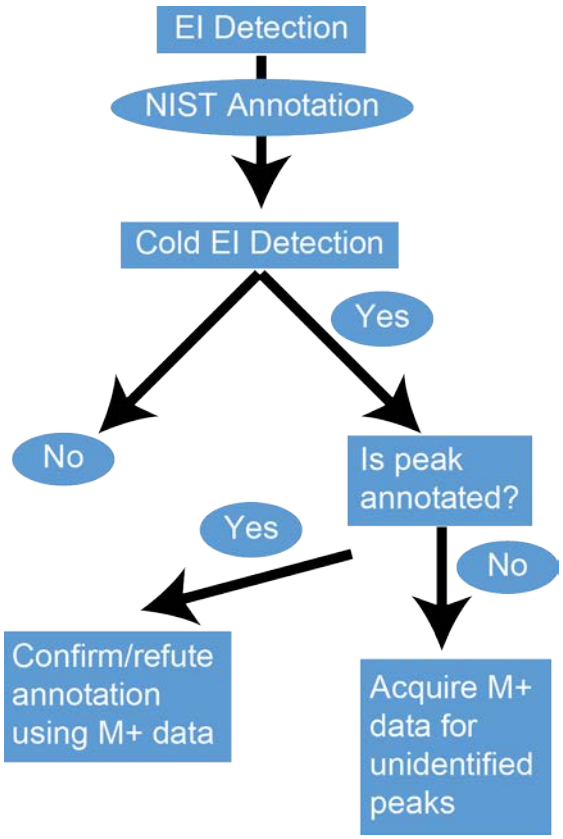

Figure 3.3: Parallel 70 eV and Cold-EI GC/MS Plant Volatile analysis workflow.

Arabidopsis leaf and tomato fruit volatiles were extracted *via* SPME and analysed using 70 eV EI and Cold-EI GC/MS. Peaks detected in EI were first annotated by NIST spectral library search (60% confidence). EI peaks were then matched to peaks detected in Cold-EI GC/MS analysis. For those peaks detected across both platforms, Cold-EI-derived $M^{+\bullet}$ data was then analysed: NIST annotations were confirmed or refuted and $M^{+\bullet}$ data was acquired for unidentified peaks. See **Table 3.4** for a summary of results from this workflow.

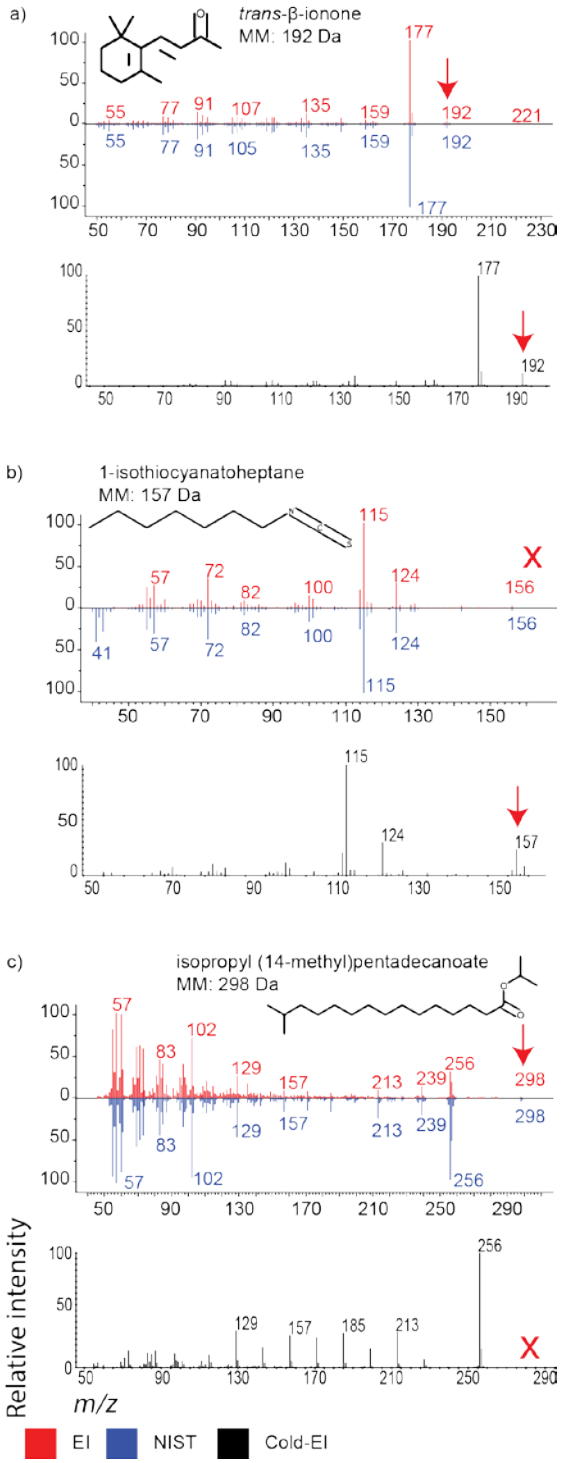

Figure 3.4: Examples of additional spectral data obtainable from Cold-EI.

Conventional EI mass spectra can be queried against the NIST library, resulting in the example spectra matches to (a) β-ionone, (b) 1-isothiocyanatoheptane and (c) isopropyl-(14-methyl)-pentadecanoate (red = queries, blue = NIST library entry). The corresponding Cold-EI spectra (black) provided $M^{+\bullet}$ data for these peaks, concurring with the library matches for (a) and (b). For compounds such as (b), where $M^{+\bullet}$ was not present in the EI spectrum, Cold-EI is particularly useful. In the case of peak (c) however, the Cold-EI data indicated a MM of 256 Da for the analyte peaks, refuting the NIST annotation which would be expected to have a $M^{+\bullet}$ at 298 *m/z*.

Table 3.1: Molecular ion relative intensity under 70 eV EI versus Cold-EI GC/MS ionisation conditions.

			Relative Intensity of Molecular Ion		
Compound	Molecular mass	Observed molecular ion m/z	50 ml/min Cold-EI	4 ml/min Cold-EI	EI
6-methyl-5-hepten-2-one	126.20	126	29.0	29.0	7.4
α-cyclocitral	152.23	152	26.8	22.0	5.3
β-cyclocitrol	154.25	154	63.2	23.4	34.0
β-cyclocitral	152.23	152	100.0	100.0	85.0
Cis-citral	152.23	152	3.3	7.3	0.0
Trans-citral	152.23	152	49.0	55.8	4.5
β-ionol	194.31	194	100.0	100.0	7.8
α-ionone	192.30	192	84.0	59.0	2.0
Trans-Geranylacetone	194.31	194	39.9	39.3	0.0
β-ionone	192.30	192	25.0	21.0	4.0
3-*trans*-5-*cis*-pseudoionone	192.30	192	20.5	33.0	4.0
Dihydroactinidiolide	180.12	180	66.0	75.0	22.0
Trans-pseudoionone	192.30	192	100.0	100.0	4.5
Farnesylacetone-1	262.23	262	91.7	57.1	0.0
Farnesylacetone-3	262.23	262	83.1	87.0	0.0
Trans-farnesylacetone	262.23	262	40.0	41.6	0.0
Median			56.1	48.7	4.3

For each compound, the condition or conditions giving the best $M^{+\bullet}$ relative abundance has been shaded green.

Table 3.2: Molecular ion abundances (%) for the optimisation mix compounds under different Cold-EI conditions.

			Make-up Gas Flow (ml/min)					Ionisation Energy (eV)				
Name	MW	RI	4	25	50	75	100	16	30	50	70	100
3-Methyl-2-buten-1-ol	86.1	732	64.7	89.7	70.3	78.2	75.8	-	82.4	100.	70.3	100
Hexanal	100.2	774	1.2	3.0	7.3	7.9	10.9	-	8.5	7.9	7.3	9.1
Isovaleric acid	102.1	847	0.0	0.0	0.0	0.0	0.0	-	0.0	0.0	0.0	0.0
α-Pinene	136.2	935	15.0	33.9	29.1	33.3	35.8	36.4	21.8	41.8	29.1	33.3
1-Heptanol	116.2	974	0.0	0.0	0.0	0.0	0.0	-	0.0	0.0	0.0	0.0
6-Methyl-5-hepten-2-one	126.2	988	11.0	16.4	25.5	37.6	50.3	13.9	24.9	22.4	25.5	21.8
1,2,4-Trimethylbenzene	120.2	996	56.6	74.0	59.4	63.0	77.6	100	86.7	61.8	59.4	61.2
2-Ethyl-1-hexanol	130.2	1033	0.0	0.0	0.0	0.0	0.0	0.0	0.0	0.0	0.0	0.0
Ocimene	136.2	1041	2.2	7.9	13.9	19.4	24.2	9.8	13.3	17.0	13.9	32.7
α-Cyclocitral	152.2	1130	6.6	21.2	21.2	38.2	38.2	23.6	19.4	23.6	21.2	21.8
Methyl salicylate	152.2	1201	91.5	84.2	74.6	100	89.7	100	73.3	70.9	74.6	54.6
3-Phenyl-1-propanol	136.2	1240	48.7	61.8	72.1	74.6	86.7	100	46.7	67.3	72.1	66.1
α-Ionone	192.3	1432	37.0	66.1	88.5	100	100	97.0	63.6	50.0	88.5	43.0
(*S*)-Dihydroactinidiolide	180.2	1554	39.8	55.8	79.4	100	100	55.8	65.5	59.4	79.4	50.9
Methyl jasmonate	224.3	1638	46.1	100	100	90.3	64.5	75.8	100	100	100	79.4
Median			15.0	33.9	29.1	38.2	50.3	23.6	24.9	41.8	29.1	33.3

Table 3.3: Comparison of EI and Cold EI molecular ion abundance and NIST spectral matching.

			F Match		R Match		Probability		$M^{+\bullet}$ rel. int.		
Compound	RI	MM	70 eV	Cold	70 eV	Cold	70 eV	Cold	70 eV	Cold	M fold-change
Isovaleric acid	847	102	805	694	809	740	77.0	76.2	0.0	0.0	0.00
Alcohols											
2-Methyl-3-buten-1-ol	608	86	939	872	939	873	90.5	67.6	20.0	7.1	0.35
3-Methyl-3-buten-1-ol	648	86	872	788	872	790	87.0	72.3	41.0	100.0	2.44
2-Methyl-1-butanol	666	88	945	861	945	864	47.9	36.4	2.0	2.0	0.98
3-Methyl-2-buten-1-ol	732	86	845	792	845	795	40.7	10.5	22.0	77.9	3.54
cis-4-Methylcyclohexanol	953	114	936	814	936	826	56.4	37.0	5.0	19.9	3.99
trans-4-Methyl-cyclohexanol	956	114	957	819	957	822	47.9	35.9	0.0	3.0	2980.00
1-Heptanol	974	116	973	704	973	834	52.5	35.1	0.0	0.0	0.00
2-Octanol	1003	130	962	707	962	787	40.3	38.3	0.0	0.0	0.00
2-Ethyl-1-hexanol	1033	130	936	802	936	815	51.1	11.4	0.0	0.0	0.00
Eucalyptol	1039	154	894	852	897	854	79.0	79.7	44.0	100.0	2.27
1-Octanol	1078	130	972	843	972	845	34.6	11.8	0.0	0.0	0.00
(+)-Fenchol	1131	154	928	894	928	901	29.1	41.5	1.0	7.7	7.67
2,6,6-Trimethyl-1-cyclohexene-1-Methanol	1214	154							35.0	91.4	2.61
1-Decanol	1277	158	813	847	813	870	38.6	12.7	0.0	0.0	0.00
β-Ionol	1420	194	834	815	834	816	13.4	11.8	8.0	54.6	6.83
Median			936	817	936	830	47.9	36.2	2.0	7.1	2.27
Aldehydes											
Hexanal	774	100	957	818	957	820	87.2	66.4	0.0	7.1	7060.00
trans-2-Hexen-1-al	849	98	937	841	937	849	44.3	52.2	22.0	97.5	4.43
α-Cyclocitral	1130	152	915	863	916	866	65.1	74.0	5.0	23.0	4.60
β-Cyclocitral	1230	152	938	874	938	880	88.1	68.3	84.0	100.0	1.19
cis-Citral	1246	152	854	808	854	809	49.9	41.9	1.0	6.8	6.75
trans-Citral	1276	152	627	847	627	849	64.2	64.8	1.0	26.4	26.38
Median			926	844	927	849	64.7	65.6	3.0	24.7	5.68
Alkanes											
Nonane	900	128	963	720	963	724	43.6	39.2	9.0	94.8	10.53
Decane	1000	142	728	750	884	756	37.2	62.5	8.0	99.4	12.42
Dodecane	1200	170	962	796	962	801	44.7	75.3	6.0	89.6	14.93
Tetradecane	1400	198	840	770	840	775	44.1	54.9	5.0	84.7	16.93
Hexadecane	1600	226	860	865	860	873	39.6	91.9	4.0	100.0	25.00
Octadecane	1800	254	829	775	829	782	10.9	65.5	4.0	91.1	22.78
Eicosane	2000	282	876	845	876	851	41.4	84.9	3.0	81.3	27.10
Median			860	775	876	782	41.4	65.5	5.0	91.1	16.93
Benzenoids											
1,2,4-Trimethylbenzene	996	120	943	868	943	878	18.2	29.1	49.0	66.0	1.35
Phenylmethanol	1043	108	976	865	976	876	62.1	23.4	90.0	100.0	1.11
1-Phenylethanol	1124	122	962	882	962	884	86.4	88.1	27.0	47.6	1.76
Methyl salicylate	1201	152	969	919	969	921	85.6	67.0	50.0	80.1	1.60
3-Phenyl-1-propanol	1240	136	959	880	959	885	85.8	87.2	22.0	72.7	3.30
Median			962	880	962	884	85.6	67.0	49.0	72.7	1.60

Esters											
phenylethylmethanoate	1182	150	827	868	924	885	34.2	23.7	0.0	0.0	0.00
(S)-Dihydroactinidiolide	1554	180	924	873	924	893	88.7	84.4	21.0	80.1	3.81
Methyl Jasmonate	1638	224	861	865	863	888	79.0	78.9	43.0	100.0	2.33
Methyl Jasmonate-2	1654	224	938	698	940	720	79.6	38.1	37.0	100.0	2.70
Median			893	867	924	887	79.3	58.5	29.0	90.0	2.51
Ketones											
6-methyl-5-hepten-2-one	988	126	938	839	938	848	85.1	74.4	15.0	25.8	1.72
(+)-carvone	1256	150	900	855	900	859	34.8	39.4	8.0	30.7	3.83
alpha ionone	1432	192	822	829	822	849	39.4	43.2	15.0	94.8	6.32
cis-geranylacetone	1433	194	783	863	797	867	21.0	31.8	2.0	40.0	19.99
trans-geranylacetone	1453	194	725	867	725	870	65.2	47.5	2.0	27.0	13.50
beta ionone	1492	192	842	860	842	864	42.6	41.5	5.0	16.9	3.37
trans-pseudoionone	1589	192	782	763	791	797	71.5	14.8	4.0	36.2	9.05
farnesylacetone-1	1861	262							2.0	28.5	14.27
farnesylacetone-2	1891	262							2.0	31.9	15.95
all-*trans*-farnesylacetone	1917	262	761	713	761	713	13.6	50.5	1.4	14.7	10.51
Median			803	847	810	854	41.0	42.4	3.0	29.6	9.78
Terpenes											
α-pinene	935	136	943	855	943	857	16.6	5.6	8.0	30.7	3.83
(-)-β-pinene	980	136	938	804	938	813	25.0	12.1	9.0	26.7	2.97
myrcene	991	136	963	664	963	727	65.7	8.5	4.0	34.1	8.51
R-(-)-α-phellandrene	1009	136	906	739	906	865	39.3	30.1	23.0	37.7	1.64
3-carene (5% 2-carene)	1011	136	956	863	956	871	12.1	10.8	17.0	54.9	3.23
α-terpinene	1021	136	944	870	948	872	16.6	10.0	52.0	82.2	1.58
p-cymene	1030	134	932	862	932	865	26.1	6.6	28.0	54.6	1.95
R-(+)-limonene	1035	136	963	856	963	859	27.8	16.1	22.0	99.0	4.50
ocimene	1041	136	896	790	920	807	15.1	2.6	2.0	14.4	7.21
γ-terpinene	1066	136	962	862	962	872	40.2	29.0	38.0	77.3	2.03
terpinolene	1094	136	968	875	970	880	36.5	13.7	88.0	100.0	1.14
(1*S*)-(-)-camphor	1160	152	969	897	969	912	15.8	41.4	32.0	72.1	2.25
(-)-trans-caryophyllene	1435	204	920	871	920	880	45.3	7.2	6.0	31.9	5.32
(+)-aromadendrene	1455	204	948	886	949	890	32.0	7.9	42.0	100.0	2.38
(-)-alloaromadendrene	1478	204	927	870	927	872	14.0	8.6	37.0	93.6	2.53
m-camphorene	1955	272	886	731	886	735	71.6	30.8	9.0	88.6	9.84
Median			944	862	946	868	27.0	10.4	22.5	63.5	2.75
All-compound Median			932	847	932	857	43.6	38.3	8.0	51.1	3.46

Compounds with $M^{+\bullet}$s undetectable by EI were assigned a nominal EI $M^{+\bullet}$ intensity of 0.001% for the purpose of calculating fold-change.

N.B: two stereoisomers of methyl jasmonate (configurations undetermined) were detected from the standard mixture, leading to designation of one as 'methyl jasmonate-2'. Similarly, two *cis* stereoisomers of farnesylacetone were detected in addition to *trans*-farnesylacetone, designated farnesylacetones 1 and 2.

Table 3.4: Plant Volatile GC/MS Compound Data Summary.

	Arabidopsis	Tomato
All peaks found in 70 eV EI analysis	64	50
NIST Annotated	50	24
Detected by Cold EI	52	19
Annotations with MW confirmed in both EI and Cold EI	29	7
Annotations with MW confirmed by Cold EI only	11	7
Annotations with MW refuted by Cold EI	3	0
Unidentified peaks with M+ data provided by Cold EI	9	5

Table 3.5: *Arabidopsis* volatiles detected *via* 70 eV and Cold-EI GC/MS

Arabidopsis Volatiles Data from 70 eV EI								Data from Cold EI		
RT	RI	NIST Annotation	F Score	R Score	Prob	Putative MW	M+ Present in EI	Cold EI M+	Annotation confirmed by Cold EI
1.584	729	1-Penten-3-one	701	731	57.1	84	Y	84	Y
2.046	743	2-Pentenal, (E)-	742	750	34.6	84	Y	84	Y
2.368	752	2-Penten-1-ol, (Z)-	708	715	52.0	86	Y	86	Y
3.608	787	2-Hexenal, (E)-	779	791	50.6	98	n.d.	98	Y
5.189	832	Heptanal	861	889	49.6	114	n.d.	114	Y
9.111	945	Butane, 1-isothiocyanato-	715	735	33.4	115	Y	115	Y
9.991	970	2,4-Heptadienal, (E,E)-	868	873	59.4	110	Y	110	Y
10.323	979	cis-2-(2-Pentenyl)furan	829	874	42.6	136	Y	136	Y
11.750	1020	Butane, 1-isothiocyanato-3-methyl-	751	754	69.6	129	Y	129	Y
13.274	1064	Unknown @ 13.274 min					n.a.	129	
14.110	1087	Nonanal	793	800	47.4	142	n.d.	142	Y
15.600	1130	4-Methylpentyl isothiocyanate	830	845	95.4	143	Y	143	Y
16.081	1144	Pentanenitrile, 5-(methylthio)-	867	905	97.0	129	Y	129	Y
16.389	1153	Unknown @ 16.389 min					n.a.	145	
16.788	1164	Hexane, 1-isothiocyanato-	727	760	67.5	143	n.d.	143	Y
17.288	1178	Unknown @ 17.288 min					n.a.	n.d.	
17.513	1185	1-Cyclohexene-1-carboxaldehyde, 2,6,6-trimethyl-	938	944	86.4	152	Y	152	Y
17.821	1194	Unknown @ 17.821 min					n.a.	184	
18.023	1199	Dodecane	777	802	20.3	170	Y	170	Y
18.177	1205	Aziridine, 2-methyl-2-(2,2,4,4-tetramethylpentyl)-	703	732	7.4	183	n.d.	126	N
18.730	1225	Unknown @ 18.73 min					n.a.	157	
19.436	1250	Propane, 1-isothiocyanato-3-(methylthio)-	875	925	97.2	147	Y	147	Y
19.825	1264	Heptane, 1-isothiocyanato-	857	868	93.0	157	n.d.	157	Y
20.181	1277	Unknown @ 20.181 min					n.a.	n.d.	
20.993	1306	Benzene, (isothiocyanatomethyl)-	816	867	61.6	149	Y	149	Y
21.652	1330	Octane, 1-isothiocyanato-	815	846	87.9	171	n.d.	171	Y
22.940	1377	Erucin	887	902	93.1	161	Y	161	Y
23.402	1394	α-Ionone	811	821	39.2	192	Y	192	Y
23.493	1397	Tetradecane	778	830	12.0	198	Y	198	Y
23.575	1400	Benzene, (2-isothiocyanatoethyl)-	949	949	92.4	163	Y	163	Y
24.075	1421	Unknown @ 24.075 min					n.a.	208	
24.305	1430	Nonyl isothiocyanate	638	750	16.1	185	n.d.	n.d.	
24.685	1446	3-Buten-2-one, 4-(2,2,6-trimethyl-7-oxabicyclo[4.1.0]hept-1-yl)-	843	855	61.8	208	Y	208	Y
24.579	1442	Unknown @ 24.579 min					n.a.	163	
24.796	1451	trans-β-Ionone	928	929	51.9	192	Y	192	Y
24.974	1458	2(4H)-Benzofuranone, 5,6,7,7a-tetrahydro-4,4,7a-trimethyl-, (R)-	816	880	75.3	180	Y	180	Y
25.522	1481	Berteroin	874	889	95.4	175	Y	175	Y

25.618	1485	2-Propen-1-ol, 3-(2,6,6-trimethyl-1-cyclohexen-1-yl)-4,6,10,10-Tetramethyl-5-	725	774	13.1	180	n.d.	165	N
25.757	1491	oxatricyclo[4.4.0.0(1,4)]dec-2-en-7-ol	747	757	18.4	208	Y	208	Y
25.969	1500	2-Methyl-4-(2,6,6-trimethylcyclohex-1-enyl)but-2-en-1-ol	805	831	20.2	208	Y	n.d.	
27.050	1545	Unknown @ 27.05 min					n.a.	200	
27.262	1554	Isoshyobunone	751	782	8.5	220	Y	n.d.	
27.449	1561	Benzophenone	733	950	55.6	182	Y	182	Y
27.598	1568	Benzenemethanol, α-phenyl-	711	809	57.6	184	Y	n.d.	
28.218	1593	Hexadecane	859	859	24.1	226	Y	226	Y
28.954	1627	1,1'-Biphenyl, 3,4-diethyl-	716	738	39.2	210	Y	210	Y
29.237	1641	Unknown @ 29.237 min					n.a.	161	
29.420	1649	Octane, 1,1'-oxybis-	732	801	12.6	242	n.d.	242	Y
29.829	1669	Dodecyl acrylate	758	835	12.4	240	n.d.	n.d.	
30.189	1686	Unknown @ 30.189 min					n.a.	n.d.	
30.372	1695	(7-Isothiocyanatoheptyl)(methyl)sulfane	811	828	91.8	203	Y	203	Y
31.213	1734	Unknown @ 31.213 min					n.a.	n.d.	
31.333	1740	Tetradecanoic acid	807	879	59.0	228	Y	228	Y
32.458	1793	Octadecane	857	857	17.1	254	n.d.	254	Y
32.602	1800	Jirsutin	753	845	79.2	217	Y	217	Y
35.409	1949	n-Hexadecanoic acid	902	903	75.7	256	Y	256	Y
36.313	1996	Eicosane	882	885	28.9	282	Y	n.d.	
36.525	2008	i-Propyl 14-methyl-pentadecanoate	796	853	55.6	298	n.d.	256	N
37.058	2039	Unknown @ 37.058 min					n.a.	256	
37.159	2045	Palmitoleic acid	758	808	6.8	254	n.d.	254	Y
37.798	2082	Unknown @ 37.798 min					n.a.	n.d.	
38.111	2100	Unknown @ 38.111 min					n.a.	n.d.	
38.933	2147	Octadecanoic acid	885	885	66.0	284	Y	284	Y
40.803	2259	Octadecenoic acid	801	833	8.9	282	n.d.	282	Y

Unknown compounds have been listed as ‘unknown’, appended with their observed retention times

n.a = not applicable

n.d = not detected

Y = yes, N = no

Table 3.6: Tomato volatiles detected *via* 70 eV and Cold-EI.

Tomato Volatiles Data from 70 eV EI								Cold-EI Data		
RT	RI	NIST Annotation	F Score	R Score	Prob	Putative MW	$M^{+\bullet}$ Present in EI	Cold EI $M^{+\bullet}$	Annotation confirmed by Cold EI	
2.656	760	Unknown @ 2.656 min					n.a.	n.d.		
3.632	788	2-Hexenal, (E)-	772	781	49.3	98	Y	98	Y	
3.959	797	3-Hexen-1-ol, (E)-	762	820	40.3	100	n.d.	100	Y	
4.415	810	Unknown @ 4.415 min					n.a.	84		
4.487	812	Unknown @ 4.487 min					n.a.	n.d.		
6.819	879	(E)-4-Oxohex-2-enal	632	766	24.2	112	n.d.	112	Y	
7.270	892	Benzaldehyde	654	888	14.5	106	n.d.	106	Y	
9.155	946	Unknown @ 9.155 min					n.a.	n.d.		
9.356	952	5-Hepten-2-one, 6-methyl-	777	802	63.7	126	Y	126	Y	
10.097	973	Unknown @ 10.097 min					n.a.	n.d.		
10.299	979	Unknown @ 10.299 min					n.a.	112		
11.707	1019	Unknown @ 11.707 min					n.a.	120		
13.062	1058	Benzenemethanol, α,α-dimethyl-	799	834	73.5	136	Y	136	Y	
13.293	1064	Unknown @ 13.293 min					n.a.	n.d.		
13.457	1069	Unknown @ 13.457 min					n.a.	n.d.		
13.567	1072	Unknown @ 13.567 min					n.a.	124		
13.942	1083	Phenylethyl Alcohol	813	869	65.4	122	Y	122	Y	
14.129	1088	Nonanal	709	736	15.3	142	n.d.	n.d.		
14.826	1108	Unknown @ 14.826 min					n.a.	n.d.		
16.403	1153	Unknown @ 16.403 min					n.a.	n.d.		
16.677	1161	Unknown @ 16.677 min					n.a.	109		
17.013	1170	Unknown @ 17.013 min					n.a.	n.d.		
17.509	1185	1-Cyclohexene-1-carboxaldehyde, 2,6,6-trimethyl-	850	898	54.5	152	n.d.	152	Y	
18.032	1200	Unknown @ 18.032 min					n.a.	n.d.		
18.239	1207	2,6-Octadienal, 3,7-dimethyl-, (Z)-	722	739	3.9	152	n.d.	n.d.		
18.691	1223	1-Cyclohexene-1-acetaldehyde, 2,6,6-trimethyl-	739	758	22.6	166	Y	n.d.		
18.979	1234	Unknown @ 18.979 min					n.a.	n.d.		
19.905	1267	Citral	818	827	52.4	152	Y	152	Y	
19.763	1262	Nonanoic acid	600	646	10.5	158	n.d.	n.d.		
20.412	1285	Undecanal	672	764	2.4	170	n.d.	n.d.		
20.792	1299	Unknown @ 20.792 min					n.a.	n.d.		
20.864	1302	Tridecane	639	722	1.3	184	n.d.	n.d.		
20.993	1306	Unknown @ 20.993 min					n.a.	n.d.		
21.032	1308	Unknown @ 21.032 min					n.a.	n.d.		
21.863	1338	Unknown @ 21.863 min					n.a.	n.d.		
23.099	1383	Dodecanal	790	862	15.8	184	n.d.	n.d.		
23.488	1397	Unknown @ 23.488 min					n.a.	n.d.		
24.079	1421	5,9-Undecadien-2-one, 6,10-dimethyl-, (Z)-	821	823	39.1	194	n.d.	194	Y	
24.248	1428	5,9-Undecadien-2-ol, 6,10-dimethyl-	699	743	2.2	196	n.d.	n.d.		

24.651	1445	3-Buten-2-one, 4-(2,2,6-trimethyl-7-oxabicyclo[4.1.0]hept-1-yl)-	716	792	10.0	208	n.d.	208	Y
24.747	1449	trans-β-Ionone	868	888	44.8	192	n.d.	192	Y
24.944	1457	2(4H)-Benzofuranone, 5,6,7,7a-tetrahydro-4,4,7a-trimethyl-, (R)-	790	842	56.8	180	Y	180	Y
27.083	1546	3,5,9-Undecatrien-2-one, 6,10-dimethyl-, (E,Z)-	621	663	2.9	192	n.d.	n.d.	
27.372	1558	Unknown @ 27.372 min					n.a.	n.d.	
27.963	1583	Unknown @ 27.963 min					n.a.	n.d.	
29.660	1661	Dibenzylamine	702	859	46.6	197	n.d.	n.d.	
30.049	1679	Benzenemethanamine, N-(phenylmethylene)-	778	892	50.3	195	Y	n.d.	
30.256	1689	Unknown @ 30.256 min					n.a.	n.d.	
30.458	1699	Unknown @ 30.458 min					n.a.	n.d.	
34.144	1882	5,9,13-Pentadecatrien-2-one, 6,10,14-trimethyl-, (E,E)-	799	819	12.9	262	n.d.	262	Y

Unknown compounds have been listed as ‘unknown’, appended with their observed retention times

n.a. = not applicable, n.d. = not detected

Y = yes

Table 3.7: Summary of apocarotenoids detected in parallel EI and Cold-EI GC/MS analyses of *Arabidopsis* leaf and tomato fruit.

Arabidopsis leaf apocarotenoids not observed in EI/Cold-EI parallel analysis						
	6-methyl-5-hepten-2-one					
	β-homo-citral					
	Trans-citral					
	Trans-geranylacetone					
	Hexahydro-pseudoionone					
	Hexahydrofarnesyl-acetone					
Peak	NIST Match	Common name	Expected $M^{+\bullet}$	Detected with Cold-EI	EI $M^{+\bullet}$	Cold EI $M^{+\bullet}$
Apocarotenoids with M+ observed in both EI and Cold-EI						
17	2,6,6-Trimethyl-1-cyclohexene-1-carboxaldehyde	β-cyclocitral	152	Y	Y	Y
28	α-Ionone	α-Ionone	192	Y	Y	Y
35	*trans*-β-Ionone	*trans*-β-Ionone	192	Y	Y	Y
36	(*R*)-5,6,7,7a-Tetrahydro-4,4,7a-trimethyl-2(4H)-benzofuranone	DHA	180	Y	Y	Y
Apocarotenoids with M+ observed only in Cold-EI						
33	4-(2,2,6-Trimethyl-7-oxabicyclo[4.1.0]hept-1-yl)-3-buten-2-one	5,6-epoxy-β-ionone	208	208	n.d	Y
Tomato fruit apocarotenoids not observed in EI/Cold-EI parallel analysis						
	β-cyclocitrol					
	Trans-citrol					
	α-ionone					
	7,8-dihydro-β-ionone					
	Trans-geranylacetone					
	Trans-pseudoionone					
	Hexahydrofarnesylacetone					
Peak	NIST Match	Common name	Expected $M^{+\bullet}$	Detected with Cold-EI	EI $M^{+\bullet}$	Cold EI $M^{+\bullet}$
Apocarotenoids observed in EI but not Cold-EI analysis						
25	(*Z*)-3,7-Dimethyl-2,6-octadienal	*cis*-citral	152	n.d	n.d	n.d
26	2,6,6-Trimethyl-1-cyclohexene-1-acetaldehyde	β-homocitral	166	n.d	Y	n.d
39	6,10-Dimethyl-5,9-undecadien-2-ol	geranylacetone alcohol	196	n.d	n.d	n.d
43	(*E,Z*)-6,10-Dimethyl-3,5,9-undecatrien-2-one	3-*trans*-5-*cis*-pseudoionone	192	n.d	n.d	n.d
Apocarotenoids with M+ observed in both EI and Cold-EI						
9	6-Methyl-5-hepten-2-one	6-methyl-5-hepten-2-one	126	126	Y	Y
23	2,6,6-Trimethyl-1-cyclohexene-1-carboxaldehyde	β-cyclocitral	152	152	Y	Y
28	*trans*-Citral	*trans*-Citral	152	152	Y	Y

42	(*R*)-5,6,7,7a-Tetrahydro-4,4,7a-trimethyl-2(4H)-benzofuranone	dihydroactinidiolide	180	180	Y	Y
Apocarotenoids with M+ observed only in Cold-EI						
38	(*Z*)-6,10-Dimethyl-5,9-undecadien-2-one	*cis*-geranylacetone	194	194	n.d	Y
40	4-(2,2,6-Trimethyl-7-oxabicyclo[4.1.0]hept-1-yl)-3-buten-2-one	5,6-epoxy-β-ionone	208	208	n.d	Y
41	*trans*-β-Ionone	*trans*-β-Ionone	192	192	n.d	Y
50	(*E,E*)-6,10,14-Trimethyl-5,9,13-pentadecatrien-2-one	*trans*-farnesylacetone	262	262	n.d	Y

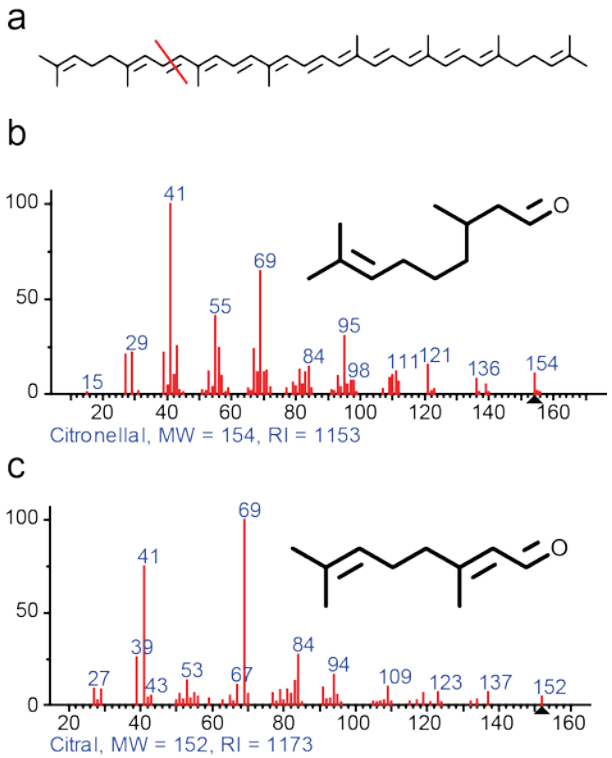

Supplementary Figure 3.1: Comparison of GC/MS spectral characteristics for two putative lycopene-derived apocarotenoids

Cleavage of lycopene at the marked position (a) could yield citral (c), which could be further desaturated to (b). The NIST library 70 eV EI spectra for these two compounds are depicted. It is important to note that particularly characteristic GC/MS peaks for these two compounds (e.g.121 *m/z* for citronellal, and 123 *m/z* for citral, plus their respective $M^{+\bullet}$s) could easily be obscured in experimentally-obtained spectra due to co-eluting interferences. Using Cold-EI, the $M^{+\bullet}$s would be enriched, allowing for differentiation of these compounds.

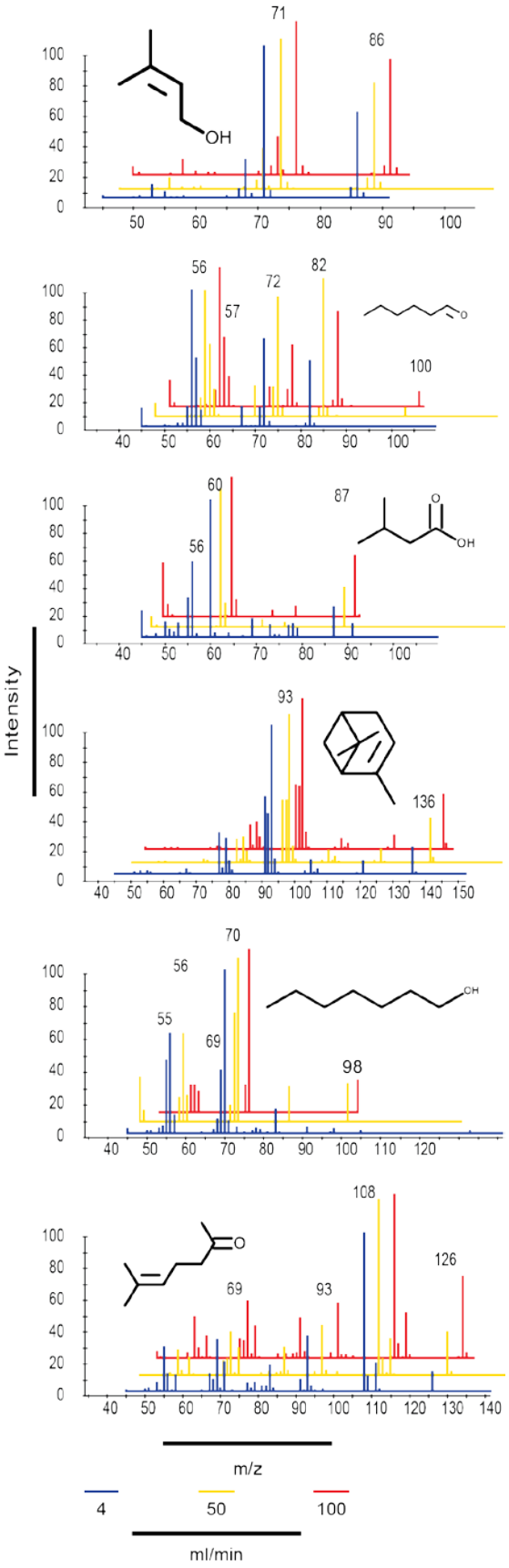
Intensity
m/z
4
50
100
ml/min

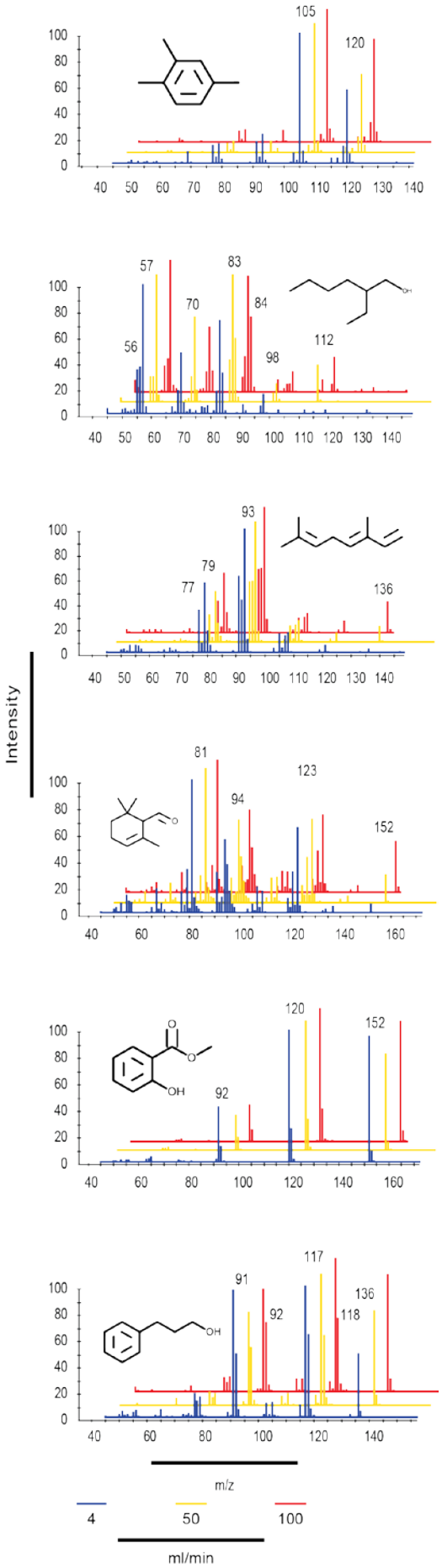
105
120
57
83
70
84
56
112
98
93
79
77
136
81
123
94
152
120
152
92
117
91
136
92
118
Intensity
m/z
4
50
100
ml/min

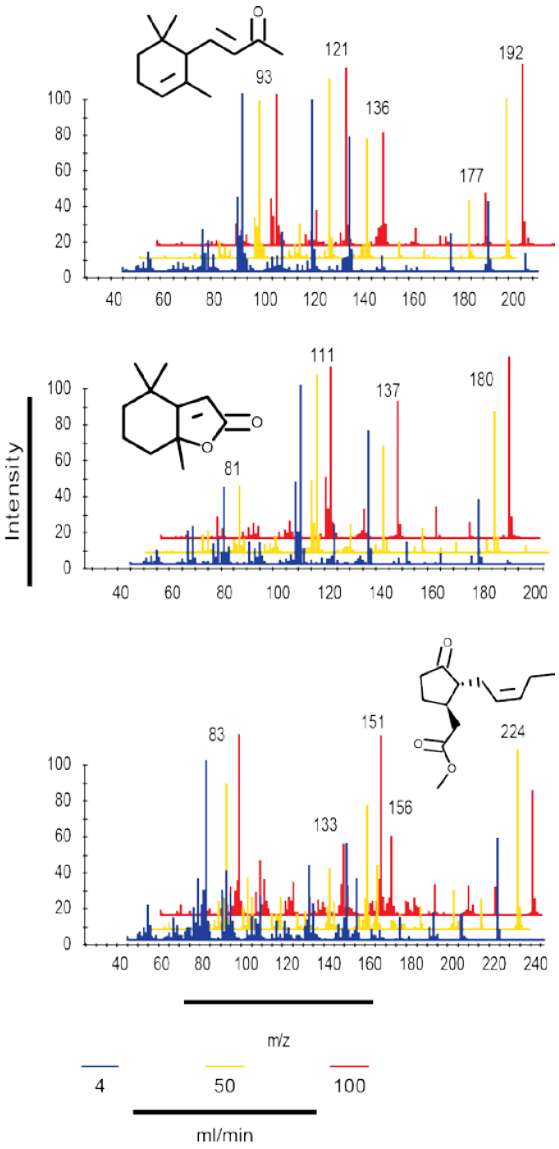

Supplementary Figure 3.2: Cold-EI mass spectra under different make-up gas-flow rates.

As I varied the make-up gas flow rate (ml/min) during Cold-EI method development, I recorded the mass spectra of the optimisation mix compounds. These spectra have been colour-coded and offset-overlaid to allow for comparison.

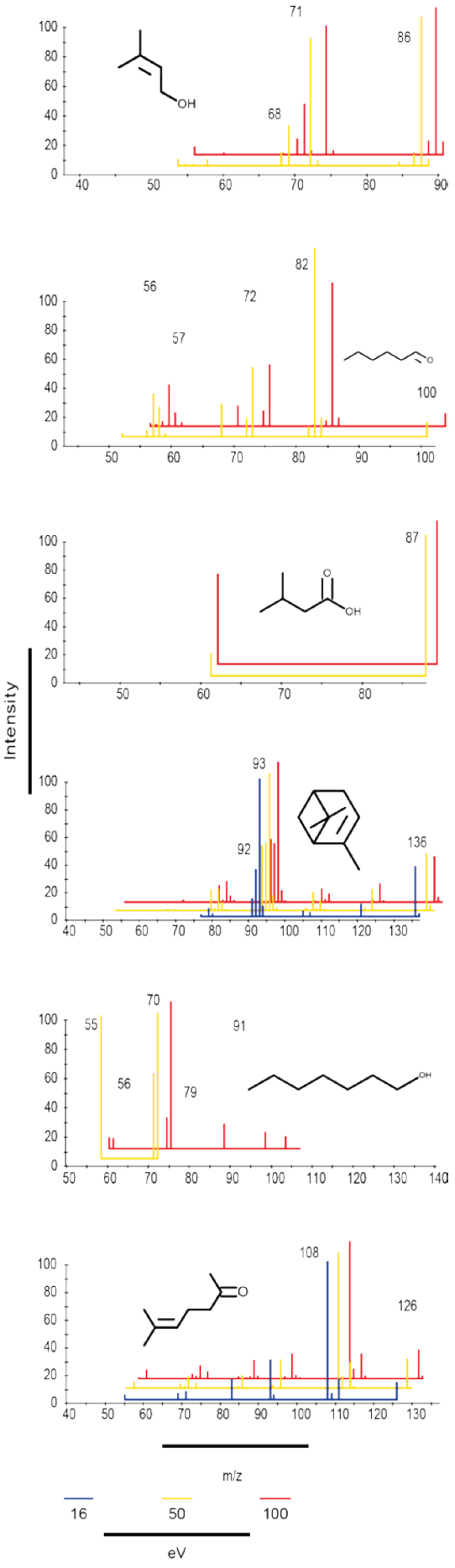
71
86
68
OH
82
56
72
57
100
87
O
OH
Intensity
93
92
136
70
55
91
56
79
OH
108
126
O
m/z
16
50
100
eV

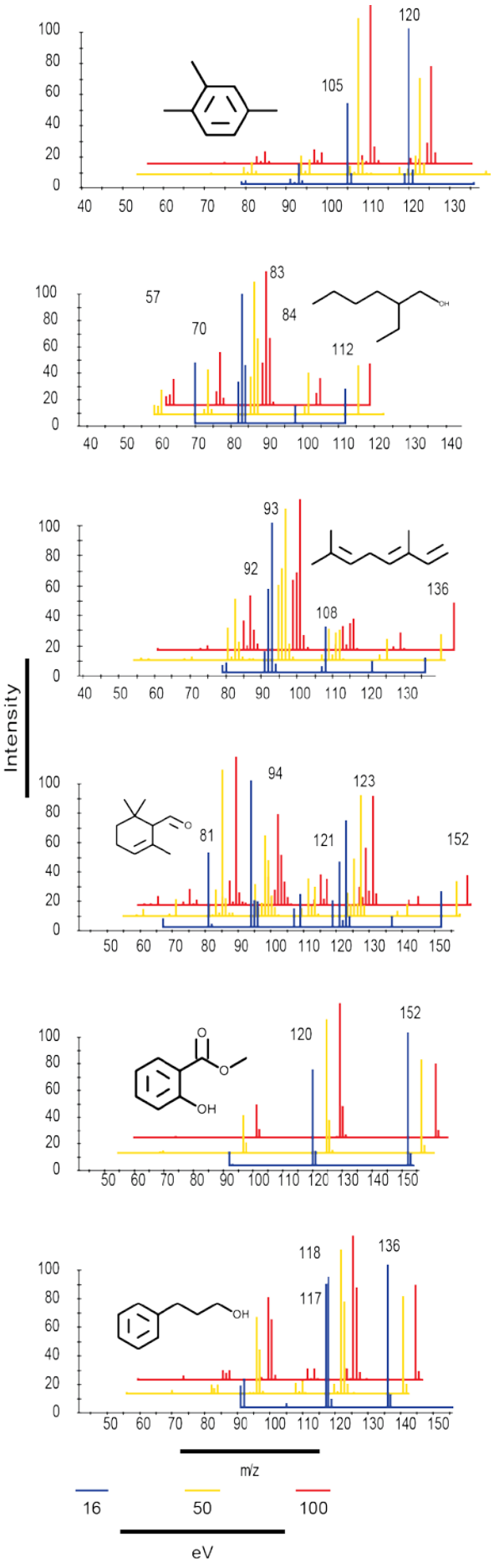
Intensity
120
105
83
57
70
84
112
93
92
136
108
94
123
81
121
152
120
152
118
136
117
m/z
16
50
100
eV

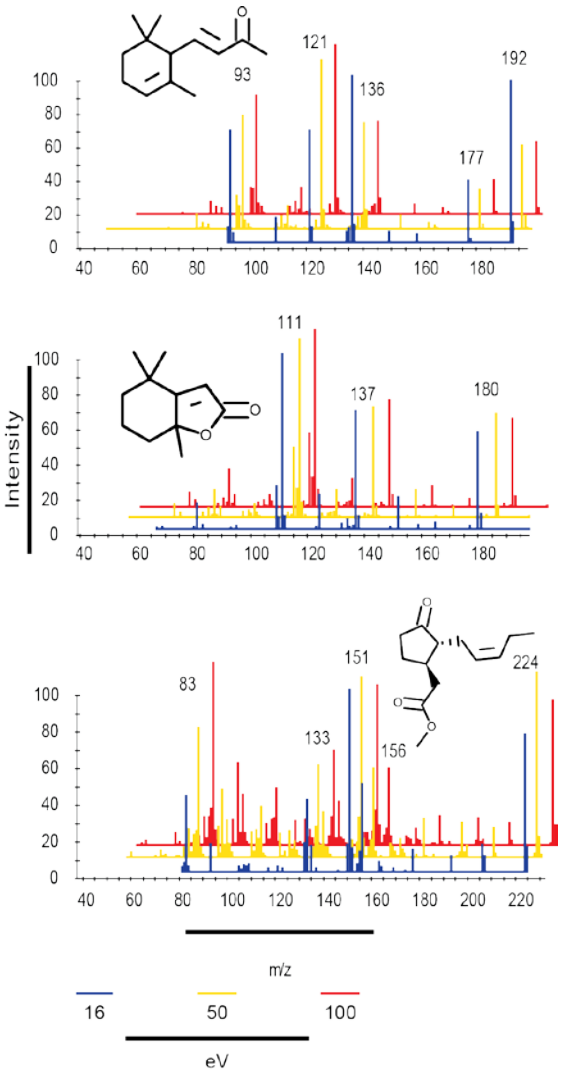

Supplementary Figure 3.3: Cold-EI mass spectra under different ionisation energies.

As I varied the ionisation energy (eV) during Cold-EI method development, I recorded the mass spectra of optimisation mix compounds. These spectra have been colour-coded and offset-overlaid to allow for comparison.

Chapter Four: Studying CCD activity *in planta* using SPME-GC/MS

4.1 Overview

Having developed a new *in planta* method for volatile apocarotenoid analysis, I proceeded to analyse volatile apocarotenoid metabolism and the *in planta* function of *Arabidopsis* CCD enzymes in *Arabidopsis* Col-0 and *ccd* loss-of-function single and double mutants. Metabolomics approaches (SPME-GC/MS and HPLC) were complemented with *CCD* gene expression studies across the genotypes. This chapter aimed to address thesis research aims One and Two (see Chapter One):

1) identify novel volatile apocarotenoids produced *in planta* in *Arabidopsis,* and
2) profile volatile apocarotenoids to help determine if they are produced by CCD or non-enzymatic activity.

4.2 Results

4.2.1 Confirmation of *ccd1, ccd4, ccd7* and *ccd8* mutants and generation of *ccd* double mutants

The *ccd* loss-of-function single mutant alleles used were as follows: *ccd1-1,* SALK097984C (*ccd4*), *max3-11* (*ccd7*) and *max4-1* (*ccd8*). The *ccd1-1* T-DNA insertion is within the sixth intron of *CCD1,* the *ccd4* insertion is within the one-and-only exon of the *CCD4* gene, the *max3-11* insertion lies in a region around exons 5 and 6 of *CCD7* and the *max4-1* insertion is in the first intron of *CCD8* (Table 4.1; (Alonso *et al.* 2003, Auldridge, *et al.* 2006)). The T-DNA insertions were confirmed using primers spanning the expected insertion sites (Supplementary Figure 4.1) *ccd1-1*, *ccd4* and *ccd7* insertions were also confirmed using border primer assays (Supplementary Figure 4.1)

ccd1, ccd4 and *ccd7* lines were crossed with one another (reciprocal crosses e.g. *ccd1* pollen crossed to *ccd4* carpels and *vice versa*, were performed), and F1 populations generated. The subsequent F2 populations were genotyped (using both spanning primer and border primer assays) for the desired *ccd* double mutants. The *ccd1;4* F2 population yielded three putative *ccd1;4* double mutants from 64 individuals from the *ccd1;4* F2

population. The corresponding numbers from the *ccd1;7* and *ccd4;7* F2 populations were 3 and 5 double mutants out of 64 screened individuals respectively. Examples of the screening results are depicted in Figure 4.1. These ratios were very close to the expected ratio of 1:16 (from which 4 double mutants would be expected per population).

4.2.2 Volatile apocarotenoid profiles consistent with Chapter Two results

Using *ccd* single and double mutants, comparisons of volatile apocarotenoid profile were made. Leaves and inflorescences were examined. Essentially the same apocarotenoid compounds observed in Chapter Two were observed in these experiments; this was expected given the same sampling and growth conditions were employed (Chapter Eight).

In this chapter however, chromatogram deconvolution (CD) was implemented to augment manual GC/MS peak identification. Raw MS total ion chromatograms (TICs) were algorithmically refined, removing baseline interferences and separating out partially co-eluting GC/MS peaks, allowing greater power to identify known or putative apocarotenoid compounds that may have been previously obscured. As a result of CD, seven new peaks were identified as putative leaf apocarotenoids on the basis of their proposed structures: dihydro-6MHO, 2,6,6-trimethylcyclohexanone, isophorol (3,5,5-trimethyl-2-cyclohexen-1-ol), menthalactone (5,6,7,7a-tetrahydro-3,6-dimethyl-2(4H)-benzofuranone), *cis*-β-ionone, 3a,4,5,6-tetrahydro-3a,6,6-trimethyl-2(3H)-benzofuranone (abbreviated to 2(3H)-B herein), and 3,7,11-trimethyl-1-dodecanol. These compounds were identified by matching deconvoluted MS spectra and observed RI values to the NIST library (Figure 4.2 and Table A.1). For dihydro-6MHO and 2,6,6-trimethylcyclohexanone, compelling literature exists suggesting a connection to the apocarotenoid pathway. Dihydro-6MHO was previously reported by Tikunov *et al* (2005) in tomato fruit. In that previous study (and here), its abundance was closely correlated with 6MHO, suggesting it may be produced *via* desaturation of 6MHO. On many previous occasions, positive correlations of secondary metabolites within the same pathway have been reported (Rizhsky *et al.* 2016, Schenkel *et al.* 2015, Tikunov, *et al.* 2005). 2,6,6-trimethylcyclohexanone was also previously reported in fresh water samples containing cyanobacteria from the *Microsystis* genus, and was proposed to be carotenoid derived; the ring structure tends to support this claim; (Arii *et al.* 2015). Similarly, isophorol's ring structure also suggests it is carotenoid derived, although this compound

has not been previously described in the apocarotenoid literature. In the case of the peak annotated as *cis*-β-ionone (RI 1337), the observed spectrum was much like that of *trans*-β-ionone (Figure 2, RI 1487), leading me to attribute this peak to the *cis* isomer of β-ionone. A synthesised standard of *cis*-β-ionone would help verify this finding, but only *trans*-β-ionone was commercially available.

Three additional leaf compounds were identified with structures suggesting they are apocarotenoid derived: menthalactone, 2(3H)-B, and 3,7,11-trimethyl-1-dodecanol. The two lactone compounds share a ring structure reminiscent of dihydroactinidiolide, suggesting they may also be derived from oxidation and cyclisation of apocarotenoids (Alder *et al.* 2012a, Ramel, *et al.* 2012b). Notably, menthalactone has been synthesised artificially from citronellal and citronellol, compounds plausibly derived from citral (Gao *et al.* 2009, Shishido *et al.* 1992), suggesting a biosynthetic pathway is also plausible. The latter-most compound is plausibly derived *via* 11,12-cleavage of lycopene followed by desaturation of the alkene and aldehyde moieties.

These compounds were presumably undetected in the previous survey of leaf compounds given the presence of interferences from co-eluting peaks and MS background noise, masking analytes, in the case of the lower-abundance peaks (menthalactone, *cis*-β-ionone, 2(3H)-B, 3,7,11-trimethyl-1-dodecanol), or distorting analyte spectra to such an extent they could not be manually matched to their NIST library entries (dihydro-6MHO, 2,6,6-trimethyl-cyclohexanone, isophorol).

For inflorescence volatiles, three compounds identified in *Arabidopsis* Col-0 anthesis inflorescence samples from Chapter Two (*cis*-citrol acetate, hexahydropseudoionone and 7,8-dihydro-β-ionone) were not observed in this analysis (Table 4.4 and Table 4.5). There may be unknown environmental factors that dictate the accumulation of these volatiles (e.g. an undetected fluctuation in growth chamber humidity or light quality/intensity). Alternatively, the emission of these volatiles may be tightly regulated according to flower developmental stage. Whilst care was taken to collect only those flower buds containing anthesis flowers - along with attached developing buds, sepals and adjoining cauline leaves - the specific age of the anthesis inflorescence samples was not determined; age differences may account for the change in observed volatiles. The change in accumulation of specific volatile apocarotenoids over the course of anthesis inflorescence development,

from opening to fertilisation and silique development, may be of interest for further study: volatiles such as the ones described here may change in abundance in response to ecological cues (Cáceres, et al. 2016, Wei, *et al.* 2011). Interestingly, quantities of other apocarotenoids remained consistent between batches (Table 4.4 and Table 4.5), suggesting different factors regulate their accumulation.

4.2.3 Leaf volatile apocarotenoid levels were largely unchanged across genotypes

The abundances of individual volatile apocarotenoids, in both leaves and flowers, were subsequently examined for differences across genotypes (Tables 4.2-4.5). Total volatile apocarotenoids were also calculated and compared. Given the uncertainty surrounding the accumulation of *cis*-citrol acetate, and 7,8-dihydro-β-ionone, these compounds have been excluded from the measure of total inflorescence volatile apocarotenoids (Table 4.4 and Table 4.5).

Considering the leaf data, there were no significant differences in volatile apocarotenoid levels between genotypes, nor did total volatile apocarotenoid concentration differ significantly. The known volatile apocarotenoids β-cyclocitral, β-ionone and DHA were abundant, with concentrations of 40 ± 8, 24 ± 5 and 7 ± 1 ng/g respectively in Col-0 leaves. Putative volatile apocarotenoids 2,2,6-trimethylcyclohexanone and isophorol were also abundant (Col-0 leaf concentrations of 39 ± 5.5 and 16 ± 3.0 ng/g respectively).

4.2.4 Marked variation in inflorescence volatile apocarotenoid levels

More pronounced changes in levels of β-carotene-derived apocarotenoids were observed in inflorescence tissues. Levels of β-ionone were markedly reduced in *ccd1* relative to Col-0, from 79 ± 45 to 14 ± 3 ng/g, and other β-carotene-derived apocarotenoids (β-cyclocitral and DHA, and the putative β-homocitral and 5,6-epoxy-β-ionone) also exhibited a downward trend (Table 4.4). In the other single mutants, no significant change was observed (Table 4.4). Interestingly however, the other two *ccd* double mutants *ccd1;7* and *ccd4;7* exhibited *elevated* β-carotene-derived apocarotenoids (β-cyclocitral and β-ionone levels reached a high of 1521 and 622 ng/g in *ccd4;7* compared to 185 and 78 ng/g in Col-0; Table 4.5).

The correlation between β-carotene-derived volatile apocarotenoids in inflorescences was seen across all genotypes, with β-cyclocitral, β-homocitral, β-ionone and 5,6-epoxy-β-ionone levels exhibiting essentially identical fold-changes relative to Col-0 (Figure 4.3). DHA exhibited a similar trend to the other compounds, but changes relative to Col-0 were less pronounced (Figure 4.3).

Considering the other inflorescence volatile apocarotenoids, there appeared to be two main patterns of accumulation, one that mirrored the aforementioned β-carotene-derived apocarotenoids, being decreased in *ccd1*, and *ccd1;4*, elevated in *ccd1;7* and *ccd4;7*, and unchanged in other genotypes, and another, exhibited by hexahydrofarnesylacetone, in which accumulation was largely unchanged across the genotypes (Tables 4.2-4.5).

To better-visualise the genotype-dependent changes in volatile apocarotenoid abundance observed for *ccd1*, *ccd1;4*, *ccd1;7* and *ccd4;7* inflorescences, a Principal Component Analysis was performed upon Col-0 normalised, $\log_2$-tranformed, fold-change values for volatile apocarotenoid abundance (Figure 4.4). PCA is an exploratory statistical procedure that allows representation of a set of observations (e.g. apocarotenoids levels in plant tissue samples) on a set of orthogonal (uncorrelated) axes (principal components, PCs) in which the original variables (in this case, apocarotenoids abundances) that contribute most to between-sample variation are weighted the most-heavily. The PCs can then be used as axes, allowing the original samples to be plotted in a multi-dimensional (usually two or three-dimensional) space.

The five genotypes separated relatively clearly along the first principal component (PC1, Figure 4.4). *ccd1* was closely, negatively, correlated with PC1, whilst Col-0 clustered at the centre of PC1 axis due to the normalisation applied. *ccd1;4* was largely negatively-correlated with PC1 whilst *ccd1;7* and *ccd4;7* were positively correlated. No genotype dependent trend was observed along the PC2 axis.

Consistent with casual observations, the loadings for PC1, accounting for 82% of variation in the samples, were made up of positive values for all the apocarotenoids except hexahydrofarnesylacetone (Figure 4.4). PC2, accounting for 13% of the observed variation, was predominately made up of a negative correlation with hexahydrofarnesylacetone.

4.2.5 Carotenoid levels remain constant despite changes in volatile apocarotenoid abundance

High-performance liquid chromatography (HPLC) coupled to a diode array detector (DAD) was then used for the analyses of the precursor carotenoids (Table 4.6 and Table 4.7). The carotenoid profile of the *ccd* mutants was qualitatively consistent with previous reports for Col-0, with violaxanthin, neoxanthin, antheraxanthin, lutein and β-carotene all observed (Kim and DellaPenna 2006, Van Norman, *et al.* 2014). In Col-0 leaf tissues (Table 4.6), lutein was the most abundant leaf carotenoid (~190 μg/g fresh weight) followed by β-carotene (~140 μg/g), violaxanthin (~44 μg/g) and neoxanthin (~34 μg/g). Inflorescence carotenoid concentrations were similar. Small amounts (> 1 μg/g fresh weight) of phytoene were also observed in all samples. A representative HPLC-DAD chromatogram of Col-0 leaf tissue is presented in Supplementary Figure 4.2.

Notably, levels of all carotenoids, in both leaves and inflorescences, remained constant across all genotypes (Table 4.6 and Table 4.7). This in turn yielded ratios of volatile apocarotenoid to carotenoid abundance (expressed as volatile apocarotenoid ng/g: carotenoid μg/g) that remained constant in leaves (0.427 ± 0.027 across all genotypes; Table 4.6), but which varied dramatically in inflorescences (Table 4.7). Whilst Col-0 inflorescence ratio was 0.88, the ratio in *ccd1* was markedly low, at 0.27. *ccd1;4* inflorescences also exhibited a lower ratio (0.49), whilst *ccd1;7* and *ccd4;7* had dramatically higher ratios of 1.873 and 5.05 respectively.

4.2.6 Loss of CCD function does not influence expression of other *CCD* genes

Next, *CCD* expression levels were assayed *via* real-time quantitative PCR (qPCR), across both tissues and all genotypes. qPCR results were largely as expected from the T-DNA insertions in *ccd* mutants (Figure 4.5 and Figure 4.6). *CCD1* and *CCD4* expression levels were reduced to >10% of Col-0 in all *ccd1* and *ccd4* backgrounds respectively. *CCD7* and *CCD8* expression results were more equivocal: *CCD7* expression was significantly reduced in *ccd7* and *ccd1;7* inflorescences, and *ccd4;7* leaves (~10-40% of Col-0 levels), but was not significantly reduced in other backgrounds (Figure 4.5 and Figure 4.6).

Similarly, *CCD8* expression was significantly reduced by 80% in *ccd8* inflorescence tissue, but had Col-0 levels in leaf tissue (Figure 4.5).

These discrepancies may be a result of T-DNA insertion read-through, which would lead to continued amplification of the target transcript despite knockout of the gene (due to the insertion disrupting subsequent translation of the mRNA). In this case, the *CCD7* and *CCD8* qPCR primers are downstream of, not flanking the T-DNA insertion sites, making read-through a plausible explanation. It is also possible the low expression of *CCD7* and *CCD8* in leaves results in higher variability of observed expression, leading to the absence of significantly decreased target-gene expression in *ccd7* and *ccd8* leaves.

4.2.7 Clustering analyses reveals biochemically linked compounds

To better-understand the volatile apocarotenoid data, two exploratory methods were employed, a correlation plot (visualised as a heat map; Figure 4.7) and hierarchical clustering analysis (HCA; Figure 4.8). Notably, only positive correlations were observed across leaf and inflorescence analyses (, a phenomenon that has been noted in previous metabolomics datasets (Sánchez, *et al.* 2012). From the leaf data, when data for all compounds was incorporated, a group of compounds clearly correlated. This group included the aforementioned β-carotene-derived compounds, further validating the casual observations made earlier (Figure 4.7 and Figure 4.8).

There were many instances where putative apocarotenoids annotations appeared to be validated by the clustering data (Figure 4.8). Putative apocarotenoids β-homocitral and 5,6-epoxy-β-ionone were closely correlated with β-cyclocitral, β-ionone and DHA, supporting the theory they are biochemically related (Chapter Two). Interestingly, isophorol also clustered with this group, suggesting it is an apocarotenoid derived from carotenoid non-enzymatic oxidation, similarly to β-cyclocitral to which it is most closely clustered in the HCA.

cis-β-ionone, in contrast, did not cluster with other β-carotene-derived apocarotenoids although it did cluster with a known apocarotenoid (*trans*-citral) and a ‘highly-likely’ putative apocarotenoid (dihydro-6MHO; Figure 4.8). This may suggest production of *cis*-β-ionone is regulated by a different rate-limiting step to other β-carotene-derived compounds (e.g. *via* prior 7,8-β-carotene isomerisation) similarly to the 9,10-

isomerisation step in the strigolactone pathway (Lin, *et al.* 2009). Alternatively, this compound may have been incorrectly identified as *cis*-β-ionone.

The two lactone compounds also clustered in unexpected ways, with 2(3H)-B clustering alongside the β-carotene cluster and *trans*-geranylacetone, whilst menthalactone clustered with 6MHO (Figure 4.8A). This latter correlation is interesting given 6MHO and citral, a plausible precursor of menthalactone (Gao, *et al.* 2009, Shishido, *et al.* 1992), share a precursor carotenoid, lycopene (Vogel, *et al.* 2008).

It is also noteworthy that three structurally similar compounds, hexahydropseudoionone, 3,7,11-trimethyl-1-dodecanol and hexahydrofarnesylacetone, clustered with one another, albeit not with other known apocarotenoids. This would suggest they are biochemically related, even if they are not apocarotenoids.

To gain greater confidence in these findings, the HCA was repeated with only those compounds which were particularly likely to be apocarotenoid-derived (Figure 4.8). β-cyclocitral, β-ionone, 5,6-epoxy-β-ionone and DHA remained clustered. Interestingly, with '*cis*-β-ionone' and menthalactone excluded, dihydro-6MHO clustered with 6MHO and *trans*-citral, recapitulating the observation of Tikunov *et al*. (2005) and providing further evidence dihydro-6MHO is an apocarotenoid, most-likely derived *via* 6MHO desaturation.

Similar results were obtained from correlation plot and HCA of inflorescence volatile apocarotenoid levels (Figure 4.9), with the aforementioned β-carotene-derived apocarotenoids correlating strongly with one another (Figure 4.9A) and clustering in the HCA (Figure 4.9B). Interestingly, hexahydrofarnesylacetone inflorescence abundance clustered with the known apocarotenoid *trans*-geranylacetone. The significance of this is debatable however, given the correlation between the compounds was not strong ($R^2 < 0.7$, Figure 4.9A).

4.2.8 Summary

Having developed a new *in planta* method for volatile apocarotenoid analysis, I proceeded to analyse the volatile apocarotenoid profile of *Arabidopsis* in three contexts, the first being wild-type (Col-0) leaves and inflorescences. These two tissue types were sampled given they both have high volatile apocarotenoid levels (Chapter Two);

perturbation in the enzymes contributing to apocarotenoid production might thus be expected to yield prominent changes. Moreover, inflorescences were chosen to complement studies in leaves given the differences in CCD expression (Supplementary Figure 4.3); CCD7 and CCD8 are, relatively speaking, highly expressed in inflorescences compared to leaves. To investigate the roles of CCDs in carotenoid and volatile apocarotenoid metabolism, the four *ccd* loss-of-function mutants were analysed alongside Col-0, as were the *ccd1;4, ccd1;7* and *ccd4;7* double mutants. The volatile apocarotenoid data were augmented with carotenoid measurements and *CCD* transcriptomic data, providing further insight.

Three observations from this chapter are particularly noteworthy:

1. There were significantly lower β-ionone concentrations in *ccd1* inflorescences relative to Col-0, suggesting a role for CCD1 in β-ionone synthesis. But, the unchanged β-ionone concentration across *ccd* mutant leaf tissue, and the elevated β-ionone concentrations in *ccd1;7* and *ccd4;7* inflorescences indicated CCD1 is not exclusively responsible for β-ionone synthesis.
2. No other genotype-dependent decreases in volatile apocarotenoid concentrations were observed, suggesting other CCDs have no major role in volatile apocarotenoid production under the conditions tested.
3. There was a dramatic increase in volatile apocarotenoid concentration in *ccd1;7* and *ccd4;7*, which may be related to increased oxidative stress and increased non-enzymatic production of volatile apocarotenoids.

4.3 Figures and Tables

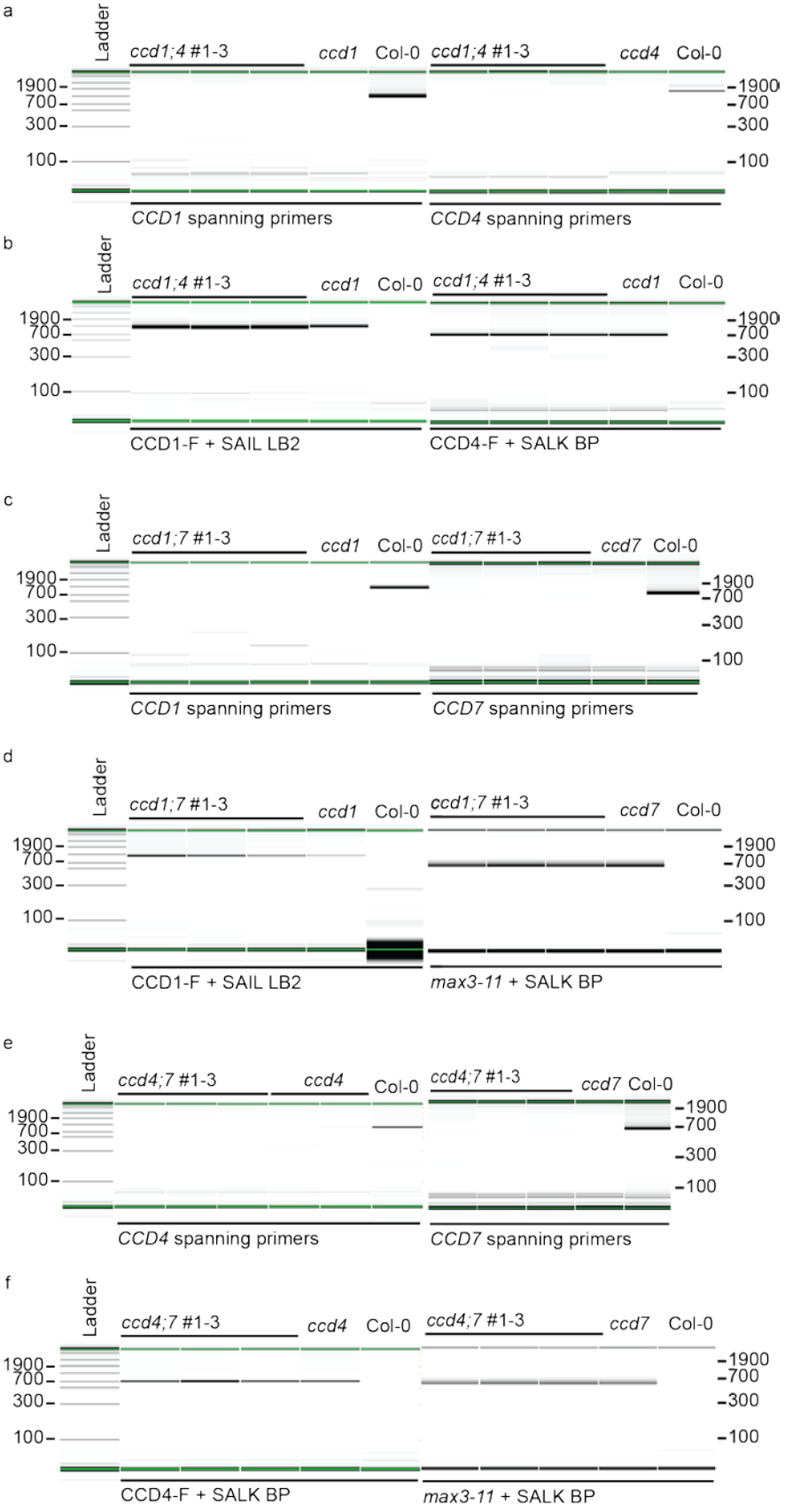
a
Ladder
ccd1;4 #1-3
ccd1
Col-0
ccd1;4 #1-3
ccd4
Col-0
1900
700
300
100
CCD1 spanning primers
CCD4 spanning primers
b
Ladder
ccd1;4 #1-3
ccd1
Col-0
ccd1;4 #1-3
ccd1
Col-0
CCD1-F + SAIL LB2
CCD4-F + SALK BP
c
Ladder
ccd1;7 #1-3
ccd1
Col-0
ccd1;7 #1-3
ccd7
Col-0
CCD1 spanning primers
CCD7 spanning primers
d
Ladder
ccd1;7 #1-3
ccd1
Col-0
ccd1;7 #1-3
ccd7
Col-0
CCD1-F + SAIL LB2
max3-11 + SALK BP
e
Ladder
ccd4;7 #1-3
ccd4
Col-0
ccd4;7 #1-3
ccd7
Col-0
CCD4 spanning primers
CCD7 spanning primers
f
Ladder
ccd4;7 #1-3
ccd4
Col-0
ccd4;7 #1-3
ccd7
Col-0
CCD4-F + SALK BP
max3-11 + SALK BP

Figure 4.1: Confirmation of T-DNA mutations in the *ccd1;4, ccd1;7* and *ccd4;7* double mutant lines

Following isolation of putative *ccd1;4*, *ccd1;7*, and *ccd4;7* double mutants from the relevant F2 populations, the disruption of *CCD1*, *CCD4* and/or *CCD7 via* T-DNA insertions was verified by PCR. DNA extracts from the putative double mutant lines (three representative, independent, lines per genotype are depicted here) were assayed using primers that span the expected insertion sites for the *CCD1* (a and c), *CCD4* (a and e) and *CCD7* (c and e) genes. T-DNA insertions were further validated using a primer set comprised of a T-DNA border primer and a primer annealing to a portion of the endogenous gene, for *CCD1* (b and d), *CCD4* (b and f), and *CCD7* (d and f). For each assay, the relevant single *ccd* loss-of-function mutant and Col-0 (wild type) controls were also included. Capillary electrophoresis results are depicted in the above figure as digital gel images. Ladder fragment sizes are (bottom to top): 100, 300, 500, 700, 1100, 1900, 2900, 4900 and 7000.

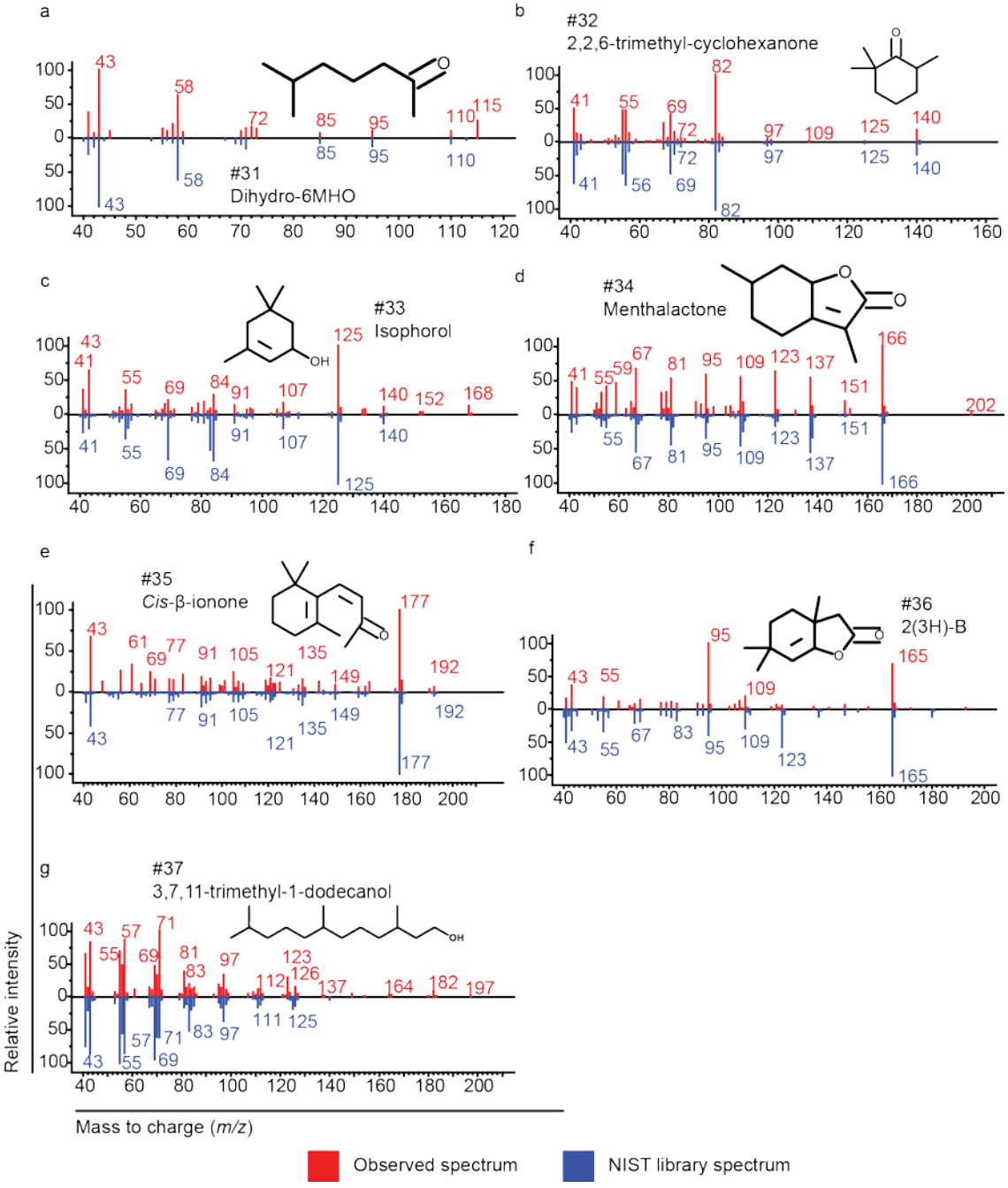

Figure 4.2: Novel, putative, apocarotenoids identified in *Arabidopsis* tissue from analyses in this chapter

The above compounds (details provided in the Appendix), numbered 31-37, were tentatively identified following chromatogram deconvolution. Compound 35, putatively *cis*-β-ionone, spectrum was compared to the NIST library spectrum for *trans*-β-ionone.

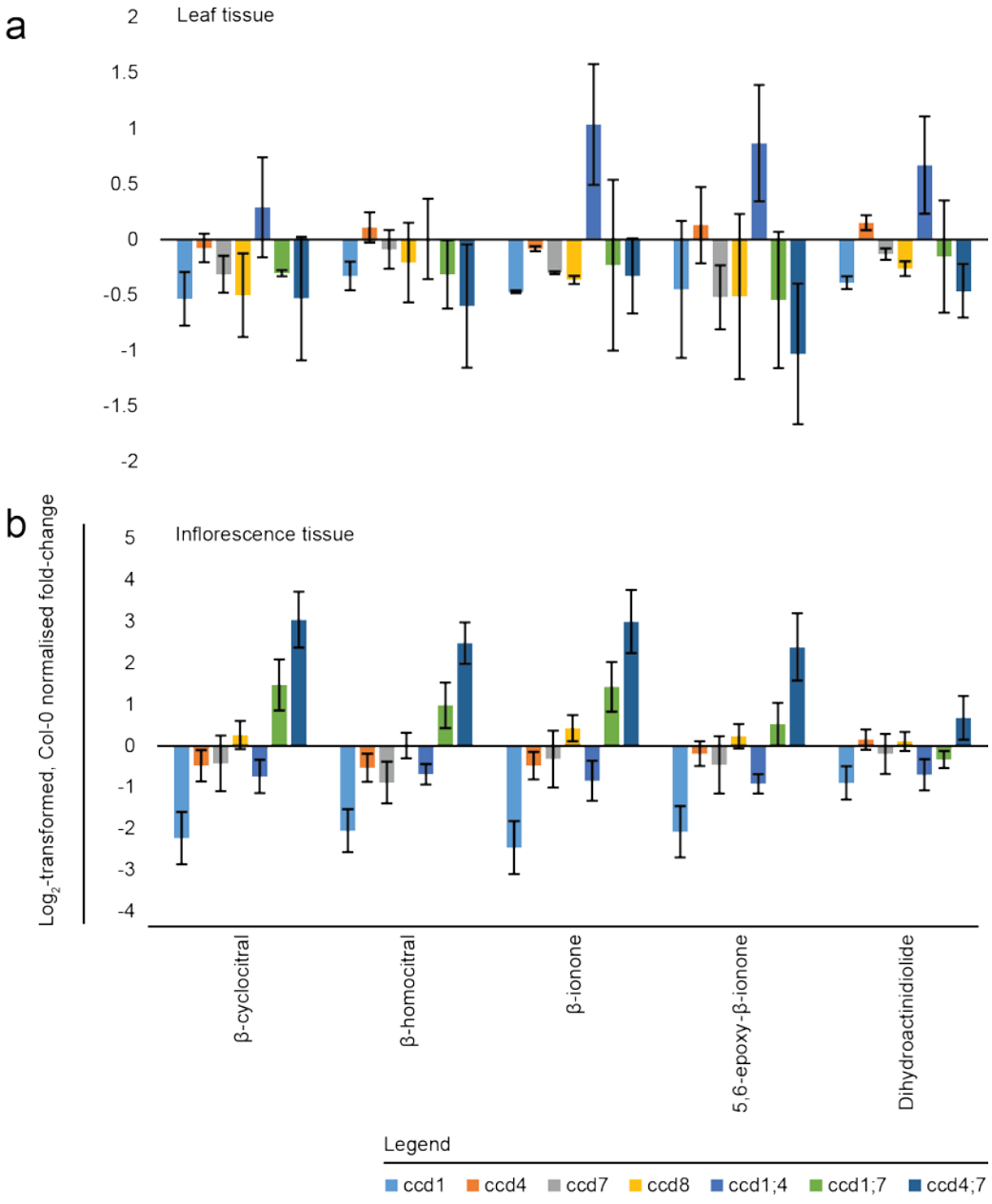

Figure 4.3: Change in β-carotene-derived volatile apocarotenoid abundance across *ccd* mutants

Col-0 normalised, log_2-transformed compound abundances for five β-carotene-derived apocarotenoids over the seven *ccd7* mutant genotypes have been plotted for both leaves (a) and inflorescences (b). Values are ± standard error, n = 4 for all genotypes.

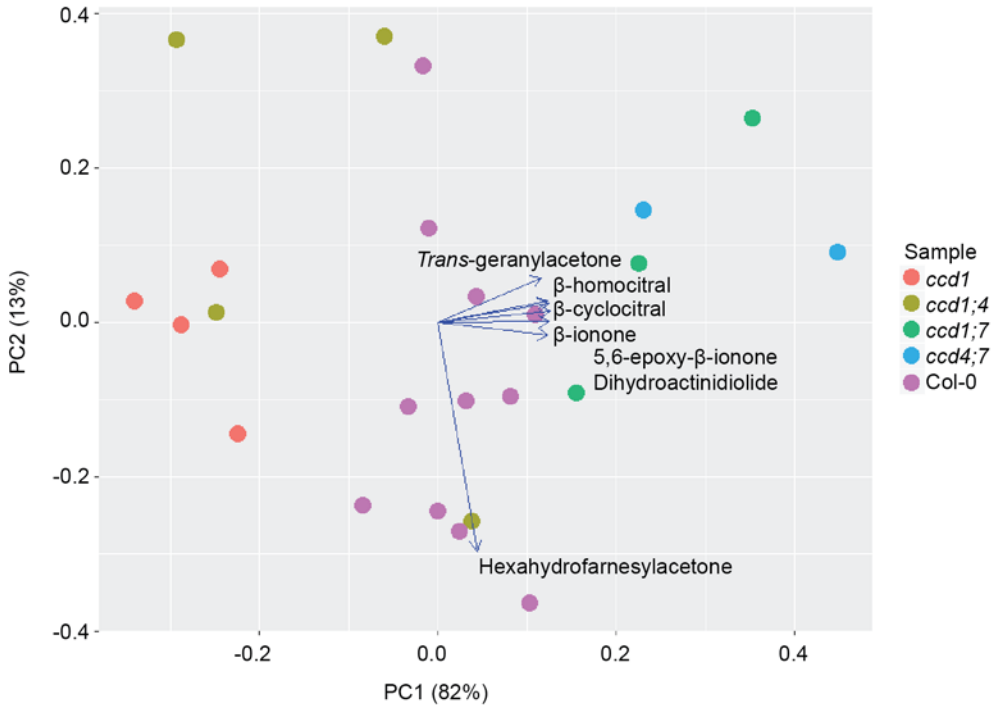

Figure 4.4: Principal component analysis of *ccd1, ccd1;4, ccd1;7, ccd4;7* and Col-0 inflorescence volatile apocarotenoid levels

Log_2-transformed metabolite abundances (expressed as fold-changes relative to the mean Col-0 values) from the aforementioned genotypes were incorporated into a PCA analysis. A loadings plot was included to depict the contributions of metabolite values to the first two principal components.

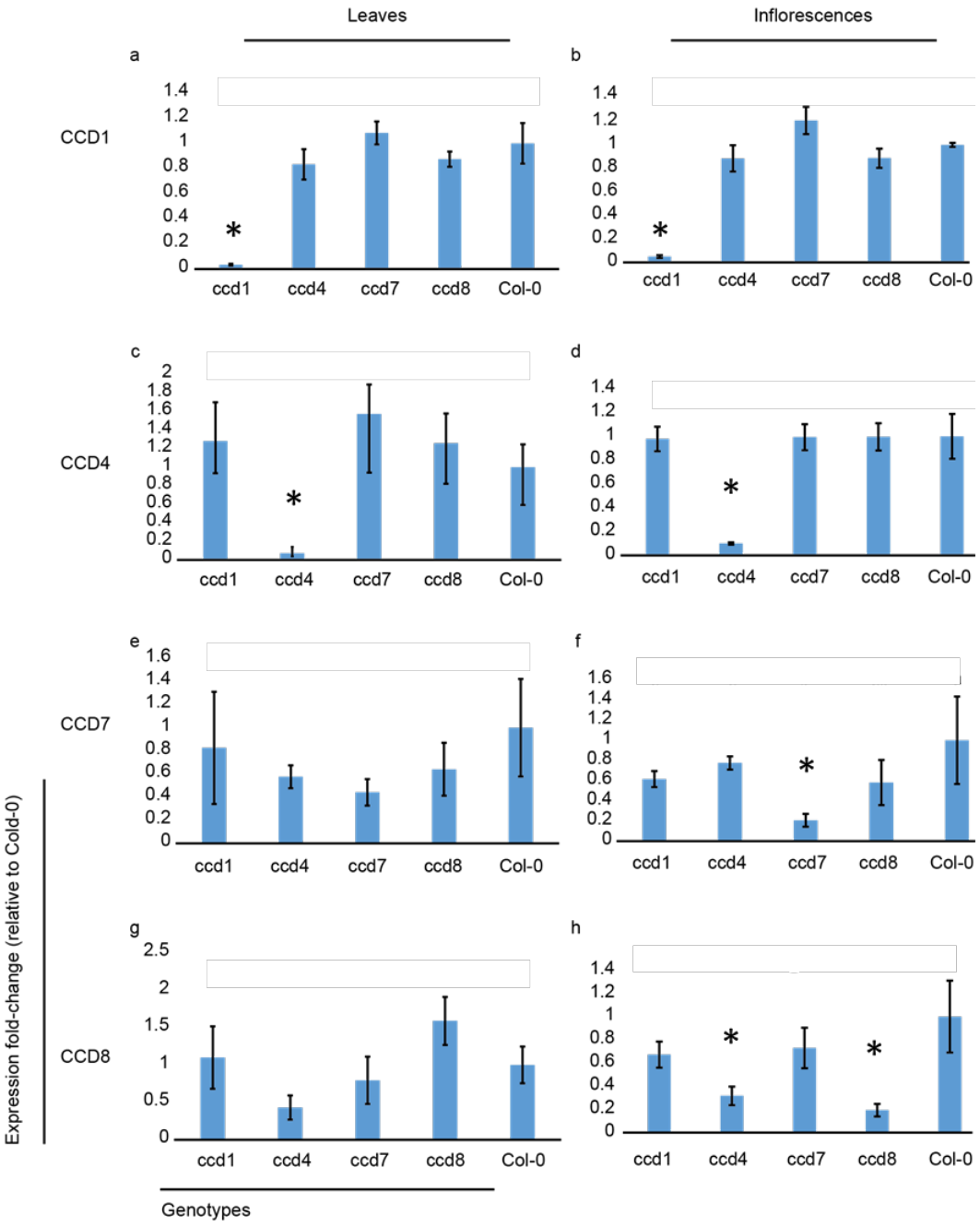

Figure 4.5: Expression of *CCD* genes in *ccd* single mutants versus Col-0

Leaf (a, c, e, g) and flower (b, d, f, h) tissue from *ccd1*, *ccd4*, *ccd7*, *ccd8* and Col-0 (wild-type) were analysed for expression of *CCD1* (a, b), *CCD4* (c, d), *CCD7* (e, f) and *CCD8* (g, h). Values are expressed as fold-change relative to wild-type, with error bars representing standard error. Statistical significance was calculated *via* pairwise Student's t-test against Col-0 values. * = $p < 0.05$. n = 4 per genotype.

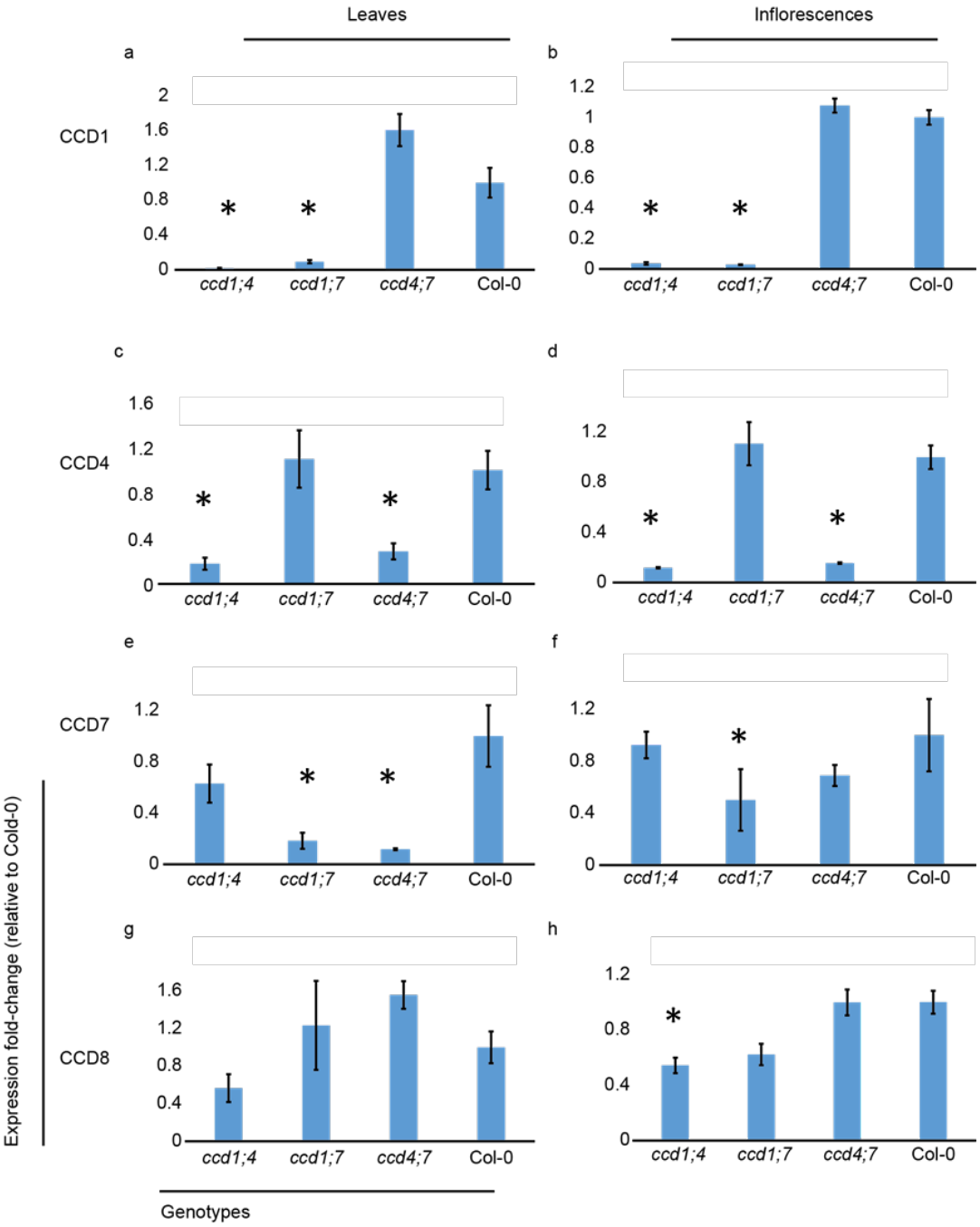

Figure 4.6: Expression of *CCD* genes in *ccd* double mutants versus Col-0

Leaves (a, c, e, g) and flowers (b, d, f, h) of *ccd1;4, ccd1;7, ccd4;7* and Col-0 were assayed for expression of *CCD1* (a, b), *CCD4* (c, d), *CCD7* (e, f) and *CCD8* (g, h). Values are expressed as fold-change relative to Col-0, with error bars representing standard error. Statistical significance was calculated *via* pairwise Student's t-test against Col-0 values. * = $p < 0.05$ level. n = 4 per genotype.

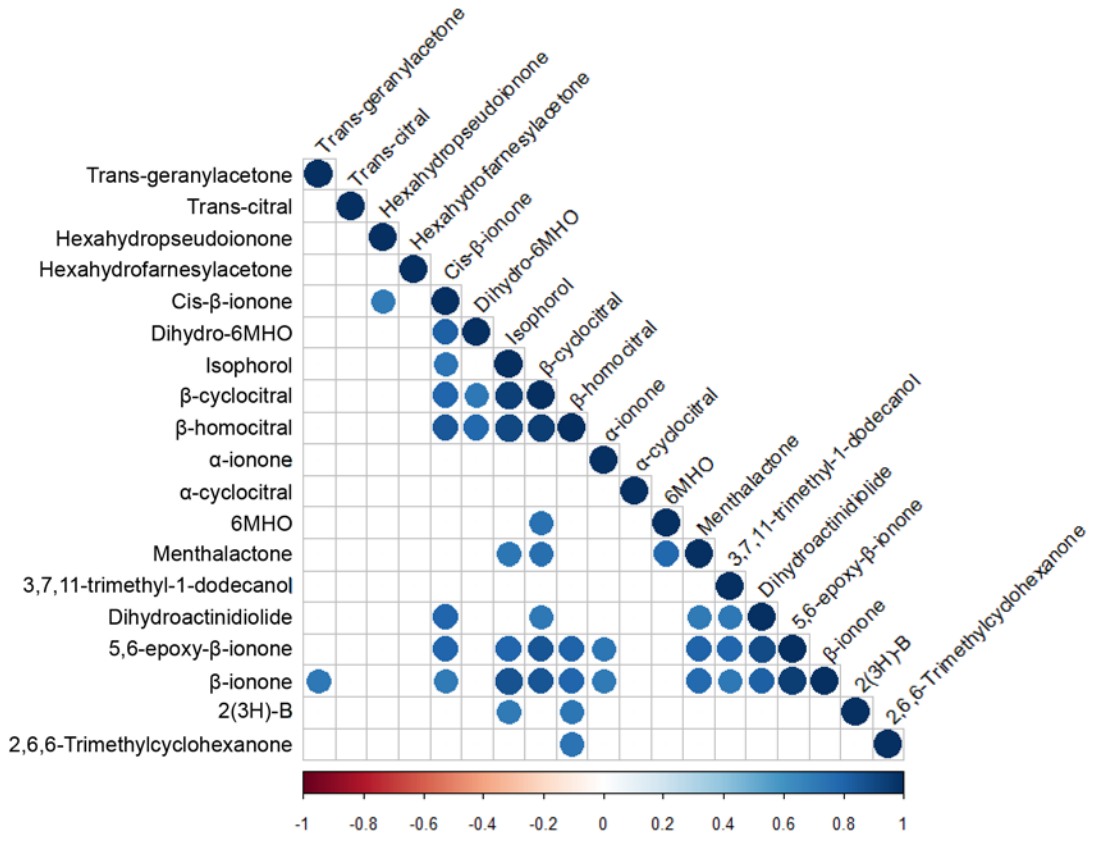

Figure 4.7: Abundance correlation heat-map of known and putative leaf volatile apocarotenoids

The correlation heat-map has a red-blue colour-intensity scale (from Pearson's Correlation Co-efficient R^2 = -1 to +1). The heat-map has been filtered to only depict correlations that have absolute R^2 > 0.7 and that are significant at the p < 0.05 level.

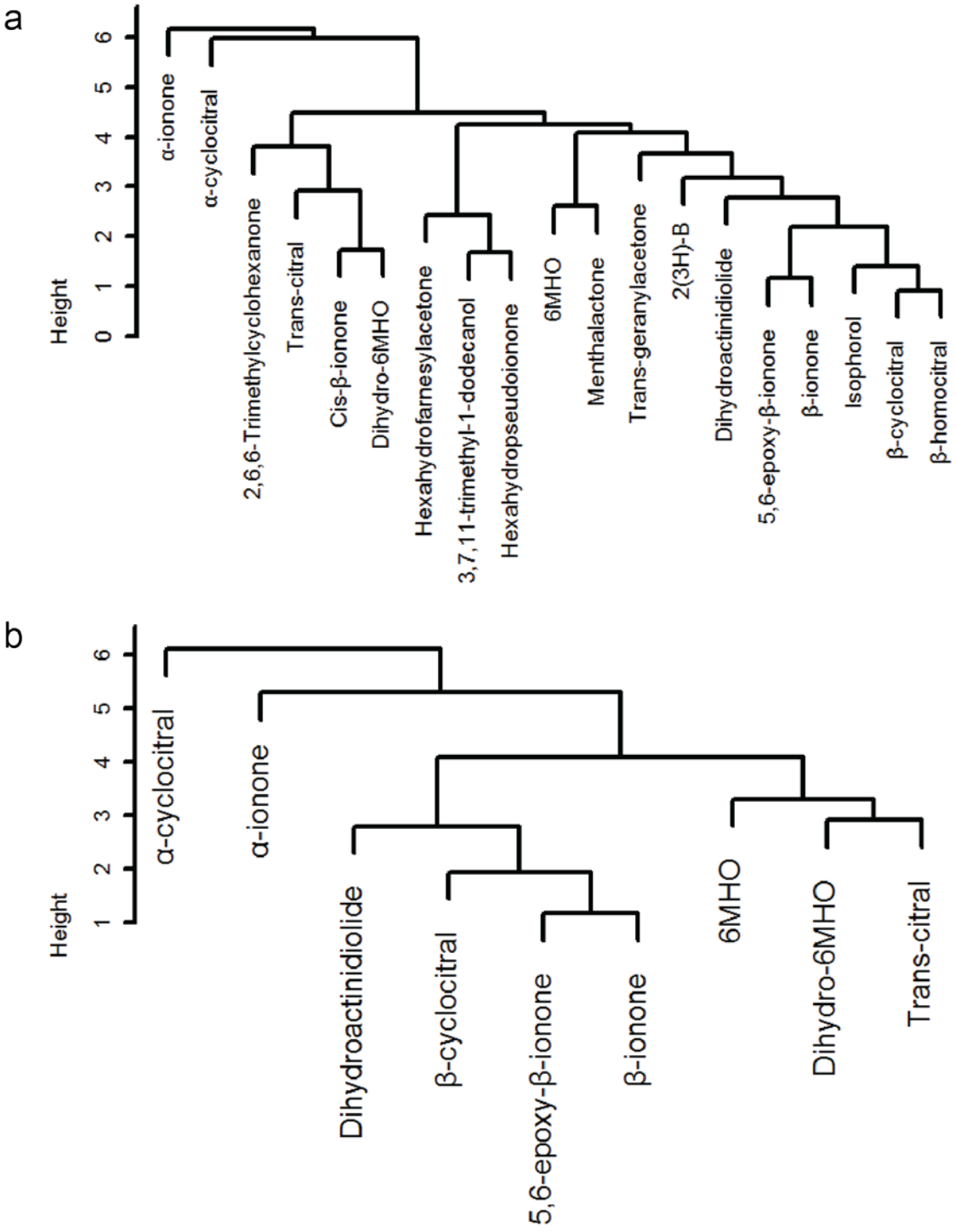

Figure 4.8: Hierarchical clustering analysis of leaf volatile apocarotenoid abundance across Col-0 and *ccd* mutants

HCAs were performed on log_2-transformed metabolite abundances (expressed as fold-changes relative to the mean Col-0 values) for a) all observed compounds and b) only known apocarotenoids and those 'highly likely' to be apocarotenoids.

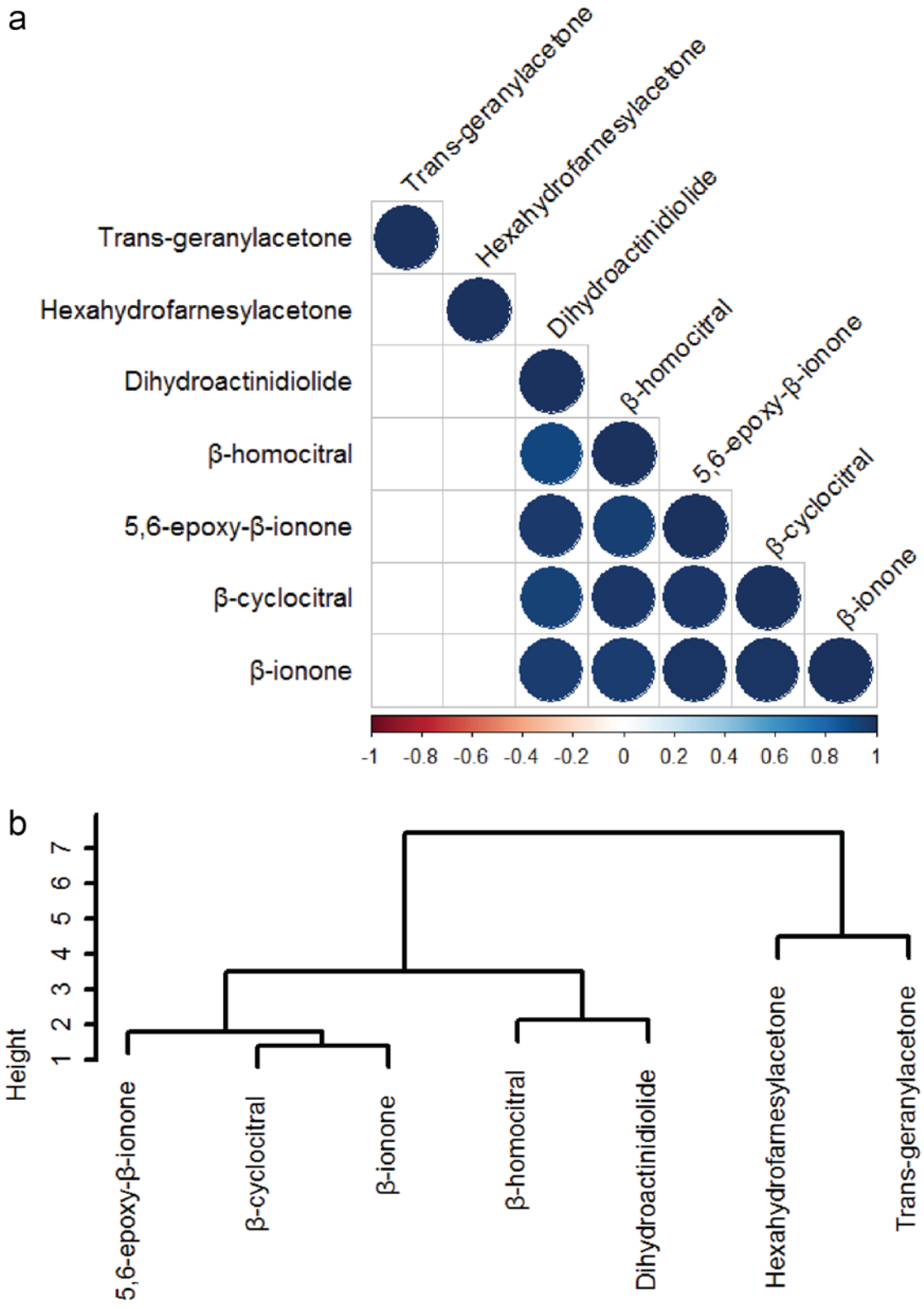
a
Trans-geranylacetone
Hexahydrofarnesylacetone
Dihydroactinidiolide
β-homocitral
5,6-epoxy-β-ionone
β-cyclocitral
β-ionone
-1 -0.8 -0.6 -0.4 -0.2 0 0.2 0.4 0.6 0.8 1
b
Height
1 2 3 4 5 6 7
5,6-epoxy-β-ionone
β-cyclocitral
β-ionone
β-homocitral
Dihydroactinidiolide
Hexahydrofarnesylacetone
Trans-geranylacetone

Figure 4.9: Correlation heat-map and hierarchical clustering analysis of inflorescence volatile apocarotenoid abundances across Col-0 and *ccd* mutants

The correlation heat-map (a) has a red-blue colour-intensity scale (from Pearson's Correlation Co-efficient R^2 = -1 to +1), and has been filtered to only depict correlations that have absolute $R^2 > 0.7$ and that are significant at the $p < 0.05$ level. HCA (b) was performed on log_2-transformed metabolite abundances (expressed as fold-changes relative to the mean Col-0 values) for inflorescence volatile apocarotenoids.

Table 4.1: Summary of the loss-of-function *ccd* alleles and screening strategies for this study

CCD enzyme	Mutant Allele	Genetic basis	Screening strategy	Reference
CCD1	ccd1-1	SAIL T-DNA insertion, intron 6	Spanning primers	Auldridge, 2006
CCD4	ccd4	SALK T-DNA insertion, exon 1 (and only)	Spanning primers	Gonzalez-Jorge, 2013
CCD7	Max3-11	SALK T-DNA insertion, between exon 5 and exon 6	Spanning primers	Auldridge 2006
CCD8	Max4-1	SLAT T-DNA insertion, intron 1	Spanning primers	Auldridge, 2006

Table 4.2: Volatile apocarotenoids observed in leaves from *Arabidopsis* Col-0 and *ccd* single mutants

		Volatile apocarotenoid concentration (ng/g FW)				
#	Compound	Col	ccd1	ccd4	ccd7	ccd8
31	Dihydro-6MHO	6.6 ± 1.44	5.913 ± 0.64	8.605 ± 1.01	6.528 ± 0.78	5.208 ± 1.24
1	6MHO	14 ± 2.98	8.851 ± 1.72	14.206 ± 2.78	9.303 ± 1.83	6.52 ± 1.5
32	2,2,6-trimethylcyclohexanone	38.9 ± 7.78	31.491 ± 2.66	39.251 ± 3.79	29.342 ± 3.15	26.456 ± 4.61
3	α-cyclocitral	8.23 ± 2.36	7.805 ± 0.46	10.124 ± 1.43	6.311 ± 0.4	6.095 ± 1.35
33	Isophorol	16.98 ± 2.53	13.578 ± 2.34	16.822 ± 0.6	16.435 ± 1.54	12.973 ± 3.49
5	β-cyclocitral	42.13 ± 7.47	29.082 ± 5.3	39.959 ± 3.71	33.905 ± 4.1	29.747 ± 8.87
9	β-homocitral	2.8 ± 0.46	t (2.231 ± 0.21)	3.019 ± 0.3	2.631 ± 0.34	t (2.426 ± 0.68)
10	Trans-citral	4.125 ± 0.51	3.382 ± 0.35	3.795 ± 0.16	4.315 ± 0.62	3.058 ± 0.77
34	Menthalactone ǂ	t (0.008 ± 0)	t (0.004 ± 0)	t (0.007 ± 0)	t (0.004 ± 0)	t (0.003 ± 0)
35	Cis-β-ionone	0.8 ± 0.13	0.711 ± 0.04	0.907 ± 0.07	0.804 ± 0.07	0.748 ± 0.15
12	Hexahydropseudoionone	0.467 ± 0.08	0.446 ± 0.03	0.512 ± 0.06	0.439 ± 0.05	0.449 ± 0.09
14	α-ionone	2.737 ± 0.3	2.57 ± 0.56	3.268 ± 0.85	1.681 ± 0.33	2.454 ± 0.78
36	2(3H)-B	t (0.076 ± 0.2)	t (0.056 ± 0.1)	t (0.072 ± 0.31)	t (0.078 ± 0.11)	t (0.08 ± 0.8)
17	Trans-geranylacetone	0.126 ± 2.06	0.089 ± 1.05	0.167 ± 1.2	0.116 ± 0.84	0.27 ± 2.78
19	β-ionone	25.02 ± 0.58	18.035 ± 0.16	23.605 ± 0.39	20.338 ± 0.18	19.442 ± 0.5
20	5,6-epoxy-β-ionone	2.532 ± 1.78	1.855 ± 0.99	2.771 ± 0.74	1.765 ± 0.39	1.773 ± 1.2
23	Dihydroactinidiolide	6.6 ± 0.37	5.041 ± 0.21	7.33 ± 0.35	6.027 ± 0.22	5.504 ± 0.26
37	3,7,11-trimethyl-1-dodecanol	4.06 ± 4.17	4.693 ± 2.56	4.588 ± 3.86	3.823 ± 2.34	3.889 ± 1.53
25	Hexahydrofarnesylacetone	9.78 ± 0	10.091 ± 0	9.535 ± 0	6.878 ± 0	9.546 ± 0
	Total Apocarotenoids	186 ± 35	146 ± 19	189 ± 22	151 ± 17	137 ± 31

t = trace compound detected at concentration below the limit-of-quantification; ǂ = trace compound detected at concentration below limit-of-detection (estimated concentrations provided in parentheses)

n.d = not detected

Values are ± standard error; n = 4 per genotype

Table 4.3: Volatile apocarotenoids observed in leaves from *Arabidopsis* Col-0 and *ccd1;4, ccd1;7* and *ccd4;7*

		Volatile apocarotenoid concentration (ng/g FW)			
#	Compound	Col-0	ccd1;4	ccd1;7	ccd4;7
31	Dihydro-6MHO	6.459 ± 1.52	5.487 ± 0.507	5.704 ± 1.37	4.262 ± 0.94
1	6MHO	14.003 ± 2.5	14.018 ± 2.75	14.924 ± 1.58	14.245 ± 2.93
32	2,2,6-trimethylcyclohexanone	39.234 ± 5.46	26.462 ± 6.942	40.588 ± 8.21	31.816 ± 3.52
3	α-cyclocitral	7.3 ± 2.25	10.064 ± 2.909	6.132 ± 1.2	4.338 ± 1.03
33	Isophorol	16.087 ± 2.95	22.213 ± 6.467	16.873 ± 4.15	15.688 ± 2.4
5	β-cyclocitral	40.171 ± 8.97	49.117 ± 18.049	32.552 ± 8.01	27.794 ± 5.31
9	β-homocitral	2.756 ± 0.36	2.769 ± 0.789	t (2.216 ± 0.54)	t (1.82 ± 0.33)
10	*Trans*-citral	4.251 ± 1.52	4.398 ± 0.7	4.072 ± 0.59	3.354 ± 0.22
34	Menthalactone ǂ	t (0.007 ± 0)	t (0.016 ± 0.008)	t (0.007 ± 0)	t (0.008 ± 0)
35	*Cis*-β-ionone	0.729 ± 0.11	0.861 ± 0.159	0.571 ± 0.06	0.476 ± 0.1
12	Hexahydropseudoionone	0.479 ± 0.08	0.497 ± 0.028	0.444 ± 0.05	0.338 ± 0.01
14	α-ionone	2.373 ± 0.76	2.035 ± 0.798	1.409 ± 0.4	1.074 ± 0.43
36	2(3H)-B	t (0.08 ± 0.01)	0.118 ± 0.04	t (0.077 ± 0.02)	t (0.084 ± 0)
17	*Trans*-geranylacetone	0.138 ± 0.02	0.198 ± 0.057	0.143 ± 0.03	0.164 ± 0.01
19	β-ionone	24.028 ± 4.59	49.257 ± 22.558	20.472 ± 4.16	19.128 ± 1.49
20	5,6-epoxy-β-ionone	2.56 ± 0.6	4.671 ± 2.047	1.756 ± 0.34	1.254 ± 0.08
23	Dihydroactinidiolide	6.94 ± 0.85	11.046 ± 3.927	6.241 ± 0.76	5.02 ± 0.31
37	3,7,11-trimethyl-1-dodecanol	4.164 ± 0.34	4.72 ± 0.321	4.257 ± 0.35	4.364 ± 0.08
25	Hexahydrofarnesylacetone	9.96 ± 0.74	11.015 ± 1.21	11.704 ± 1	13.629 ± 0.92
	Total Apocarotenoids	186 ± 35	219 ± 70	170 ± 33	149 ± 20

t = trace compound detected at concentration below the limit-of-quantification; ǂ = trace compound detected at concentration below limit-of-detection (estimated concentrations provided in parentheses)

n.d = not detected

Values are ± standard error; n = 4 per genotype

Table 4.4: Volatile apocarotenoids observed in inflorescences from *Arabidopsis* Col-0 and *ccd* single mutants

		Volatile apocarotenoid concentration (ng/g FW)				
#	Compound	Col-0	ccd1	ccd4	ccd7	ccd8
5	β-cyclocitral	182.98 ± 110	38.885 ± 21.35	130.859 ± 39.42	136.132 ± 81.16	218.931 ± 58.45
9	β-homocitral	9.25 ± 5.96	t (2.226 ± 0.96)	6.392 ± 1.69	4.989 ± 2.08	9.281 ± 2.21
11	*Cis*-citrol acetate*	n.d	n.d	n.d	n.d	n.d
12	Hexahydropseudoionone	n.d	n.d	n.d	n.d	n.d
16	7,8-dihydro-β-ionone*	n.d	n.d	n.d	n.d	n.d
17	*Trans*-geranylacetone	1.043 ± 0.42	0.453 ± 0.07	0.668 ± 0.19	0.505 ± 0.13	0.594 ± 0.12
19	β-ionone	79.427 ± 45.35	14.398 ± 8.05	57.012 ± 14.7	63.54 ± 39.01	106.443 ± 26.05
20	5,6-epoxy-β-ionone	5.164 ± 2.75	1.222 ± 0.66	4.519 ± 1.04	3.753 ± 2.32	6.059 ± 1.38
23	Dihydroactinidiolide	20.667 ± 7.65	11.099 ± 3.58	22.934 ± 4.27	18.038 ± 7.18	22.273 ± 3.89
38	Hexahydrofarnesylacetone	53.6 ± 6.25	52.267 ± 11.21	59.901 ± 11.51	57.545 ± 11.11	53.363 ± 8.71
	Total apocarotenoids	352 ± 178	121 ± 46	282 ± 73	285 ± 143	417 ± 101

t = trace compound detected at concentration below the limit-of-quantification; ǂ = trace compound detected at concentration below limit-of-detection (estimated concentrations provided in parentheses)

n.d = not detected

* = compound excluded from calculation of total volatile apocarotenoids

Values are ± standard error; n = 4 per genotype

Table 4.5: Volatile apocarotenoids observed in inflorescences from *Arabidopsis* Col-0 and *ccd1;4, ccd1;7* and *ccd4;7*

		Volatile apocarotenoid concentration (ng/g FW)			
#	Compound	Col	ccd1;4	ccd1;7	ccd4;7
5	β-cyclocitral	185 ± 25.68	110.486 ± 33.309	512.567 ± 275.47	1521.013 ± 903.5
9	β-homocitral	t (9.99 ± 1.048)	t (6.201 ± 1.937)	19.679 ± 9.21	55.73 ± 23.06
11	*Cis*-citrol acetate*	n.d	n.d	n.d	n.d
12	Hexahydropseudoionone	n.d	n.d	n.d	n.d
16	7,8-dihydro-β-ionone*	n.d	n.d	n.d	n.d
17	*Trans*-geranylacetone	1.055 ± 0.114	0.629 ± 0.162	1.571 ± 0.43	3.279 ± 1.84
19	β-ionone	78.01 ± 7.464	43.386 ± 17.146	209.596 ± 108.17	622.308 ± 430.86
20	5,6-epoxy-β-ionone	5.21 ± 0.661	2.759 ± 1.199	7.48 ± 3.23	27.112 ± 20.37
23	Dihydroactinidiolide	22.05 ± 2.162	13.539 ± 4.008	17.5 ± 2.72	35.248 ± 15.7
25	Hexahydrofarnesylacetone	56.91 ± 12.606	42.152 ± 10.249	32.741 ± 4.86	45.847 ± 11.62
	Total apocarotenoids	359 ± 156	219 ± 68	802 ± 404	2311 ± 1407

t = trace compound detected at concentration below the limit-of-quantification; ǂ = trace compound detected at concentration below limit-of-detection (estimated concentrations provided in parentheses)

n.d = not detected

* = compound excluded from calculation of total volatile apocarotenoids

Values are ± standard error; n = 4 per genotype

Table 4.6: Leaf carotenoid concentrations in Col-0 and *ccd* mutants

	Leaf carotenoid concentration (µg/g, fresh weight)							
Compound	Col-0	ccd1	ccd4	ccd7	ccd8	ccd1;4	ccd1;7	ccd4;7
Lutein	190 ± 2.01	197 ± 14.44	167 ± 16.22	216 ± 32.83	178 ± 9.77	185 ± 25.04	170 ± 46.57	176 ± 3.05
Antheraxanthin	13 ± 2.72	16 ± 4.41	14 ± 1.08	16 ± 8.02	16 ± 3.63	12 ± 2.14	10 ± 1.49	12 ± 0.75
Neoxanthin	34 ± 0.59	36 ± 2.92	31 ± 4.31	40 ± 6.66	34 ± 1.99	33 ± 5.47	29 ± 7.98	32 ± 0.5
Violaxanthin	44 ± 2.76	45 ± 6.13	38 ± 0.31	48 ± 6.22	41 ± 2.66	43 ± 7.08	38 ± 11.39	40 ± 0.22
β-carotene	138 ± 2.53	140 ± 12.33	125 ± 7.8	143 ± 16	129 ± 5.46	137 ± 14.95	123 ± 29.18	129 ± 3.22
Phytoene	0.165 ± 0.012	0.151 ± 0.026	0.13 ± 0.018	0.133 ± 0.006	0.1 ± 0.004	0.15 ± 0.025	0.134 ± 0.025	0.139 ± 0.006
Total Carotenoids	419 ± 10.63	435 ± 40.26	375 ± 29.74	463 ± 69.73	397 ± 23.51	409 ± 54.7	371 ± 96.63	388 ± 7.75
Total Volatile Apocarotenoids	186 ± 35	146 ± 19	188 ± 22	151 ± 17	136 ± 31	219 ± 70	170 ± 33	149 ± 20
Apocarotenoid/Carotenoid ratio (ng:µg, FW)	0.444 ± 0.011	0.336 ± 0.028	0.501 ± 0.037	0.326 ± 0.043	0.343 ± 0.019	0.535 ± 0.063	0.459 ± 0.095	0.384 ± 0.008

Values are ± standard error; n = 4 for all genotypes

Table 4.7: Inflorescence carotenoid concentrations in Col-0 and *ccd* mutants

	Inflorescence carotenoid concentration (µg/g, fresh weight)							
Compound	Col-0	ccd1	ccd4	ccd7	ccd8	ccd1;4	ccd1;7	ccd4;7
Lutein	192 ± 14.35	202 ± 4.47	200 ± 7.71	190 ± 2.53	185 ± 7.83	203 ± 6.19	196 ± 9.49	206 ± 3.87
Antheraxanthin	7.54 ± 0.68	5.56 ± 1.91	5.21 ± 1.04	6.27 ± 0.73	6.59 ± 0.81	9.28 ± 2.44	7 ± 0.68	6.6 ± 0.23
Violaxanthin	56 ± 4.57	57 ± 0.94	57 ± 4.03	58 ± 0.62	55 ± 2.5	62 ± 2.49	58 ± 2.2	62 ± 2.15
Neoxanthin	31 ± 2.06	31 ± 0.56	32 ± 1.45	31 ± 0.59	31 ± 1.22	32 ± 0.97	31 ± 1.48	33 ± 1.65
β-carotene	138 ± 9.44	149 ± 4.75	145 ± 6.25	138 ± 4.27	138 ± 8.56	145 ± 4.77	138 ± 4.41	151 ± 3.97
Phytoene	0.266 ± 0.014	0.339 ± 0.032	0.313 ± 0.04	0.281 ± 0.043	0.265 ± 0.039	0.33 ± 0.031	0.274 ± 0.024	0.332 ± 0.036
Total Carotenoids	425 ± 31.11	446 ± 12.67	440 ± 20.53	424 ± 8.79	416 ± 20.96	452 ± 16.9	430 ± 18.29	459 ± 11.91
Total Volatile Apocarotenoids	352 ± 178	121 ± 46	282 ± 73	285 ± 143	417 ± 101	219 ± 68	801 ± 404	2311 ± 1407
Apocarotenoid/Carotenoid ratio (ng:µg, FW)	0.828 ± 0.056	0.271 ± 0.008	0.641 ± 0.029	0.672 ± 0.014	1.002 ± 0.048	0.485 ± 0.017	1.862 ± 0.076	5.033 ± 0.127

Values are ± standard error; n = 4 for all genotypes

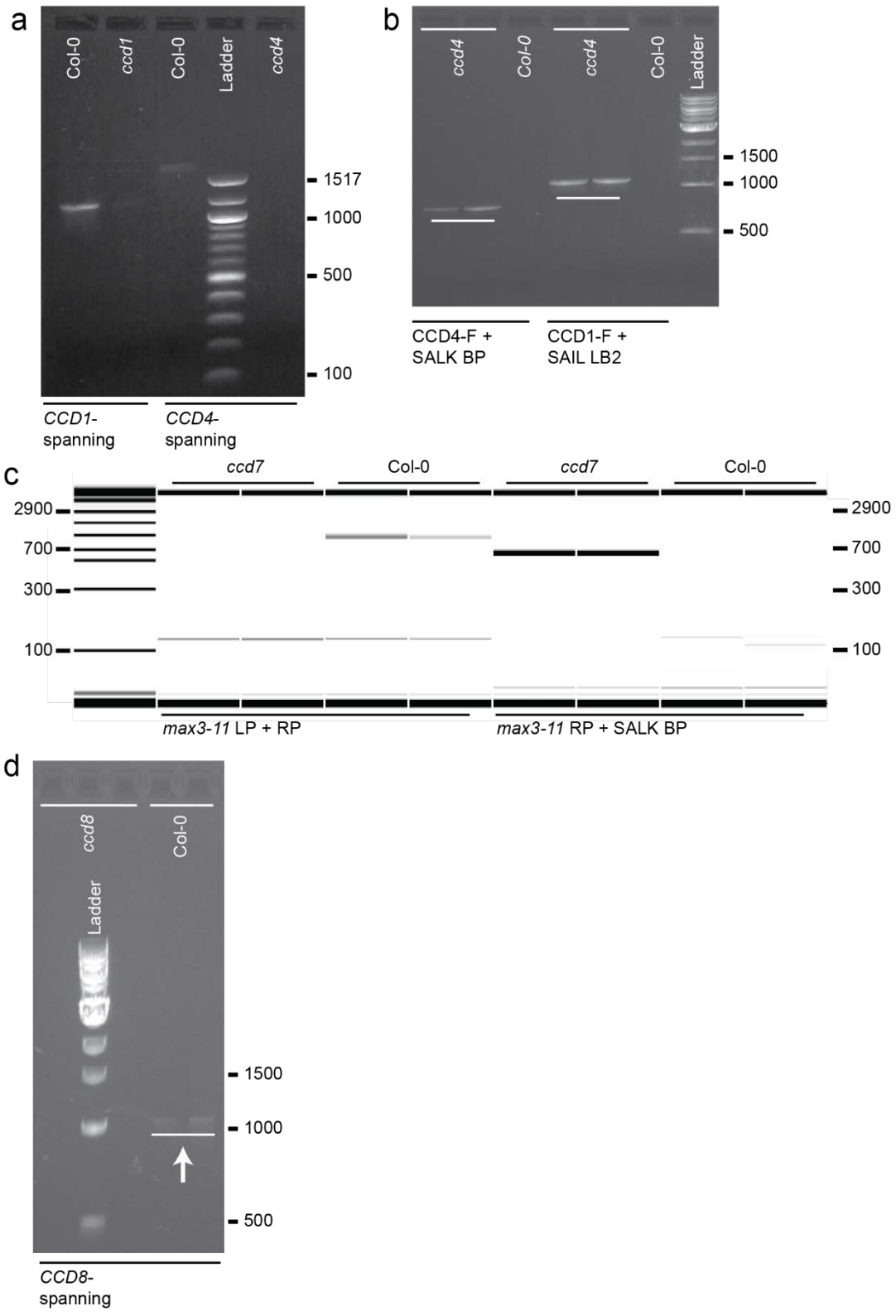

Supplementary Figure 4.1: Validation of PCR screening assays for *ccd1, ccd4, ccd7* and *ccd8* T-DNA insertions

The T-DNA insertions responsible for the *ccd1-1, ccd4* (SALK097984C), *ccd7* (*max3-11*) and *ccd8* (*max4-1*) were screened for using PCR assays with primers that span the insertion sites (a, c, d). The *ccd1, ccd4* and *ccd7* T-DNA insertions were further confirmed using assays combining the spanning primers with a T-DNA insertion border primer (SALK BP for *ccd4* and *ccd7*, and SAIL LB2 for *ccd1* insertions respectively; b, c). The above gel electrophoresis (a, b, d)

and capillary electrophoresis-derived digital gel images (c) were acquired upon electrophoresis of PCR products on a 1% agarose-TBE gel containing 0.5 µg/ml ethidium bromide at 130 V (210 mA) for 30 min (a, b, d) or on a LabChip GXII instrument as per the manufacturer's instructions (c). The 100 bp ladder (a) fragment sizes are (bottom to top): 100, 200, 300, 400, 500, 600, 700, 800, 900, 1000, 1100, 1200 and 1517. The 1 kb ladder (b, d) fragment sizes are (bottom to top): 500, 1000, 1500, 2000, 3000, 4000, 5000, 6000, 8000 and 10,000. Digital gel ladder sizes (c) are (bottom to top): 10, 300, 500, 700, 1100, 1900, 2900, 4900, 7000).

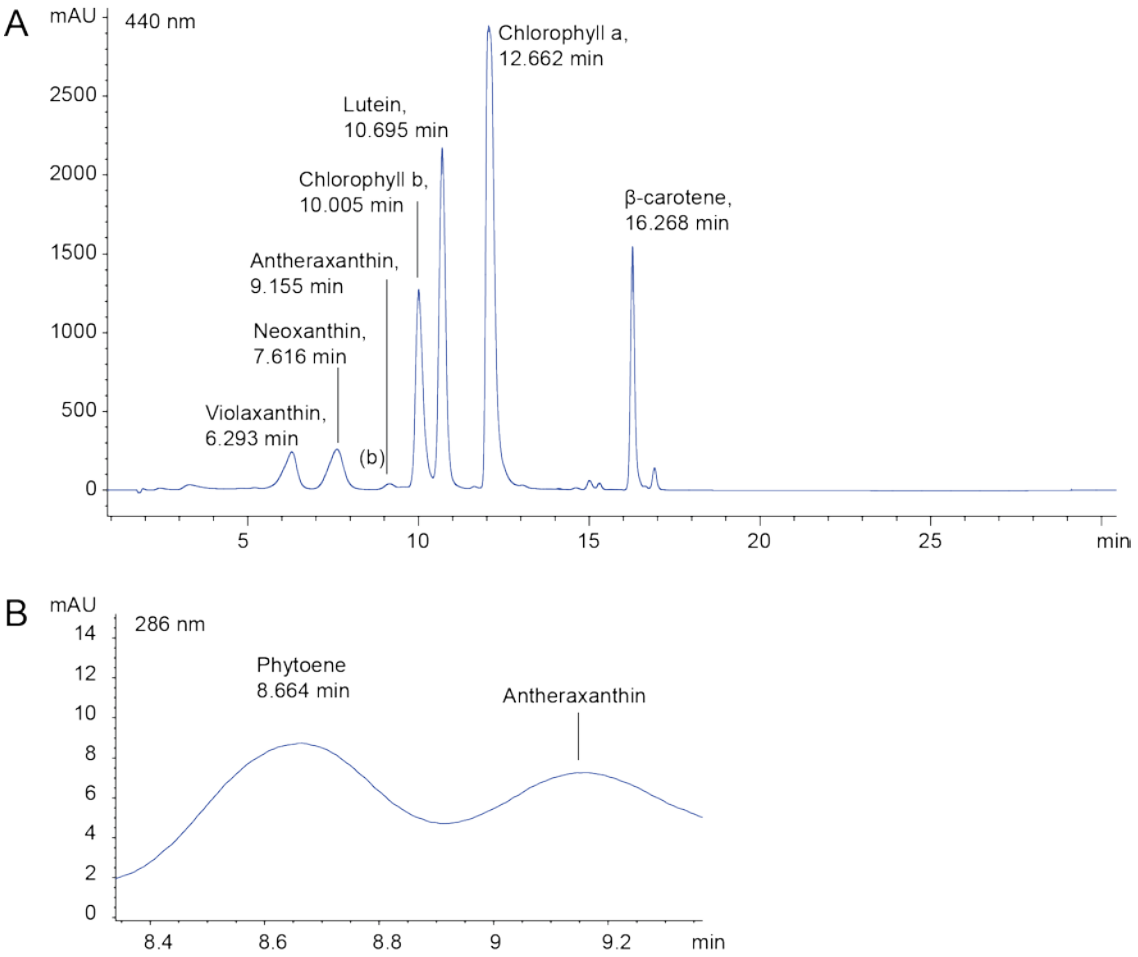

Supplementary Figure 4.2: Representative HPLC-DAD chromatogram depicting carotenoids and chlorophylls

A sample chromatogram from HPLC analysis of carotenoids and chlorophylls in Col-0 leaf tissue is presented here to depict the orders of elution for the HPLC analytes. In addition to the main chromatogram, recorded at 440 nm (a), a zoomed-in chromatogram (measured at 286 nm) is presented to show the lower-abundance phytoene peak (b). Typical UV-visible spectra obtained for the labelled analytes, and structures of the carotenoid analytes, are presented in Figure A.2

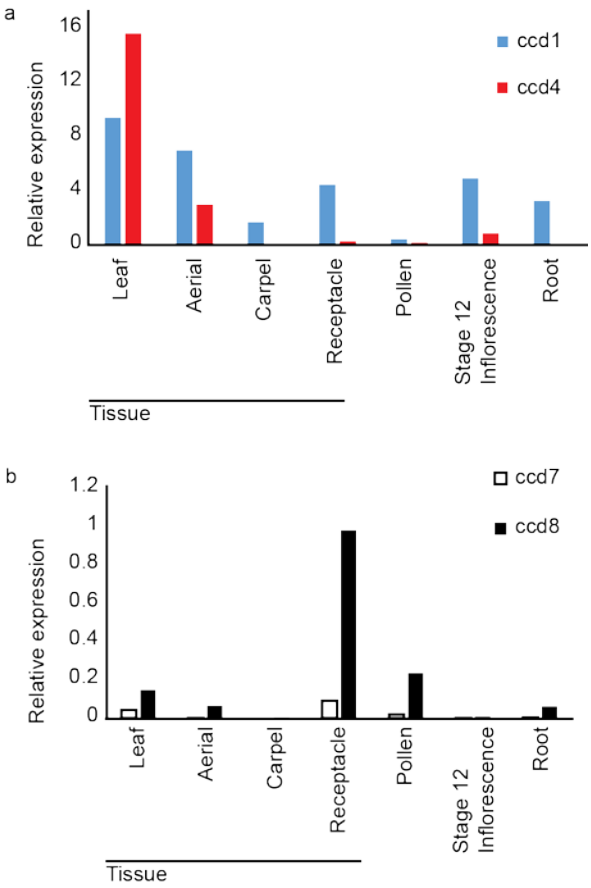

Supplementary Figure 4.3: Expression of *Arabidopsis CCD1, CCD4, CCD7* and *CCD8* in different tissues

RNA sequencing reads (obtained from Thalemine, https://www.araport.org/, (Krishnakumar *et al.* 2015)) for *CCD1* and *CCD4* (a) and *CCD7* and *CCD8* (b) from different *Arabidopsis* tissues were plotted, following normalisation of gene read numbers to *AtPP2A* (AT1G10430) read number.

Chapter Five: Insight into *cis*-carotenoid metabolism in the *Arabidopsis ccr2* mutant

5.1 Overview

The profiling of volatile apocarotenoids (Chapter Four) was extended to *ccd x ccr2* mutants, grown under 8 h photoperiod conditions (so as to induce accumulation of linear carotenes), in this chapter. The aims were as follows:

1. Provide further validation that specific (aforementioned) apocarotenoids are linear carotene-derived, and identify new linear carotene-derived apocarotenoids.
2. Identify if any CCDs are responsible for the production of these apocarotenoids, and also investigate whether specific CCDs are more/less active as a result of linear carotene accumulation.
3. Identify volatile apocarotenoids as being ACS2 candidates, searching for links between candidate apocarotenoid abundance and *ccr2* phenotype reversion in *ccd x ccr2* mutants. Concurrently, examine linear carotene-derived volatile apocarotenoids to identify candidate ACS1 structures.

5.2 Results

5.2.1 Generation of *ccd x ccr2* double mutants and initial phenotyping of *ccd x ccr2* mutants: no *ccr2* reversion observed

As described for the Col-0 background *ccd* mutants, the *ccd x ccr2* single mutants were confirmed *via* spanning and border primer assays (Chapter Four, Supplementary Figure 4.1). These mutants were then crossed, with the subsequent F2 populations screened for homozygous *ccd1;4, ccd1;7* and *ccd4;7* mutants (Supplementary Figure 5.1). Out of 64 *ccd1;4 x ccr2* F2 individuals, four homozygous mutants were identified. The corresponding statistics for *ccd1;7 x ccr2* and *ccd4;7 x ccr2* F2 populations were three and five (respectively) out of 64; the ratios are essentially consistent with the expected ratio of 1:16.

Subsequently, *ccr2* and the various *ccd x ccr2* mutants were grown under extended dark photoperiod (i.e. 8 h days), checking for any effect of CCD loss-of-function on the *ccr2* yellow-leaf phenotype. Consistent with previous observations, 8 h photoperiod *ccr2* plants exhibited yellowing in newly-emerged leaves, but Col-0 did not (Figure 5.1); this was noticeable in both rosette and cauline leaves (leaves from both the primary inflorescence and first internode were examined).

Contrary to expectations, all *ccd x ccr2* mutants exhibited a comparable leaf-yellowing phenotype (Figure 5.1). Nor did any of the *ccd x ccr2* mutants revert rosette or inflorescence lutein concentration to Col-0 levels, although *ccd1;4 x ccr2* rosette lutein concentration was significantly higher than that of *ccr2* (Figure 5.2A). The higher leaf lutein level in the *ccd1;4* mutant is somewhat unexpected, and may suggest a role for CCD4 and CCD1 in lutein catabolism under specific conditions, a possibility explored further in Chapter Six. Nevertheless, it remains apparent that the *ccr2* phenotype is still prevalent in this genotype. Interestingly, *ccd x ccr2* single mutant inflorescence lutein concentrations were significantly lower than both Col-0 and *ccr2* (and *ccd x ccr2* double mutants; Figure 5.2B). This discrepancy is discussed later, in section 5.2.5.

Chlorophyll results were more equivocal (Figure 5.2C and D). Only *ccr2* and *ccd4 x ccr2* rosette leaf chlorophyll *a* measurements were significantly lower relative to Col-0 (Figure 5.2C). Rosette chlorophyll *b* levels were significantly reduced in *ccr2* and *ccd x ccr2* single mutants, but not in *ccd x ccr2* double mutants (Figure 5.2C).

Chlorophyll *a* and *b* levels in *ccr2* in inflorescences were slightly *higher* than Col-0, as were *ccd1;7* and *ccd4;7 x ccr2*, whilst *ccd x ccr2* single mutant chlorophylls were significantly lower than Col-0 (Figure 5.2D). The chlorophyll results are not entirely unexpected, as the *ccr2* reduced chlorophyll phenotype has previously been found to arise from delayed greening of newly-emerged tissue (Hou 2015), and may thus be masked in the presence of mature leaf tissue. Thus, the green portions of the *ccr2*-background leaves (Figure 5.1) are largely indistinguishable from Col-0.

5.2.2 Volatile apocarotenoid survey: identification of linear carotene-derived compounds unique to *ccr2*-background

Known and putative leaf volatile apocarotenoids detected in Col-0-background plants (Chapter Two and Four) were also detected in *ccr2*-background samples, with only one exception: dihydro-6MHO could not be detected in the analyses comparing Col-0, *ccr2* and the *ccd x ccr2* double mutants (Table 5.2), despite being observed in the batch comparing Col-0 and *ccr2* to *ccd x ccr2* single mutants (Table 5.1). This is likely due to minor deterioration in integrity of the SPME fibre used for this set of analyses. I have previously observed that the sensitivity of PDMS/DVB/CAR SPME fibres toward low-MW compounds is preferentially lost during the onset of fibre deterioration. Given the Col-0, *ccr2* and *ccd x ccr2* double mutant data did not differ qualitatively or quantitatively form other Col-0 leaf SPME measurements for any other compounds, the rest of the apocarotenoid data was retained for analysis.

There was also one addition to the apocarotenoid profile detected across the genotypes: citronellal (Figure 5.3). This compound is likely to be a putative apocarotenoid given it appears to be derived from desaturation of citral in a manner analogous to the speculated desaturation of 6MHO to dihydro-6MHO (Tikunov, *et al.* 2005).

Apocarotenoids in inflorescences grown under 8 h photoperiod however (Table 5.3 and Table 5.4), appeared to differ dramatically to those observed under 16 h (Chapter Four). In addition to the apocarotenoids observed under 16 h photoperiod (Table 4.4 and 4.5), short-day inflorescences had quantifiable levels of 6MHO, 2,6,6-trimethylcyclohexanone, *cis*-citral, *trans*-citral, *cis*-β-ionone and α-ionone (Table 5.3 and Table 5.4). These compounds were detected at substantial levels across both Col-0 and the *ccr2*-background genotypes. This qualitative change appears to be a general response to reduced photoperiod, possibly as a result of altered oxidative conditions affecting non-enzymatic volatile apocarotenoid production.

In addition to the apocarotenoids observed across Col-0 and *ccr2*-background plants, three compounds appeared exclusive to *ccr2*-background samples: *cis*-geranylacetone, 3-*trans*-5-*cis*-pseudoionone and *trans*-farnesylacetone (Tables 5.1-5.4). The structures of these three compounds are consistent with cleavage from linear carotenes (phytofluene/ζ-

carotene, neurosporene/lycopene and phytoene/phytofluene, respectively; Figure 1.2). This, combined with their occurrence exclusively in *ccr2*-background samples, provides strong evidence that these compounds are volatile apocarotenoids produced from *in planta* cleavage of linear carotenes that accumulate in *ccr2*-background plants, and which are a novel addition to the detectable *Arabidopsis* apocarotenoid profile.

In addition, a number of other putatively linear carotene-derived leaf volatile apocarotenoids, common to all genotypes, were also elevated in *ccr2*-background (Tables 5.1-5.4, Figure 5.4), providing further evidence they are indeed linear carotene-derived: 6MHO, citronellal, *trans*-geranylacetone. In inflorescences, these compounds exhibited similar trends, as did *cis*-citral, *trans*-citral, hexahydropseudoionone and hexahydrofarnesylacetone, further supporting suggestions these are linear carotene-derived (Table 5.3 and 5.4, Figure 5.5). On the other hand, whilst *trans*-citral, hexahydropseudoionone and hexahydrofarnesylacetone are also present in leaves, they were not elevated in *ccr2*-background compared to Col-0; nor were dihydro-6MHO or 3,7,11-trimethyl-1-dodecanol concentrations (Table 5.1 and Table 5.2, Figure 5.4). These observations may point to the presence of a rate-limiting steps downstream of carotenoid cleavage that prevents increases in particular volatiles alongside their putative precursor linear carotenes. The alternative explanation - that these compounds do not originate from the apocarotenoid pathway - must also be considered.

5.2.3 Clustering analysis reveals *ccr2* and *ccd x ccr2* genotypes primarily differentiated by volatile apocarotenoid abundance

HCA of leaf volatile apocarotenoid abundances in Col-0, *ccr2* and *ccd x ccr2* mutants indicated a large cluster of correlated volatile apocarotenoids (Supplementary Figure 5.2A). The nature of this cluster was largely similar to that reported for leaf volatile apocarotenoids in Chapter Four, Figure 4.8. In addition to this cluster however, *cis*-geranylacetone, 3-*trans*-5-*cis*-pseudoionone and *trans*-farnesylacetone, three compounds observed exclusively in *ccr2*-background tissues, registered as a distinct cluster. The cluster dendrogram derived from inflorescence volatile apocarotenoid abundances was similar to the *ccr2*-background leaf volatile abundance dendrogram (Supplementary Figure 5.2B).

PCA of variation in volatile apocarotenoids revealed interesting trends. As expected, inability to detect *cis*-geranylacetone, 3-*trans*-5-*cis*-pseudoionone or *trans*-farnesylacetone in Col-0, markedly lower levels of *trans*-geranylacetone, 6MHO and *trans*-citral, and significantly higher α-ionone levels, all contributed to Col-0 leaf and inflorescence samples being clearly separated from their *ccr2*-background counterparts (Figure 5.6). These differences were reflected in the compositions of PC2 in both the leaf (Figure 5.6A) and inflorescence (Figure 5.6B) apocarotenoid analyses (accounting for 30 and 24% of variation respectively).

PCA also revealed differences between *ccr2* and *ccd x ccr2* single mutants on the one hand, and *ccd x ccr2* double mutants on the other. PC1 of leaf (Figure 5.6A) and inflorescence (Figure 5.6B) PCAs (accounting for 53 and 47% of variation respectively) were essentially able to discriminate these two groups into distinct clusters, with *ccd x ccr2* double mutants positively associated with increased abundance of β-cyclocitral and DHA. The double mutants were also highly-correlated with β-ionone and 5,6-epoxy-β-ionone in leaves (Figure 5.6A) and 6MHO and *cis*-citral in inflorescences (Figure 5.6B). This is consistent with observations that volatile apocarotenoid production increased markedly in the *ccd x ccr2* double mutants (Table 5.2 and Table 5.4).

5.2.4 HPLC-DAD analysis: Col-0, *ccr2* and *ccd x ccr2* mutants also differ in carotenoid profile

Volatile apocarotenoid measurements were placed in greater context by measurement of the precursor carotenoids. Phytoene, violaxanthin, neoxanthin, antheraxanthin, lutein and β-carotene were all observable at roughly the same quantities as described in Chapter Four (Supplementary Figure 5.3). In addition to the carotenoids previously described for 16 h photoperiod, Col-0-background plants however, 8 h photoperiod *ccr2*-background plants had a number of additional linear carotenes not observed in Col-0 samples: isomers of phytofluene, ζ-carotene, neurosporene and lycopene (Table 5.5 and Table 5.6; no additional isomers of phytoene were observed). The presence of linear carotenes (other than phytoene) in *ccr2* but not Col-0-background was consistent with previous *ccr2* studies (Cuttriss, *et al.* 2007, Park, *et al.* 2002).

Of the linear carotenes, two phytofluene isomers were detected across some *ccr2*-background samples, whilst some samples had only one. Given the small quantities of both isomers, the quantities have been summed for analysis. Similarly, small quantities of between three and six *cis*-lycopene isomers were detected across *ccr2*-background samples, leading me to analyse the sum of *cis*-lycopene peak areas. Neurosporene isomers were by far the most abundant linear carotenes observed; two distinct groups of isomers could be discerned: those eluting prior to β-carotene, and those eluting after. In an attempt to gain greater insight into linear carotene catabolism - should it involve preferential consumption of some neurosporene isomers over others - these two groups (dubbed 'neurosporene-pre' and 'neurosporene-aft') were reported separately (Table 5.5 and Table 5.6).

Quantities of many carotenoids varied substantially across the genotypes (Table 5.5 and Table 5.6). As noted above (Figure 5.2A and B), lutein was reduced in the *ccr2* and *ccd x ccr2* mutants to between 13 and 23% of Col-0 concentration in leaves and 13 – 48% in inflorescences. Of the other carotenoids in *ccr2* and *ccd x ccr2* mutant leaves (Table 5.5), phytoene, β-carotene and neoxanthin remained largely unchanged, whilst antheraxanthin and violaxanthin were elevated. This elevation has been previously observed in *ccr2* leaves grown under 8 h photoperiod, and may reflect altered oxidative conditions (Chai, *et al.* 2011, Cuttriss, *et al.* 2007). Expression studies of the relevant carotenoid biosynthetic genes (e.g. *ZEP, VDE*) could be performed to better-understand the basis of this change in carotenoid profile.

Ccr2 and *ccr2 x ccd* mutant inflorescences (Table 5.6) exhibited the same trends for phytoene, β-carotene, neoxanthin, antheraxanthin and violaxanthin concentrations as in leaves. Violaxanthin levels were reduced in *ccd x ccr2* single mutants relative to *ccr2* however, such that only *ccd1 x ccr2* violaxanthin concentration exhibited a significant increase above Col-0 (Table 5.6). This phenomenon was similar to the differences between *ccr2* and *ccd x ccr2* single mutant inflorescences observed for lutein and chlorophylls (Figure 5.2B); antheraxanthin was also markedly reduced in *ccd x ccr2* single mutants relative to *ccr2*. Whilst potentially of interest, these observations may be an artefact of difficulties in sampling inflorescences from the same developmental stage. Although every effort was taken to sample anthesis flowers (with adjacent cauline leaves

of the same age), differences in the rate of flower ageing and/or cauline leaf mass (perhaps part of pleiotropic effects of *ccd* mutations) may have confounded comparisons of carotenoid profile. Should these observations be of future interest, a study of *ccd x ccr2* mutant inflorescence development could be done to mitigate confounding factors.

Phytofluene and *cis*-lycopene concentrations also showed interesting changes in leaves (Table 5.5), with levels substantially reduced relative to *ccr2* in *ccd1 x ccr2* and *ccd7 x ccr2*, whilst remaining similar to *ccr2* in *ccd4 x* ccr2 and *ccd8 x ccr2*. ζ-carotene was not observed in *ccd1 x ccr2, ccd7 x ccr2* and *ccd8 x ccr2*, whilst retaining *ccr2* levels in *ccd4 x ccr2* (Table 5.5).

Of the two neurosporene isomer groups, neurosporene-aft exhibited a pattern somewhat similar to that of the aforementioned linear carotenes: elevated relative to *ccr2* in *ccd4 x ccr2* and *ccd8 x ccr2*, whilst maintaining *ccr2* levels in other *ccr2*-background genotypes. Neurosporene-pre, in contrast, had levels largely unchanged from *ccr2* in *ccd1 x ccr2* and *ccd8 x ccr2*, whilst being reduced in *ccd4 x ccr2, ccd7 x ccr2* and the *ccd x ccr2* double mutants (Table 5.5).

Linear carotene trends are perhaps best-depicted in a PCA examining variation in leaf linear carotene concentrations across genotypes (Figure 5.7A). PC1 accounts for 66% of the observed variation, and appears to separate the samples into three distinct clusters. PC1 is strongly weighted toward the linear carotenes exclusive to *ccr2*-background tissues, all of which were essentially correlated with one another. PC2, accounting for 18% of between-sample variation, is dominated by phytoene abundance; from the plot of the PC loadings one can see abundances of phytoene and the other linear carotenes are virtually independent of (i.e. orthogonal to) one another (Figure 5.7A).

As expected, Col-0 samples were very distinct from the *ccr2*-background samples, having undetectable levels of all PC1 linear carotenes (Figure 5.7). The *ccr2*-background samples formed two clusters, with *ccr2, ccd4 x ccr2, ccd8 x ccr2* and *ccd4;7 x ccr2* being associated with higher levels of linear carotenes other than phytoene (Figure 5.7A). This was also reflected in the total linear carotenes measured in different genotypes (Figure 5.7B). *Ccr2, ccd4 x ccr2, ccd8 x ccr2* and *ccd4;7 x ccr2* had significantly higher linear carotenes than *ccd7 x ccr2, ccd1;4 x ccr2*_and *ccd1;7 x ccr2*. All aforementioned genotypes, except for *ccr2*, also had significantly higher linear carotenes compared with

ccd1 x ccr2. All *ccr2*-background genotypes had higher linear carotenes compared to Col-0.

The same trends were observed for ζ-carotene and neurosporenes in inflorescences, whilst *cis*-lycopene inflorescence concentration was lowest in *ccr2* (0.018 µg), intermediate in the *ccd x ccr2* double mutants (> 1 µg/g), and higher in *ccd x ccr2* single mutants, being highest in *ccd4 x ccr2* (4.3 µg/g). Phytofluene levels were constant across *ccr2* and *ccd x ccr2* single mutants, and lower in the *ccd x ccr2* double mutants. At this stage, it is unclear why leaf and inflorescence across-genotype trends in linear carotene concentration should be different (and whether or not it is an artefact of inflorescence sampling, as discussed above).

5.2.5 Expression analysis: Possibility of compensatory *CCD* induction in *ccr2* and *ccd x ccr2* backgrounds

CCD expression in *ccr2* and *ccd x ccr2* backgrounds appeared perturbed by various factors. *CCD1* expression was not repressed in *ccd1 x ccr2* in either leaves or inflorescences (Figure 5.8), although *ccd1;4 x ccr2* and *ccd1;7 x ccr2* leaves and inflorescences all exhibited significantly decreased *CCD1* expression (Figure 5.9).

Similarly, *CCD4* was repressed in *ccd4 x ccr2* and *ccd4;7 x ccr2*, but not in *ccd1;4 x ccr2* tissues (Figure 5.8 and Figure 5.9). *CCD7* expression exhibited little or no downward trend in *ccd7*-background samples, only being significantly repressed (to 40% of Col-0/*ccr2* levels) in *ccd1;7 x ccr2* inflorescence tissue (Figure 5.9). *CCD8* expression was only significantly reduced (50% of Col-0, 25% of *ccr2* levels) in *ccd8 x ccr2* inflorescences (Figure 5.8).

Given the previously noted possibility of RNA-Polymerase read-through of the T-DNA insertion sequence, leading to transcription of the qPCR primer target amplicons, these results are not completely unexpected. It was more noteworthy that *CCD* expression levels in *ccr2* did not generally differ from Col-0 levels (Figure 5.8 and Figure 5.9), suggesting *CCD* activity (at transcriptional level) is not perturbed by the presence of linear carotenes.

5.2.6 Summary

As observed for *ccd* mutants in the Col-0 background (Chapter Four), there were no obvious volatile apocarotenoid-CCD relationships, which would be exemplified by the absence of a given apocarotenoid in a specific *ccd* background. It would appear non-enzymatic carotenoid cleavage is similarly responsible for the bulk of volatile apocarotenoid production, regardless of the addition of linear carotenes in the *ccr2*-background. As an example: whilst β-carotene derived leaf volatile apocarotenoids were somewhat reduced relative to Col-0 in *ccd1 x ccr2*, these apocarotenoids are markedly elevated above both Col-0 and *ccr2* in the *ccd1;4 x ccr2* mutant. This rules out CCD1 as being necessary for production of β-carotene-derived volatile apocarotenoids in leaves. Neither do CCD4 nor CCD7 appear necessary, with β-carotene-derived volatile apocarotenoids also elevated above Col-0/*ccr2* levels in *ccd1;7 x ccr2* and *ccd4;7 x ccr2* as well.

I also noted *ccr2* and *ccd x ccr2* single mutants exhibited two to eight-fold reductions in α-cyclocitral and α-ionone leaf concentrations relative to Col-0 (Figure 5.4). The same trend was also observed in *ccr2* inflorescences, where *ccd x ccr2* single mutant α-ionone concentrations were measured to at or below 1 ng/g compared to 6 ng/g in Col-0 (Figure 5.5). Reductions in these two α-carotene derived volatiles is consistent with the reduction in εLCY activity, required for lycopene cyclisation to produce α-carotene, previously reported for *ccr2* (Cuttriss, *et al.* 2007). Whilst α-carotene is below trace levels in both Col-0 and *ccr2*, consistently reduced εLCY activity in the *ccd x ccr2* mutants appears likely given the reduced levels of lutein (a xanthophyll derivative of α-carotene) in *ccr2*-background mutants (Figure 5.2). Presumably, the reduced α-carotene pool in *ccr2*-background plants leads to reduced volatile apocarotenoids, in addition to reduced lutein.

Curiously however, *ccd x ccr2* double mutants had levels of α-cyclocitral and α-ionone comparable to Col-0. This would appear to result from increased cleavage of the diminished α-carotene pool, consistent with the spike in levels of other volatile apocarotenoids. The marked increases of volatile apocarotenoid levels in all *ccd x ccr2* double mutant tissues (Figure 5.4 and Figure 5.5) was perhaps the most interesting observation, made all the more notable given the limited changes in substrate carotenoid levels (changes only observed in a few linear carotenes; Table 5.5 and Table 5.6).

5.3 Figures and Tables

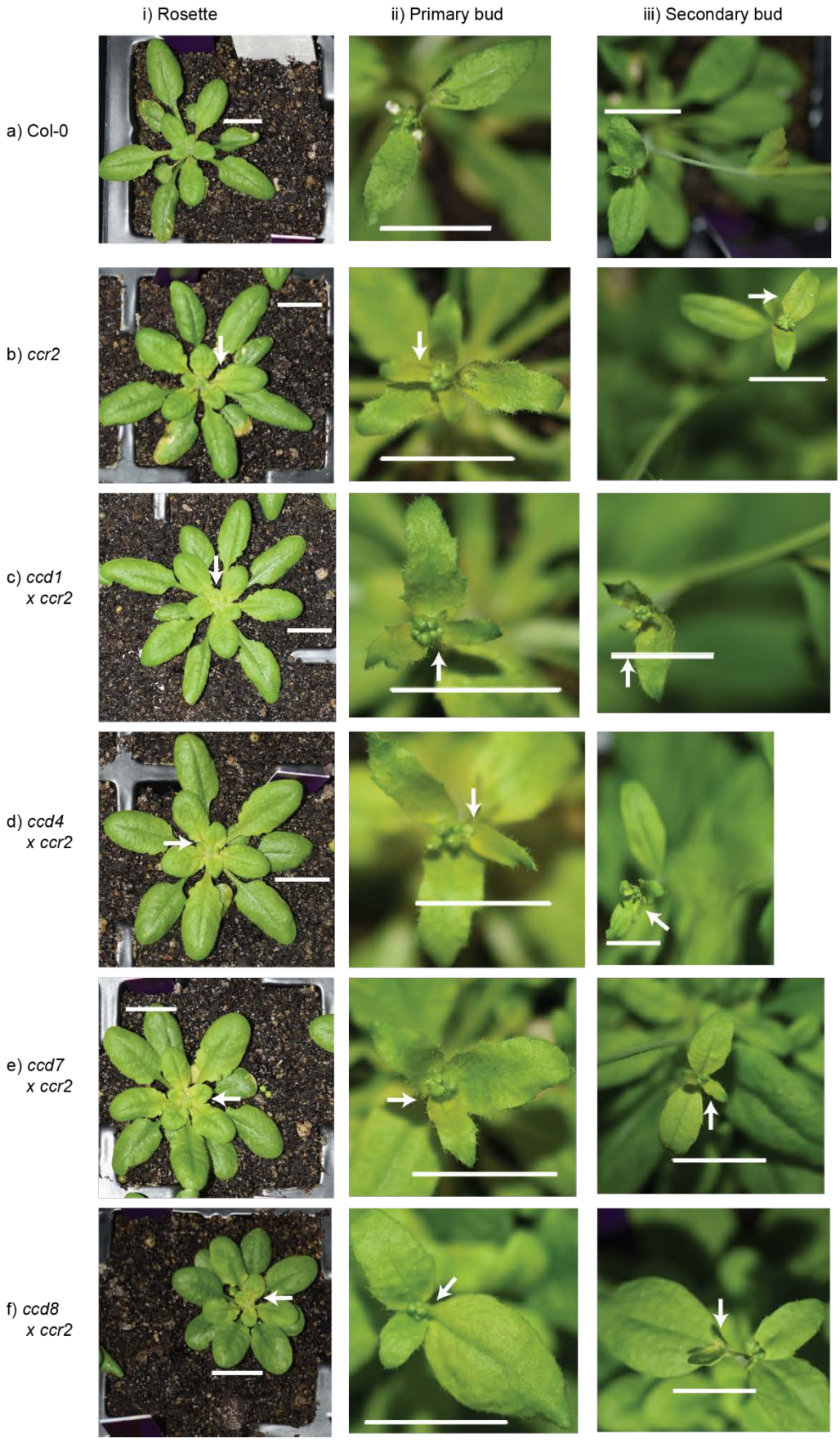
i) Rosette
ii) Primary bud
iii) Secondary bud
a) Col-0
b) *ccr2*
c) *ccd1* x *ccr2*
d) *ccd4* x *ccr2*
e) *ccd7* x *ccr2*
f) *ccd8* x *ccr2*

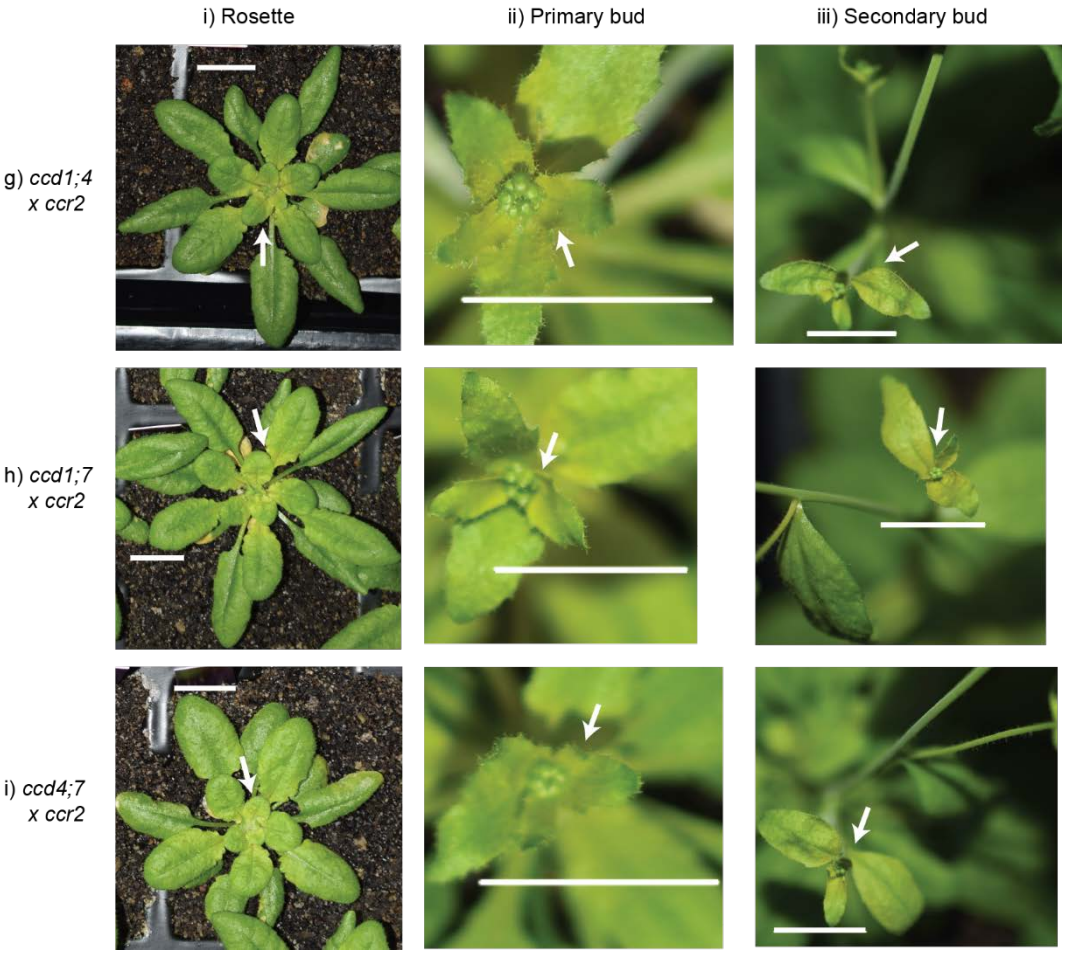

Figure 5.1: Rosette and cauline leaves of *ccr2 x ccd* single and double mutants

Col-0 (wild-type, a), *ccr2* (b), *ccd1 x ccr2* (c), *ccd4 x ccr2* (d), *ccd7 x ccr2* (e), *ccd8 x ccr2* (f), *ccd1;4 x ccr2* (g), *ccd1;7 x ccr2* (h), and *ccd4;7 x ccr2* (i) plants were grown for 21 days under 16 h photoperiod before being shifted to 8 h photoperiod. Rosette images (I) were taken of 35 d.o. plants (approximately growth stage 5.1), whilst primary bolt (II) images were taken at roughly 49 d.o., as plants reached growth stage 6. Images of secondary bolt buds (III) were taken as secondary bolts branched from the primary bolt. All images were taken within 1 h of start of the light photoperiod. Scale bars represent 1 cm in all images. White arrows highlight the yellow-leaf phonotype associated with *ccr2*.

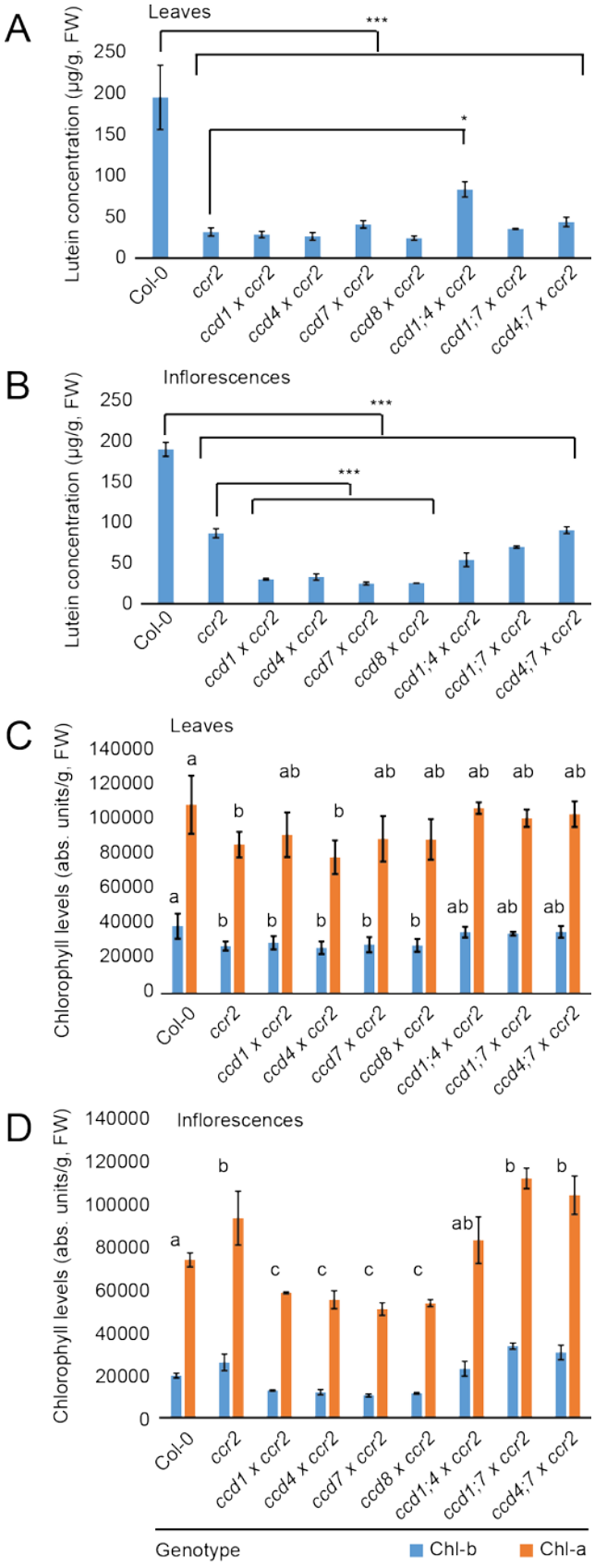
A
Leaves
Lutein concentration (µg/g, FW)
250
200
150
100
50
0
***
*
Col-0
ccr2
ccd1 x ccr2
ccd4 x ccr2
ccd7 x ccr2
ccd8 x ccr2
ccd1;4 x ccr2
ccd1;7 x ccr2
ccd4;7 x ccr2
B
Inflorescences
Lutein concentration (µg/g, FW)
250
200
150
100
50
0
***
***
Col-0
ccr2
ccd1 x ccr2
ccd4 x ccr2
ccd7 x ccr2
ccd8 x ccr2
ccd1;4 x ccr2
ccd1;7 x ccr2
ccd4;7 x ccr2
C
Leaves
Chlorophyll levels (abs. units/g, FW)
140000
120000
100000
80000
60000
40000
20000
0
a
b
ab
Col-0
ccr2
ccd1 x ccr2
ccd4 x ccr2
ccd7 x ccr2
ccd8 x ccr2
ccd1;4 x ccr2
ccd1;7 x ccr2
ccd4;7 x ccr2
D
Inflorescences
Chlorophyll levels (abs. units/g, FW)
140000
120000
100000
80000
60000
40000
20000
0
a
b
c
ab
Col-0
ccr2
ccd1 x ccr2
ccd4 x ccr2
ccd7 x ccr2
ccd8 x ccr2
ccd1;4 x ccr2
ccd1;7 x ccr2
ccd4;7 x ccr2
Genotype
Chl-b
Chl-a

Figure 5.2: *ccr2* and *ccd x ccr2* lutein and chlorophyll abundance

Lutein (A and B) and chlorophyll *a* and *b* (C and D) concentrations were measured in Col-0, *ccr2* and *ccd x ccr2* mutant rosette leaves (A and C) and inflorescences (B and D). Statistical significance was calculated *via* pairwise Student's t-tests relative to Col-0 and *ccr2* levels; asterisks in A and B represent $p < 0.05$ (*) and $p < 0.001$ (***), difference statistical symbols in C and D represent significance at $p < 0.05$ level. Values are expressed ± standard error. $n = 3$ per genotype.

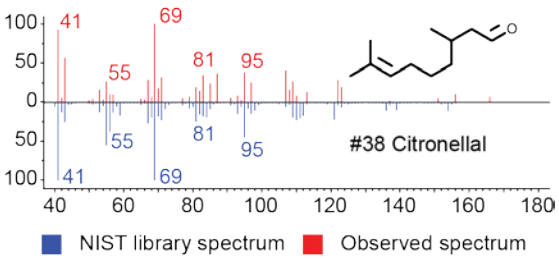

Figure 5.3: Citronellal compound data

Citronellal was tentatively identified following chromatogram deconvolution of GC/MS spectrum and match of deconvoluted spectrum (red) to NIST14 database spectrum (blue; A). Additional data, including observed and NIST RI, is available in the Appendix.

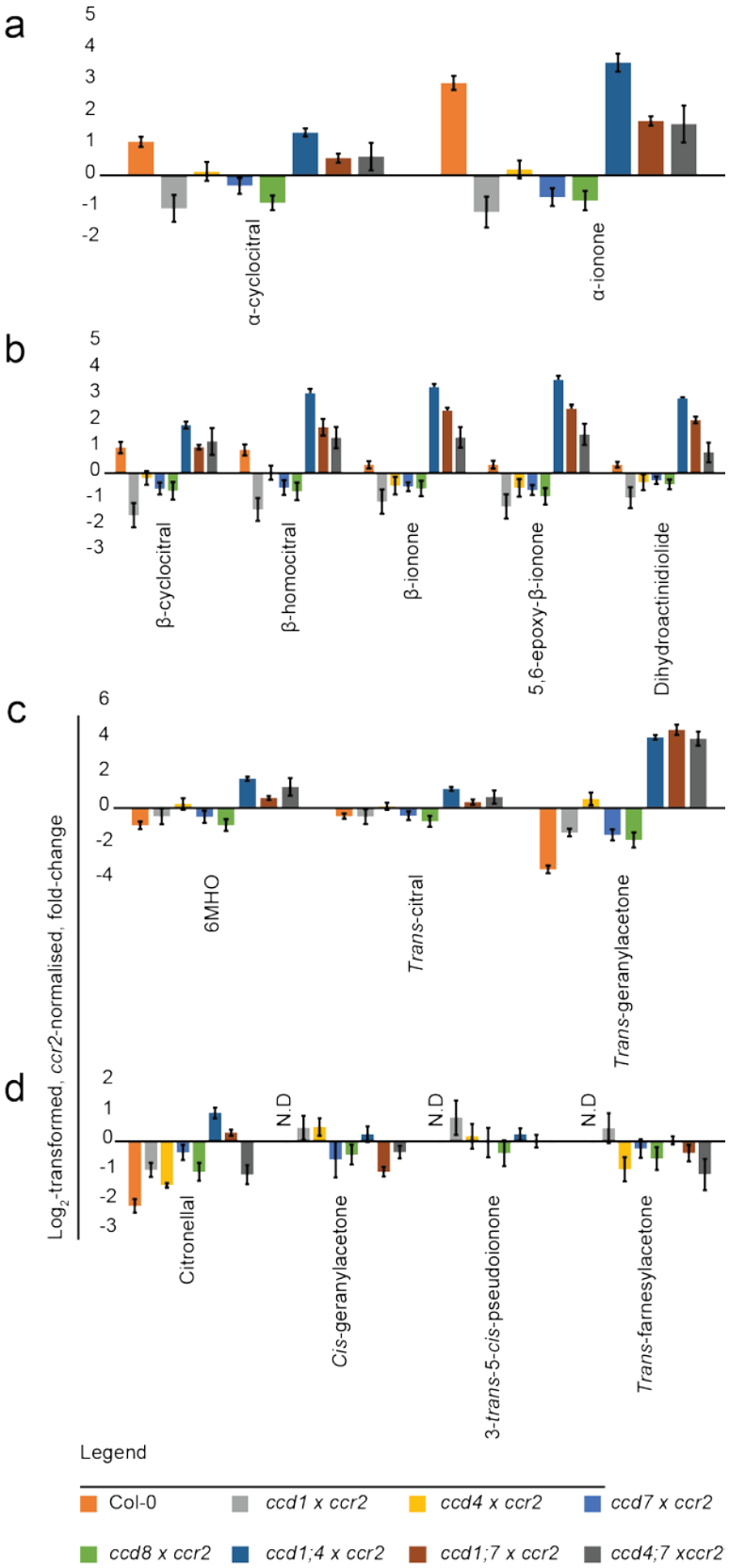
a
α-cyclocitral
α-ionone
b
β-cyclocitral
β-homocitral
β-ionone
5,6-epoxy-β-ionone
Dihydroactinidiolide
c
6MHO
Trans-citral
Trans-geranylacetone
d
Log2-transformed, ccr2-normalised, fold-change
N.D
N.D
N.D
Citronellal
Cis-geranylacetone
3-trans-5-cis-pseudoionone
Trans-farnesylacetone
Legend
Col-0
ccd1 x ccr2
ccd4 x ccr2
ccd7 x ccr2
ccd8 x ccr2
ccd1;4 x ccr2
ccd1;7 x ccr2
ccd4;7 xccr2

Figure 5.4: Change in abundance of selected leaf volatile apocarotenoids across Col-0 and *ccd x ccr2* mutants

Ccr2-normalised, log_2-transformed compound abundances for selected (putative and known) volatile apocarotenoids across Col-0 and the seven *ccd x ccr2* mutant genotypes have been plotted. a) α-cyclocitral and α-ionone. b) β-cyclocitral, β-homocitral, β-ionone, 5,6-epoxy-β-ionone and dihydroactinidiolide. c) 6MHO, *trans*-citral and *trans*-geranylacetone. d) Citronellal, *cis*-geranylacetone, 3-*trans*-5-*cis*-pseudoionone and *trans*-farnesylacetone. Values are ± standard error, n = 4 for all genotypes. N.D = not detected.

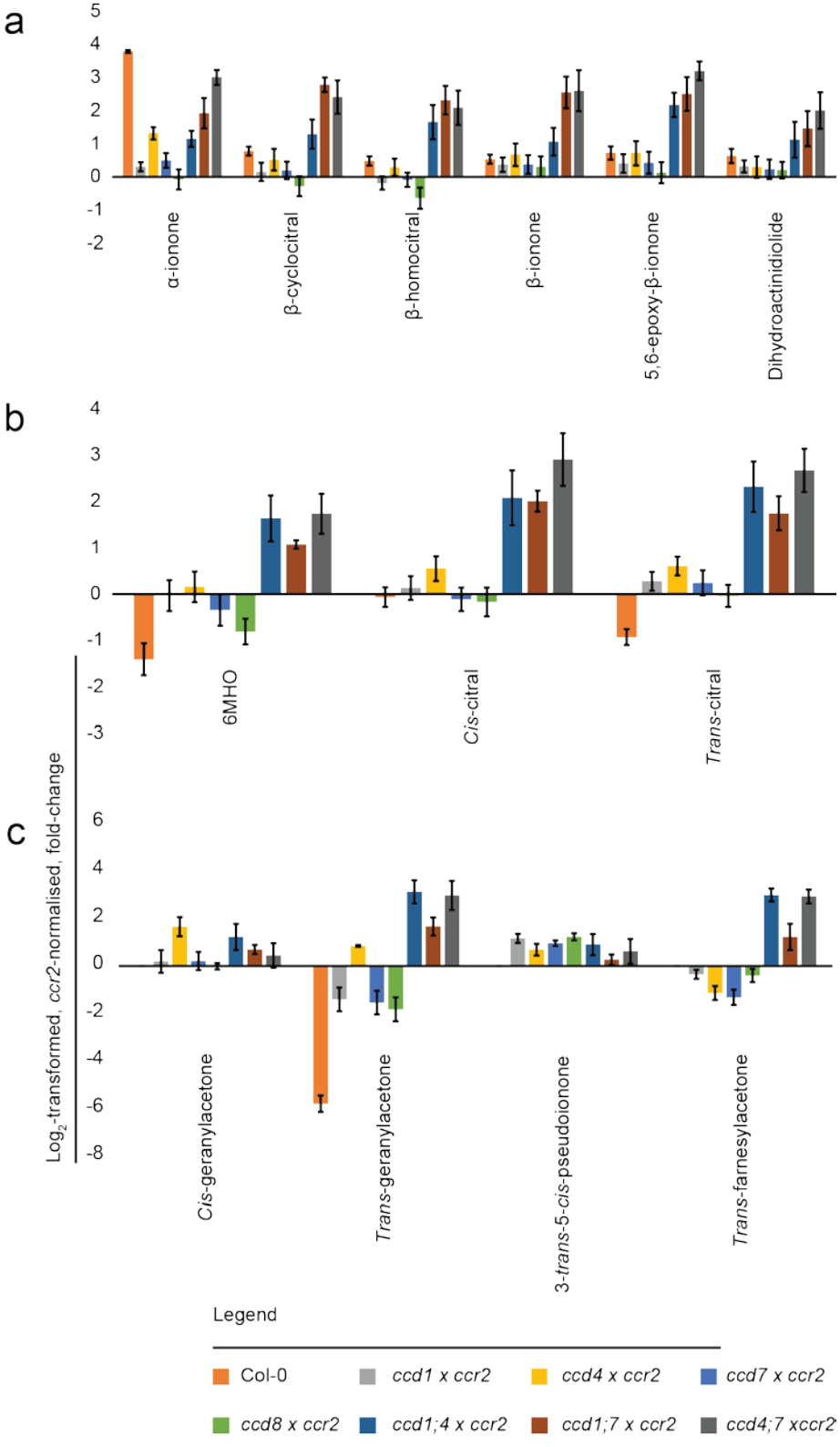
a
b
c
α-ionone
β-cyclocitral
β-homocitral
β-ionone
5,6-epoxy-β-ionone
Dihydroactinidiolide
6MHO
Cis-citral
Trans-citral
Cis-geranylacetone
Trans-geranylacetone
3-trans-5-cis-pseudoionone
Trans-farnesylacetone
Log2-transformed, ccr2-normalised, fold-change
Legend
Col-0
ccd1 x ccr2
ccd4 x ccr2
ccd7 x ccr2
ccd8 x ccr2
ccd1;4 x ccr2
ccd1;7 x ccr2
ccd4;7 xccr2

Figure 5.5: Change in abundance of selected inflorescence volatile apocarotenoids across Col-0 and *ccd x ccr2* mutants

Ccr2-normalised, log_2-transformed compound abundances for selected (putative and known) volatile apocarotenoids across Col-0 and the seven *ccd x ccr2* mutant genotypes have been plotted. a) α-ionone, β-cyclocitral, β-homocitral, β-ionone, 5,6-epoxy-β-ionone and dihydroactinidiolide. b) 6MHO, *cis*-citral and *trans*-citral. d) *Cis*-geranylacetone, *trans*-geranylacetone, 3-*trans*-5-*cis*-pseudoionone and *trans*-farnesylacetone. Values are ± standard error, n = 4 for all genotypes. N.D = not detected.

A) Leaves

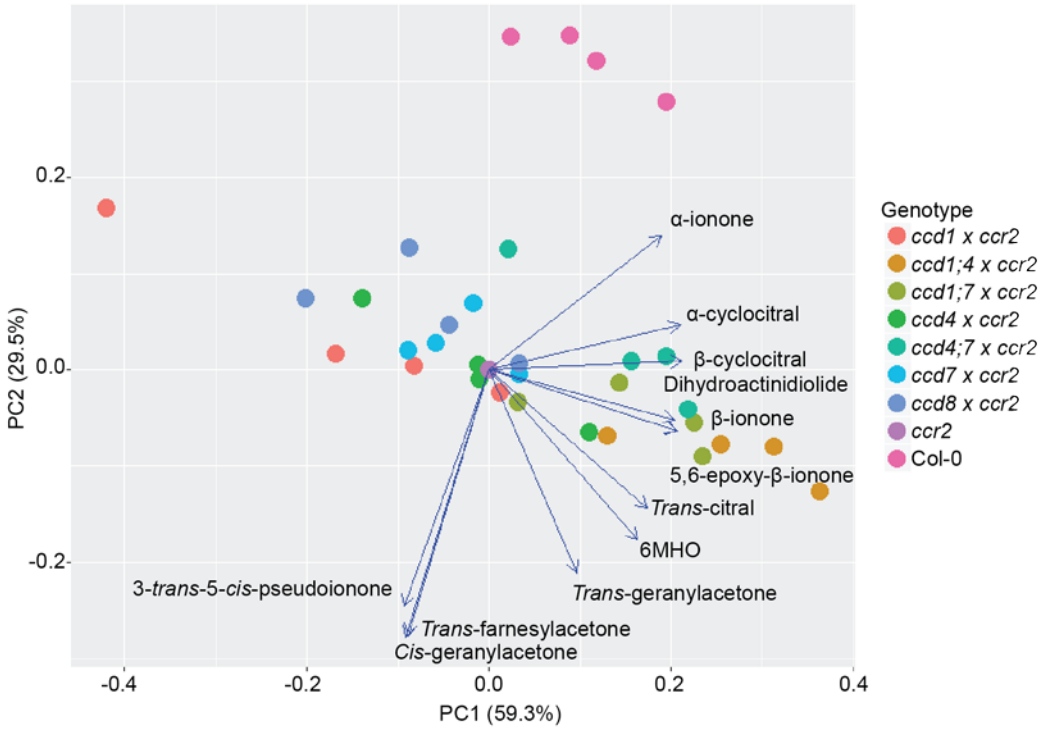

B) Inflorescences

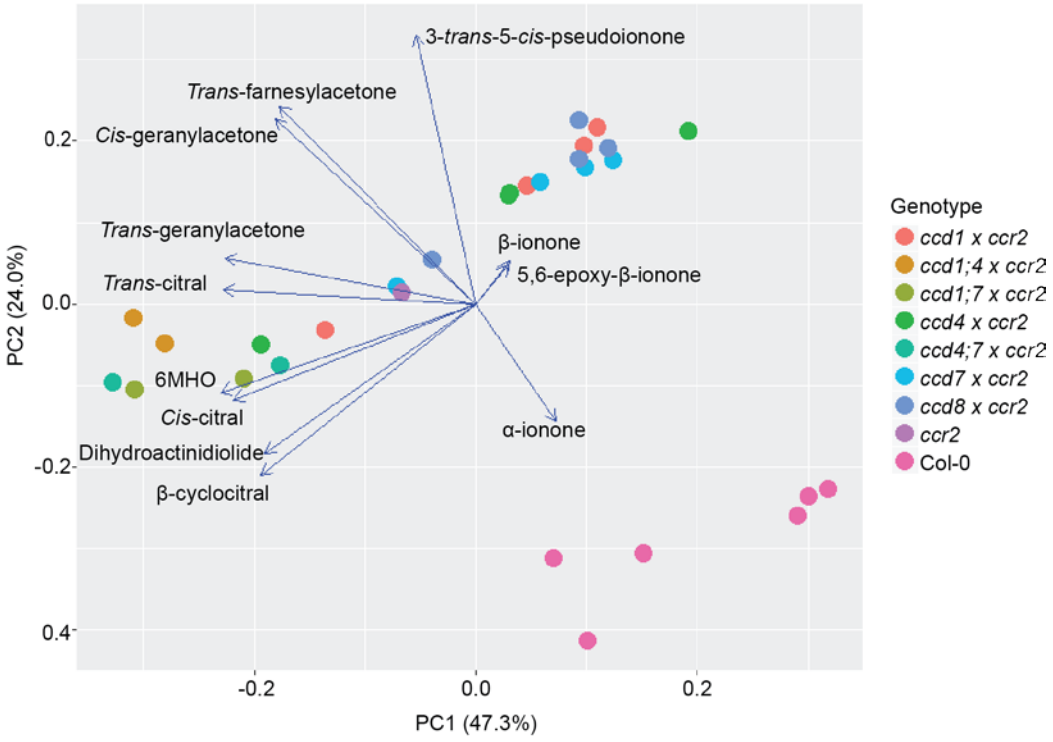

Figure 5.6: Principal Component Analysis of *Col-0*, *ccr2* and *ccd x ccr2* leaf and inflorescence volatile apocarotenoid abundances

Log_2-transformed volatile apocarotenoid abundances (expressed as fold-changes relative to mean *ccr2* values) for leaf (a) and inflorescence (b) tissues were incorporated into PCA analyses. Volatile apocarotenoid loadings are overlaid onto the plots of the first two principal components.

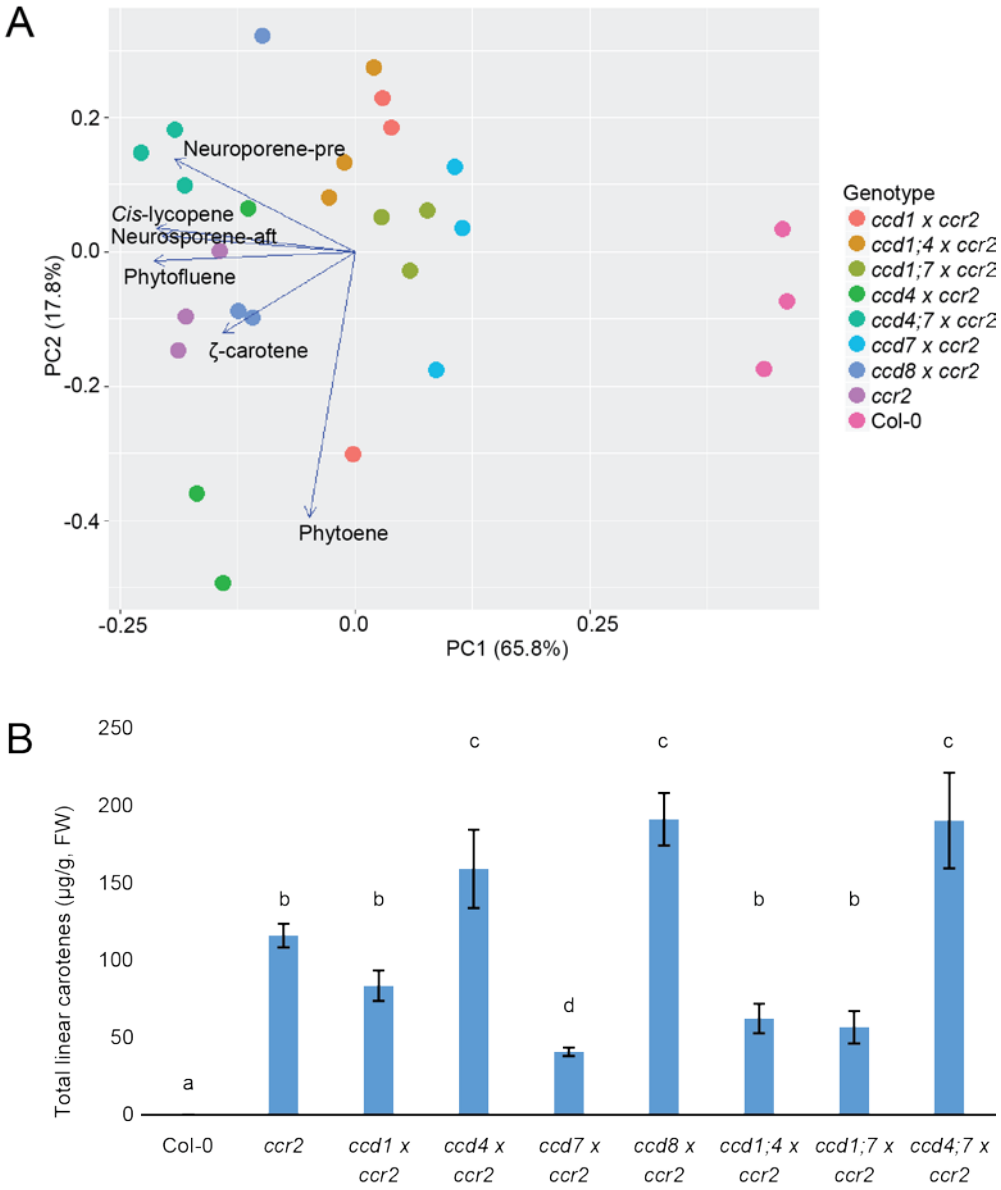

Figure 5.7: Linear carotene abundances in Col-0, *ccr2* and *ccd x ccr2* leaf tissue

A) Log_2-transformed, normalised, carotene abundances from the aforementioned genotypes were incorporated into a PCA analysis. PC loadings were added to the plot of the first two principal components. B) Total linear carotene concentrations were plotted for all genotypes. Values are ± standard error. Statistical symbols in (b) represent significance at $p < 0.05$ level using ANOVA and post-hoc Tukey's Test. $n = 3$.

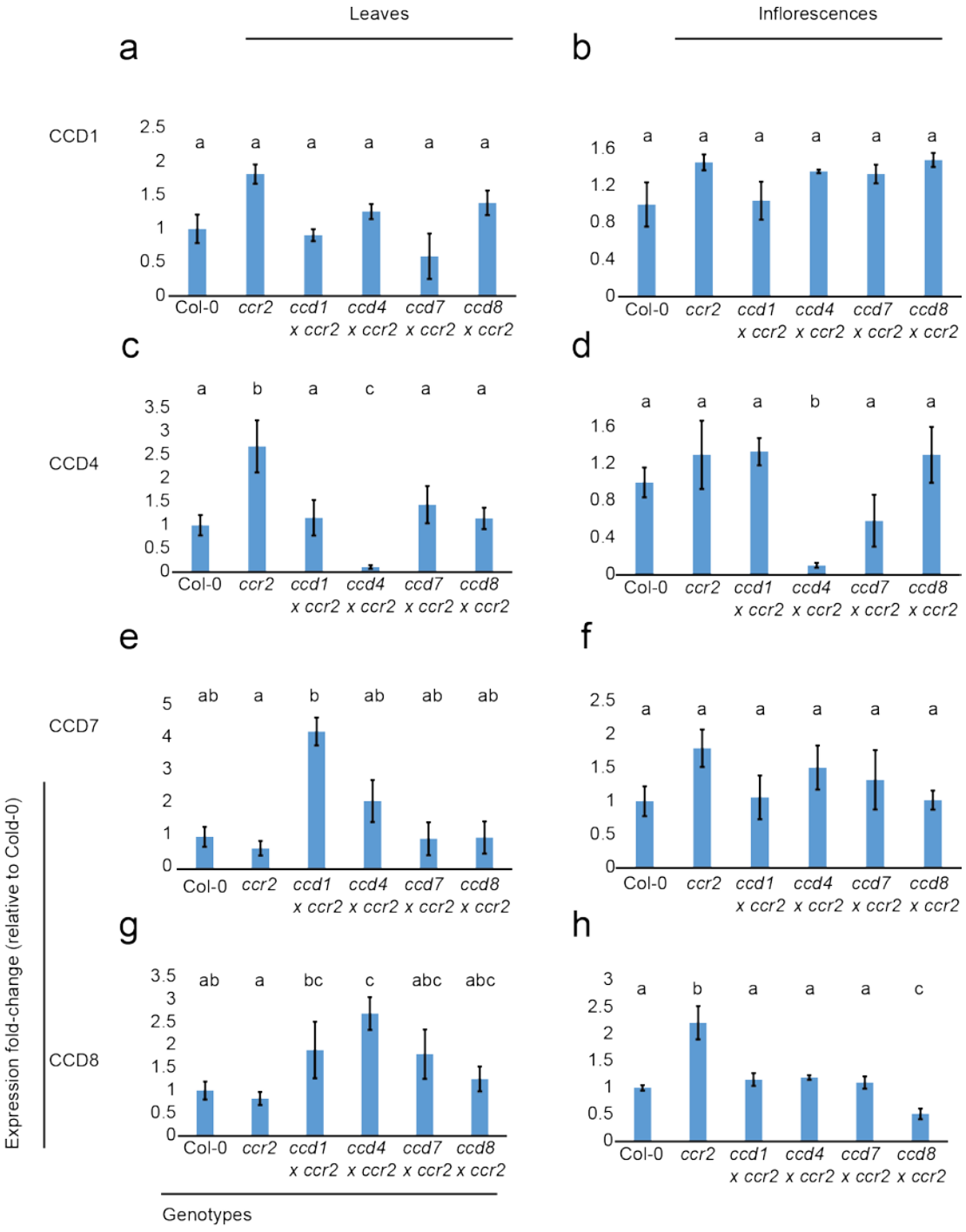

Figure 5.8: Expression of *CCD* genes in *Col-0*, *ccr2* and *ccd x ccr2* single mutants

Leaf (a, c, e, g) and inflorescence (b, d, f, h) tissues from Col-0, *ccr2* and *ccr2 x ccd1*, *ccr2 x ccd4*, *ccr2 x ccd7* and *ccr2 x ccd8* were analysed for expression of *CCD1* (a, b), *CCD4* (c, d), *CCD7* (e, f) and *CCD8* (g, h). Values are expressed as fold-change relative to Col-0 with error bars representing standard error. Statistical significance was calculated *via* ANOVA with post-hoc Tukey's Test. Different statistical symbols represent significance at the $p < 0.05$. $n = 4$ per genotype.

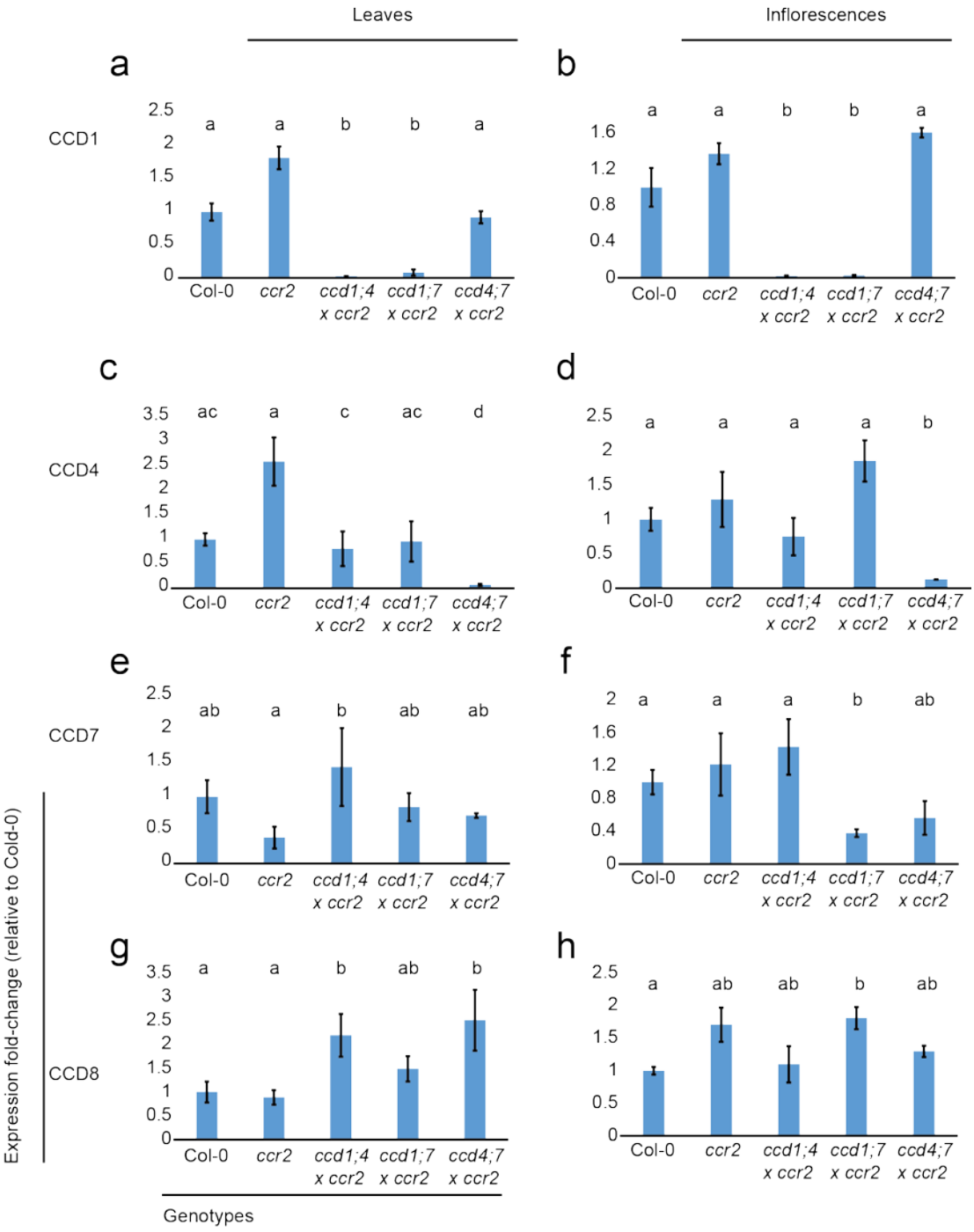

Figure 5.9: Expression of *CCD* genes in *Col-0*, *ccr2* and *ccd x ccr2* double mutants

Leaf (a, c, e, g) and inflorescence (b, d, f, h) tissues from Col-0, *ccr2*, *ccd1;4 x ccr2*, *ccd1;7 x ccr2* and *ccd4;7 x ccr2* were analysed for expression of *CCD1* (a, b), *CCD4* (c, d), *CCD7* (e, f) and *CCD8* (g, h). Values are expressed as fold-change relative to Col-0 with error bars representing standard error. Statistical significance was calculated *via* ANOVA with post-hoc Tukey's Test. Different statistical symbols represent significance at the $p < 0.05$. $n = 4$ per genotype.

Table 5.1: Volatile apocarotenoids observed in leaves from Col-0, *ccr2*, and *ccd x ccr2* single mutants

		Volatile apocarotenoid concentration (ng/g FW)					
#	Compound	Col-0	*ccr2*	*ccd1 x ccr2*	*ccd4 x ccr2*	*ccd7 x ccr2*	*ccd8 x ccr2*
31	Dihydro-6MHO	6.8 ± 1.6	5.5 ± 1.5	3.4 ± 0.9	7.4 ± 2.3	4.5 ± 0.9	3 ± 1
1	6MHO	13.5 ± 2.3	26.8 ± 7	19.3 ± 7.3	31.6 ± 8.1	18.9 ± 5.1	13.6 ± 3.5
32	2,6,6-trimethylcyclohexanone	37.9 ± 7.4	26.3 ± 5.2	13.9 ± 3.6	27 ± 2.4	17.9 ± 3.6	15.1 ± 3.4
3	α-cyclocitral	8.7 ± 1	4.2 ± 0.8	2 ± 0.7	4.6 ± 1.1	3.3 ± 0.6	2.3 ± 0.4
39	Citronellal	5.1 ± 0.9	23.3 ± 6.2	11.9 ± 2.2	8.3 ± 0.4	17.9 ± 3.6	11.3 ± 2.7
33	Isophorol	17 ± 2.8	10.4 ± 2	4.3 ± 1.4	9.4 ± 1.9	7.6 ± 1.3	7 ± 1.6
5	β-cyclocitral	43 ± 7.1	21.8 ± 4.4	7.1 ± 2.7	19.1 ± 3.9	14.4 ± 2.5	13.6 ± 3.6
9	β-homocitral	3 ± 0.5	t (1.6 ± 0.3)	ǂ (0.6 ± 0.2)	1.6 ± 0.3	1.1 ± 0.2	1 ± 0.3
10	Trans-citral	4.3 ± 0.5	6 ± 1.2	4.2 ± 1.4	6.4 ± 1	4.4 ± 0.8	3.5 ± 0.9
34	Menthalactone	ǂ (0.008 ± 0.0016)	ǂ (0.004 ± 0.0009)	ǂ (0.001 ± 0.0005)	ǂ (0.002 ± 0.0006)	ǂ (0.002 ± 0.0003)	ǂ (0.002 ± 0.0005)
35	Cis-β-ionone	0.8 ± 0.08	0.54 ± 0.06	0.26 ± 0.06	0.61 ± 0.14	0.4 ± 0.08	0.37 ± 0.07
12	Hexahydropseudoionone	0.48 ± 0.06	0.33 ± 0.05	0.2 ± 0.05	0.34 ± 0.03	0.22 ± 0.04	0.2 ± 0.05
14	α-ionone	2.59 ± 0.43	0.34 ± 0.06	0.15 ± 0.06	0.39 ± 0.09	0.21 ± 0.05	0.2 ± 0.05
37	2(3H)-B	t (0.073 ± 0.008)	t (0.045 ± 0.006)	ǂ (0.019 ± 0.0071)	t (0.041 ± 0.009)	ǂ (0.034 ± 0.0058)	ǂ (0.03 ± 0.0054)
15	Cis-geranylacetone	n.d	0.005 ± 0.001	0.007 ± 0.002	0.007 ± 0.002	0.003 ± 0.002	0.004 ± 0.001
17	Trans-geranylacetone	0.12 ± 0.02	1.4 ± 0.14	0.53 ± 0.09	2.01 ± 0.57	0.48 ± 0.12	0.4 ± 0.14
19	β-ionone	26.5 ± 2.8	21.2 ± 2.5	9.9 ± 3.8	15.1 ± 4.1	14.7 ± 1.8	14.1 ± 3.2
20	5,6-epoxy-β-ionone	2.6 ± 0.3	2 ± 0.3	0.8 ± 0.3	1.4 ± 0.4	1.3 ± 0.2	1.1 ± 0.3
21	3-trans-5-cis-pseudoionone	n.d	1.2 ± 0.3	2.1 ± 1.1	1.3 ± 0.5	1.1 ± 0.5	0.9 ± 0.3
23	Dihydroactinidiolide	6.4 ± 0.5	5.1 ± 0.5	2.7 ± 0.9	4 ± 1	4.2 ± 0.4	3.8 ± 0.5
38	3,7,11-trimethyl-1-dodecanol	4 ± 0.4	4.8 ± 0.7	3.6 ± 0.8	4.1 ± 0.6	3.6 ± 0.4	3.8 ± 0.9
25	Hexahydrofarnesylacetone	9.9 ± 0.6	15.3 ± 1.6	12.8 ± 2.6	10.4 ± 2.6	11.4 ± 1.1	10.8 ± 3
29	Trans-farnesylacetone	n.d	55.8 ± 9.6	76.1 ± 32.6	28.7 ± 9.5	46.9 ± 11.7	37 ± 11.6
	Total Apocarotenoids	193 ± 29	234 ± 44	176 ± 63	184 ± 41	175 ± 35	143 ± 37

t = trace compound detected at concentration below the limit-of-quantification; ǂ = trace compound detected at concentration below limit-of-detection (estimated concentrations provided in parentheses)

n.d = not detected

Values are ± standard error; n = 4 per genotype

Table 5.2: Volatile apocarotenoids observed in leaves from Col-0, *ccr2* and *ccd x ccr2* double mutants

		Volatile apocarotenoid concentration (ng/g FW)				
#	Compound	Col-0	*ccr2*	*ccd1;4 x ccr2*	*ccd1;7 x ccr2*	*ccd4;7 xccr2*
31	Dihydro-6MHO	n.d	n.d	n.d	n.d	n.d
1	6MHO	13 ± 4.9	26 ± 6.7	85 ± 7.7	40 ± 3.2	62 ± 25
32	2,2,6-trimethyl-cyclohexanone	38 ± 14	29 ± 5.7	37 ± 10	22 ± 6	27 ± 6
3	α-cyclocitral	8.1 ± 2.7	3.8 ± 0.7	10.7 ± 1	6.1 ± 0.6	6.3 ± 2.2
39	Citronellal	4.9 ± 1.7	25 ± 6.5	45.9 ± 6.1	28.7 ± 2.1	10.6 ± 2.7
33	Isophorol	16 ± 5.5	10 ± 1.89	23.4 ± 2.3	14.6 ± 0.4	15.2 ± 5.4
5	β-cyclocitral	45 ± 22	22 ± 4.5	78 ± 8	44 ± 3	51 ± 22
9	β-homocitral	3.5 ± 0.41	1.5 ± 0.3	13.35 ± 1.66	5.49 ± 1.37	4.15 ± 1.37
10	Trans-citral	4 ± 1	6.5 ± 1.33	12.6 ± 1.1	7.6 ± 0.8	9.2 ± 2.8
34	Menthalactone	ǂ (0.008 ± 0.0059)	ǂ (0.004 ± 0.001)	ǂ (0.012 ± 0.004)	ǂ (0.005 ± 0.0007)	ǂ (0.008 ± 0.005)
35	Cis-β-ionone	0.88 ± 0.38	0.56 ± 0.06	1.71 ± 0.19	1.08 ± 0.03	1.18 ± 0.35
12	Hexahydropseudoionone	0.52 ± 0.06	0.32 ± 0.05	0.55 ± 0.04	0.35 ± 0.01	0.5 ± 0.06
14	α-ionone	2.73 ± 0.47	0.34 ± 0.07	4.04 ± 0.88	1.12 ± 0.12	1.05 ± 0.53
37	2(3H)-B	0.073 ± 0.048	0.04 ± 0.006	0.188 ± 0.028	0.107 ± 0.012	0.105 ± 0.058
15	Cis-geranylacetone	n.d	t (0.006 ± 0.001)	t (0.006 ± 0.0012)	t (0.002 ± 0.0003)	t (0.004 ± 0.0006)
17	Trans-geranylacetone	0.15 ± 0.01	1.31 ± 0.1	22.6 ± 2.4	30.5 ± 6.9	21.5 ± 6.8
19	β-ionone	25 ± 4	22 ± 2	207 ± 19	112 ± 9	55 ± 17
20	5,6-epoxy-β-ionone	3 ± 1	2 ± 0.3	24 ± 3	11 ± 1	6 ± 2
21	3-trans-5-cis-pseudoionone	n.d	1.3 ± 0.3	1.4 ± 0.22	1.2 ± 0.2	n.d
23	Dihydroactinidiolide	3.5 ± 0.4	4.8 ± 0.5	13.3 ± 1.7	5.5 ± 1.4	4.1 ± 1.4
38	3,7,11-trimethyl-1-dodecanol	4 ± 1	4.9 ± 0.7	12.6 ± 1.1	7.6 ± 0.8	9.2 ± 2.8
25	Hexahydrofarnesylacetone	10.5 ± 0.6	14 ± 1.6	17 ± 1.2	13 ± 1.6	13.5 ± 1.4
29	Trans-farnesylacetone	n.d	59 ± 9.6	57 ± 5.7	42.2 ± 9.2	25.5 ± 11.2
	Total Apocarotenoids	186 ± 61	234 ± 44	684 ± 71	407 ± 48	323 ± 111

t = trace compound detected at concentration below the limit-of-quantification; ǂ = trace compound detected at concentration below limit-of-detection (estimated concentrations provided in parentheses)

n.d = not detected

Values are ± standard error; n = 4 per genotype

Table 5.3: Volatile apocarotenoids observed in inflorescences from Col-0, *ccr2* and *ccd x ccr2* single mutants

		Volatile apocarotenoid concentration (ng/g FW)					
#	Compound	Col-0	*ccr2*	*ccd1 x ccr2*	*ccd4 x ccr2*	*ccd7 x ccr2*	*ccd8 x ccr2*
1	6MHO	41 ± 11	109 ± 21	106 ± 28	121 ± 31	86 ± 23	62 ± 13
32	2,2,6-trimethylcyclohexanone	120 ± 15	131 ± 31	109 ± 21	109 ± 21	89 ± 3	61 ± 7
3	β-cyclocitral	181 ± 17	105 ± 8	117 ± 25	151 ± 39	120 ± 24	87 ± 20
7	*Cis*-citral	24 ± 4	25 ± 7	28 ± 5	37 ± 7	23 ± 4	22 ± 5
		8.01 ±	5.72 ±	5.04 ±		5.39 ±	3.67 ±
9	β-homocitral	0.81	1.63	0.75	7.01 ± 1.4	0.88	0.91
10	*Trans*-citral	12 ± 1.57	23 ± 9.88	28 ± 4.35	36 ± 5.4	28 ± 5.71	23 ± 4.12
			1.71 ±		2.26 ±		1.59 ±
35	*Cis*-β-ionone	2.25 ± 0.2	0.12	1.7 ± 0.25	0.55	1.9 ± 0.44	0.45
		0.51 ±	0.024 ±	0.4 ±	0.469 ±	0.426 ±	0.333 ±
12	Hexahydropseudoionone	0.022	0.01	0.072	0.058	0.022	0.058
		6.43 ±	0.47 ±	0.58 ±	1.16 ±	0.66 ±	
14	α-ionone	0.18	0.23	0.06	0.16	0.11	0.44 ± 0.1
			0.168 ±	0.192 ±	0.528 ±	0.195 ±	0.167 ±
15	*Cis*-geranylacetone	n.d	0.028	0.076	0.17	0.06	0.016
		0.43 ±	23.47 ±		42.15 ±	8.12 ±	6.65 ±
17	*Trans*-geranylacetone	0.12	9.67	8.9 ± 3.67	1.03	3.34	2.74
19	β-ionone	77 ± 8	53 ± 3	69 ± 11	85 ± 23	69 ± 15	66 ± 16
		5.16 ±	3.13 ±	4.13 ±		4.21 ±	3.42 ±
20	5,6-epoxy-β-ionone	0.76	0.71	0.88	5.14 ± 1.5	1.08	0.86
			1.58 ±	3.54 ±	2.54 ±	3.07 ±	
21	3-*trans*-5-*cis*-pseudoionone	n.d	0.49	0.51	0.47	0.26	3.71 ± 0.4
23	Dihydroactinidiolide	22 ± 3.48	14 ± 3.88	17 ± 2.36	17 ± 4.34	16 ± 3.72	16 ± 2.98
25	Hexahydrofarnesylacetone	54 ± 12	49 ± 28	76 ± 15	76 ± 12	63 ± 8	106 ± 20
29	*Trans*-farnesylacetone	n.d	217 ± 60	171 ± 24	99 ± 22	87 ± 22	165 ± 35
	Total Apocarotenoids	552 ± 73	785 ± 186	736 ± 138	792 ± 170	597 ± 110	621 ± 127

t = trace compound detected at concentration below the limit-of-quantification; ǂ = trace compound detected at concentration below limit-of-detection (estimated concentrations provided in parentheses)

n.d = not detected

Values are ± standard error; n = 4 per genotype

Table 5.4: Volatile apocarotenoids observed in inflorescences from Col-0, *ccr2* and *ccd x ccr2* double mutants

		Volatile apocarotenoid concentration (ng/g FW)				
#	Compound	Col	*ccr2*	*ccd1;4 x ccr2*	*ccd1;7 x ccr2*	*ccd4;7 x ccr2*
1	6MHO	41 ± 14	162 ± 81	503 ± 206	340 ± 22	538 ± 189
32	2,2,6-trimethylcyclohexanone	126 ± 37	131 ± 29	268 ± 106	327 ± 57	274 ± 107
3	β-cyclocitral	183 ± 91	109 ± 40	267 ± 95	751 ± 122	580 ± 244
7	*Cis*-citral	18 ± 2.74	23 ± 14.33	98 ± 49.82	93 ± 15.86	174 ± 83.72
9	β-homocitral	8.3 ± 4.44	7.04 ± 3.25	22.22 ± 9.51	35.1 ± 12.25	29.96 ± 13.02
10	*Trans*-citral	11 ± 4.69	31 ± 17.88	154 ± 70.69	104 ± 29.88	197 ± 75.51
35	*Cis*-β-ionone	2.71 ± 0.79	2.38 ± 1.07	4.67 ± 1.32	6.74 ± 1.2	6.48 ± 1.46
12	Hexahydropseudoionone	0.48 ± 0.084	0.432 ± 0.172	1.107 ± 0.454	0.825 ± 0.376	0.924 ± 0.305
14	α-ionone	7.95 ± 0.16	10.49 ± 1.89	23.26 ± 4.2	39.83 ± 14.85	84.15 ± 13.95
15	*Cis*-geranylacetone	n.d	0.017 ± 0.006	0.04 ± 0.019	0.028 ± 0.004	0.024 ± 0.01
17	*Trans*-geranylacetone	0.48 ± 0.12	7.93 ± 2.8	68.67 ± 27.64	25.1 ± 7.6	61.94 ± 32.61
19	β-ionone	79 ± 33	48 ± 17	100 ± 34	279 ± 109	288 ± 154
20	5,6-epoxy-β-ionone	5.3 ± 0.78	3.32 ± 0.71	14.99 ± 4.38	18.86 ± 7.94	30.54 ± 6.64
21	3-*trans*-5-*cis*-pseudoionone	n.d	3.85 ± 0.43	7.2 ± 2.59	4.62 ± 0.78	5.91 ± 2.55
23	Dihydroactinidiolide	10 ± 3.71	10 ± 4.33	22 ± 10.15	28 ± 12.49	41 ± 19.18
25	Hexahydrofarnesylacetone	53 ± 19	47 ± 16	152 ± 53	56 ± 19	165 ± 74
29	*Trans*-farnesylacetone	n.d	195 ± 41	1541 ± 317	456 ± 215	1474 ± 330
	Total Apocarotenoids	546 ± 211	791 ± 272	3248 ± 992	2565 ± 647	3953 ± 1347

t = trace compound detected at concentration below the limit-of-quantification; ǂ = trace compound detected at concentration below limit-of-detection (estimated concentrations provided in parentheses)

n.d = not detected

Values are ± standard error; n = 4 per genotype

Table 5.5: Leaf carotenoid concentrations in Col-0, *ccr2* and *ccd x ccr2* mutants

	Leaf carotenoid concentration (µg/g, fresh weight)								
	Col	ccr2	ccd1 x ccr2	ccd4 x ccr2	ccd7 x ccr2	ccd8 x ccr2	ccd1;4 x ccr2	ccd1;7 x ccr2	ccd4;7 x ccr2
Cyclic Carotenes and Xanthophylls									
Lutein	195 ± 39.05	32 ± 5.02	29 ± 3.82	26 ± 4.54	41 ± 4.53	24 ± 2.58	83 ± 9.27	35 ± 0.59	44 ± 5.68
Antheraxanthin	12 ± 2.14	38 ± 4.66	31 ± 4.31	34 ± 5.13	30 ± 3.9	46 ± 0.91	29 ± 3.6	32 ± 1.38	32 ± 3.6
Neoxanthin	35 ± 7.33	24 ± 2.52	26 ± 3.19	24 ± 3.86	25 ± 3.94	24 ± 3.84	31 ± 2.56	30 ± 1.46	30 ± 2.96
Violaxanthin	45 ± 6.82	69 ± 7.59	96 ± 11.05	91 ± 14.7	86 ± 9.7	89 ± 13.61	100 ± 5.08	102 ± 3.09	102 ± 6.43
β-carotene	160 ± 28.48	134 ± 13.04	137 ± 16.98	127 ± 17.98	129 ± 19.76	141 ± 14.58	163 ± 16.21	151 ± 4.01	161 ± 19.68
Linear Carotenes									
Phytoene	0.16 ± 0.01	0.18 ± 0.01	0.18 ± 0.03	0.21 ± 0.03	0.18 ± 0.02	0.18 ± 0.02	0.16 ± 0.01	0.17 ± 0	0.15 ± 0.01
Phytofluene	n.d	5.17 ± 0.24	0.65 ± 0.09	5.27 ± 0.77	0.42 ± 0.09	7.29 ± 0.59	0.42 ± 0.04	0.51 ± 0.06	3.94 ± 0.2
ζ-carotenes	n.d	0.66 ± 0.08	n.d	0.44 ± 0.07	n.d	n.d	n.d	n.d	0.27 ± 0.07
Neurosporene-pre	n.d	40.35 ± 4.47	22.1 ± 2.91	7.8 ± 1.45	10.74 ± 1.65	27.48 ± 7.58	15.07 ± 0.97	6.16 ± 0.61	79.95 ± 19.65
Neurosporene-aft	n.d	67.51 ± 2.54	60.59 ± 6.76	143.84 ± 22.53	29.54 ± 0.96	155.31 ± 8.6	45.57 ± 8.36	49.77 ± 9.77	104.43 ± 10.74
Cis-lycopenes	n.d	2.23 ± 0.29	0.14 ± 0	1.65 ± 0.4	0.03 ± 0.01	1.12 ± 0.16	1.25 ± 0.14	0.13 ± 0.02	1.81 ± 0.27
Cyclic Carotenes and Xanthophylls Total	446 ± 83.83	297 ± 32.83	318 ± 39.35	301 ± 46.22	310 ± 41.82	324 ± 35.52	406 ± 36.73	350 ± 10.54	369 ± 38.34
Linear Carotenes Total	0 ± 0.11	116 ± 7.63	84 ± 9.81	159 ± 25.25	41 ± 2.73	191 ± 16.95	62 ± 9.51	57 ± 10.47	191 ± 30.93
Total Carotenoids	446 ± 83.94	413 ± 40.46	402 ± 49.16	460 ± 71.47	351 ± 44.55	515 ± 52.46	468 ± 46.24	407 ± 21.01	560 ± 69.27
Total Volatile Apocarotenoids	186 ± 61	234 ± 44	176 ± 63	184 ± 41	175 ± 35	143 ± 37	684 ± 71	407 ± 48	323 ± 111
Apocarotenoid/Carotenoid ratio (ng:µg, FW)	0.417 ± 0.066	0.566 ± 0.051	0.438 ± 0.048	0.4 ± 0.054	0.499 ± 0.056	0.278 ± 0.026	1.461 ± 0.131	1 ± 0.049	0.577 ± 0.064

Values are ± standard error; n = 4 for all genotypes

Table 5.6: Inflorescence carotenoid concentrations in Col-0, *ccr2* and *ccd x ccr2* mutants

	Inflorescence carotenoid concentrations (µg/g, fresh weight)								
	Col	*ccr2*	*ccd1 x ccr2*	*ccd4 x ccr2*	*ccd7 x ccr2*	*ccd8 x ccr2*	*ccd1;4 x ccr2*	*ccd1;7 x ccr2*	*ccd4;7 x ccr2*
Cyclic Carotenes and Xanthophylls									
Lutein	190 ± 8.66	87 ± 5.68	30 ± 1.18	33 ± 3.89	25 ± 1.78	26 ± 0.2	54 ± 8.55	70 ± 1.47	91 ± 4.19
Antheraxanthin	7.54 ± 0.57	42.82 ± 6.88	13.76 ± 0.2	11.56 ± 1.29	11 ± 0.94	13.01 ± 0.85	33.47 ± 4.52	56.52 ± 3.41	45.39 ± 0.45
Violaxanthin	58 ± 3.13	148 ± 17.72	85 ± 1.46	78 ± 7.29	69 ± 4.65	70 ± 1.58	143 ± 21.27	197 ± 8.18	183 ± 19.05
Neoxanthin	31 ± 1.53	38 ± 5.36	22 ± 0.46	20 ± 2.25	18 ± 1.23	18 ± 0.64	34 ± 5.58	49 ± 2.7	47 ± 5.78
β-carotene	138 ± 6.54	193 ± 21.44	115 ± 5.28	120 ± 11.51	95 ± 6.64	99 ± 3.53	218 ± 32.89	254 ± 14.91	247 ± 27.18
Linear Carotenes									
Phytoene	0.208 ± 0.012	0.184 ± 0.012	0.154 ± 0.005	0.176 ± 0.005	0.142 ± 0.006	0.179 ± 0.019	0.247 ± 0.029	0.202 ± 0.018	0.207 ± 0.021
Phytofluene	n.d	5.64 ± 0.75	5.83 ± 0.33	6.64 ± 0.2	5.01 ± 0.35	2.78 ± 0.1	15.99 ± 2.45	8.29 ± 0.89	14.69 ± 1.38
ζ-carotene	n.d	0.635 ± 0.021	0.264 ± 0.027	1.07 ± 0.041	0.615 ± 0.02	0.533 ± 0.022	1.16 ± 0.165	1.015 ± 0.124	1.402 ± 0.082
Neurosporene-pre	n.d	61 ± 1.59	31 ± 0.13	52 ± 2.22	24 ± 0.76	23 ± 2.23	38 ± 4.45	58 ± 5.5	21 ± 3.02
Neurosporene-aft	n.d	122 ± 2.25	129 ± 5.5	110 ± 5.8	96 ± 10.41	109 ± 17.29	180 ± 19.32	163 ± 5.87	196 ± 19.32
Cis-lycopenes	n.d	0.018 ± 0.004	1.497 ± 0.189	4.322 ± 0.055	1.319 ± 0.079	1.09 ± 0.199	0.104 ± 0.014	0.211 ± 0.007	0.135 ± 0.019
Cyclic Carotenes and Xanthophylls Total	424.44 ± 20.43	508.95 ± 57.08	266.23 ± 8.58	262.42 ± 26.23	217.19 ± 15.24	226.22 ± 6.79	482.75 ± 72.81	627.28 ± 30.67	612.61 ± 56.66
Linear Carotenes Total	0.21 ± 0.05	189.64 ± 4.63	167.32 ± 6.18	174.4 ± 8.32	127.93 ± 11.63	136.55 ± 19.87	234.75 ± 26.42	230.1 ± 12.4	232.73 ± 23.84
Total Carotenoids	425 ± 20.48	699 ± 61.71	434 ± 14.76	437 ± 34.55	345 ± 26.87	363 ± 26.65	717 ± 99.24	857 ± 43.07	845 ± 80.5
Total Volatile Apocarotenoids	552 ± 73	785 ± 198	754 ± 143	800 ± 172	611 ± 114	627 ± 128	3248 ± 992	2565 ± 647	3953 ± 1347
Apocarotenoid/Carotenoid ratio (ng:µg, FW)	1.3 ± 0.06	1.124 ± 0.091	1.739 ± 0.057	1.831 ± 0.134	1.77 ± 0.128	1.728 ± 0.118	4.527 ± 0.55	2.992 ± 0.143	4.676 ± 0.407

Values are ± standard error; n = 4 for all genotypes

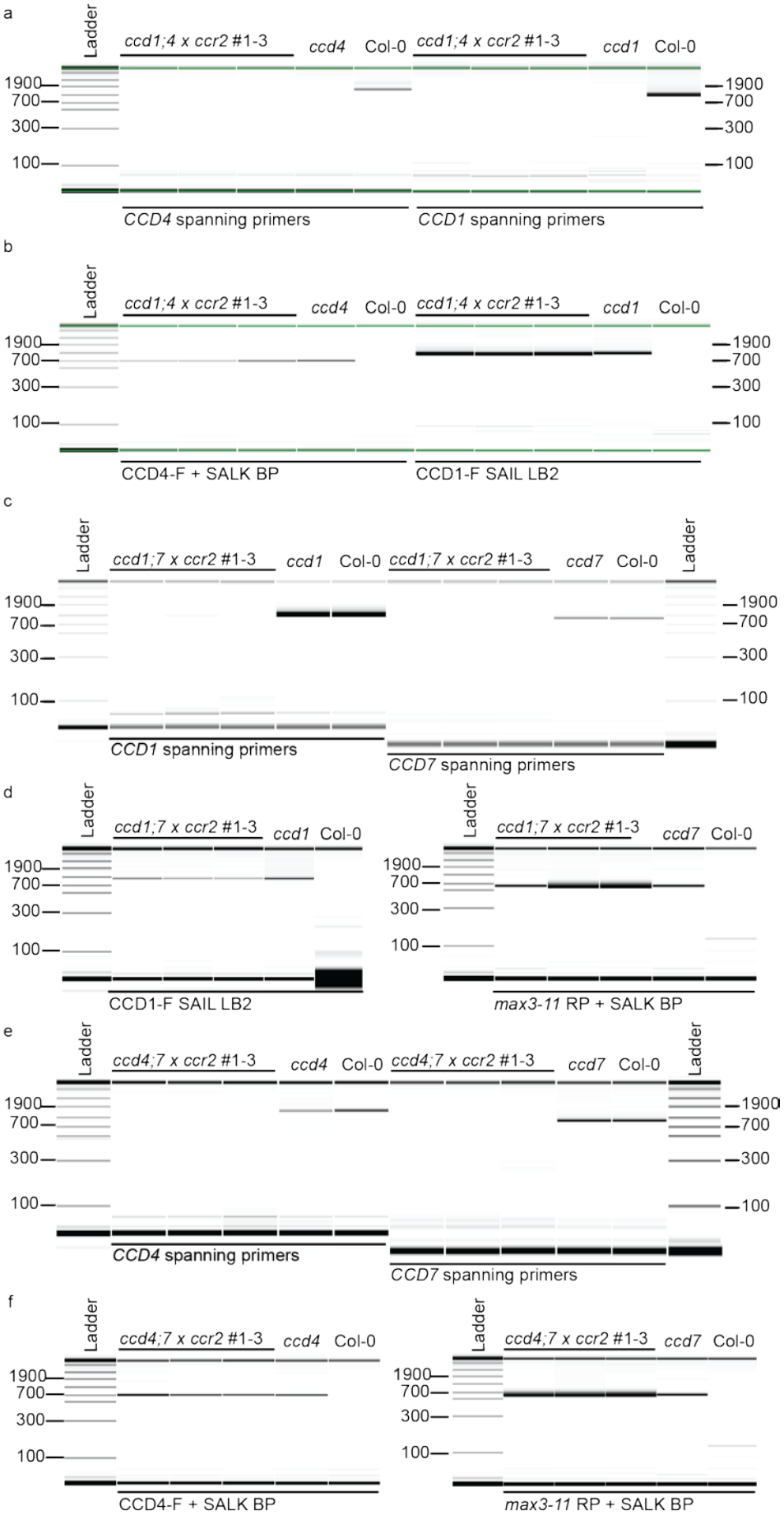
a
Ladder
ccd1;4 x ccr2 #1-3
ccd4
Col-0
ccd1;4 x ccr2 #1-3
ccd1
Col-0
1900
700
300
100
CCD4 spanning primers
CCD1 spanning primers
b
Ladder
ccd1;4 x ccr2 #1-3
ccd4
Col-0
ccd1;4 x ccr2 #1-3
ccd1
Col-0
CCD4-F + SALK BP
CCD1-F SAIL LB2
c
Ladder
ccd1;7 x ccr2 #1-3
ccd1
Col-0
ccd1;7 x ccr2 #1-3
ccd7
Col-0
Ladder
CCD1 spanning primers
CCD7 spanning primers
d
Ladder
ccd1;7 x ccr2 #1-3
ccd1
Col-0
CCD1-F SAIL LB2
Ladder
ccd1;7 x ccr2 #1-3
ccd7
Col-0
max3-11 RP + SALK BP
e
Ladder
ccd4;7 x ccr2 #1-3
ccd4
Col-0
ccd4;7 x ccr2 #1-3
ccd7
Col-0
Ladder
CCD4 spanning primers
CCD7 spanning primers
f
Ladder
ccd4;7 x ccr2 #1-3
ccd4
Col-0
CCD4-F + SALK BP
Ladder
ccd4;7 x ccr2 #1-3
ccd7
Col-0
max3-11 RP + SALK BP

Supplementary Figure 5.1: Confirmation of T-DNA mutations in the *ccr2*-background *ccd1;4*, *ccd1;7* and *ccd4;7* double mutant lines.

Following isolation of putative *ccr2*-background *ccd1;4*, *ccd1;7*, and *ccd4;7* double mutants from the relevant F2 populations, the disruption of *CCD1*, *CCD4* and/or *CCD7 via* T-DNA insertions was verified by PCR. DNA extracts from the putative double mutant lines (three representative, independent, lines per genotype are depicted here) were assayed using primers that span the expected insertion sites for the *CCD1* (a and c), *CCD4* (a and e) and *CCD7* (c and e) genes. T-DNA insertions were further validated using a primer set comprised of a T-DNA border primer and a primer annealing to a portion of the endogenous gene, for *CCD1* (b and d), *CCD4* (b and f), and *CCD7* (d and f). For each assay, the relevant single *ccd* loss-of-function mutant and Col-0 (wild type) controls were also included. Capillary electrophoresis results are depicted in the above figure as digital gel images. Ladder fragment sizes are (bottom to top): 100, 300, 500, 700, 1100, 1900, 2900, 4900 and 7000.

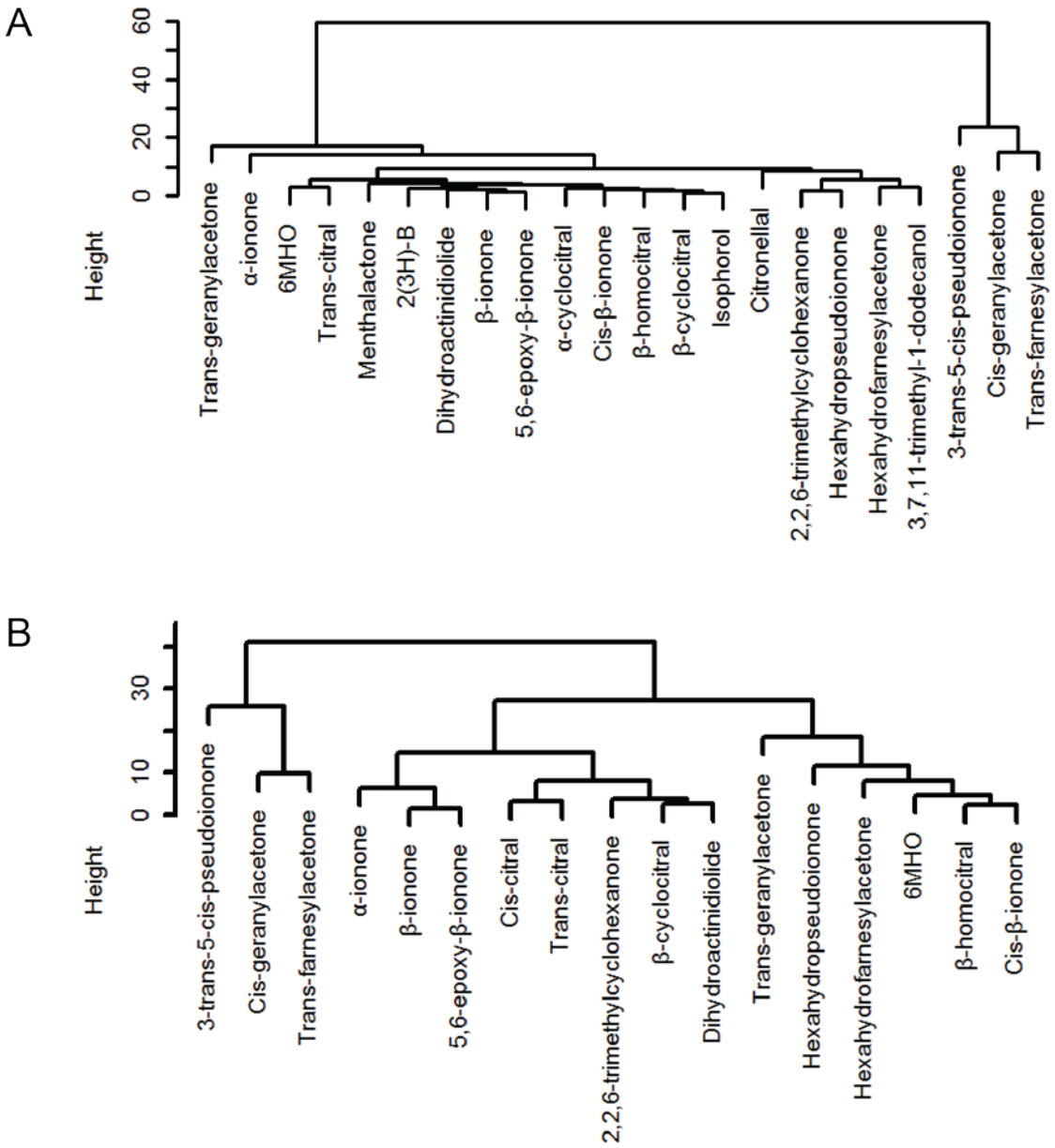

Supplementary Figure 5.2: Hierarchical clustering analysis of volatile apocarotenoid abundance across Col-0, *ccr2*, and *ccd x ccr2* mutants

HCAs were performed on log_2-transformed metabolite abundance, expressed as fold-changes relative to the mean *ccr2* values) for a) leaf and b) inflorescence volatiles.

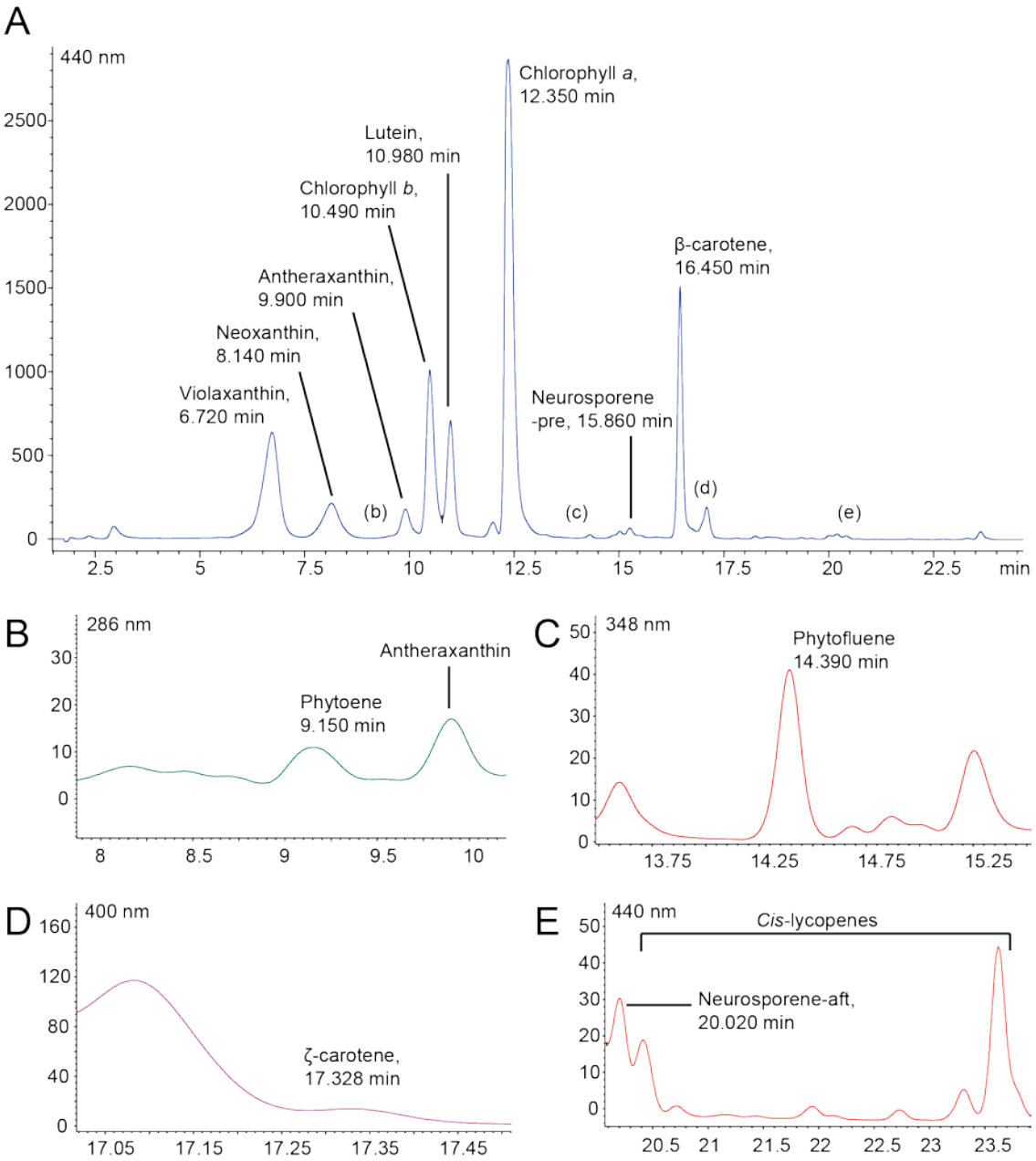

Supplementary Figure 5.3: Representative HPLC-DAD chromatogram depicting carotenoids and chlorophylls

A sample chromatogram from HPLC analysis of carotenoids and chlorophylls in *ccr2* leaf tissue is presented here to depict the orders of elution for the HPLC analytes. In addition to the main chromatogram, recorded at 440 nm (a), zoomed-in chromatograms at varying wavelengths are presented to show lower-abundance peaks (b-e). Typical UV-visible spectra obtained for the labelled analytes, and structures of the carotenoid analytes, are presented in Figure A.2.

Chapter Six: CCD4 and CCD1 function and volatile apocarotenoid abundance during leaf senescence

6.1 Overview

A more targeted approach was taken in this chapter, with volatile apocarotenoids profiled in Col-0, *ccd1*, *ccd4* and *ccd1;4* leaves over a dark-induced senescence time-course. The aims of this chapter can be described as follows:

1. To quantify changes in volatile apocarotenoids during *Arabidopsis* dark-induced leaf senescence,
2. To describe CCD1 and CCD4 function during leaf senescence in terms of volatile apocarotenoid production and/or carotenoid catabolism, and
3. To explore the possibility an ACS is involved in negative regulation of thylakoid degradation/senescence.

6.2 Results

6.2.1 Dark-induced senescence protocol successfully applied

This senescence assay was carried out as described by Rottet *et al.* (2016), to best-replicate the observed changes in carotenoid concentration and observe any attendant changes in volatile apocarotenoids. Briefly, dark-induction was carried out by detaching whole rosettes and placing them on moistened filter paper at room temperature in a darkened chamber. The 0 d time-point was sampled 1 h after start of dark-induction, and 3 d and 7 d time-points were subsequently also photographed and analysed. As revealed by photographs, the dark-induction regime successfully induced senescence, with extensive senescent leaf-yellowing visible in all genotypes by 7 d post-dark-induction (Figure 6.1). As expected (Grassl *et al.* 2012), photos taken at the 3 d time-point revealed few visible signs of senescence (Figure 6.1B). No difference in extent or rate of senescence was obvious from rosette images (Figure 6.1), nor was there any difference when senescence was assessed using the SGR1 senescence marker gene (see section 6.2.4).

6.2.2 Volatile apocarotenoid abundance varies in response to dark-induced senescence; no CCD-dependence apparent

Examining the volatile apocarotenoid profiles for Col-0, *ccd1*, *ccd4* and *ccd1;4* over the three dark-induction time-points, few genotype-dependent differences in volatile apocarotenoid abundance were observed (Figure 6.2). *ccd1;4* exhibited significantly higher levels of 3,7,11-trimethyl-1-dodecanol compared to Col-0 3 d post dark-induction, and significantly higher levels of 6MHO 7 d post dark-induction. Additionally, *ccd1* had significantly higher levels of 5,6-epoxy-β-ionone 7 d post dark-induction. The bases of these differences from wild-type behaviour is unclear, although subtle differences in chloroplastic conditions may be responsible.

These phenomena notwithstanding, volatile apocarotenoids exhibited remarkably similar senescence-dependent changes in abundance across all genotypes. With the aid of HCA, three patterns of senescence-dependent volatile apocarotenoid response were discerned (Figure 6.3A): 1) apocarotenoids that progressively decreased in abundance with increased time post dark-induction, 2) apocarotenoids that exhibited a more limited senescence-dependent decrease in abundance (~50% decline between 0 and 7 d post dark-induction) and 3) apocarotenoids that increased in abundance post dark-induction. Additionally, dark-induced senescence seemed to introduce immediate changes in apocarotenoid profile compared to that of normally-sampled leaf tissue (likely due to changes in oxidative conditions arising from cessation of photosynthesis): in 0 h time-point samples, neither 5,6-epoxy-β-ionone nor *trans*-geranylacetone were detected in leaf samples, although both increased in abundance 3 and 7 d post dark-induction.

Considering the changes to volatile apocarotenoid profile with increased time post dark-induction however, 0 d post dark-induction samples were clearly separated from 3 and 7 d post dark-induction samples in the PCA (Figure 6.3B), along an axis defined by a combination of PC1 (accounting for 59% of between-sample variation) and PC2 (14% of variation). As expected, Group 1 compounds were associated with 0 d post dark-induction samples whilst Group 3 compounds were associated with 3 and 7 d post dark-induction samples. Genotypes however, were not distinguished by these two principal components, reflecting the inability to observe many significant differences in apocarotenoid abundance between genotypes. The smaller Group 2 volatile apocarotenoid subset appeared to be largely orthogonal to the 0, 3 and 7 d post dark-induction axis. Still, compound abundance did not vary in any way linked to either time-point or genotype.

6.2.3 Carotenoid concentrations elevated in *ccd4* and *ccd1*-backgrounds

Col-0, *ccd1, ccd4* and *ccd1;4* leaves were analysed *via* HPLC at 0, 3 and 7 d post dark-induced senescence. The observed 0 d carotenoid profiles (Figure 6.4A) were essentially consistent with those observed for leaves under normal conditions (Table 4.6), with β-carotene, lutein, neoxanthin and violaxanthin all detected. Interestingly however, antheraxanthin was present in small quantities in Col-0 and *ccd1;4* leaves at 0 d post dark-induction but was not detected in *ccd1* and *ccd4* samples. Apart from antheraxanthin, carotenoid concentrations did not differ significantly between genotypes at the 0 d time-point (Figure 6.4).

Considering the senescence time-course, findings were consistent with previous work. *Ccd4* exhibited elevated (2-2.5-fold) β-carotene and lutein concentrations relative to Col-0 7 d post dark-induction (Figure 6.4). Significantly higher levels of both violaxanthin and antheraxanthin were observed in *ccd4* at 7 d post dark-induction (approximately two-fold relative to Col-0). No significant differences were observed for neoxanthin (Figure 6.4).

Unexpectedly, these trends in carotenoid concentration were not entirely replicated in *ccd1;4*. At 7 d post dark-induction, neither β-carotene nor lutein concentrations were significantly higher than Col-0, although violaxanthin and antheraxanthin levels were. *ccd1* levels of violaxanthin were also higher relative to Col-0 7 d post dark-induction, being comparable to *ccd1;4*. No differences in either chlorophyll *a* or *b* abundances were observed (Figure 6.4B).

The differences in final carotenoid concentration between *ccd4* and *ccd1;4* notwithstanding, loss of function of CCD4 and, to a lesser extent, CCD1 had clear effects upon carotenoid catabolism, as reflected in the percent-changes in carotenoid concentration for the different genotypes going from 0 to 7 post dark-induction (Figure 6.5).

Whilst levels of β-carotene, lutein, violaxanthin and neoxanthin all declined in Col-0 after 7 d dark-induction (~50% decrease; Figure 6.5), carotenoid abundances responded differently in the other genotypes. In *ccd4*, β-carotene concentration actually increased marginally after 7 d dark-induction, whilst *ccd1* and *ccd1;4* concentrations only declined 35% and 25% respectively.

CCD4 loss-of-function had an even clearer effect upon senescence-dependent percent-change in lutein, neoxanthin and violaxanthin. *ccd1;4* levels of these carotenoids were unchanged 7 d post dark-induction and *ccd4* lutein and violaxanthin concentrations were elevated ~25% over the senescence time-course (Figure 6.5).

No comparisons of antheraxanthin senescence-dependent percent-change could be made given percent-changes could not be calculated for *ccd1* or *ccd4*, although it seems clear antheraxanthin increases markedly in all genotypes upon senescence. The significance of this remains unclear.

Overall, these differences in carotenoid percent-change translated into significantly higher total carotenoid concentration in *ccd4* relative to Col-0 7 d post dark-induced senescence (Figure 6.6A). It is also of note that, whilst *ccd1* and Col-0 total carotenoids decline on going from the 0 to 3 to 7 d time-points, *ccd1;4* total carotenoids were unchanged over this time-course (Figure 6.6A).

Higher total carotenoids in *ccd4*, and similar total volatile apocarotenoids across genotypes (Figure 6.6B), meant that *ccd4* apocarotenoid:carotenoid ratio was significantly lower than all other genotypes at 7 d post dark-induced senescence (Figure 6.6C).

6.2.4 Dark-induced senescence reflected in *SGR1* induction; CCD4 also induced in response to senescence

Finally, I examined expression of *CCD1* and *CCD4*, and the senescence marker genes *SGR1*, *WRKY53* and *DGAT3*, upon dark-induced senesce in Col-0, *ccd1*, *ccd4* and *ccd1;4* (Figure 6.7). *CCD1* expression was consistently reduced in *ccd1* and *ccd1;4* relative to Col-0/*ccd4* levels over the time-course, but did not exhibit any response to dark-induction (Figure 6.7A). In contrast, *CCD4* expression peaked 3 d post dark-induction (Figure 6.7A). This trend was observed in all genotypes, with the 3 d post dark-induction *CCD4* expression significantly higher than 0 d for Col-0, *ccd1* and *ccd4* (Figure 6.7B; *ccd1;4* expression of *CCD4* at 3 d was only significantly higher relative to 7 d levels). The persistence of this senescence-dependent peak in *CCD4* expression, even in *ccd4*-background plants, suggests a strong tendency for RNA Polymerase read-through to affect assessment of T-DNA gene knockout *via* qPCR (as was likely observed in Chapters Four and Five). RNA Polymerase read-through is also believed to be responsible for the

lack of reduced *CCD4* expression in *ccd1;4* (0 d post dark-induced *CCD4* expression in *ccd1;4* is unchanged from Col-0 levels).

Considering the senescence marker genes, *SGR1* responded to dark-induction as previously reported. After 3 d dark-induction, *SGR1* expression was elevated eight-fold in all genotypes, and continued to be similarly elevated 7 d post dark-induction. No differences in expression levels were discerned between genotypes.

Unexpectedly, *WRKY53* and *DGAT3* responses to dark-induced senescence were at odds with previous reports of senescence-dependent induction (Grassl, *et al.* 2012, Lundquist, *et al.* 2012). *WRKY53* expression actually decreased around four-fold in all genotypes 3 d post dark-induction; 7 d levels were unchanged from 3 d or were further decreased. At the same time, *DGAT3* expression did not significantly vary in response to dark-induced senescence in any of the genotypes (Figure 7).

This inability to replicate *WRKY53* and *DGAT3* senescence-dependent expression induction may stem from differences in type of senescence conditions analysed. Lundquist *et al*. (2012) observed *DGAT3* induction by comparing leaves from plants of markedly different ages: young, green, pre-bolting leaves compared to senescent leaves from anthesis and post-anthesis plants, whilst Grassl *et al*. (2012) observed *WRKY53* upregulation upon dark-induction in individual leaves (attached to whole plants) covered in foil. In contrast, I adhered to the dark-induced senescence protocol employed by Rottet *et al*. (2016), in which whole rosettes were detached and left in the dark (on moistened filter paper). Inability to induce *WRKY53* and *DGAT3* might point to additional environmental cues being required for *WRKY53* and *DGAT3* senescence-dependent induction. Such factors were however beyond the scope of this study.

The alternative possibility, that this study did not induce senescence effectively, seems unlikely given the other senescence phenotypes observed. In any case, dark-induction has replicated the changes in carotenoid abundance reported by Rottet *et al*. (2016), meaning the conclusions concerning CCD function and senescence-dependent apocarotenoid and carotenoid metabolism are valid.

6.2.5 Summary

In this chapter, I directly observed volatile apocarotenoids produced by senescence-dependent carotenoid breakdown. Carotenoid content changes led Rottet *et al*. (2016) to conclude CCD4 degrades β-carotene and lutein during senescence. Here, SPME-GC/MS

was used to verify if β-carotene cleavage to β-ionone occurs, and whether CCD4 is indeed responsible. Other volatile apocarotenoids were also profiled. Results by Rottet *et al*. (2016) were also extended with analysis of the *ccd1* and *ccd1;4* mutants, testing for contribution by CCD1 to senescence-dependent volatile apocarotenoid production/carotenoid catabolism. *ccd1;4* was also analysed to address the possibility of redundancy. Plants were sampled 0, 3 and 7 days post dark-induced senescence; the 3 d time point was chosen given previous studies have demonstrated that 3 d post dark-incubation represents a good model for studying initiation of senescence (Grassl, *et al.* 2012). The 7 d time-point was chosen given it was the point at which Rottet *et al*. (2016) observed significant differences in carotenoid levels between Col-0 and *ccd4*.

Senescing-leaf apocarotenoid biology was also of interest given the possibility of a senescence-retarding ACS. If such a CCD4-derived ACS exits, I anticipated it might manifest itself in *accelerated* thylakoid membrane degradation in *ccd4*-background leaves. Leaf appearance and chlorophyll abundance were monitored across the different genotypes. Progress of thylakoid degradation was also assessed by assaying expression of senescence reporter genes: *STAYGREEN1* (*SGR1*), *DIACYLGLYCEROL ACYLTRANSFERASE 3* (*DGAT3*), and *WRKY DNA-BINDING PROTEIN 53* (*WRKY53*). *SGR1* complexes with light-harvesting complex protein II (LHCPII) in thylakoid membranes and recruits chlorophyll catabolising enzymes to break down LHCPII-associated chlorophyll (Grassl, *et al.* 2012, Park *et al.* 2007). *DGAT3* is a plastoglobule-localised enzyme speculated to be involved in production of triacylglycerols (Hernández *et al.* 2012, Lundquist, *et al.* 2012). *WRKY35* is a senescence-induced transcription factor (Lundquist, *et al.* 2012, Zentgraf *et al.* 2010). Absence of the senescence-retarding ACS might be expected to perturb marker induction in the *ccd4*-background genotypes.

The results appear to rule out CCD4-mediated cleavage of β-carotene to β-ionone, given all genotypes' β-ionone levels uniformly declined over the senescence time-course. CCD4-dependent β-ionone production would only be feasible if there was rapid turnover of β-ionone such that levels remain indistinguishable between *ccd4* and the other genotypes. Such a possibility has not been discussed in the literature. Given the majority of volatile apocarotenoids mirror β-ionone in a genotype-independent, decrease in abundance over the senescence time-course, it is most likely that production of β-ionone and other volatile apocarotenoids is entirely independent of CCD4 and CCD1, as proposed in Chapters Four and Five. Instead, results suggest CCD4 cleaves lutein, and possibly neoxanthin and violaxanthin as well, which would be consistent with previous

studies (Lätari, *et al.* 2015, Rottet, *et al.* 2016). The findings here could be extended with further information regarding the expression of carotenogenic genes and/or abundance of proteins – this would clarify for example, if the observed increases in β-carotene, lutein, violaxanthin, and antheraxanthin result from reduced xanthophyll-cleavage alone, or if changes in carotenoid biosynthetic activity are also a factor.

There was also no evidence for the previously mooted senescence-retarding ACS, with expression of senescence marker *SGR1* unchanged between genotypes over the duration of the time-course. Possibilities regarding the senescence-retarding ACS are discussed further in the next chapter.

6.3 Figures and Tables

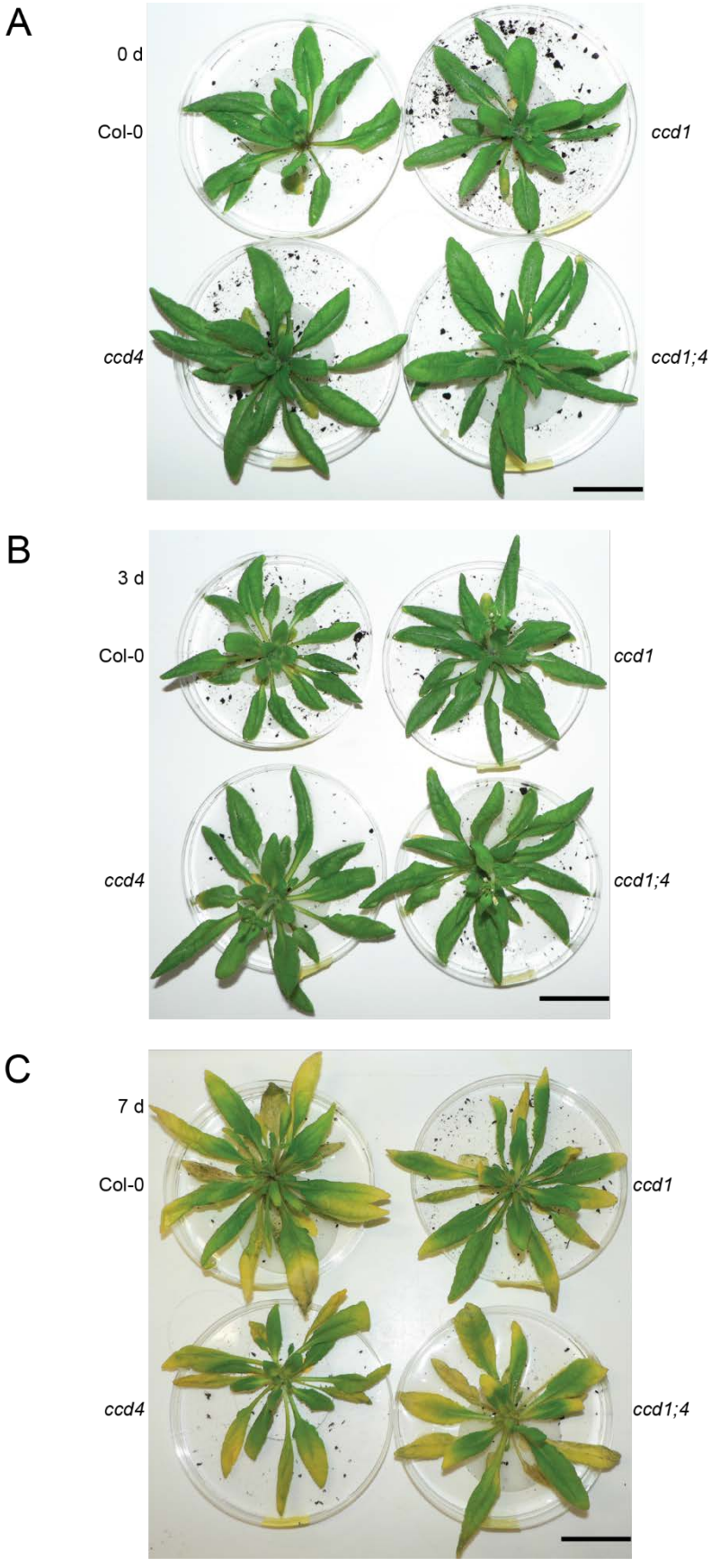

Figure 6.1: Col-0, *ccd1*, *ccd4* and *ccd1;4* rosettes 0, 3 and 7 d post-dark-induction

Col-0, *ccd1*, *ccd4* and *ccd1;4* rosettes from 35 d old plants were excised and dark-incubated for 1 h (so-called “0 d” time-point, A), 3 d (B) and 7 d (C). Black scale bars represent 3 cm in all images.

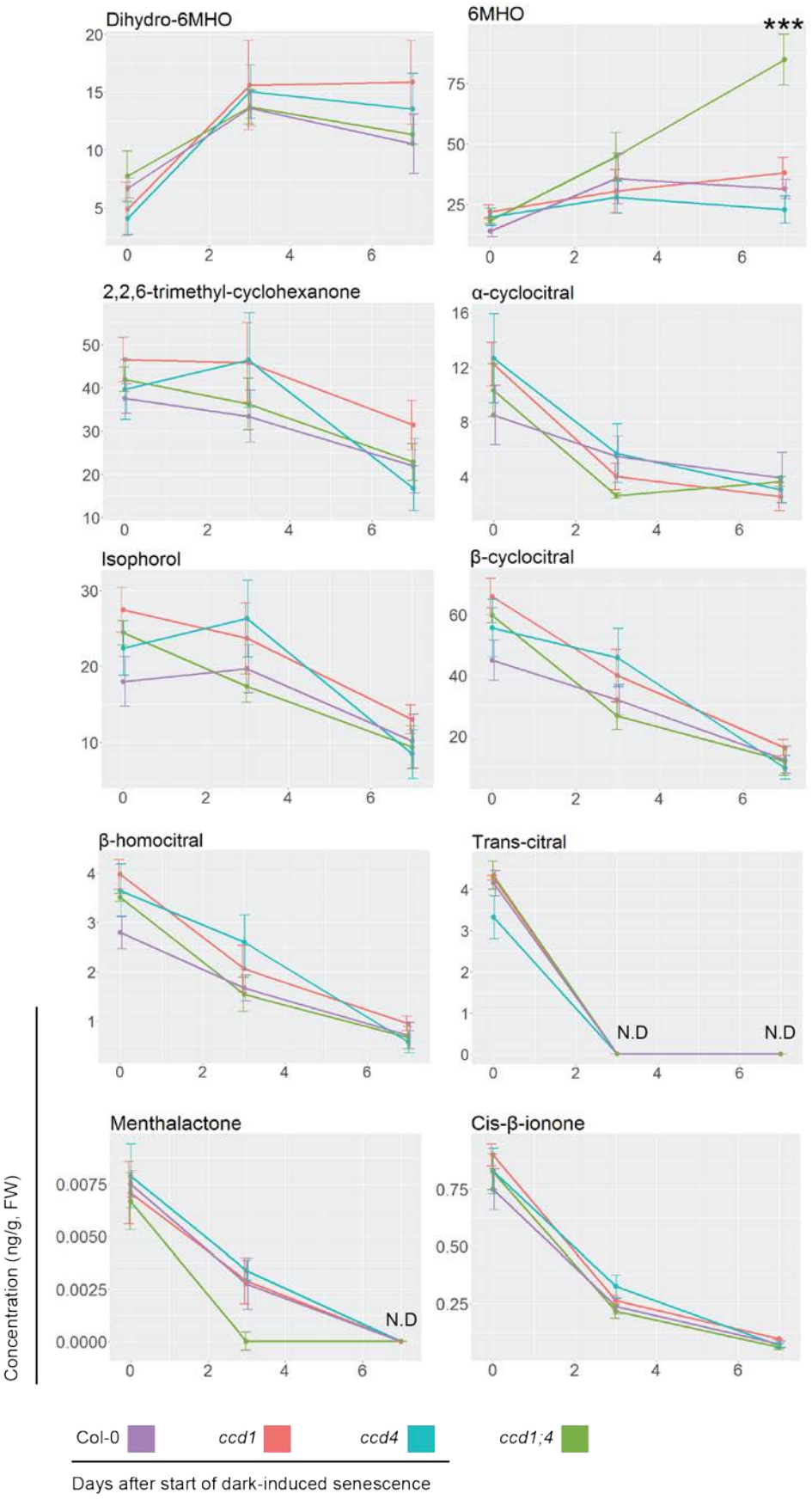
Dihydro-6MHO
6MHO
***
2,2,6-trimethyl-cyclohexanone
α-cyclocitral
Isophorol
β-cyclocitral
β-homocitral
Trans-citral
N.D
N.D
Menthalactone
N.D
Cis-β-ionone
Concentration (ng/g, FW)
Col-0
ccd1
ccd4
ccd1;4
Days after start of dark-induced senescence

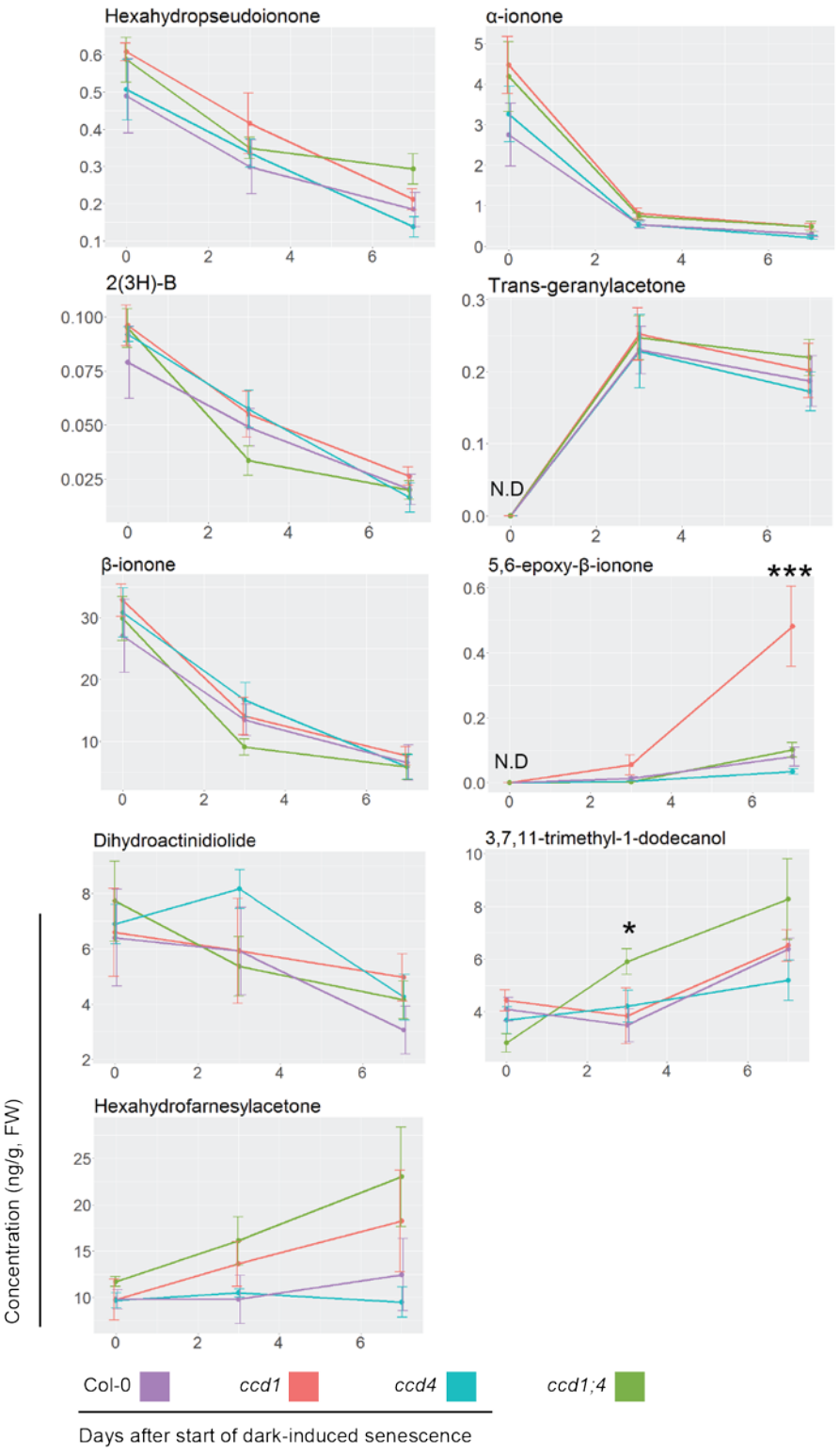

Figure 6.2: Change in volatile apocarotenoid concentration during dark-induced senescence

The concentrations for all volatile apocarotenoids detected in senescing leaves were plotted 0, 3 and 7 d post dark-induction, for Col-0 (purple), *ccd1* (red), *ccd4* (cyan) and *ccd1;4* (green). Values are plotted ± standard error. Statistical significance was calculated for selected genotype compound concentrations, relative to Col-0 concentration, at specific timepoints. * = $p < 0.05$, *** = $p < 0.001$, Student's t-test. N.D = not detected. *n* = 4 per genotype.

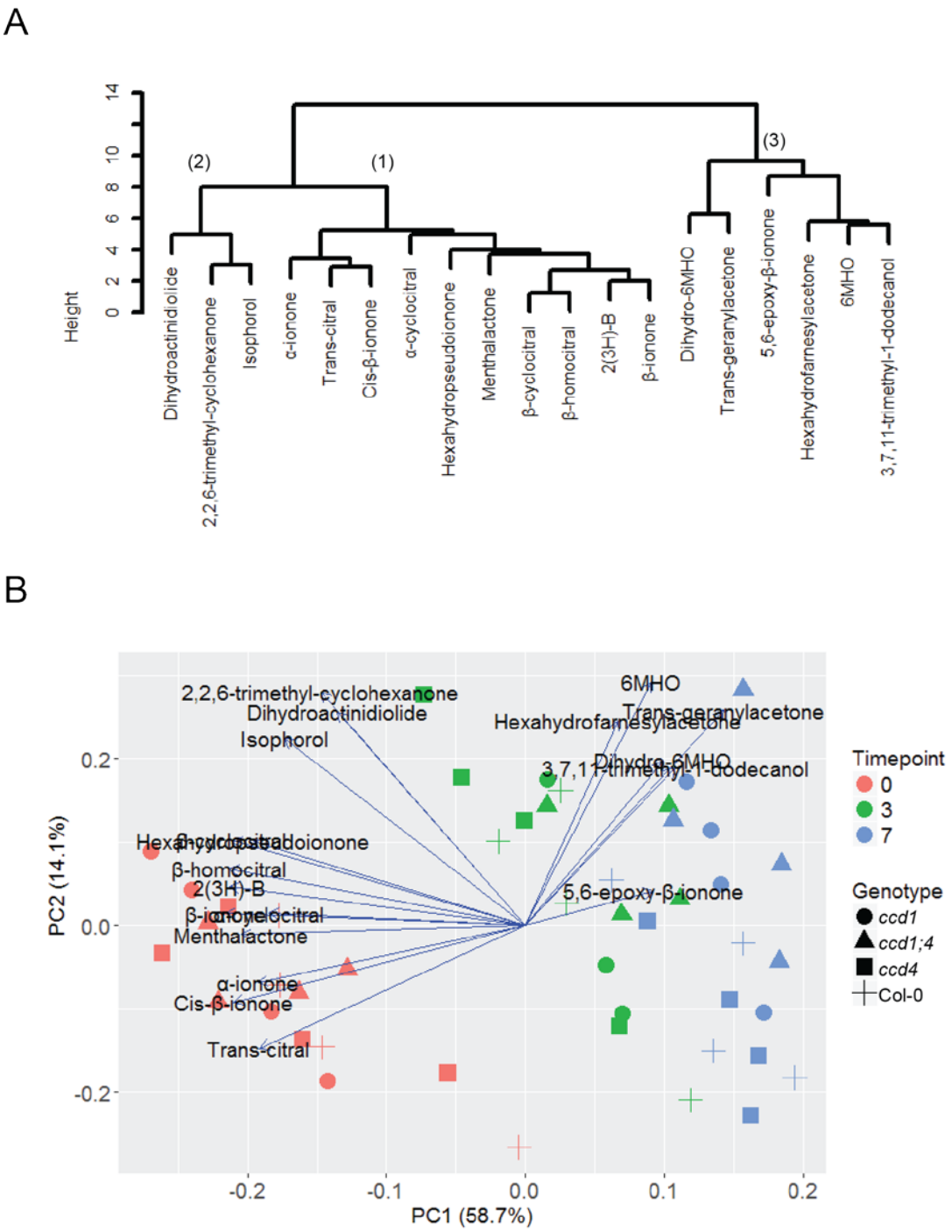

Figure 6.3: Clustering analyses of senescence-dependent leaf volatile apocarotenoid response in Col-0, *ccd1*, *ccd4* and *ccd1;4*

HCA (a) and PCA (b) were conducted upon normalised volatile apocarotenoid concentrations observed in Col-0, *ccd1*, *ccd4* and *ccd1;4* leaves 0, 3 and 7 d post dark-induction. Clusters numbered 1-3 have been used to highlight prominent compound clusters in the HCA cluster dendrogram. Samples on the PCA plot of the first two principal components have been colour-coded according to senescence time-point; shapes represent genotypes. The loadings for the first two principal components have been projected onto the plot.

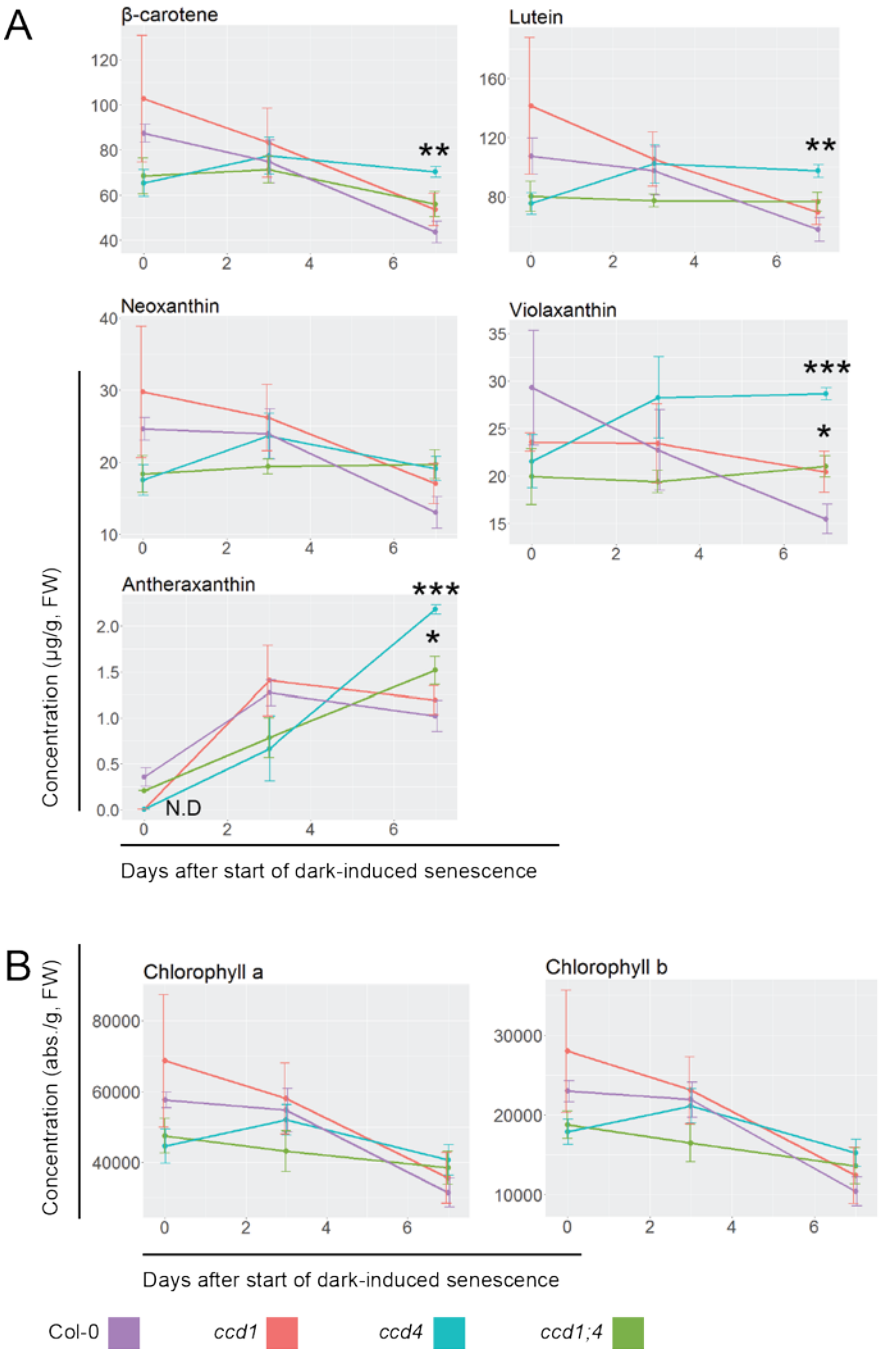

Figure 6.4: Change in carotenoid and chlorophyll abundance during dark-induced senescence

The concentrations for all carotenoids detected in senescing leaves were plotted 0, 3 and 7 d post dark-induction for Col-0 (purple), *ccd1* (red), *ccd4* (cyan) and *ccd1;4* (green; a). Chlorophyll *a* and *b* abundance (b) during senescence was similarly plotted. Values are plotted ± standard error. Statistical significance was calculated for selected genotype compound abundances, relative to Col-0 abundance, at specific time-points. * = $p < 0.05$, ** = $p < 0.01$, *** = $p < 0.001$, Student's t-test. N.D = not detected. *n* = 3 per genotype.

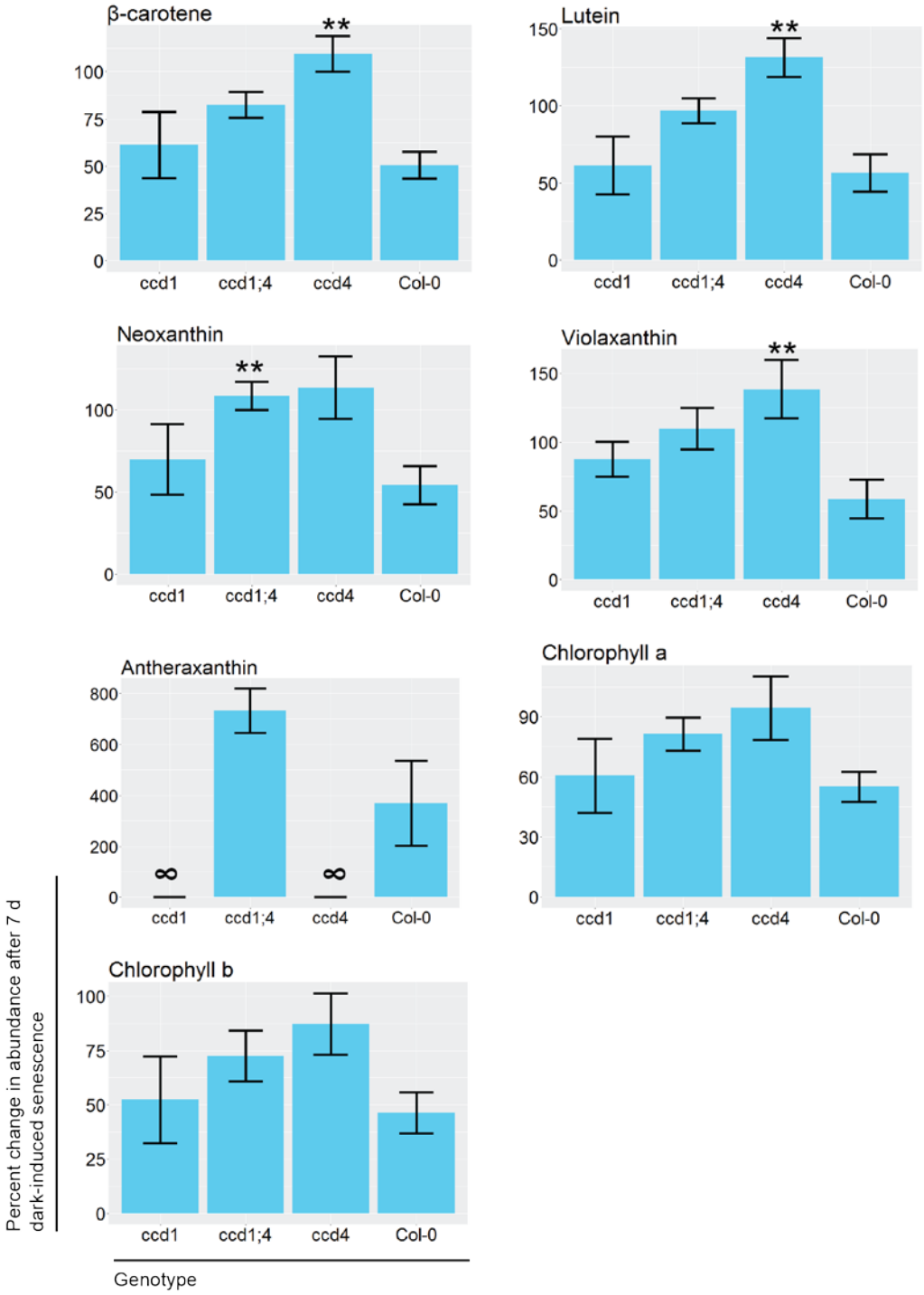

Figure 6.5: Percent-change in carotenoid and chlorophyll abundance between start and end of dark-induced senescence

Relative changes in carotenoid and chlorophyll abundances between 0 and 7 d post dark-induction were calculated for each genotype and expressed as a percent-change. Values are presented ± standard error. Statistical significance was calculated relative to Col-0 values for selected genotype compound percent-changes. ** = $p < 0.05$. ∞: antheraxanthin percent-changes could not be calculated for *ccd1* or *ccd4* given antheraxanthin was not detected in 0 d samples. $n = 3$ per genotype.

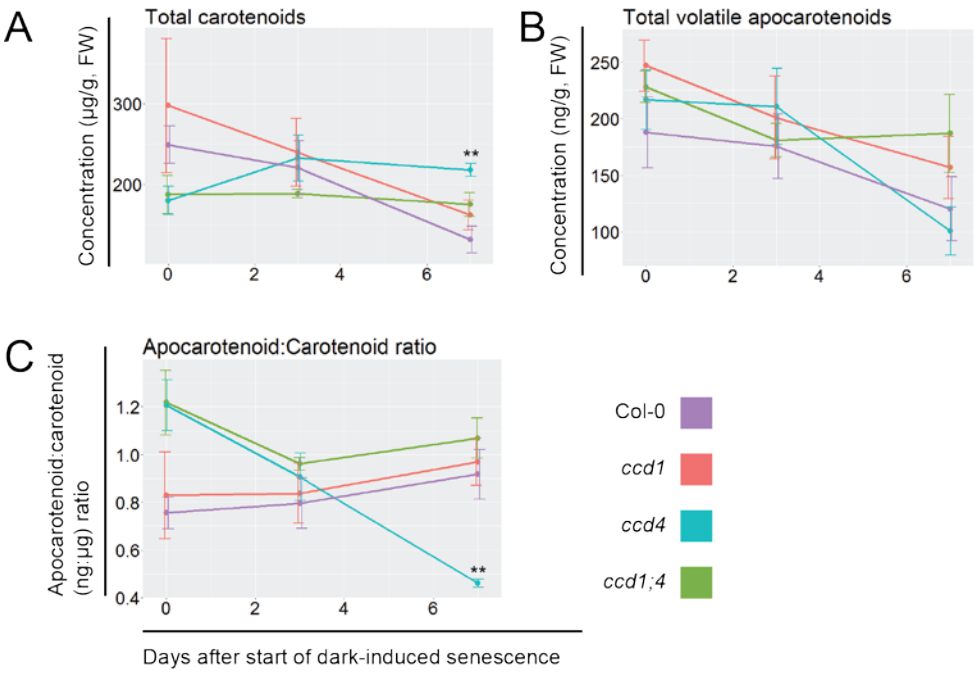

Figure 6.6: Change in total carotenoids and volatile apocarotenoids during dark-induced senescence

Total leaf carotenoids (a), volatile apocarotenoids (b) and volatile apocarotenoid:carotenoid ratio (ng:µg, c) were plotted 0, 3 and 7 d post dark-induction for Col-0 (purple), *ccd1* (red), *ccd4* (cyan) and *ccd1;4* (green). Values are plotted ± standard error. Statistical significance was calculated for selected genotype values relative to Col-0 values are specific time-points. ** = $p < 0.01$, Student's t-test. *n* = 3 per genotype.

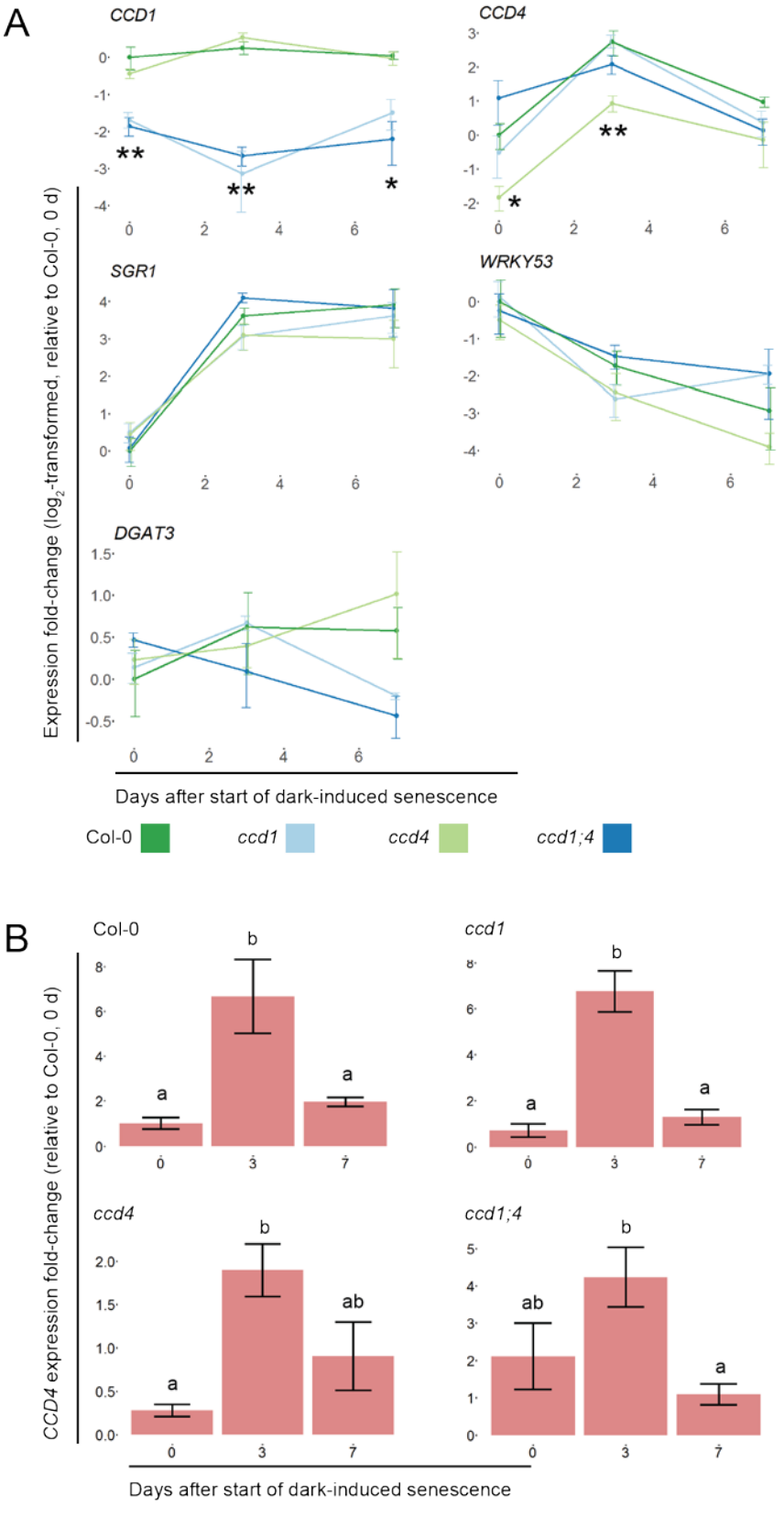

Figure 6.7: Expression of *CCD1, CCD4, SGR1, WRKY53* and *DGAT3* during dark-induced senescence

Expression of *CCD1*, *CCD4*, *SGR1*, *WRKY53* and *DGAT3* 0, 3 and 7 d post dark-induction were plotted (relative to Col-0, 0 d expression) for Col-0 (dark green), *ccd1* (light blue), *ccd4* (light green) and *ccd1;4* (dark blue; A). The induction of *CCD4* 3 d post dark-induction in the four genotypes was also plotted in panel B (relative to Col-0, 0 d post dark-induction expression) to better-depict statistically significant differences. Values are plotted ± standard error. Statistical significance

in panel A is calculated for selected genotype expression values relative to Col-0 values at specific time-points. * = $p < 0.05$, ** = $p < 0.01$, Student's t-test. Statistical symbols in panel B represent significance at $p < 0.05$, based on ANOVA and post-hoc Tukey test. *n* = 3 per genotype.

Chapter Seven: General conclusions regarding apocarotenoid biosynthesis in *Arabidopsis thaliana*

7.1 New insights have been gained by untargeted SPME-GC/MS metabolomics *in planta*

New insights into volatile apocarotenoid and carotenoid metabolism have been obtained in this project by applying SPME-GC/MS with untargeted metabolomics to *in planta* measurement of known and putative volatile apocarotenoids. Following SPME method-optimisation I confirmed that my SPME-GC/MS method provided dramatically improved sensitivity for volatile (including semi-volatile) apocarotenoids compared to other common sampling methods (i.e. organic solvent extraction/liquid-injection, static gas-tight syringe headspace sampling). This finding was consistent with observations for other classes of volatiles/semi-volatiles (Cavalli, *et al.* 2003, Pfannkoch and Whitecavage 2000).

The exceptionally high sensitivity of SPME sampling, combined with noise-filtering mass spectral chromatogram deconvolution (Du and Zeisel 2013), facilitated the detection of a wide range of novel, putative, volatile apocarotenoids, addressing my first thesis research aim. Compounds such as β-homocitral, hexahydropseudoionone, citronellal and menthalactone are described in *Arabidopsis* for the first time using this metabolomics approach. Using hierarchical clustering I also demonstrated that abundances of these putative apocarotenoids were often correlated with known apocarotenoids, providing preliminary evidence suggesting these compounds originate from the apocarotenoid pathway. This experimental approach is different to many other previous *in planta* studies of apocarotenoids, in which more-limited numbers of known apocarotenoids were selectively monitored and reported (Ramel, *et al.* 2012a, Ramel, *et al.* 2012b, Wei, *et al.* 2011).

I also used simultaneous profiling of a broad range of volatile apocarotenoids to observe interesting patterns in compound abundance such as the close correlation of β-carotene-derived apocarotenoids in Col-0-background inflorescences (Chapter Four), and the strikingly divergent responses of the two major volatile apocarotenoid groups upon dark-induced senescence (Chapter Six). These patterns, sometimes analysed more quantitatively using PCA and HCA, also gave clues as to the biosynthetic origins of these volatiles (Rizhsky, *et al.* 2016, Sánchez, *et al.* 2012), be that likely common precursors

(e.g. β-carotene, Chapter Four), or similar oxidative conditions precipitating non-enzymatic synthesis (Chapter Six).

I was also able to provide additional evidence that three volatile apocarotenoids, *cis*-geranylacetone, 3-*trans*-5-*cis*-pseudoionone and *trans*-farnesylacetone, are produced from *Arabidopsis* tissue when linear carotenes accumulate in 8 h photoperiod, *ccr2*-background plants (Chapter Five). These compounds are somewhat novel, being undetectable in wild-type *Arabidopsis*, although they have been reported in other species (Tikunov, *et al.* 2005, Vogel, *et al.* 2010a). Using 8 h photoperiod, *ccr2*-background, plants as a model for studying volatile apocarotenoid metabolism, I also observed elevated levels of 6MHO, *trans*-geranylacetone and citronellal, further suggesting these compounds are also linear carotene-derived apocarotenoids.

But, SPME is not without its challenges. The requirement for fresh tissue in the sampling protocol restricts the number of samples that can be run at a time. This can complicate experimental design. I compared Col-0 to *ccd* single and double mutants separately, for example, to keep sample queue-time low, and to ensure maintenance of biological sample integrity; the same was done for *ccr2*-background analyses. Whilst, as demonstrated here, SPME is very sensitive and useful for identifying trends and forming new hypotheses, a targeted organic extraction/liquid injection protocol may be more practical for routine analyses, once compounds of interest have been identified. The use of selected-ion-monitoring or alternative GC/MS hardware (e.g. orbitrap GC/MS) would be expected to overcome the reduced sensitivity that I observed with other sampling methods (Chapter Two).

7.2 Cold-EI technology of interest but not currently fit for purpose

Whilst the application of SPME-based untargeted metabolomics was a clear example of new technologies leading to new biological insights, my evaluation of cold-EI revealed it to be unsuitable, in its current form, for plant volatile analysis. Cold-EI-GC/MS yielded very promising results when tested against plant volatile standards (Chapter Three), markedly improving the observed $M^{+\bullet}$ relative intensities in resulting GC/MS spectra, as has been observed for other analyte classes (Dagan and Amirav 1995, Patkin 2015a, Patkin 2015b). Moreover, the compound-class-dependent differences in cold-EI induced

$M^{+\bullet}$ enrichment will be of interest in the further development of this technology. When used to analyse volatiles, and particularly volatile apocarotenoids, however, cold-EI delivered little practical benefit in terms of enhancing compound identification *via* validation of putative MM against observed $M^{+\bullet}$. This stemmed from the low sensitivity of cold-EI-GC/MS caused by the high-volume make-up gas flow entering the MS ion source. Thus, although cold-EI had previously proved useful in the analysis of samples with higher analyte concentration, such as fuels and burn residues (Fialkov, *et al.* 2008), it was impractical for my analyses of trace volatile apocarotenoids. Although there are options for concentrating volatile samples prior to introduction onto GC/MS e.g. dynamic 'purge-trap' headspace sampling (Tieman, *et al.* 2006), these were not available to us, and thus I declined to use cold-EI in my subsequent, routine analyses.

7.3 Volatile apocarotenoids are most-likely non-enzymatically-derived

Addressing my second thesis research question, one of the most surprising findings from my research was the lack of any concurrent CCD loss-of-function and apocarotenoid absence, which would provide evidence for a given CCD being responsible for a particular apocarotenoid. Instead, most volatile apocarotenoids, across studies, appeared to follow essentially similar patterns of increase/decrease across *ccd* genotypes, or else displayed limited variation irrespective of genotype. This suggests volatile apocarotenoids by and large do not require CCD function for their biosynthesis and likely form non-enzymatically. The alternative explanation, that redundancy exists between all four CCDs, and can maintain production of all volatile apocarotenoids, appears implausible.

One exception to the non-enzymatic volatile apocarotenoid production theory was the observation of reduced β-ionone in *ccd1* and *ccd1;4* inflorescences (Chapter Four), corroborating previous studies of *CCD1*-overexpression that suggested CCD1 synthesises β-ionone in inflorescences (Wei, *et al.* 2011). And yet, even in inflorescences it appears CCD1 is not exclusively responsible for β-ionone production, given β-ionone was elevated in *ccd1;7* and *ccd4;7,* presumably due to increased non-enzymatic oxidation. I also observed that changes in β-ionone concentrations across the *ccd* mutant inflorescences in Chapter Four were correlated with changes in other β-carotene-derived

compounds that are known to be non-enzymatically-derived (i.e. β-cyclocitral and DHA). This further suggested non-enzymatic oxidation was the major factor influencing the abundance of many volatile apocarotenoids in that tissue.

Findings from Chapter Six provided more evidence suggesting non-enzymatic oxidation is responsible for volatile apocarotenoid production in a wide range of situations. Despite the observed *CCD4* expression increase in senescing leaves, a majority of volatile apocarotenoids decreased in abundance over the senescence time-course. This appears to reflect the importance of ROS (perhaps singlet oxygen in particular), derived during photosynthesis, in the production of volatile apocarotenoids. β-cyclocitral and β-ionone for example, can form *via* singlet oxygen attack upon β-carotene, and undergo an approximately ten-fold reduction in abundance between 0 and 7 d post dark-induction.

Sometimes, volatile apocarotenoid production appears to be dependent upon availability of precursor carotenoids. *Cis*-geranylacetone, 3-*trans*-5-*cis*-pseudoionone and *trans*-farnesylacetone were exclusively detected in *ccr2*-background samples; other linear carotene-derived apocarotenoids (6MHO, *cis*-citral, *trans*-citral, citronellal, etc.) were markedly elevated in these samples. Reduction of α-cyclocitral and α-ionone in *ccr2*-background, where *εLCY* expression is reduced (Cuttriss, *et al.* 2007), is also consistent with the above theory. But, availability of carotenoid substrate is not the only factor. The aforementioned decrease in leaf volatile apocarotenoids over the course of dark-induced senescence (Chapter Six) was consistent in all tested genotypes, despite the senescence-dependent decline in carotenoids being abolished in *ccd4* and *ccd1;4*. This suggests availability of both carotenoid substrate and cleaving ROS (singlet oxygen is the only documented species, but others may be active too) determine the extent of volatile apocarotenoid production.

Moreover, carotenoid oxidative cleavage seems quite nuanced. Results from Chapter Five reveal non-enzymatic cleavage exhibited a considerable degree of selectivity in the linear carotenes oxidised, cleavage regioselectivity and, thus, the apocarotenoid produced. Whilst phytoene was present in all genotypes, for example, *trans*-farnesylacetone is only observable in *ccr2*-background plants that accumulate phytofluene. It seems *trans*-farnesylacetone originates essentially exclusively from cleavage of phytofluene. This might be due to some aspect of phytoene sub-plastidial localisation that prevents non-enzymatic oxidation. Furthermore, of the four neurosporene/lycopene-derived apocarotenoids observed, 6MHO, *cis*-citral, *trans*-citral and 3-*trans*-5-*cis*-pseudoionone, their concentration follows the pattern: 6MHO > citrals > pseudoionone. This may reflect

a preference for singlet oxygen attack at the ends of the neurosporene/lycopene i.e. 5,6 and 7,8-cleavage, leading to 6MHO and citral production (Chapter One, Figure 1.2). This might be expected given the inner portions of the carotenoid substrate would be embedded within a lipid membrane, hindering oxygen attack.

It was similarly of note that *trans*-geranylacetone inflorescence abundance is consistent with differences in inflorescence ζ-carotene, but not neurosporene, concentration - suggesting *trans*-geranylacetone is formed predominately *via* ζ-carotene oxidation. This relationship was observed across *ccr2* and *ccd x ccr2* single mutant leaves. Although the link broke down when *ccd x ccr2* double mutant leaves were examined, elevated levels of *trans*-geranylacetone in double mutant lines may be influenced by other factors e.g. increased singlet oxygen levels.

My thesis results do suggest, however, that loss of CCD activity can affect oxidative conditions in photosynthetic tissue - indirectly influencing volatile apocarotenoid abundance. This would account for the most striking observations from my analyses, the dramatic increases in volatile apocarotenoids seen in *ccd* double mutants. This was observed in *ccd1;7* and *ccd4;7* inflorescences (Chapter Four), and both leaves and inflorescences of *ccd x ccr2* double mutants (Chapter Five).

Provided I assume CCDs cleave xanthophyll carotenoids in *Arabidopsis* leaves and inflorescences to form non-volatile apocarotenoids, it would appear emission of volatile apocarotenoids is elevated when CCD carotenoid-cleavage is perturbed. This in turn suggests inability of CCDs to cleave carotenoids promotes the oxidative conditions required for volatile apocarotenoid formation.

There may be a requirement for carotenoid homeostasis in photosynthetic tissue, balancing carotenoid anabolism with catabolism, which can occur *via* either CCD cleavage to non-volatile apocarotenoids, or non-enzymatic cleavage to volatile apocarotenoids. There seems to be some level of redundancy amongst CCDs for xanthophyll-cleavage, which would explain why a spike in volatile apocarotenoids was not observed in *ccd* single mutant tissues (Chapter Four).

This homeostasis proposal is consistent with findings of $^{14}CO_2$ pulse-chase experiments, which revealed a surprisingly high rate of carotenoid turnover in leaves (Beisel, *et al.* 2010). The need for homeostasis was also alluded to by the leaf chlorosis observed in the cross of *Arabidopsis PSY*-overexpression lines with *ccd4;* an inability to maintain carotenoid homeostasis seems to have deleterious effects.

Unfortunately, I only have indirect evidence of CCD-dependent non-volatile apocarotenoid formation in *Arabidopsis* tissues grown under normal conditions; the LC/MS method employed by Lätari *et al.* (2015) could, however, be used to investigate this. Limitation in my data non-withstanding, I suggest CCD4 has a role in production of non-volatile apocarotenoids. CCD4 is known to contribute to production of non-volatile apocarotenoid glycosides in *Arabidopsis* leaves *via* violaxanthin and antheraxanthin cleavage (Lätari, *et al.* 2015), and the results in Chapter Six suggest lutein is also cleaved by CCD4. CCD1 may, additionally, have a role in violaxanthin cleavage, given *ccd1* maintained violaxanthin levels over the course of the senescence time-course (Chapter Six). The increased leaf lutein levels in *ccd1;4 x ccr2* relative to *ccr2*, observed in Chapter Five are also consistent with a xanthophyll-catabolising role for CCD4 and CCD1. In *vitro* and *in bacterio* cleavage of violaxanthin by CCD1 has also been reported on many occasions (Huang *et al.* 2009a, Ibdah, *et al.* 2006, Vogel, *et al.* 2008).

Considering my homeostasis model, it would also appear CCD7 has a role in carotenoid catabolism to non-volatile apocarotenoids, explaining the observations of elevated volatile apocarotenoids in *ccd* double mutants containing the *ccd7* mutation (Chapter Four and Five)

One unresolved observation in this model is the fact that 16 h photoperiod *ccd* leaves (Chapter Four) did not exhibit any changes in volatile apocarotenoid concentration. It seems carotenoid biosynthetic rate was restricted instead. This regulation likely occurs at the PSY biosynthetic step (Chapter One): PSY transcriptional (and translational) abundance is a major determinant of carotenoid concentration in many species (Bowman *et al.* 2014, Fu *et al.* 2014, Li *et al.* 2008, Maass *et al.* 2009, Rodriguez-Villalon *et al.* 2009b), and there are many examples of transcriptional, translational and post-translational mechanisms regulating PSY function (Kachanovsky, *et al.* 2012, Lao *et al.* 2011, Li, *et al.* 2008, Ruiz-Sola *et al.* 2014, Shumskaya *et al.* 2012, Zhou *et al.* 2015). Study of PSY expression or protein abundance in *ccd* mutant tissues may yield further insight into *Arabidopsis* carotenoid homeostasis.

Differences in physiology between leaves and inflorescences may explain the prevalence of different carotenoid homeostatic-regulatory mechanisms (i.e. anabolism versus catabolism) observed in Chapter Four. The fact volatile apocarotenoids were elevated in both *ccr2*-background leaves and inflorescences (Chapter Five) may point to increased singlet oxygen accumulation, resulting from *ccr2*-background photosynthetic stress (Cuttriss, *et al.* 2007) which, in the absence of adequate CCD-dependent carotenoid

turnover (Lätari, *et al.* 2015), leads to elevated non-enzymatically-generated volatile apocarotenoids (Ramel, *et al.* 2012b).

Another outstanding question is why the spike in volatile apocarotenoids was not observed in *ccd1;4* inflorescences (Chapter Four) but was observed in *ccd1;4 x ccr2* tissues (Chapter Five). Given CCD1's cytoplasmic localisation (Simkin, *et al.* 2004a), it is possible CCD1 has a limited catabolic role in normally-developing chloroplasts. Changes in plastid structure - possible in *ccr2* tissues (Park, *et al.* 2002) or during senescence (Rottet *et al.* 2015) may increase the importance of CCD1-mediated carotenoid turnover.

This theory necessarily implies, however, that CCD7 function is more important to carotenoid catabolism (in normal chloroplasts) than CCD4, given *ccd1;7* inflorescences had elevated volatile apocarotenoids relative to Col-0 (Chapter Four). Closer examination of CCD7 and its *in planta* function(s) is clearly warranted (Bruno, *et al.* 2016); if CCD7 is important for carotenoid turnover, crossing of *ccd7* to *PSY-OX* may lead to chlorosis, as in the *ccd4 x PSY-OX* line (Lätari, *et al.* 2015).

And why is there an enzymatic pathway when volatile apocarotenoid production can be elevated to maintain carotenoid turnover? Perhaps an overabundance of volatile apocarotenoids has a deleterious effect. Due to its role in photosynthetic stress signalling, permanently high β-cyclocitral levels may impair normal photosynthetic capacity (Ramel, *et al.* 2012b) There is also some suggestion β-cyclocitral and other volatile apocarotenoids may be toxic to certain species of cyanobacteria (Arii, *et al.* 2015, Harada *et al.* 2009, Ozaki *et al.* 2008). Under normal conditions, CCD carotenoid cleavage to produce non-volatile apocarotenoids, possibly sequestered in cell vacuoles as glycosides (Lätari, *et al.* 2015), may be preferred - minimising exposure of plant tissue to volatile apocarotenoids that may act as specific stress signals (Ramel, *et al.* 2012b, Shumbe, *et al.* 2014) or more generally as reactive electrophile species, also known to have signalling properties (Farmer and Mueller 2013).

Interestingly, loss of the CCD-dependent carotenoid catabolic route does not appear to affect growth of either the *ccd* single or double mutants (beyond the strigolactone-deficient phenotype in *ccd7* and *ccd8* backgrounds), under normal conditions (Chapter Four and Five). There may however be other photosynthetic and/or oxidative stress conditions e.g. cold, high-light, fluctuating light quality, that require increased carotenoid turnover (Ramel, *et al.* 2013), and in which *ccd* mutants, particularly double mutants, will

manifest a phenotype related to loss of CCD function or overabundant volatile apocarotenoids.

7.4 SPME-GC/MS as a tool for ACS discovery: inconclusive but promising

Considering the potential of SPME-GC/MS for identification of volatile apocarotenoids as candidate ACS structures - the results are inconclusive. I was unable to corroborate evidence from previous studies that ACS2 and ACS1 are CCD-derived (Avendaño-Vázquez, *et al.* 2014, Hou 2015). Moreover, the search for the putative CCD4-derived ACS involved in negative-regulation of senescence, *via* study of *ccd4*-background mutants, was inconclusive.

Phenotyping of *ccr2* and the *ccd x ccr2* mutants under 8 h photoperiod (*via* leaf-yellowing assessment and lutein/chlorophyll measurements, Chapter Five) did not yield reversion of the *ccr2* phenotype to Col-0 wild-type, suggesting no CCD is solely responsible for producing ACS2. This however, contradicts findings made by colleagues (Hou 2015). Etiolated (dark-grown) *ccr2* seedlings are known to be defective in development of the prolamellar body (PLB), a precursor to chloroplasts and other plastids (Park, *et al.* 2002). Treatment of etiolated *ccr2* seedlings with a chemical inhibitor of CCD cleavage, D15 (Sergeant *et al.* 2009), led to wild-type PLB development, providing strong evidence the *ccr2* signal is an ACS arising from CCD activity (Hou 2015).

How can these observations be reconciled? Perhaps, in photosynthetic tissues, ACS2 is non-enzymatically derived due to the greater abundance of ROS. In etiolated seedlings however, CCD cleavage may be required. Alternatively, there may be redundancy such that even when combinations of CCD1, CCD4 and CCD7 are knocked out, the remaining CCDs are able to produce ACS2 levels that lead to manifestation of the *ccr2* phenotype.

Either scenario leaves open the possibility that any of the detected linear carotene-derived volatile apocarotenoids are ACS2. Some of these volatile apocarotenoids (6MHO, stereoisomeric mixtures of citrals, geranylacetones, pseudoionones and farnesylacetones) were applied to Col-0 plants, as part of work done in our laboratory prior to this thesis. But, these treatments could not replicate the *ccr2* phenotype (Hou 2015). It is possible an additional enzymatic step is required to transform these volatiles to ACS2, and that

exogenously-applied volatiles cannot access the subcellular compartments where this reaction takes place (Hou, *et al.* 2016). Alternatively, ACS2 may be the non-volatile, 'reciprocal', portion of a cleaved linear carotene.

Concerning ACS1, I found that three phytofluene/ζ-carotene-derived volatile apocarotenoids accumulate, *via* non-enzymatic activity, when these two linear carotenes are present in *Arabidopsis* (Chapter Five). It is thus possible ACS1 is one of these volatile apocarotenoids, a reciprocal non-volatile portion, or a derivative thereof. Interpretation is complicated given the *clb5* mutant, where the ACS1-associated phenotype was first reported, was reverted upon loss of CCD4 (Avendaño-Vázquez, *et al.* 2014). This suggested CCD4 cleaves phytofluene/ζ-carotene to produce ACS1. Yet, none of these phytofluene/ζ-carotene-derived compounds were absent from the *ccd4* volatile apocarotenoid profile. Perhaps bleached *clb5* seedlings differ from normal, photosynthetic, tissues in terms of CCD4 access to carotenoid substrates and propensity for non-enzymatic cleavage. Harsher oxidative conditions in photosynthetically-active tissue may allow ACS1 to form irrespective of CCD4 activity (just as ACS2 synthesis may not require CCDs in photosynthetic *ccr2* tissue).

Furthermore, my results (Chapter Six) did not corroborate previous reports (Rottet, *et al.* 2016) of an ACS negatively regulating thylakoid membrane degradation and, potentially, other senescence processes. Senescence appears to proceed normally in *ccd4*, *ccd1* and *ccd1;4*, as judged by leaf appearance, HPLC measurements of chlorophyll abundance, and *SGR1* expression. If CCD4 is responsible for an ACS that retards thylakoid membrane degradation, one might have expected leaf yellowing, chlorophyll degradation and/or *SGR1* induction to be accelerated in the *ccd4*-background. Despite evidence that CCD4 and CCD1 loss-of-function can perturb carotenoid catabolism during senescence, broader senescence processes do not seem affected. One possibility might be that an ACS produced by CCD4 can retard senescence but, in its absence, other factors maintain the rate of thylakoid degradation. Alternatively, the ACS may specifically affect the rate of thylakoid membrane lipid degradation. Unfortunately, analysis of these lipids was considered beyond the scope of my study.

Despite the complexities, this thesis research, primarily involving volatile SPME-GC/MS metabolomics, combined with carotenoid profiling across different genetic backgrounds, tissue types and environmental conditions, has yielded novel insights into apocarotenoid

and carotenoid metabolism. I believe it will yield new hypotheses to progress investigation into this fascinating group of compounds.

Chapter Eight: Materials and Methods

8.1 Chemicals and materials

High purity grade (>90%) α-cyclocitral, α-ionone, β-carotene, β-cyclocitral, β-cyclocitrol, β-ionol, β-ionone, citral, farnesylacetone, geranylacetone, lutein, lycopene, 6-methyl-5-hepten-2-one (6MHO), pseudoionone, zeaxanthin, n-hydrocarbon mix (C_9-C_{36}, Cat. No. 49451-U), hydrochloric acid, GC/MS-grade ethyl acetate (EtOAc) and triethylamine were purchased from Sigma-Aldrich (i.e. Merck, New South Wales, Australia). Neoxanthin, neurosporene and ζ-carotene were supplied by CaroteNature GmbH (Switzerland). 13,13,13-D_3-β-ionone (>99%) was supplied by Buchem BV (the Netherlands). GC/MS-grade acetone, acetonitrile, dichloromethane (DCM), ethanol and isopropanol were supplied by Thermo Fischer (Victoria, Australia). (S)-Dihydroactinidiolide (>97%) was purchased from 4C Pharma (Ontario, Canada). Other plant volatile standards used in Chapter Three were obtained from Sigma-Aldrich, and Theta Corporation (Pennsylvania, United States). Trisaminomethane (Tris), trisaminomethane hydrochloride (Tris HCl), boric acid, ethylenediaminetetraacetic acid (EDTA), ammonium acetate and sodium chloride (NaCl) were supplied by Merck (New South Wales, Australia). Milli-Q water was used throughout.

Stock solutions for standards at 1 mg/mL were prepared in EtOAc and stored in amber glass vials at −20 °C, and diluted as required (using either EtOAc or DCM) for calibration and QC standards. n-Alkane standards (provided as a 1 mg/ml solution) were diluted accordingly using DCM and stored at room temperature in amber glass vials.

The following SPME fibres were used for SPME-GC/MS method development: 100 µm polydimethylsiloxane (PDMS; volatiles, MM 60-275), 65 µm polydimethylsiloxane/divinylbenzene (PDMS/DVB; volatiles, amines and nitro-aromatics, MM 50-300), 75 µm polydimethylsiloxane/Carboxen (PDMS/CAR; gases and low-MM compounds, MM 30-225), and 50/30 µm divinylbenzene/carboxen on polydimethylsiloxane (PDMS/DVB/CAR; volatiles and semi-volatiles, MW 40-275), purchased from Sigma Aldrich (New South Wales, Australia). For SPME-Cold-EI-GC/MS analysis, the PDMS/DVB/CAR fibre was used. Fibres were conditioned according to the manufacturer's instructions.

8.2 Plant growth and sampling

The following genotypes were used: Col-0, *ccr2-1*, *ccd1-1*, *ccd4* (SALK097981C), *max3-11* and *max4-1*. These genotypes, apart from *ccr2-1*, are available from The Arabidopsis Biological Resource Centre, Ohio State University (Ohio, United States).

Plant samples were freshly harvested, kept at room temperature and analysed immediately. For most *Arabidopsis thaliana* and tomato (*Solanum lycopersicum*) tissues, 500 mg were used per biological replicate. Given the small size of *Arabidopsis* buds, I did not harvest 500 mg of tissue for each replicate, instead normalising replicates to bud number (100 buds/replicate, ~40 mg).

Arabidopsis was grown under a 16 h photoperiod, at ~120 $\mu Em^{-2}s^{-1}$ light intensity, on Debco Seed Raising Mix (Scotts Australia, New South Wales, Australia), supplemented with 3 g/L Osmocote controlled-release fertilizer (Scotts Australia). For harvesting, *Arabidopsis* plant maturity was normalised according to the growth stages described by Boyes *et al.* (2001). The four to six youngest leaves were harvested from one plant, per biological replicate, at around growth stage 6 (approx. 32 day old plants, after the first flower has opened); this corresponded to leaves that had emerged in the preceding two weeks. Inflorescence tissues (bolts and flowers) were harvested at mid-flowering stage (6.5, approx. 44 days old), as were leaves harvested for SPME-Cold-EI-GC/MS work. Two to three plants were required to make up one biological replicate for developing and anthesis flower samples; fertilised flowers were excluded from samples. Bolt tissue i.e. internodes and nodes of primary and secondary inflorescences from one plant was sufficient per biological replicate. Total siliques, from one plant per replicate, were harvested after flowering was complete (growth stage 6.9). For dry seed samples, seeds were harvested from senescent plants and pooled (2-3 plants) for each biological replicate. Tomato tissues for SPME-GC/MS survey were harvested from mature tomato plants (approx. 50 days old) grown in a suburban garden in Canberra, Australia, from November 2015. For SPME-Cold-EI GC/MS, tomato fruits were purchased from a commercial market in Melbourne, Australia, on the day of analysis. Tomato fruit tissue was diced into 1 cm^3 cubes prior to analysis.

Dark-induction was done by excising rosettes from 5 week old plants (growth stage 5.1) grown as above under 12 h photoperiod. Following excision, rosettes were dark-incubated in petri dishes on filter paper that was kept moistened with tap water for the duration of

the senescence time-course. At the required time-points, 0 h (i.e. 1 h after dark-incubation), 3 d and 7 d, leaf tissue was harvested from dark-induced samples as described above.

8.3 Plant crossing

Single *ccd* and *ccd x ccr2* plants, previously generated in our laboratory, were grown under 16 h photoperiod as described above. Beginning from plant growth stage 6, the carpels of flowers from the maternal plant were exposed using dissecting tweezers. Excised flowers (with anthers/pollen exposed) from the paternal plant were then brushed against the maternal carpel. Following crossing, the growing siliques were kept isolated/protected by wrapping with plastic film, keeping one end open to allow for ventilation.

After silique drying, F1 seeds were collected and sown, allowing generation of the F2 population. At least 64 individuals from each F2 population were subsequently grown. Tissues were harvested from F2 plants for screening of the *ccd* mutations as plants approached growth stage 5.1.

8.4 DNA extraction

DNA extraction was performed using either the Qiagen DNeasy Plant Kit (Victoria, Australia), as per the manufacturer's instructions, or *via* the high-throughput extraction protocol developed in our laboratory. For the high-throughput extraction, approximately 50 mg of fresh tissue was harvested into a 1.5 ml tube, or alternatively into a 96 x 1.1 ml tube rack (FisherBiotec, Western Australia, Australia). Ball bearings were added to the tubes and samples were ground using a Qiagen Tissuelyzer (Victoria, Australia) for 1 min at 25 Hz. Following this, 700 µl (or 500 µl, for the 96-well format) of extraction buffer (an aqueous solution of 100 mM Tris HCl, 50 mM EDTA and 500 mM NaCl) was added to the sample. Samples were then centrifuged at 16,000 g (5,000 g) for 10 min. Then, the supernatant was transferred to a fresh tube (tube rack) and 700 µl (500 µl) of isopropanol was added. This mixture was then centrifuged at 16,000 g (5,000 g) for 5 min, after which the supernatant was discarded. The tubes were allowed to dry for 5 min and then the precipitated DNA was resuspended in 100 µl (73 µl) water. DNA samples were stored at -20 ^{o}C following extraction.

8.5 Polymerase Chain Reaction

Polymerase chain reactions (PCR) were prepared with the following reagents: 5 µL 10x reaction buffer, 1 µL 10 mM dNTPs, 1 µL DNA template, 0.25 µL *Taq* polymerase and gene-specific primers (0.2 µM final concentration) were mixed with water to a final volume of 50 µL. New England Biolabs (i.e. Genesearch, Queensland, Australia) *Taq* polymerase and Standard *Taq* Buffer were used. The PCR cycling conditions involved an initial denaturation (95 ^{o}C, 30 s) followed by 45 cycles of amplification (95 ^{o}C, 30 s; 50 ^{o}C, 15s; 68 ^{o}C, 3 min) and a final extension step (65 ^{o}C, 5 min). A ramp rate of 4.4 ^{o}C/s was applied when changing temperatures.

8.6 Gel and capillary electrophoreses

PCR products were analysed *via* either gel or capillary electrophoresis. For gel electrophoresis, PCR reactions were typically diluted five-fold with water and then mixed with blue gel loading dye (Genesearch, Queensland, Australia) in a 5:1 ratio. Gels (100 mL final volume) were then prepared with 1% agarose (Fisher Biotec, Western Australia, Australia) and 2.5 ng of ethidium bromide (Merck, New South Wales, Australia) in 'TBE' buffer (88 mM trisaminomethane, 88 mM boric acid, 10 mM EDTA, adjusted to pH 8.3 with hydrochloric acid).

After samples were loaded on the gel, electrophoresis was performed at a voltage of 130 volts (210 milliamps) for 30 min. Subsequently, the gel was photographed with a UV transilluminator (UVP, California, United States) operated using Quantum ST4 software (Fisher Biotec).

For capillary electrophoresis, PCR reactions were loaded, undiluted, onto a LabChip GXII instrument (Perkin Elmer, Victoria, Australia) as per the manufacturer's instructions. Prior to this, the LabChip instrument was washed, primed and loaded with 'DNA 5K' reagents (Perkin Elmer) as per the manufacturer's instructions. Capillary electropherogram images were exported as .png files for analysis.

8.7 RNA extraction

Approximately 80 mg of tissue per biological replicated was harvested into a 1.5 ml tube containing a ball bearing and promptly flash frozen. Samples were subsequently ground in pre-chilled racks on a Qiagen Tissuelyzer (Victoria, Australia) for 2 x 30 s, 25 Hz bursts. Tubes were kept on liquid nitrogen in between grinding bursts. Subsequently, RNA was extracted using the Sigma Spectrum Plant Total RNA Kit (i.e. Merck, New South Wales, Australia), as per manufacturer's instructions. RNA was stored at -80^{o}C.

8.8 First strand complementary DNA synthesis

First strand complementary DNA (cDNA) was synthesised from extracted RNA using the Superscript III (SSIII) First-Strand Synthesis System (Thermo Fisher, Victoria, Australia). First, RNA concentrations were normalised to 0.1 µg/µl using RNAse-free water. SSIII reagents were then added to 10 µl aliquots of normalised RNA samples as per the manufacturer's instructions. RNA and SSIII reagents were incubated at 55 ^{o}C for 30 min for the first-strand synthesis step. Following completion of the manufacturer's protocol, cDNA reactions were stored at -20 ^{o}C.

8.9 Quantitative real-time polymerase chain reaction

For quantitative real-time polymerase chain reaction (qPCR), cDNA samples were diluted ten-fold with water. Primer-specific qPCR master mixes were created by mixing LightCycler 480 SYBR Green I Master Mix (Roche, New South Wales, Australia) with water and gene-specific primers (final concentration of 1 µM) as per the manufacturer's instructions. For each reaction, 7 µL of this mix was then combined with 3 µL of diluted cDNA template. The samples were then reacted using a LightCycler 480 Instrument (Roche, New South Wales, Australia). The qPCR cycling protocol consisted of a pre-incubation step (95 ^{o}C, 10 min, 4.8 ^{o}C/s ramp rate), followed by 60 cycles of amplification (95 ^{o}C, 15 s, 4.8 ^{o}C/s; 60 ^{o}C, 15 s, 2.5 ^{o}C/s; 72 ^{o}C, 20 s, 4.8 ^{o}C/s). An additional step to

generate qPCR melt curves followed (95 ^{o}C, 30 s, 4.8 ^{o}C/s; 60 ^{o}C, 30 s, 2.5 ^{o}C/s; returning to 95 ^{0}C at 0.11 ^{o}C/s).

Data was exported in text format. The cycles-to-linear phase and qPCR efficiencies for reactions were then calculated using the LinRegPCR software (Ruijter *et al.* 2009). From this output, Cq (AKA Ct) values were obtained and results were interpreted using the ddCt method (Yuan *et al.* 2006). Gene expression fold-change and ddCt values were exported in .csv format for further statistical analysis.

8.10 Carotenoid and chlorophyll extraction and high-performance liquid chromatography analyses

Carotenoids and chlorophylls were extracted from approximately 80 mg tissue per biological replicate and analysed *via* high performance liquid chromatography (HPLC). Tissues were harvested into 1.5 mL tubes containing ball bearings. These samples were then flash frozen and ground as described for RNA extraction. Subsequently, 400 µL of 3:2 acetone:ethyl acetate solution were mixed with each sample. To each sample, 320 µL of water was added. The samples were then vortexed and centrifuged (13,000 g, 5 min). The epiphase, containing the ethyl acetate extract, was transferred to a fresh tube and centrifuged (as above) to remove any residual water and debris. The organic extract was then transferred to an amber 200 µL HPLC insert vial (Agilent Technologies, Victoria, Australia).

HPLC was performed using an Agilent 1260 Infinity Quaternary Pump and Automated Liquid Sampler, linked to an Agilent 1100 Series UV/Vis Diode Array Detector (DAD). Compound separation was achieved using a C30 250 x 4.6 mm column (YMC, Japan) and a HPLC program involving two solutions: 0.1% ammonium acetate in methanol (A) and methyl-*tert*-butyl ether (B). Solution A was initially set to 100% of flow for 5 min. Subsequently, solution B increased to 100% of flow over 20 min. Over another 5 min the proportion of A was returned to 100%; this was maintained for another 5 min. When not in use, the column was stored in acetonitrile.

Compounds were identified *via* comparison of spectra to authentic standards (see Chemicals and Materials) or literature spectra. Compounds were quantified by monitoring DAD response at 286 nm (phytoene), 348 nm (phytofluene), 400 nm (ζ-carotene) and 440 nm (all other compounds). Peak areas at the selected wavelengths were integrated using Agilent Chemstation (version B.04.03, Agilent Technologies, Victoria, Australia), and exported in .csv format for further analysis.

8.11 GC/MS sample preparation and calibration

For static HS and SPME work, samples were contained in glass vials (20 mL) sealed using aluminium foil and magnetic crimp caps with silicone septa. The volume of calibration solutions added to the vials was kept constant across the GC/MS sequence (8-10 µL) using stocks of appropriate concentration. For LI, standard solutions were contained in amber glass vials (300 µL). Final concentrations used for calibrations were as follows: 0, 1, 5, 10, 20 and 50 ppm (LI); 0, 2, 8, 40 and 200 ppb (HS); and 0, 0.2, 0.5, 1, 4, and 20 ppb (SPME). Final concentration of 13,13,13-D_3-β-ionone internal standard was added to SPME samples at 10 ppb as described. Limits of quantification and detection were calculated as, respectively, ten and three times the noise-to-signal ratio of a given analyte peak multiplied by the corresponding analyte concentration, as per the following equations:

$LOQ = 10\frac{N}{S} \times c$, and $LOD = 3\frac{N}{S} \times c$, where N is noise and S is signal (i.e. N/S is the inverse of the signal-to-noise ratio) for a given analyte peak, and c is the corresponding analyte concentration.

QC standard samples were interspersed throughout the sequence to monitor GC/MS performance and SPME fibre integrity, and contained a mixture of all apocarotenoid standards at a final concentration of 10 ppm (LI), 40 ppb (HS) or 10 ppb (SPME). Calibration levels and biological replicates were randomised within statistical ‘blocks’ to account for any systemic fluctuations in SPME fibre and/or GC/MS performance.

8.12 GC/MS system

A single quadrupole GC/MSD instrument (Agilent Technologies, Palo Alto, CA, USA) consisting of a 7890A series gas chromatograph and a 5975C inert XL MSD mass

selective detector (Triple-Axis Detector) was used. The system was retrofitted with a MPS 2 Gerstel Multipurpose sampler with LI, HS and SPME capability (GERSTEL GmbH & Co. KG, Germany). The split/splitless injector port had either a standard glass wool liner for LI or a 1.0 mm straight, no-wool liner for SPME and HS. Splitless injection with the injector temperature at 250 ºC was applied. 1 µL injections were used for LI-GCMS. Following parameter optimisation, both SPME and static HS samples and standards were incubated at 70 °C for 5 min prior to extraction. For SPME, fibres were exposed to the sample for 40 mins' extraction prior to a 40 min desorption in the GC inlet. For static HS, 1 ml of sample headspace was drawn into a gas-tight syringe, kept at 80 °C prior to injection, at a speed of 200 µL/s. The sample inlet was purged for 1 min after sample introduction. The gas chromatographic separation was achieved on an Agilent J&W VF-5 ms column (30 m × 0.25 mm × 0.25 µm), equipped with a 10 m EZ-Guard column. The oven temperature program was as follows: 40 °C for 2 min, ramping to 150 °C at 5 °C/min and held for 2 min, then to 320 °C at a ramp rate of 15 °C/min and held for another minute. The GC run time was 38 min. The helium (ultra-high purity, BOC Australia) carrier gas flow rate was 1 mL/min. Transfer line temperature was 320 °C, ion source, 250 °C and quadrupole, 150 °C. Electron impact ionisation energy (EI) was 70 eV, with full MS scan acquisition from *m/z* 40 – 500 and four minute solvent delay. Total SPME-GC/MS analysis per sample was 83 min.

8.13 Cold-EI-GC/MS system

Cold-EI analysis was performed using a Clarus 680 GC system coupled to an AxION iQT QTOFMS (GC-MS/MS; PerkinElmer, Massachusetts, USA), fitted with an auto sampler, split/splitless injector equipped with a split/splitless liner (2 mm × 4 mm × 86.2 mm; PerkinElmer). Samples were introduced into the Clarus 680 GC inlet as described for the GC-QMS system. Separation was performed using an Elite-5MS capillary column (PerkinElmer) of dimensions 30 m × 0.25 mm × 0.25 µm, with the program as described for GC-QMS analyses. Helium carrier gas flow rate was maintained at 1.2 mL min^{-1}. Transfer line temperature was 280 ˚C; and ion source 230 ˚C. A mass range of 40-300 Da was applied. Make-up gas flows of 4, 25, 50, 75 and 100 ml/min, and ionisation voltages of 16, 30, 50, 70 and 100 eV were applied. The system was operated in total transfer ion mode through the quadrupole sector.

8.14 EI-GC/MS system for EI and Cold-EI parallel analysis

A single quadrupole GC/MSD instrument was used consisting of a 7890A series gas chromatograph and a 5975C mass-selective triple-axis detector (Agilent Technologies, California, USA). The split/splitless injector port was fitted with a 78.5 mm x 6.5 mm x 0.75 mm un-lined injection sleeve suitable for SPME analysis. For standard solution analysis, 1 µL injections were made, with 10:1 split. For analysis of plant tissues *via* SPME, samples were incubated at 70 °C for 5 min prior to extraction. Fibres were manually exposed to the sample for 20 min's extraction prior to a 10 min desorption in the GC inlet. Sample inlet was purged 1 min after injection with 20 ml/min of carrier gas. Gas chromatographic separation was achieved on an Agilent J&W HP-1 column (30 m × 0.32 mm × 0.25 µm), equipped with a 10 m EZ-Guard column using the following program: 40 °C for 7 min, ramping to 260 °C at 5 °C/min and held for 2 min, then to 330 °C at a ramp rate of 20 °C/min and held for another 5.5 min. The GC run time was 42.75 min. The helium (ultra-high purity, BOC Australia) carrier gas flow rate was 1.2 mL/min. Transfer line temperature was 280 °C, and ion source 230 °C; ionisation energy was fixed at 70 eV. A mass range of 40-300 Da was scanned.

8.15 GCMS data analysis

Agilent MSD Chemstation software (version E.02) was used for data acquisition; Agilent MassHunter (version B.50), Mass IQ (PerkinElmer), AxION iQT Driver (PerkinElmer), and AxION eCipher (PerkinElmer) softwares were used for quantitative and qualitative analyses. For quantitative analyses, peak areas were integrated from compound-specific EICs; these data were subsequently exported in .csv format for further analysis. The NIST/EPA/NIH Mass Spectral Library (version 2014) was used for mass spectral matching and GC/MS peak annotation. To further verify detected compounds, Kovat's RIs were calculated for all peaks using n-alkanes C_9-C_{22} spiked into samples and compared against literature RI values in the NIST library.

8.16 Statistical analyses and data presentation

Following export of numerical data to .csv format, further graphing and analyses were performed using either Microsoft Excel (Washington, United States) or R (R Core Team 2016) with the RStudio integrated development environment (Massachusetts, United States). Data collation and visualisation in R was done using the ddply, plyr, ggplot2, ggfortify, (Wickham 2009, Wickham 2011) Hmisc and corrplot packages (https://cran.r-project.org/web/packages/corrplot/index.html, https://cran.r-project.org/web/packages/Hmisc/). PCA and HCA were performed on centred and scaled values using R base package, all other data were normalised as described in figure and table captions. Figures collated in Excel and R were cosmetically refined using Adobe Illustrator (California, United States).

8.17 Tables

Table 8.1: Primers used in this thesis

Primer Name	Gene Target	Sequence	Amplicon length	Comments
CCD1-span F	CCD1 (AT3G63520)	GCTCCCATCCGTGATGAAAC	1012	Ccd1 spanning primer assay
CCD1-span R	CCD1 (AT3G63520)	GGAGTGGGTCAATCTCTTGTC		
CCD4-span F	CCD4 (AT4G19170)	ATGGACTCTGTTTCTTCTTCTTCCT	1788	Ccd4 spanning primer assay
CCD4-span R	CCD4 (AT4G19170)	TTAAAGCTTATTAAGGTCACTTTCC		
CCD8-span F	CCD8 (AT4G32810)	AACAAAACCTCAAGTCCCTCAC	991	Ccd8 spanning primer assay
CCD8-span R	CCD8 (AT4G32810)	TCCAATGTTCCATAGACCAGG		
max3-9 F	CCD7 (AT2G44990)	GCCGCAGATTTGTTGAAACC	251	Max3-9 sequencing primers
max3-9 R	CCD7 (AT2G44990)	TGAGTATCCGTGAATGCCC		
ccd7-1F	CCD7 (AT2G44990)	GACCAAAATGTCTCTCCCTAT	325	Overlapping amplification of CCD7
ccd7-1R	CCD7 (AT2G44990)	ATGGTCGTCAGTAAATAGTCC		
ccd7-2F	CCD7 (AT2G44990)	CTTCAGCTTTCCGTGATTACCAA	480	Overlapping amplification of CCD7

ccd7-2R	CCD7 (AT2G44990)	ATCTTCCGACGGTATCCAAC		
ccd7-3F	CCD7 (AT2G44990)	CTCATAGAGGTCCTTTCTCG	369	Overlapping amplification of CCD7
ccd7-3R	CCD7 (AT2G44990)	TAATTTTACGCCGCTGTCTG		
ccd7-4F	CCD7 (AT2G44990)	ATTGGGCATTCACGGATAC	432	Overlapping amplification of CCD7
ccd7-4R	CCD7 (AT2G44990)	GAAATCGAACCATCGGTAAG		
ccd7-5F	CCD7 (AT2G44990)	CTGTCGAAGTGTCTTCTCAA	606	Overlapping amplification of CCD7
ccd7-5R	CCD7 (AT2G44990)	ACCAACGAATCTTCTAGCTC		
ccd7-6F	CCD7 (AT2G44990)	TCCGGTTATAAACTCATCCTG	610	Overlapping amplification of CCD7
ccd7-6R	CCD7 (AT2G44990)	TATATGGCTTCTGTAACACCTT		
ccd7-7F	CCD7 (AT2G44990)	GAATTTGACGTTTCCGATGG	613	Overlapping amplification of CCD7
ccd7-7R	CCD7 (AT2G44990)	GGACATAGTCTAAGAACTAGATGA		
max3-11 LP	CCD7 (AT2G44990)	TTAGGCGACACCAAAATGAAG	1129	SALK max3-11 screening primers
max3-11 RP	CCD7 (AT2G44990)	TTATGAATCTAAACCGTGGCG		
SALK BP		ATTTTGCCGATTTCGGAAC		SALK LBb1.3 border primer
LB2_SAIL		GCTTCCTATTATATCTTCCCAAATTACCAA TACA		SAIL LB2 border primer
ccd1-qF	CCD1 (AT3G63520)	ATGCATGACCCAGTCCCAAT	260	qPCR primer for ccd1
ccd1-qR	CCD1 (AT3G63520)	CAAGCATTGGCGTTGTGGAA		
ccd4-qF	CCD4 (AT4G19170)	AGCGTCGTTTTGATTGCACC	213	qPCR primers for ccd4
ccd4-qR	CCD4 (AT4G19170)	ATCTCCAATCGCCGCGTAAA		
ccd7-qF	CCD7 (AT2G44990)	TCCATTCGACATGGTCGTGA	252	qPCR primer for ccd7
ccd7-qR	CCD7 (AT2G44990)	TACACTTTGTTTACACTCGACAC		
ccd8-qF	CCD8 (AT4G32810)	GATGCTAGGATCGGGAGATTCA	230	qPCR primer for ccd8

ccd8-qR	CCD8 (AT4G32810)	TGGAAACCGATAGTTTGGGGT		
PP2A-qF	PP2A (At1g13320)	CTTCGTGCAGTATCGCTTCTC	250	qPCR primer for PP2A
PP2A-qR	PP2A (At1g13320)	ATTGGAGAGCTTGATTTGCG		
sgr1-qF	SGR1 (AT4G22920)	TCACATAAGCGGTGGCCATT	244	qPCR primer for SGR1
sgr1-qR	SGR1 (AT4G22920)	AGTCTTGTGACCATCAGGCG		
dgat3-qF	DGAT3 (AT1G48300)	AGCCACAGTAGCAACCCTTC	271	qPCR primer for DGAT3
dgat3-qR	DGAT3 (AT1G48300)	AGCAGATCCTTCGAAACCCG		
wrky53-qF	WRKY53 (AT4G23810)	GATCAGACGGGGATGCTACG	269	qPCR primer for WRKY53
wrky53-qR	WRKY53 (AT4G23810)	CTCGCCGTTGATAGTTCCGT		

Appendix

Appendix

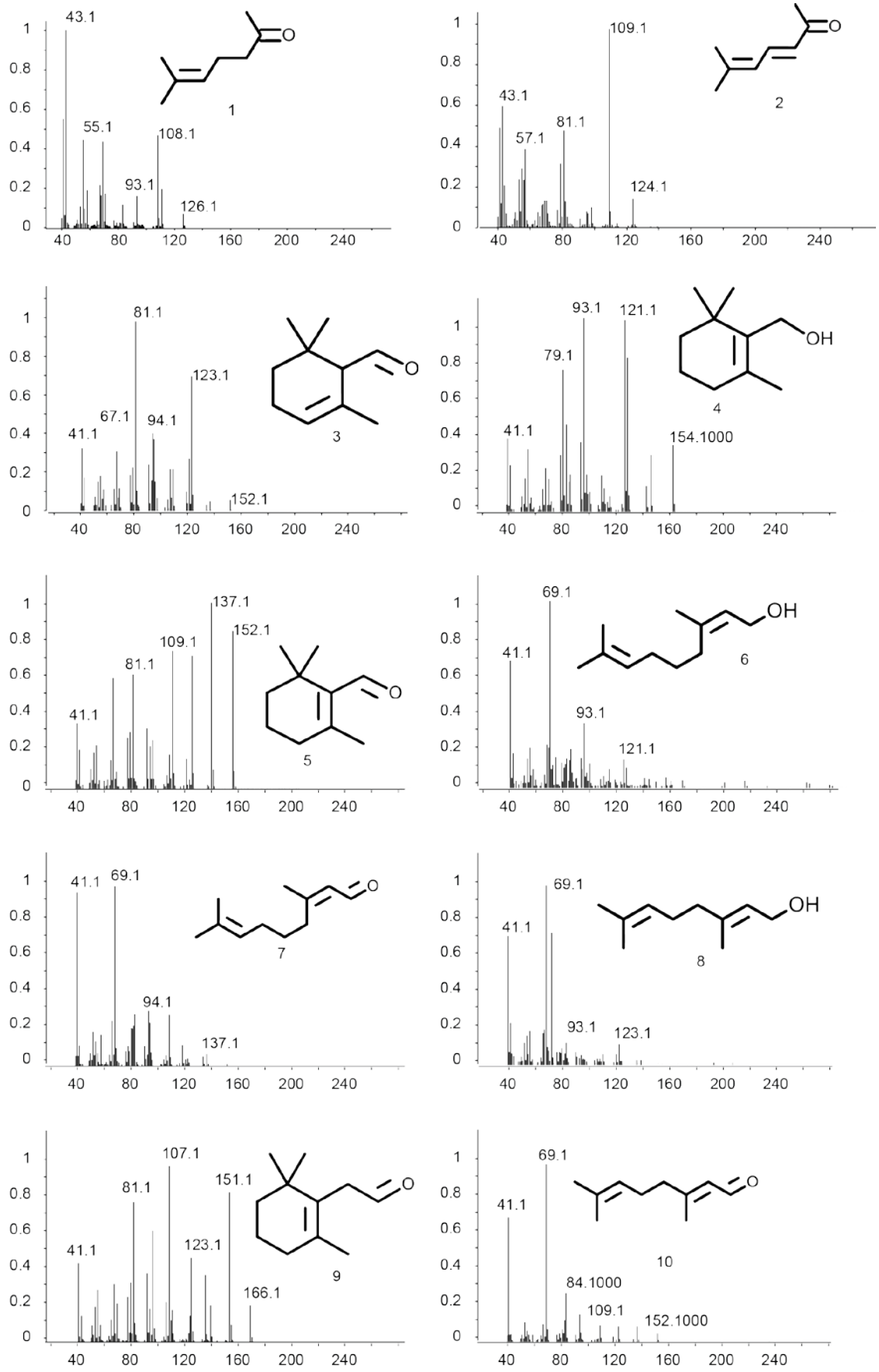

Relative intensity (x 10^2) versus mass to charge (m/z)

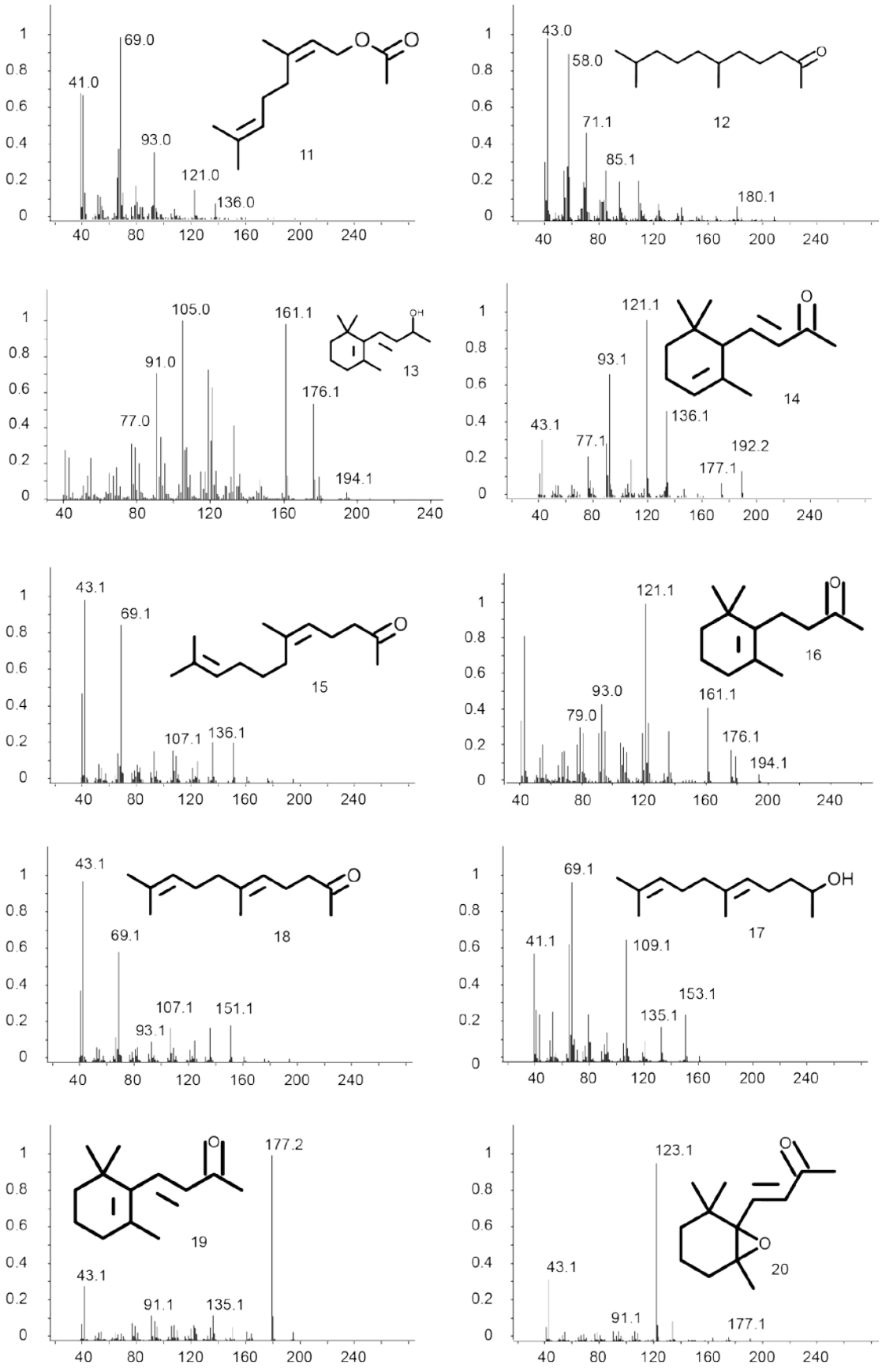

Relative intensity (x 10^2) versus mass to charge (m/z)

Appendix

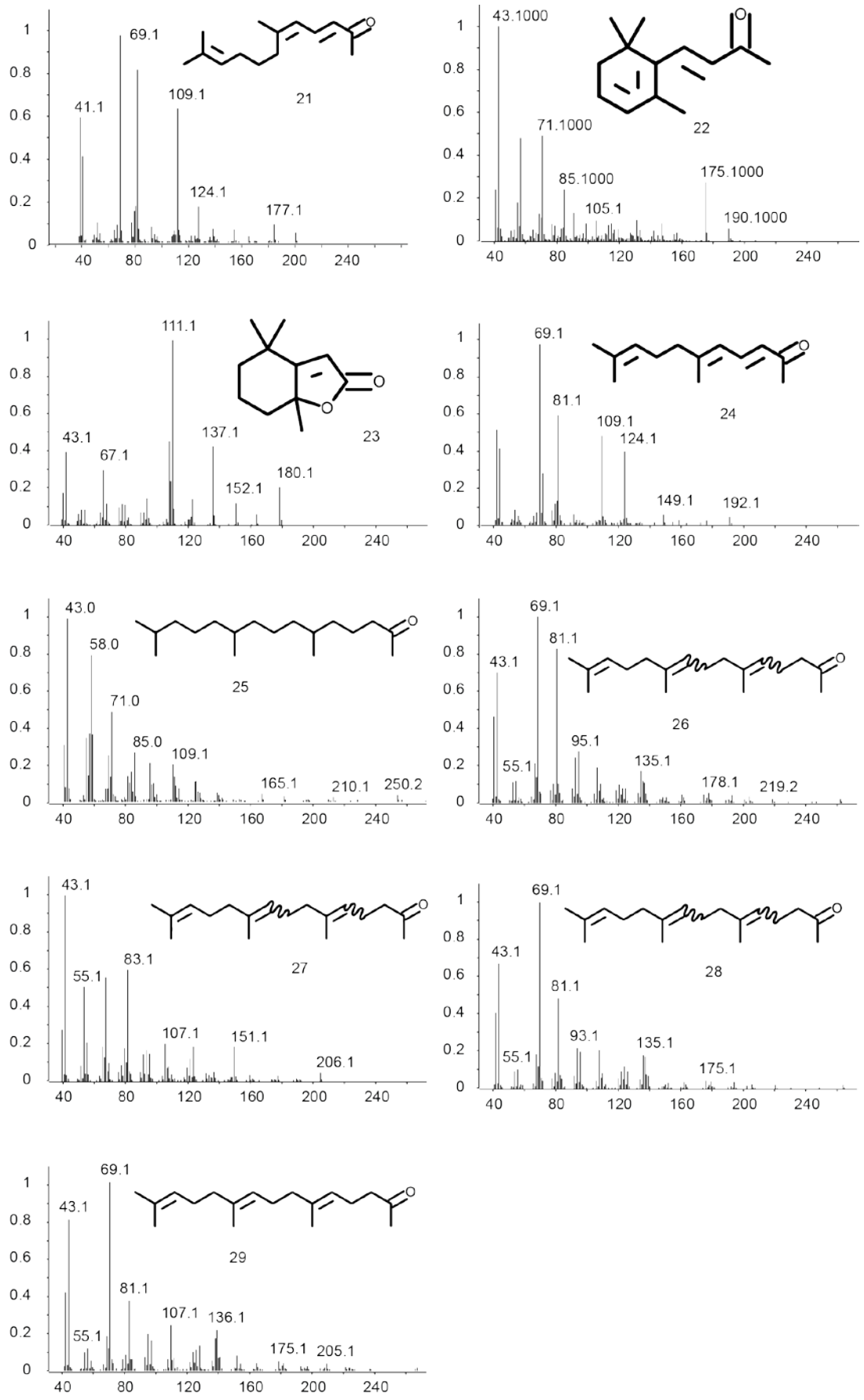

Relative intensity (x 10^2) versus mass to charge (m/z)

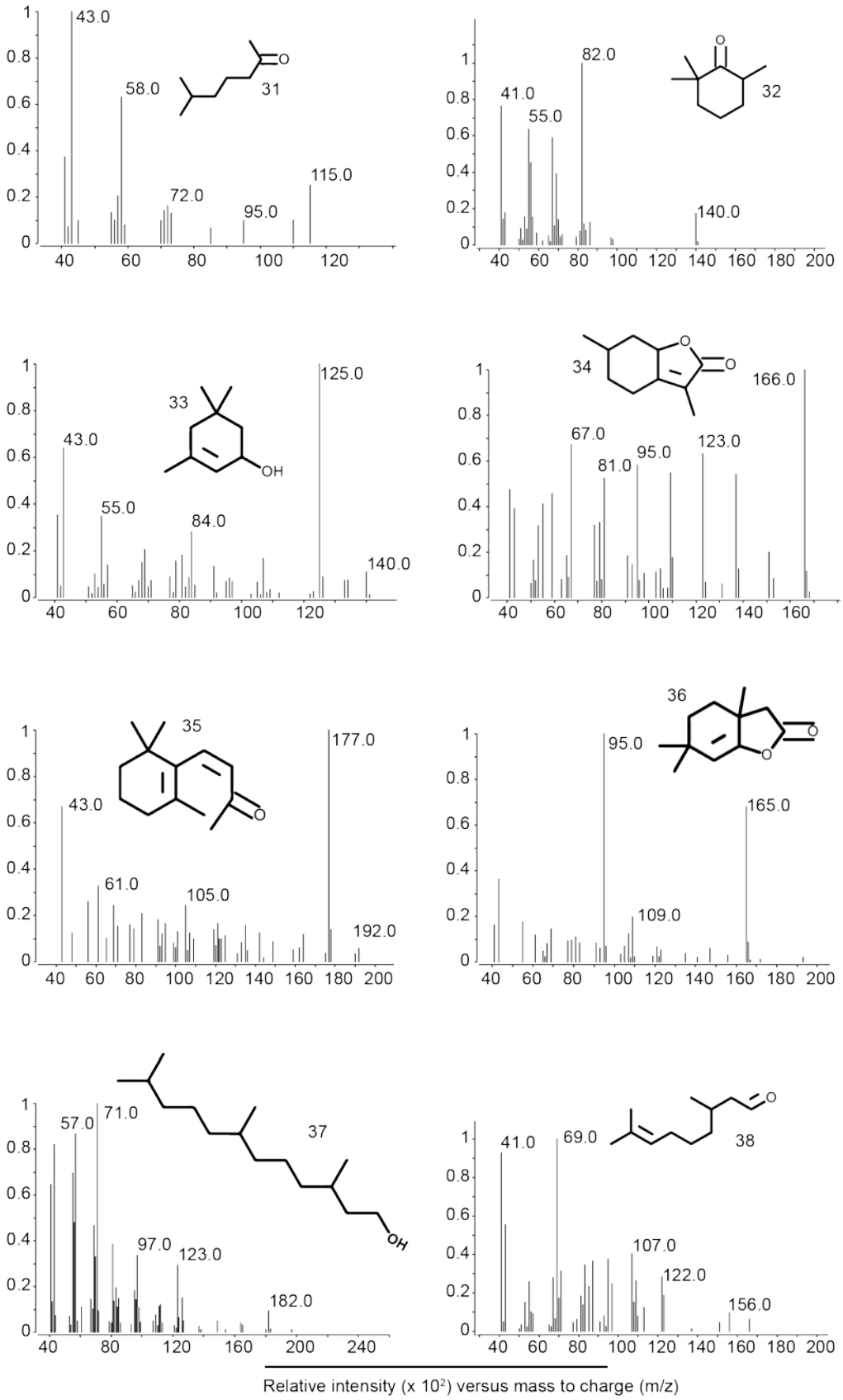

Figure A.1: Mass spectra for all known and putative apocarotenoids in this study

Compounds are numbered as in Table A.1

Appendix

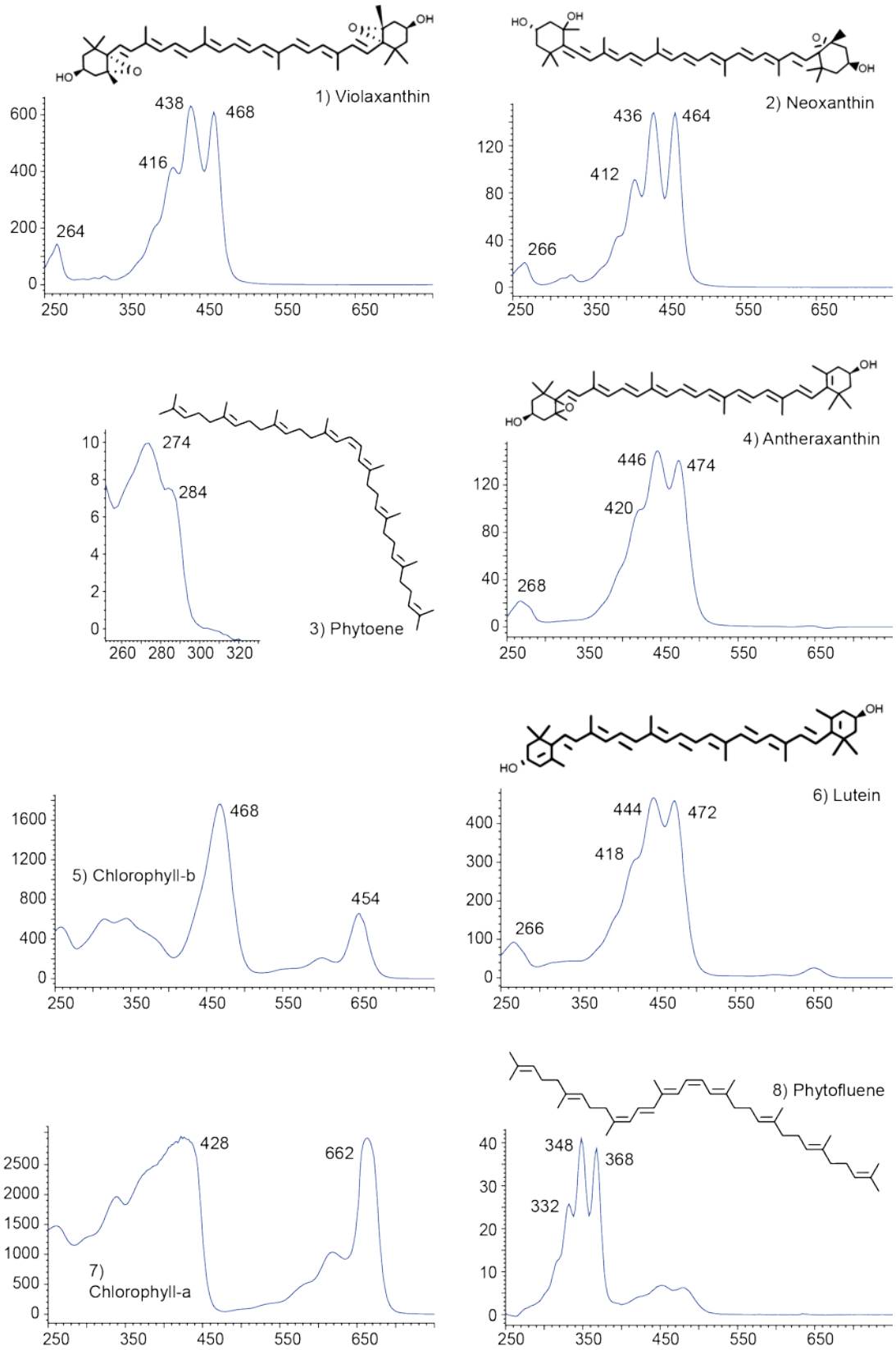
1) Violaxanthin
438
468
416
264
2) Neoxanthin
436
464
412
266
3) Phytoene
274
284
4) Antheraxanthin
446
474
420
268
5) Chlorophyll-b
468
454
6) Lutein
444
472
418
266
7)
Chlorophyll-a
428
662
8) Phytofluene
348
368
332

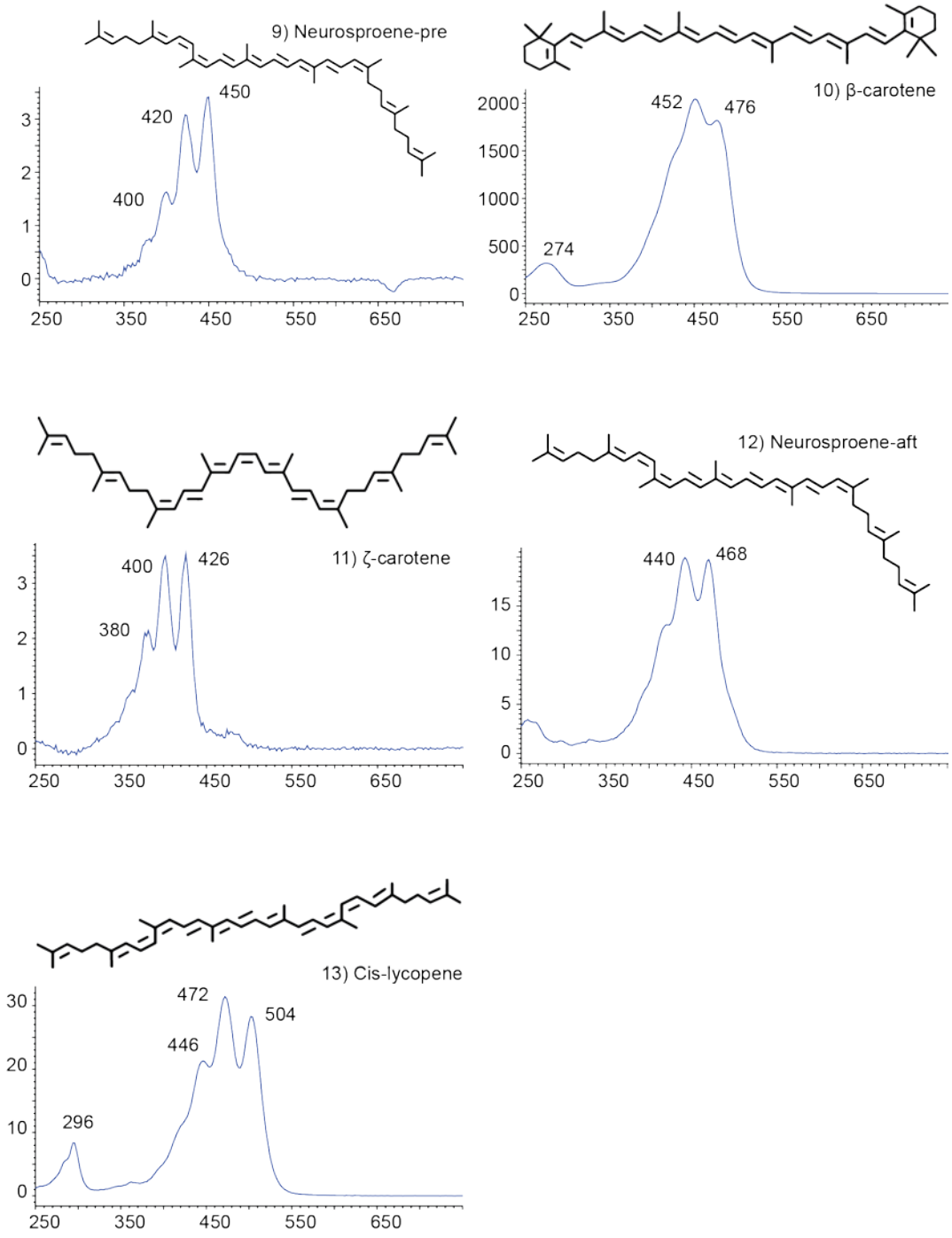

Figure A.2: UV-visible spectra for all carotenoids and chlorophylls observed in this study

Spectra are presented as absorbance units (y-axis) versus wavelength (nm). Note: stereochemistries of carotenoid structures are for illustrative purposes only (depicting stereoisomers commonly cited in the literature); stereochemistries of observed carotenoids were not determined in this study.

Table A.1: Data for all known and putative apocarotenoids observed in this study

#	Compound Name	Trivial Name	MM	CAS-NO	RI	NIST RI	NIST Forward Match	NIST Reverse Match	Verified by authentic standard	Compound used for concentration calculations	Quantifying ion	Qualifying ions
1	6-methyl-5-hepten-2-one	6-methyl-5-hepten-2-one	126	110-93-0	928	938	937	952	Y	6-methyl-5-hepten-2-one	43	108, 126
2	6-methyl-3,5-heptadiene-2-one	6-methyl-3,5-heptadiene-2-one	124	16647-04-4	1109	1107	783	876	-	6-methyl-5-hepten-2-one	109	81, 124
3	2,6,6-trimethyl-2-cyclohexene-1-carboxaldehyde	α-cyclocitral	152	432-24-6	1122	1116	937	943	Y	α-cyclocitral	81	123, 152
4	2,6,6-trimethylcyclohex-1-ene-1-methanol	β-cyclocitrol	154	NA	1209	NA	NA	NA	Y	β-cyclocitrol	93	121, 154
5	2,6,6-trimethyl-1-cyclohexene-1-carboxaldehyde	β-cyclocitral	152	432-25-7	1212	1204	951	954	Y	β-cyclocitral	137	152, 109
6	*Cis*-3,7-dimethyl-2,6-octadien-1-ol	*Cis*-citrol	154	106-25-2	1228	1228	656	841	-	*Cis*-citral	69	93, 121
7	*Cis*-3,7-dimethyl-2,6-octadienal	*Cis*-citral	152	106-26-3	1242	1240	961	961	Y	*Cis*-citral	69	94, 137
8	*Trans*-3,7-dimethyl-2,6-octadien-1-ol	*Trans*-citrol	154	106-24-1	1253	1255	707	801	-	Trans-citral	69	93, 123
9	2,6,6-trimethyl-1-cyclohexene-1-acetaldehyde	β-homo-citral	166	472-66-2	1261	1254	947	955	-	β-cyclocitral	107	151, 166
10	*Trans*-3,7-dimethyl-2,6-octadienal	Trans-citral	152	141-27-5	1270	1270	964	964	Y	Trans-citral	69	109, 152
11	*Cis*-3,7-dimethyl-2,6-octadienyl acetate	*Cis*-citrol acetate	196	141-12-8	1365	1364	876	910	-	*Cis*-citral	69	93, 121
12	6,10-dimethyl-2-undecanone	Hexahydropseudoionone	198	1604-34-8	1408	1408	820	897	-	*Trans*-geranylacetone	43	85, 180
13	*Trans*-4-(2,6,6-Trimethyl-1-cyclohexen-1-yl)-3-buten-2-ol	β-ionol	194	22029-76-1	1413	1406	886	886	Y	β-ionol	121	161, 179
14	*Trans*-4,(2,6,6-trimethyl-2-cyclohexen-1-yl)-3-buten-2-one	α-ionone	192	127-41-3	1426	1457	933	933	Y	α-ionone	121	136, 192

15	*Cis*-6,10-dimethyl-5,9-undecadien-2-one	*Cis*-geranylacetone	194	3879-26-3	1429	1435	932	939	Y	*Cis*-geranylacetone	43	107, 136
16	4-(2,6,6-trimethyl-1-cyclohexen-1-yl)-2-butanone	7,8-dihydro-β-ionone	194	17283-81-7	1436	1433	939	963	-	β-ionone	121	136, 161
17	*Trans*-6,10-dimethyl-5,9-undecadien-2-one	*Trans*-geranylacetone	194	3796-70-1	1452	1453	921	922	Y	*Trans*-geranylacetone	43	107, 151
18	6,10-Dimethyl-5,9-undecadien-2-ol	Geranylacetone alcohol	196	53837-34-6	1453	1459	875	877	-	*Trans*-geranylacetone	69	109, 153
19	*Trans*-4-(2,6,6-trimethyl-1-cyclohexen-1-yl)-3-buten-2-one	β-ionone	192	79-77-6	1487	1486	969	969	Y	β-ionone	177	91, 135
20	4-(2,2,6-trimethyl-7-oxabicyclo[4.1.0]hept-1-yl)-3-buten-2-one	5,6-epoxy-β-ionone	208	23267-57-4	1489	1473	926	930	Y	β-ionone	123	93, 177
21	3-*trans*-5-*cis*-6,10-dimethyl-3,5,9-undecatrien-2-one	3-*trans*-5-*cis*-pseudoionone	192	13927-47-4	1533	1535	899	901	Y	3-*trans*-5-*cis*-pseudoionone	69	109, 124
22	4-(2,6,6-trimethylhexa-1,3-dienyl)-but-3-en-2-one	3,4-dehydro-β-ionone	190	1203-08-3	1536	1485	751	797	-	β-ionone	43	85, 175
23	5,6,7,7a-tetrahydro-4,4,7a-trimethyl-2(4H)-benzofuranone	Dihydroactinidiolide	180	17092-92-1	1547	1532	970	971	Y	Dihydroactinidiolide	111	137, 180
24	All-*trans*-6,10-dimethyl-3,5,9-undecatrien-2-one	*Trans*-pseudoionone	192	3548-78-5	1588	1589	865	884	Y	*Trans*-pseudoionone	69	109, 124
25	6,10,14-trimethyl-2-pentadecanone	Hexahydrofarnesylacetone	168	502-69-2	1847	1844	878	927	-	Farnesylacetone-1	43	71, 109
26	NA	Farnesylacetone-1	262	NA	1864	NA	NA	NA	Y	Farnesylacetone-1	69	81, 90
27	NA	Farnesylacetone-2	262	NA	1883	NA	NA	NA	Y	Farnesylacetone-2	43	83, 107
28	NA	Farnesylacetone-3	262	NA	1893	NA	NA	NA	Y	Farnesylacetone-3	69	81, 135
29	All-*trans*-6,10,14-trimethyl-5,9,13-pentadecatrien-2-one	*Trans*-farnesylacetone	262	1117-52-8	1921	1919	877	896	Y	*Trans*-farnesylacetone	69	81, 136
30	2,6,10,10-tetramethyl-oxaspiro[4.5]dec-6-ene	(±)-Theaspirane	194	36431-72-8	1302	1306	920	949	-	α-ionone	138	82, 123
31	6-methyl-2-heptanone	6-methyl-2-heptanone	128	928-68-7	954.4	956	711	837	No	6-methyl-5-hepten-2-one	43	58
32	2,2,6-trimethyl-cyclohexanone	2,2,6-trimethylcyclohexanone	140	2408-37-9	1037.8	1036	894	935	No	6-methyl-5-hepten-2-one	82	69, 140

33	3,5,5-trimethyl-2-cyclohexen-1-ol	Isophorol	140	470-99-5	1149.9	1147	739	793	No	α-cyclocitral	125	107, 140
34	5,6,7,7a-tetrahydro-3,6-dimethyl-2(4H)-benzofuranone	Menthalactone	166	13341-72-5	1312.8	1303	737	758	No	β-cyclocitral	166	137, 109
35	3-cis-4-(2,6,6-trimethyl-1-cyclohexen-1-yl)-3-buten-2-one	Cis-β-ionone	192	NA	1337.0	NA	NA	NA	No	α-ionone	177	43
36	3a,4,5,6-tetrahydro-3a,6,6-trimethyl-2(3H)-benzofuranone	2(3H)-B	180	16778-26-0	1427.3	1426	684	769	No	α-ionone	165	123, 109
37	3,7,11-trimethyl-1-dodecanol	3,7,11-trimethyl-1-dodecanol	228	6750-34-1	1573.6	1571	775	832	No	Trans-pseudoionone	55	69, 83
38	3,7-dimethyl-6-octenal	Citronellal	154	106.23.0	1145.9	1153	587	644	No	*Cis*-citral	69	81, 95

Information has been provided above for all apocarotenoids and putative apocarotenoids in this thesis, including names, Chemical Abstracting Service (CAS) number, MM, observed and NIST library RIs, and forward and reverse matching scores using the NIST spectral library search. For each compound, the compound whose *in planta* calibration curve was used for quantification, as well as quantifying and qualifying ions, are also listed.

References

Adami, M., De Franceschi, P., Brandi, F., Liverani, A., Giovannini, D., Rosati, C., Dondini, L. and Tartarini, S. (2013) Identifying a carotenoid cleavage dioxygenase (ccd4) gene controlling yellow/white fruit flesh color of peach. *Plant Mol Biol Rep*, **31**, 1166-1175.

Adams, R.P. (2007) *Identification of Essential Oil Components by Gas Chromatography-Mass Spectrometry* Allured Publishing Corporation: Carol Stream, Illinois.

Ahrazem, O., Trapero, A., Gómez, M.D., Rubio-Moraga, A. and Gómez-Gómez, L. (2010) Genomic analysis and gene structure of the plant carotenoid dioxygenase 4 family: A deeper study in Crocus sativus and its allies. *Genomics*, **96**, 239-250.

Akiyama, K. (2007) Chemical identification and functional analysis of apocarotenoids involved in the development of arbuscular mycorrhizal symbiosis. *Bioscience, Biotechnology, and Biochemistry*, **71**, 1405-1414.

Alboresi, A., Dall'Osto, L., Aprile, A., Carillo, P., Roncaglia, E., Cattivelli, L. and Bassi, R. (2011) Reactive oxygen species and transcript analysis upon excess light treatment in wild-type *Arabidopsis thaliana* vs a photosensitive mutant lacking zeaxanthin and lutein. *BMC Plant Biology*, **11**, 62.

Alder, A., Jamil, M., Marzorati, M., Bruno, M., Vermathen, M., Bigler, P., Ghisla, S., Bouwmeester, H., Beyer, P. and Al-Babili, S. (2012b) The path from β-carotene to carlactone, a strigolactone-like plant hormone. *Science*, **335**, 1348-1351.

Alméras, E., Stolz, S., Vollenweider, S., Reymond, P., Mène-Saffrané, L. and Farmer, E.E. (2003) Reactive electrophile species activate defense gene expression in Arabidopsis. *The Plant Journal*, **34**, 205-216.

Alon, T. and Amirav, A. (2015) How enhanced molecular ions in Cold EI improve compound identification by the NIST library. *Rapid Communications in Mass Spectrometry*, **29**, 2287-2292.

Alonso, J.M., Stepanova, A.N., Leisse, T.J., Kim, C.J., Chen, H., Shinn, P., Stevenson, D.K., Zimmerman, J., Barajas, P., Cheuk, R., Gadrinab, C., Heller, C., Jeske, A., Koesema, E., Meyers, C.C., Parker, H., Prednis, L., Ansari, Y., Choy, N., Deen, H., Geralt, M., Hazari, N., Hom, E., Karnes, M., Mulholland, C., Ndubaku, R., Schmidt, I., Guzman, P., Aguilar-Henonin, L., Schmid, M., Weigel, D., Carter, D.E., Marchand, T., Risseeuw, E., Brogden, D., Zeko, A., Crosby, W.L., Berry, C.C. and Ecker, J.R. (2003) Genome-wide insertional mutagenesis of *Arabidopsis thaliana*. *Science*, **301**, 653-657.

Amirav, A., Gordin, A. and Tzanani, N. (2001) Supersonic gas chromatography/mass spectrometry. *Rapid Communications in Mass Spectrometry*, **15**, 811-820.

Amirav, A., Keshet, U. and Danon, A. (2015) Soft Cold EI – approaching molecular ion only with electron ionization. *Rapid Communications in Mass Spectrometry*, **29**, 1954-1960.

Arii, S., Tsuji, K., Tomita, K., Hasegawa, M., Bober, B. and Harada, K.-I. (2015) Cyanobacterial blue color formation during lysis under natural conditions. *Applied and Environmental Microbiology*, **81**, 2667-2675.

Ashikawa, I., Kito, M., Satoh, K., Koike, H., Inoue, Y., Saiki, K., Tsukida, K. and Koyama, Y. (1987) All-*trans* β-carotene-5,6-epoxide in thylakoid membranes. *Photochemistry and Photobiology*, **46**, 269-275.

Auldridge, M.E., Block, A., Vogel, J.T., Dabney-Smith, C., Mila, I., Bouzayen, M., Magallanes-Lundback, M., DellaPenna, D., McCarty, D.R. and Klee, H.J.

(2006) Characterization of three members of the Arabidopsis carotenoid cleavage dioxygenase family demonstrates the divergent roles of this multifunctional enzyme family. *The Plant Journal*, **45**, 982-993.

Avendaño-Vázquez, A.-O., Cordoba, E., Llamas, E., San Román, C., Nisar, N., De la Torre, S., Ramos-Vega, M., Gutiérrez-Nava, M.d.l.L., Cazzonelli, C.I., Pogson, B.J. and León, P. (2014) An uncharacterized apocarotenoid-derived signal generated in ζ-carotene desaturase mutants regulates leaf development and the expression of chloroplast and nuclear genes in *Arabidopsis*. *The Plant Cell*.

Baldermann, S., Kato, M., Kurosawa, M., Kurobayashi, Y., Fujita, A., Fleischmann, P. and Watanabe, N. (2010) Functional characterization of a carotenoid cleavage dioxygenase 1 and its relation to the carotenoid accumulation and volatile emission during the floral development of *Osmanthus fragrans* Lour. *Journal of Experimental Botany*, **61**, 2967-2977.

Baldwin, E.A., Scott, J.W., Shewmaker, C.K. and Schuch, W. (2000) Flavor trivia and tomato aroma: Biochemistry and possible mechanisms for control of important aroma components. *HortScience*, **35**, 1013-1022.

Beisel, K.G., Jahnke, S., Hofmann, D., Köppchen, S., Schurr, U. and Matsubara, S. (2010) Continuous turnover of carotenes and chlorophyll *a* in mature leaves of *Arabidopsis* revealed by $^{14}CO_2$ pulse-chase labeling. *Plant Physiology*, **152**, 2188-2199.

Booker, J., Auldridge, M., Wills, S., McCarty, D., Klee, H. and Leyser, O. (2004) MAX3/CCD7 is a Carotenoid Cleavage Dioxygenase required for the synthesis of a novel plant signaling molecule. *Current Biology*, **14**, 1232-1238.

Bowman, M.J., Willis, D.K. and Simon, P.W. (2014) Transcript abundance of Phytoene Synthase 1 and Phytoene Synthase 2 is associated with natural variation of storage root carotenoid pigmentation in carrot. *Journal of the American Society for Horticultural Science*, **139**, 63-68.

Bradbury, L.M.T., Shumskaya, M., Tzfadia, O., Wu, S.-B., Kennelly, E.J. and Wurtzel, E.T. (2012) Lycopene cyclase paralog CruP protects against reactive oxygen species in oxygenic photosynthetic organisms. *Proceedings of the National Academy of Sciences*, **109**, E1888–E1897.

Brandi, F., Bar, E., Mourgues, F., Horvath, G., Turcsi, E., Giuliano, G., Liverani, A., Tartarini, S., Lewinsohn, E. and Rosati, C. (2011) Study of 'Redhaven' peach and its white-fleshed mutant suggests a key role of CCD4 carotenoid dioxygenase in carotenoid and norisoprenoid volatile metabolism. *BMC Plant Biology*, **11**, 24.

Bruno, M., Beyer, P. and Al-Babili, S. (2015) The potato carotenoid cleavage dioxygenase 4 catalyzes a single cleavage of β-ionone ring-containing carotenes and non-epoxidated xanthophylls. *Archives of Biochemistry and Biophysics*, **572**, 126-133.

Bruno, M., Koschmieder, J., Wuest, F., Schaub, P., Fehling-Kaschek, M., Timmer, J., Beyer, P. and Al-Babili, S. (2016) Enzymatic study on AtCCD4 and AtCCD7 and their potential to form acyclic regulatory metabolites. *Journal of Experimental Botany*, **67**, 5993-6005.

Butkhup, L., Jeenphakdee, M., Jorjong, S., Samappito, S., Samappito, W. and Chowtivannakul, S. (2011) HS-SPME-GC-MS analysis of volatile aromatic compounds in alcohol related beverages made with mulberry fruits. *Food Science and Biotechnology*, **20**, 1021-1032.

Cáceres, L.A., Lakshminarayan, S., Yeung, K.K.-C., McGarvey, B.D., Hannoufa, A., Sumarah, M.W., Benitez, X. and Scott, I.M. (2016) Repellent and attractive effects of α-, β-, and dihydro-β-ionone to generalist and specialist herbivores. *Journal of Chemical Ecology*, **42**, 107-117.

Campbell, R., Ducreux, L.J.M., Morris, W.L., Morris, J.A., Suttle, J.C., Ramsay, G., Bryan, G.J., Hedley, P.E. and Taylor, M.A. (2010) The metabolic and developmental roles of carotenoid cleavage dioxygenase 4 from potato (Solanum tuberosum L). *Plant Physiology*.

Cavalli, J.-F., Fernandez, X., Lizzani-Cuvelier, L. and Loiseau, A.-M. (2003) Comparison of static headspace, headspace solid phase microextraction, headspace sorptive extraction, and direct thermal desorption techniques on chemical composition of French olive oils. *Journal of Agricultural and Food Chemistry*, **51**, 7709-7716.

Cazzonelli, C.I. and Pogson, B.J. (2010) Source to sink: regulation of carotenoid biosynthesis in plants. *Trends in Plant Science*, **15**, 266-274.

Chai, C., Fang, J., Liu, Y., Tong, H., Gong, Y., Wang, Y., Liu, M., Wang, Y., Qian, Q., Cheng, Z. and Chu, C. (2011) *ZEBRA2*, encoding a carotenoid isomerase, is involved in photoprotection in rice. *Plant Molecular Biology*, **75**, 211-221.

Chan, K.X., Phua, S.Y., Crisp, P., McQuinn, R. and Pogson, B.J. (2016) Learning the languages of the chloroplast: Retrograde signaling and beyond. *Annual Review of Plant Biology*, **67**, 25-53.

Cunningham, F.X. and Gantt, E. (1998) Genes and enzymes of carotenoid biosynthesis in plants. *Annual Review of Plant Physiology and Plant Molecular Biology*, **49**, 557-583.

Cuttriss, A.J., Chubb, A.C., Alawady, A., Grimm, B. and Pogson, B.J. (2007) Regulation of lutein biosynthesis and prolamellar body formation in *Arabidopsis*. *Functional Plant Biology*, **34**, 663-672.

Dagan, S. and Amirav, A. (1995) Electron impact mass spectrometry of alkanes in supersonic molecular beams. *Journal of the American Society for Mass Spectrometry*, **6**, 120-131.

Du, X. and Zeisel, S.H. (2013) Spectral deconvolution for gas chromatography mass spectrometry-based metabolomics: Current status and future perspectives. *Computational and Structural Biotechnology Journal*, **4**. e201301013.

Dueñas, M.E., Klein, A.T., Alexander, L.E., Yandeau-Nelson, M.D., Nikolau, B.J. and Lee, Y.J. (2017) High spatial resolution mass spectrometry imaging reveals the genetically programmed, developmental modification of the distribution of thylakoid membrane lipids among individual cells of maize leaf. *The Plant Journal*, **89**, 825-838.

Duncan, M.W. (2012) Good mass spectrometry and its place in good science. *Journal of Mass Spectrometry*, **47**, 1671-1671.

Dunkel, M., Schmidt, U., Struck, S., Berger, L., Gruening, B., Hossbach, J., Jaeger, I.S., Effmert, U., Piechulla, B., Eriksson, R., Knudsen, J. and Preissner, R. (2009) SuperScent—a database of flavors and scents. *Nucleic Acids Research*, **37**, D291-D294.

Eggink, P.M., Maliepaard, C., Tikunov, Y., Haanstra, J.P.W., Bovy, A.G. and Visser, R.G.F. (2012) A taste of sweet pepper: Volatile and non-volatile chemical composition of fresh sweet pepper (Capsicum annuum) in relation to sensory evaluation of taste. *Food Chemistry*, **132**, 301-310.

El-Sayed, A. (2016) The Pherobase: Database of Pheromones and Semiochemicals.

Enfissi, E.M.A., Nogueira, M., Bramley, P.M. and Fraser, P.D. (2017) The regulation of carotenoid formation in tomato fruit. *The Plant Journal*, **89**, 774-788.

Eroglu, A., Hruszkewycz, D.P., dela Sena, C., Narayanasamy, S., Riedl, K.M., Kopec, R.E., Schwartz, S.J., Curley, R.W., Jr. and Harrison, E.H. (2012) Naturally occurring eccentric cleavage products of provitamin A beta-carotene function as antagonists of retinoic acid receptors. *Journal of Biological Chemistry*, **287**, 15886-15895.

Estavillo, G.M., Chan, K.X., Phua, S.Y. and Pogson, B.J. (2012) Reconsidering the nature and mode of action of metabolite retrograde signals from the chloroplast. *Frontiers in Plant Science*, **3**, 300.

Farmer, E.E. and Mueller, M.J. (2013) ROS-mediated lipid peroxidation and RES-activated signaling. *Annual Review of Plant Biology*, **64**, 429-450.

Feng, H., Skinkis, P.A. and Qian, M.C. (2017) Pinot noir wine volatile and anthocyanin composition under different levels of vine fruit zone leaf removal. *Food Chemistry*, **214**, 736-744.

Fester, T., Hause, B., Schmidt, D., Halfmann, K., Schmidt, J., Wray, V., Hause, G. and Strack, D. (2002a) Occurrence and localization of apocarotenoids in arbuscular mycorrhizal plant roots. *Plant and Cell Physiology*, **43**, 256-265.

Fester, T., Schmidt, D., Lohse, S., Walter, M.H., Giuliano, G., Bramley, P.M., Fraser, P.D., Hause, B. and Strack, D. (2002b) Stimulation of carotenoid metabolism in arbuscular mycorrhizal roots. *Planta*, **216**, 148-154.

Fialkov, A.B., Gordin, A. and Amirav, A. (2008) Hydrocarbons and fuels analyses with the supersonic gas chromatography mass spectrometry—The novel concept of isomer abundance analysis. *Journal of Chromatography A*, **1195**, 127-135.

Fiedor, J. and Burda, K. (2014) Potential role of carotenoids as antioxidants in human health and disease. *Nutrients*, **6**, 466-488.

Floss, D.S., Schliemann, W., Schmidt, J., Strack, D. and Walter, M.H. (2008) RNA Interference-mediated repression of *MtCCD1* in Mycorrhizal Roots of *Medicago truncatula* causes accumulation of C_{27} apocarotenoids, shedding light on the functional role of CCD1. *Plant Physiology*, **148**, 1267-1282.

Fraser, P.D. and Bramley, P.M. (2004) The biosynthesis and nutritional uses of carotenoids. *Progress in Lipid Research*, **43**, 228-265.

Fraser, P.D., Truesdale, M.R., Bird, C.R., Schuch, W. and Bramley, P.M. (1994) Carotenoid biosynthesis during tomato fruit development (evidence for tissue-specific gene expression). *Plant Physiology*, **105**, 405-413.

Frusciante, S., Diretto, G., Bruno, M., Ferrante, P., Pietrella, M., Prado-Cabrero, A., Rubio-Moraga, A., Beyer, P., Gomez-Gomez, L., Al-Babili, S. and Giuliano, G. (2014) Novel carotenoid cleavage dioxygenase catalyzes the first dedicated step in saffron crocin biosynthesis. *Proceedings of the National Academy of Sciences*, **111**, 12246-12251.

Fu, X., Feng, C., Wang, C., Yin, X., Lu, P., Grierson, D., Xu, C. and Chen, K. (2014) Involvement of multiple phytoene synthase genes in tissue- and cultivar-specific accumulation of carotenoids in loquat. *Journal of Experimental Botany*, **65**, 4679-4689.

Gallon, C.Z., Fuller, S.C., Fanning, K.J., Smyth, H.E., Pun, S., Martin, I.F. and O'Hare, T.J. (2013) Increase in β-ionone, a carotenoid-derived volatile in zeaxanthin-biofortified sweet corn. *Journal of Agricultural and Food Chemistry*, **61**, 7181-7187.

Galpaz, N., Burger, Y., Lavee, T., Tzuri, G., Sherman, A., Melamed, T., Eshed, R., Meir, A., Portnoy, V., Bar, E., Shimoni-Shor, E., Feder, A., Saar, Y., Saar, U., Baumkoler, F., Lewinsohn, E., Schaffer, A.A., Katzir, N. and Tadmor, Y. (2013) Genetic and chemical characterization of an EMS induced mutation in Cucumis melo CRTISO gene. *Archives of Biochemistry and Biophysics*, **539**, 117-125.

Galpaz, N., Ronen, G., Khalfa, Z., Zamir, D. and Hirschberg, J. (2006) A chromoplast-specific carotenoid biosynthesis pathway is revealed by cloning of the tomato white-flower locus. *The Plant Cell*, **18**, 1947-1960.

Gao, P., Xu, P.-F. and Zhai, H. (2009) Expeditious construction of (+)-mintlactone *via* intramolecular Hetero-Pauson−Khand reaction. *The Journal of Organic Chemistry*, **74**, 2592-2593.

García-Limones, C., Schnäbele, K., Blanco-Portales, R., Luz Bellido, M., Caballero, J.L., Schwab, W. and Muñoz-Blanco, J. (2008) Functional characterization of FaCCD1: A Carotenoid Cleavage Dioxygenase from strawberry involved in lutein degradation during fruit ripening. *Journal of Agricultural and Food Chemistry*, **56**, 9277-9285.

George, M.J., Marjanovic, L. and Williams, D.B.G. (2015) Solvent-assisted headspace sampling using solid phase microextraction for the analysis of phenols in water. *Analytical Chemistry*, **87**, 9559-9562.

Gonzalez-Jorge, S., Ha, S.-H., Magallanes-Lundback, M., Gilliland, L.U., Zhou, A., Lipka, A.E., Nguyen, Y.-N., Angelovici, R., Lin, H., Cepela, J., Little, H., Buell, C.R., Gore, M.A. and DellaPenna, D. (2013) CAROTENOID CLEAVAGE DIOXYGENASE4 is a negative regulator of β-carotene content in *Arabidopsis* seeds. *The Plant Cell* **25**, 4812-4826.

Gonzalez-Jorge, S., Mehrshahi, P., Magallanes-Lundback, M., Lipka, A.E., Angelovici, R., Gore, M.A. and DellaPenna, D. (2016) ZEAXANTHIN EPOXIDASE activity potentiates carotenoid degradation in maturing *Arabidopsis* seed. *Plant Physiology*.

González-Pérez, S., Gutiérrez, J., García-García, F., Osuna, D., Dopazo, J., Lorenzo, Ó., Revuelta, J.L. and Arellano, J.B. (2011) Early transcriptional defense responses in *Arabidopsis* cell suspension culture under high-light conditions. *Plant Physiology*, **156**, 1439-1456.

Grassl, J., Pružinská, A., Hörtensteiner, S., Taylor, N.L. and Millar, A.H. (2012) Early events in plastid protein degradation in stay-green *Arabidopsis* reveal differential regulation beyond the retention of LHCII and chlorophyll. *Journal of Proteome Research*, **11**, 5443-5452.

Han, S.-H., Sakuraba, Y., Koh, H.-J. and Paek, N.-C. (2012) Leaf variegation in the rice *zebra2* mutant is caused by photoperiodic accumulation of tetra-*cis*-lycopene and singlet oxygen. *Mol Cells*, **33**, 87-97.

Harada, K.-I., Ozaki, K., Tsuzuki, S., Kato, H., Hasegawa, M., Kuroda, E.K., Arii, S. and Tsuji, K. (2009) Blue color formation of cyanobacteria with β-cyclocitral. *Journal of Chemical Ecology*, **35**, 1295-1301.

Harrison, A.G. (1992) *Chemical Ionization Mass Spectrometry* 2 edn. Boca Raton: CRC Press.

Harrison, P.J. and Bugg, T.D.H. (2014) Enzymology of the carotenoid cleavage dioxygenases: Reaction mechanisms, inhibition and biochemical roles. *Archives of Biochemistry and Biophysics*, **544**, 105-111.

Havaux, M. (2013) Carotenoid oxidation products as stress signals in plants. *The Plant Journal*, **79**, 597-606

Hernández, M.L., Whitehead, L., He, Z., Gazda, V., Gilday, A., Kozhevnikova, E., Vaistij, F.E., Larson, T.R. and Graham, I.A. (2012) A cytosolic acyltransferase contributes to triacylglycerol synthesis in sucrose-rescued *Arabidopsis* seed oil catabolism mutants. *Plant Physiology*, **160**, 215-225.

Hirschberg, J. (2001) Carotenoid biosynthesis in flowering plants. *Current Opinion in Plant Biology*, **4**, 210-218.

Hocart, C.H. (2010) 9.10 - Mass Spectrometry: An Essential Tool for Trace Identification and Quantification. In *Comprehensive Natural Products II*. Oxford: Elsevier, pp. 327-388.

Hou, X. (2015) Results of ccr2 studies. Personal Communication.

Hou, X., Rivers, J., León, P., McQuinn, R.P. and Pogson, B.J. (2016) Synthesis and function of apocarotenoid signals in plants. *Trends in Plant Science*. **21**, 792–803

Huang, F.-C., Horváth, G., Molnár, P., Turcsi, E., Deli, J., Schrader, J., Sandmann, G., Schmidt, H. and Schwab, W. (2009a) Substrate promiscuity of RdCCD1, a carotenoid cleavage oxygenase from *Rosa damascena*. *Phytochemistry*, **70**, 457-464.

Huang, F.-C., Molnár, P. and Schwab, W. (2009b) Cloning and functional characterization of carotenoid cleavage dioxygenase 4 genes. *Journal of Experimental Botany*, **60**, 3011-3022.

Hummel, J., Strehmel, N., Selbig, J., Walther, D. and Kopka, J. (2010) Decision tree supported substructure prediction of metabolites from GC-MS profiles. *Metabolomics*, **6**, 322-333.

Ibdah, M., Azulay, Y., Portnoy, V., Wasserman, B., Bar, E., Meir, A., Burger, Y., Hirschberg, J., Schaffer, A.A., Katzir, N., Tadmor, Y. and Lewinsohn, E. (2006) Functional characterization of CmCCD1, a carotenoid cleavage dioxygenase from melon. *Phytochemistry*, **67**, 1579-1589.

Ilg, A., Beyer, P. and Al-Babili, S. (2009) Characterization of the rice carotenoid cleavage dioxygenase 1 reveals a novel route for geranial biosynthesis. *FEBS Journal*, **276**, 736-747.

Ilg, A., Bruno, M., Beyer, P. and Al-Babili, S. (2014) Tomato carotenoid cleavage dioxygenases 1A and 1B: Relaxed double bond specificity leads to a plenitude of dialdehydes, mono-apocarotenoids and isoprenoid volatiles. *FEBS Open Bio*, **4**, 584-593.

Ilg, A., Yu, Q., Schaub, P., Beyer, P. and Al-Babili, S. (2010) Overexpression of the rice carotenoid cleavage dioxygenase 1 gene in Golden Rice endosperm suggests apocarotenoids as substrates in planta. *Planta*, **232**, 691-699.

Isaacson, T., Gil, R., Dani, Z. and Hirschberg, J. (2002) Cloning of tangerine from tomato reveals a carotenoid isomerase essential for the production of β-carotene and xanthophylls in plants. *The Plant Cell*. **14**, 333-342

Jefferies, R.A. and Mackerron, D.K.L. (1987) Effect of second growth on the quality of tubers as seed in the cultivar Record. *Potato Research*, **30**, 337-340.

Joichi, A., Nakamura, Y., Haze, S., Ishikawa, T., Atoji, H., Nishida, T. and Sakurai, K. (2013) Volatile constituents of blue-coloured hybrid tea rose flowers. *Flavour and Fragrance Journal*, **28**, 180-187.

Kachanovsky, D.E., Filler, S., Isaacson, T. and Hirschberg, J. (2012) Epistasis in tomato color mutations involves regulation of phytoene synthase 1 expression by cis-carotenoids. *Proceedings of the National Academy of Sciences*, **109**, 19021-19026.

Kato, M., Matsumoto, H., Ikoma, Y., Okuda, H. and Yano, M. (2006) The role of carotenoid cleavage dioxygenases in the regulation of carotenoid profiles during maturation in citrus fruit. *Journal of Experimental Botany*, **57**, 2153-2164.

Kelly, A.A., Kalisch, B., Hölzl, G., Schulze, S., Thiele, J., Melzer, M., Roston, R.L., Benning, C. and Dörmann, P. (2016) Synthesis and transfer of galactolipids in the chloroplast envelope membranes of *Arabidopsis thaliana*. *Proceedings of the National Academy of Sciences*, **113**, 10714-10719.

Kim, C., Meskauskiene, R., Zhang, S., Lee, K.P., Lakshmanan Ashok, M., Blajecka, K., Herrfurth, C., Feussner, I. and Apel, K. (2012) Chloroplasts of *Arabidopsis* are the source and a primary target of a plant-specific programmed cell death signaling pathway. *The Plant Cell*, **24**, 3026-3039.

Kim, J. and DellaPenna, D. (2006) Defining the primary route for lutein synthesis in plants: The role of Arabidopsis carotenoid β-ring hydroxylase CYP97A3. *Proceedings of the National Academy of Sciences*, **103**, 3474-3479.

Klingner, A., Hundeshagen, B., Kernebeck, H. and Bothe, H. (1995) Localization of the yellow pigment formed in roots of gramineous plants colonized by arbuscular fungi. *Protoplasma*, **185**, 50-57.

Kobayashi, K., Endo, K. and Wada, H. (2016) Roles of lipids in photosynthesis. In *Lipids in Plant and Algae Development* (Nakamura, Y. and Li-Beisson, Y. eds). Cham: Springer International Publishing, pp. 21-49.

Konig, W.A., Joulain, D. and Hochmuth, D.H. König WA, Joulain D, Hochmuth DH: GC/MS Library: Terpenoids and Related Constituents of Essential Oils.[http://www.massfinder.com].

Krishnakumar, V., Hanlon, M.R., Contrino, S., Ferlanti, E.S., Karamycheva, S., Kim, M., Rosen, B.D., Cheng, C.-Y., Moreira, W., Mock, S.A., Stubbs, J., Sullivan, J.M., Krampis, K., Miller, J.R., Micklem, G., Vaughn, M. and Town, C.D. (2015) Araport: the *Arabidopsis* Information Portal. *Nucleic Acids Research*, **43**, D1003-D1009.

Kusano, M., Iizuka, Y., Kobayashi, M., Fukushima, A. and Saito, K. (2013) Development of a direct headspace collection method from *Arabidopsis* seedlings using HS-SPME-GC-TOF-MS analysis. *Metabolites*, **3**, 223.

Kwok, E.Y. and Hanson, M.R. (2004) Stromules and the dynamic nature of plastid morphology. *Journal of Microscopy-Oxford*, **214**, 124-137.

Lao, Y.-M., Xiao, L., Ye, Z.W., Jiang, J.-G. and Zhou, S.-S. (2011) In silico analysis of phytoene synthase and its promoter reveals hints for regulation mechanisms of carotenogenesis in Duanliella bardawil. *Bioinformatics*, **27**, 2201-2208.

Lashbrooke, J., Young, P., Dockrall, S., Vasanth, K. and Vivier, M. (2013) Functional characterisation of three members of the *Vitis vinifera* L. carotenoid cleavage dioxygenase gene family. *BMC Plant Biology*, **13**, 156.

Lätari, K., Wüst, F., Hübner, M., Schaub, P., Beisel, K., Gabriele, Matsubara, S., Beyer, P. and Welsch, R. (2015) Tissue-specific apocarotenoid glycosylation contributes to carotenoid homeostasis in *Arabidopsis* leaves. *Plant Physiology*. 00243.2015

Lerch, O. and Gil, C. (2008) Determination of aldehydes and ketones in oily matrices using a novel dynamic headspace sampler coupled to GC/MS. *Gerstel AppNote*, **3/2008**.

Levonen, A.-L., Landar, A., Ramachandran, A., Ceaser, E.K., Dickinson, D.A., Zanoni, G., Morrow, J.D. and Darley-Usmar, V.M. (2004) Cellular mechanisms of redox cell signalling: role of cysteine modification in controlling antioxidant defences in response to electrophilic lipid oxidation products. *Biochemical Journal*, **378**, 373-382.

Li, F., Murillo, C. and Wurtzel, E.T. (2007) Maize *Y9* Encodes a product essential for 15-*cis*-ζ-carotene isomerization. *Plant Physiology*, **144**, 1181-1189.

Li, F., Vallabhaneni, R. and Wurtzel, E.T. (2008) PSY3, a new member of the phytoene synthase gene family conserved in the Poaceae and regulator of abiotic stress-induced root carotenogenesis. *Plant Physiology*, **146**, 1333-1345.

Lin, H., Wang, R., Qian, Q., Yan, M., Meng, X., Fu, Z., Yan, C., Jiang, B., Su, Z., Li, J. and Wang, Y. (2009) DWARF27, an iron-containing protein required for the biosynthesis of strigolactones, regulates rice tiller bud outgrowth. *The Plant Cell*, **21**, 1512-1525.

Linnewiel, K., Ernst, H., Caris-Veyrat, C., Ben-Dor, A., Kampf, A., Salman, H., Danilenko, M., Levy, J. and Sharoni, Y. (2009) Structure activity relationship of carotenoid derivatives in activation of the electrophile/antioxidant response element transcription system. *Free Radical Biology and Medicine*, **47**, 659-667.

Liu, J.R., Sun, X.R., Dong, H.W., Sun, C.H., Sun, W.G., Chen, B.Q., Song, Y.Q. and Yang, B.F. (2008) β-ionone suppresses mammary carcinogenesis, proliferative

activity and induces apoptosis in the mammary gland of the Sprague-Dawley rat. *International Journal of Cancer*, **122**, 2689-2698.

Lundquist, P.K., Poliakov, A., Bhuiyan, N.H., Zybailov, B., Sun, Q. and van Wijk, K.J. (2012) The functional network of the *Arabidopsis* plastoglobule proteome based on quantitative proteomics and genome-wide coexpression analysis. *Plant Physiology*, **158**, 1172-1192.

Lv, F., Zhou, J., Zeng, L. and Xing, D. (2015) β-cyclocitral upregulates salicylic acid signalling to enhance excess light acclimation in *Arabidopsis*. *Journal of Experimental Botany*, **66**, 4719-4732.

Ma, G., Zhang, L., Matsuta, A., Matsutani, K., Yamawaki, K., Yahata, M., Wahyudi, A., Motohashi, R. and Kato, M. (2013) Enzymatic formation of β-citraurin from β-cryptoxanthin and zeaxanthin by carotenoid cleavage dioxygenase 4 in the flavedo of citrus fruit. *Plant Physiology*, **163**, 682-695.

Maass, D., Arango, J., Wüst, F., Beyer, P. and Welsch, R. (2009) Carotenoid crystal formation in *Arabidopsis* and carrot roots caused by increased phytoene synthase protein levels. *PLoS ONE*, **4**, e6373.

Maier, W., Peipp, H., Schmidt, J., Wray, V. and Strack, D. (1995) Levels of a terpenoid glycoside (blumenin) and cell wall-bound phenolics in some cereal mycorrhizas. *Plant Physiology*, **109**, 465-470.

Maresca, J., Graham, J. and Bryant, D. (2008) The biochemical basis for structural diversity in the carotenoids of chlorophototrophic bacteria. *Photosynthesis Research*, **97**, 121-140.

Mathieu, S., Terrier, N., Procureur, J., Bigey, F. and Günata, Z. (2005) A carotenoid cleavage dioxygenase from *Vitis vinifera* L.: functional characterization and expression during grape berry development in relation to C_{13}-norisoprenoid accumulation. *Journal of Experimental Botany*, **56**, 2721-2731.

Matsui, K., Sugimoto, K., Mano, J.i., Ozawa, R. and Takabayashi, J. (2012) Differential metabolisms of green leaf volatiles in injured and intact parts of a wounded leaf meet distinct ecophysiological requirements. *PLoS ONE*, **7**, e36433.

McQuinn, R.P., Giovannoni, J.J. and Pogson, B.J. (2015) More than meets the eye: from carotenoid biosynthesis, to new insights into apocarotenoid signaling. *Current Opinion in Plant Biology*, **27**, 172-179.

Mehrshahi, P., Johnny, C. and DellaPenna, D. (2014) Redefining the metabolic continuity of chloroplasts and ER. *Trends in Plant Science*, **19**, 501-507.

Melendez-Martinez, A.J., Stinco, C.M., Liu, C. and Wang, X.-D. (2013) A simple HPLC method for the comprehensive analysis of cis/trans (Z/E) geometrical isomers of carotenoids for nutritional studies. *Food Chemistry*, **138**, 1341-1350.

Nambara, E. and Marion-Poll, A. (2005) Abscisic acid biosynthesis and catabolism. *Annual Review of Plant Biology*, **56**, 165-185.

Nisar, N., Li, L., Lu, S., Khin, Nay C. and Pogson, Barry J. (2015) Carotenoid metabolism in plants. *Molecular Plant*, **8**, 68-82.

Nishino, H., Tokuda, H., Murakoshi, M., Satomi, Y., Masuda, M., Onozuka, M., Yamaguchi, S., Takayasu, J., Tsuruta, J., Okuda, M., Khachik, F., Narisawa, T., Takasuka, N. and Yano, M. (2000) Cancer prevention by natural carotenoids. *Biofactors*, **13**, 89-94.

NIST (2014) NIST/EPA/NIH Mass Spectral Library. In *NIST Standard Reference Database 1A*.

Noctor, G. and Foyer, C.H. (2016) Intracellular redox compartmentation and ROS-related communication in regulation and signaling. *Plant Physiology*, **171**, 1581-1592.

Oberschall, A., Deák, M., Török, K., Sass, L., Vass, I., Kovács, I., Fehér, A., Dudits, D. and Horváth, G.V. (2000) A novel aldose/aldehyde reductase protects

transgenic plants against lipid peroxidation under chemical and drought stresses. *The Plant Journal*, **24**, 437-446.

Ohmiya, A., Kishimoto, S., Aida, R., Yoshioka, S. and Sumitomo, K. (2006) Carotenoid Cleavage Dioxygenase (CmCCD4a) contributes to white color formation in chrysanthemum petals. *Plant Physiology*, **142**, 1193-1201.

Ozaki, K., Ohta, A., Iwata, C., Horikawa, A., Tsuji, K., Ito, E., Ikai, Y. and Harada, K.-i. (2008) Lysis of cyanobacteria with volatile organic compounds. *Chemosphere*, **71**, 1531-1538.

Park, H., Kreunen, S.S., Cuttriss, A.J., DellaPenna, D. and Pogson, B.J. (2002) Identification of the carotenoid isomerase provides insight into carotenoid biosynthesis, prolamellar body formation, and photomorphogenesis. *The Plant Cell*, **14**, 321-332.

Park, S.-Y., Yu, J.-W., Park, J.-S., Li, J., Yoo, S.-C., Lee, N.-Y., Lee, S.-K., Jeong, S.-W., Seo, H.S., Koh, H.-J., Jeon, J.-S., Park, Y.-I. and Paek, N.-C. (2007) The senescence-induced staygreen protein regulates chlorophyll degradation. *The Plant Cell*, **19**, 1649-1664.

Patkin, A. (2015a) Analysis of FAMEs using cold EI GC/MS for enhanced molecular ion sensitivity. Shelton, CT, USA: PerkinElmer.

Patkin, A. (2015b) Cold EI GC/MS enhancement of high MW hydrocarbon molecular weight information. Shelton, CT, USA: PerkinElmer.

Pfannkoch, E. and Whitecavage, J. (2000) Comparison of the sensitivity of static headspace GC, solid phase microextraction, and direct thermal extraction for analysis of volatiles in solid matrices. Linthicum, MD, USA: Gerstel Inc.

Pogson, B., McDonald, K.A., Truong, M., Britton, G. and DellaPenna, D. (1996) Arabidopsis carotenoid mutants demonstrate that lutein is not essential for photosynthesis in higher plants. *The Plant Cell*, **8**, 1627-1639.

Pogson, B.J., Woo, N.S., Förster, B. and Small, I.D. (2008) Plastid signalling to the nucleus and beyond. *Trends in Plant Science*, **13**, 602-609.

R Core Team (2016) R: A language and environment for statistical computing. Austria: R Foundation for Statistical Computing.

Ramel, F., Birtic, S., Cuiné, S., Triantaphylidès, C., Ravanat, J.-L. and Havaux, M. (2012a) Chemical quenching of singlet oxygen by carotenoids in plants. *Plant Physiology*, **158**, 1267-1278.

Ramel, F., Birtic, S., Ginies, C., Soubigou-Taconnat, L., Triantaphylidès, C. and Havaux, M. (2012b) Carotenoid oxidation products are stress signals that mediate gene responses to singlet oxygen in plants. *Proceedings of the National Academy of Sciences*, **109**, 5535-5540.

Ramel, F., Mialoundama, A.S. and Havaux, M. (2013) Nonenzymic carotenoid oxidation and photooxidative stress signalling in plants. *Journal of Experimental Botany*, **64**, 799-805.

Renold, W., Näf-Müller, R., Keller, U., Willhalm, B. and Ohloff, G. (1974) An investigation of the tea aroma. Part I. New volatile black tea constituents. *Helvetica Chimica Acta*, **57**, 1301-1308.

Restek (2000) A technical guide for static headspace analysis using GC. Bellefonte, PA, USA: Restek Corporation.

Risticevic, S., Lord, H., Gorecki, T., Arthur, C.L. and Pawliszyn, J. (2010) Protocol for solid-phase microextraction method development. *Nature Protocols*, **5**.

Rizhsky, L., Jin, H., Shepard, M.R., Scott, H.W., Teitgen, A.M., Perera, M.A., Mhaske, V., Jose, A., Zheng, X., Crispin, M., Wurtele, E.S., Jones, D., Hur, M., Góngora-Castillo, E., Buell, C.R., Minto, R.E. and Nikolau, B.J. (2016) Integrating metabolomics and transcriptomics data to discover a biocatalyst that

can generate the amine precursors for alkamide biosynthesis. *The Plant Journal*, **88**, 775-793.

Rodriguez-Villalon, A., Gas, E. and Rodriguez-Concepcion, M. (2009a) Colors in the dark: a model for the regulation of carotenoid biosynthesis in etioplasts. *Plant Signaling & Behavior*, **4**, 965-967.

Rodriguez-Villalon, A., Gas, E. and Rodriguez-Concepcion, M. (2009b) Phytoene synthase activity controls the biosynthesis of carotenoids and the supply of their metabolic precursors in dark-grown *Arabidopsis* seedlings. *The Plant Journal*, **60**, 424-435.

Rohloff, J. (2004) Essential oil drugs — terpene composition of aromatic herbs. In *Production Practices and Quality Assessment of Food Crops: Quality Handling and Evaluation* (Dris, R. and Jain, S.M. eds). Dordrecht: Springer Netherlands, pp. 73-128.

Rohloff, J. and Bones, A.M. (2005) Volatile profiling of *Arabidopsis thaliana* – Putative olfactory compounds in plant communication. *Phytochemistry*, **66**, 1941-1955.

Rottet, S., Besagni, C. and Kessler, F. (2015) The role of plastoglobules in thylakoid lipid remodeling during plant development. *Biochimica et Biophysica Acta (BBA) - Bioenergetics*, **1847**, 889-899.

Rottet, S., Devillers, J., Glauser, G., Douet, V., Besagni, C. and Kessler, F. (2016) Identification of plastoglobules as a site of carotenoid cleavage. *Frontiers in Plant Science*, **7**. 1855.

Rowan, D.D. (2011) Volatile Metabolites. *Metabolites*, **1**, 41.

Rubio-Moraga, A., Rambla, J., Fernández-de-Carmen, A., Trapero-Mozos, A., Ahrazem, O., Orzáez, D., Granell, A. and Gómez-Gómez, L. (2014) New target carotenoids for CCD4 enzymes are revealed with the characterization of a novel stress-induced carotenoid cleavage dioxygenase gene from *Crocus sativus*. *Plant Molecular Biology*, **86**, 555-569.

Rubio, A., Rambla, J.L., Santaella, M., Gómez, M.D., Orzaez, D., Granell, A. and Gómez-Gómez, L. (2008) Cytosolic and plastoglobule-targeted carotenoid dioxygenases from *Crocus sativus* are both involved in β-ionone release. *Journal of Biological Chemistry*, **283**, 24816-24825.

Ruijter, J.M., Ramakers, C., Hoogaars, W.M.H., Karlen, Y., Bakker, O., van den Hoff, M.J.B. and Moorman, A.F.M. (2009) Amplification efficiency: linking baseline and bias in the analysis of quantitative PCR data. *Nucleic Acids Research*, **37**, e45.

Ruiz-Sola, M.Á., Arbona, V., Gómez-Cadenas, A., Rodríguez-Concepción, M. and Rodríguez-Villalón, A. (2014) A root specific induction of carotenoid biosynthesis contributes to ABA production upon salt stress in *Arabidopsis*. *PLOS ONE*, **9**, e90765.

Ruiz-Sola, M.A. and Rodriguez-Concepcion, M. (2012) Carotenoid biosynthesis in *Arabidopsis*: a colorful pathway. *Arabidopsis Book*, **10**, e0158.

Sánchez, G., Besada, C., Badenes, M.L., Monforte, A.J. and Granell, A. (2012) A non-targeted approach unravels the volatile network in peach fruit. *PLOS ONE*, **7**, e38992.

Schenkel, D., Lemfack, M., Piechulla, B. and Splivallo, R. (2015) A meta-analysis approach for assessing the diversity and specificity of belowground root and microbial volatiles. *Frontiers in Plant Science*, **6**. 707.

Scholtes, C., Nizet, S., Massart, H., Gerbaux, P. and Collin, S. (2015) Occurrence of theaspirane and its odorant degradation products in hop and beer. *Journal of Agricultural and Food Chemistry*, **63**, 8247-8253.

Schwab, W., Davidovich-Rikanati, R. and Lewinsohn, E. (2008) Biosynthesis of plant-derived flavor compounds. *The Plant Journal*, **54**, 712-732.

Schwartz, S.H., Qin, X. and Loewen, M.C. (2004) The biochemical characterization of two carotenoid cleavage enzymes from *Arabidopsis* indicates that a carotenoid-derived compound inhibits lateral branching. *Journal of Biological Chemistry*, **279**, 46940-46945.

Schwartz, S.H., Tan, B.C., McCarty, D.R., Welch, W. and Zeevaart, J.A.D. (2003) Substrate specificity and kinetics for VP14, a carotenoid cleavage dioxygenase in the ABA biosynthetic pathway. *Biochimica et Biophysica Acta (BBA) - General Subjects*, **1619**, 9-14.

Sergeant, M.J., Li, J.-J., Fox, C., Brookbank, N., Rea, D., Bugg, T.D.H. and Thompson, A.J. (2009) Selective inhibition of carotenoid cleavage dioxygenases: phenotypic effects on shoot branching. *Journal of Biological Chemistry*, **284**, 5257-5264.

Serrano, M., Silva, M. and Gallego, M. (2015) Determination of 14 haloketones in treated water using solid–phase microextraction and gas chromatography–mass spectrometry. *Journal of Chromatography A*, **1407**, 208-215.

Shishido, K., Irie, O. and Shibuya, M. (1992) An efficient total synthesis of (−)-mintlactone and (+)-isomintlactone. *Tetrahedron Letters*, **33**, 4589-4592.

Shumbe, L., Bott, R. and Havaux, M. (2014) Dihydroactinidiolide, a high light-induced β-carotene derivative that can regulate gene expression and photoacclimation in *Arabidopsis*. *Molecular Plant*, **7**, 1248-1251.

Shumskaya, M., Bradbury, L.M.T., Monaco, R.R. and Wurtzel, E.T. (2012) Plastid localization of the key carotenoid enzyme phytoene synthase is altered by isozyme, allelic variation, and activity. *The Plant Cell*, **24**, 3725-3741.

Simkin, A.J., Schwartz, S.H., Auldridge, M., Taylor, M.G. and Klee, H.J. (2004a) The tomato carotenoid cleavage dioxygenase 1 genes contribute to the formation of the flavor volatiles β-ionone, pseudoionone, and geranylacetone. *The Plant Journal*, **40**, 882-892.

Simkin, A.J., Underwood, B.A., Auldridge, M., Loucas, H.M., Shibuya, K., Schmelz, E., Clark, D.G. and Klee, H.J. (2004b) Circadian regulation of the PhCCD1 carotenoid cleavage dioxygenase controls emission of β-ionone, a fragrance volatile of petunia flowers. *Plant Physiology*, **136**, 3504-3514.

Skogerson, K., Wohlgemuth, G., Barupal, D.K. and Fiehn, O. (2011) The volatile compound BinBase mass spectral database. *BMC Bioinformatics*, **12**, 1-15.

Snodderly, D.M. (1995) Evidence for protection against age-related macular degeneration by carotenoids and antioxidant vitamins. *The American Journal of Clinical Nutrition*, **62**, 1448S-1461S.

Stein, S.E. (1995) Chemical substructure identification by mass spectral library searching. *Journal of the American Society for Mass Spectrometry*, **6**, 644-655.

Stigliani, A.L., Giorio, G. and D'Ambrosio, C. (2011) Characterization of P450 carotenoid β- and ε-hydroxylases of tomato and transcriptional regulation of xanthophyll biosynthesis in root, leaf, petal and fruit. *Plant and Cell Physiology*, **52**, 851-865.

Supelco (2016) Selection guide for Supelco SPME fibers: Sigma-Aldrich.

Takaichi, S., Sandmann, G., Schnurr, G., Satomi, Y., Suzuki, A. and Misawa, N. (1996) The carotenoid 7, 8-dihydro-ψ end group can be cyclized by the lycopene cyclases from the bacterium *Erwinia uredovora* and the higher plant *Capsicum Annuum*. *European Journal of Biochemistry*, **241**, 291-296.

Tan, B.-C., Joseph, L.M., Deng, W.-T., Liu, L., Li, Q.-B., Cline, K. and McCarty, D.R. (2003) Molecular characterization of the Arabidopsis 9-cis epoxycarotenoid dioxygenase gene family. *The Plant Journal*, **35**, 44-56.

Tian, L., DellaPenna, D. and Zeevaart, J.A.D. (2004) Effect of hydroxylated carotenoid deficiency on ABA accumulation in Arabidopsis. *Physiologia Plantarum*, **122**, 314-320.

Tieman, D.M., Zeigler, M., Schmelz, E.A., Taylor, M.G., Bliss, P., Kirst, M. and Klee, H.J. (2006) Identification of loci affecting flavour volatile emissions in tomato fruits. *Journal of Experimental Botany*, **57**, 887-896.

Tikunov, Y., Lommen, A., de Vos, C.H.R., Verhoeven, H.A., Bino, R.J., Hall, R.D. and Bovy, A.G. (2005) A novel approach for nontargeted data analysis for metabolomics. Large-scale profiling of tomato fruit volatiles. *Plant Physiology*, **139**, 1125-1137.

Trivedi, D.K., Gill, S.S. and Tuteja, N. (2016) Abscisic acid (ABA): Biosynthesis, regulation, and role in abiotic stress tolerance. In *Abiotic Stress Response in Plants*: Wiley-VCH Verlag GmbH & Co. KGaA, pp. 315-326.

Urbanová, K., Vrkoslav, V., Valterová, I., Háková, M. and Cvačka, J. (2012) Structural characterization of wax esters by electron ionization mass spectrometry. *Journal of Lipid Research*, **53**, 204-213.

Utama, I.M.S., Wills, R.B.H., Ben-yehoshua, S. and Kuek, C. (2002) *In vitro* efficacy of plant volatiles for inhibiting the growth of fruit and vegetable decay microorganisms. *Journal of Agricultural and Food Chemistry*, **50**, 6371-6377.

Vallabhaneni, R., Bradbury, L.M.T. and Wurtzel, E.T. (2010) The carotenoid dioxygenase gene family in maize, sorghum, and rice. *Archives of Biochemistry and Biophysics*, **504**, 104-111.

Van Norman, J.M., Zhang, J., Cazzonelli, C.I., Pogson, B.J., Harrison, P.J., Bugg, T.D.H., Chan, K.X., Thompson, A.J. and Benfey, P.N. (2014) Periodic root branching in *Arabidopsis* requires synthesis of an uncharacterized carotenoid derivative. *Proceedings of the National Academy of Sciences*, 201403016.

Vierheilig, H., Maier, W., Wyss, U., Samson, J., Strack, D. and Piché, Y. (2000) Cyclohexenone derivative- and phosphate-levels in split-root systems and their role in the systemic suppression of mycorrhization in precolonized barley plants. *Journal of Plant Physiology*, **157**, 593-599.

Vogel, J.T., Tan, B.-C., McCarty, D.R. and Klee, H.J. (2008) The carotenoid cleavage dioxygenase 1 enzyme has broad substrate specificity, cleaving multiple carotenoids at two different bond positions. *Journal of Biological Chemistry*, **283**, 11364-11373.

Vogel, J.T., Tieman, D.M., Sims, C.A., Odabasi, A.Z., Clark, D.G. and Klee, H.J. (2010a) Carotenoid content impacts flavor acceptability in tomato (*Solanum lycopersicum*). *Journal of the Science of Food and Agriculture*, **90**, 2233-2240.

Vogel, J.T., Walter, M.H., Giavalisco, P., Lytovchenko, A., Kohlen, W., Charnikhova, T., Simkin, A.J., Goulet, C., Strack, D., Bouwmeester, H.J., Fernie, A.R. and Klee, H.J. (2010b) SlCCD7 controls strigolactone biosynthesis, shoot branching and mycorrhiza-induced apocarotenoid formation in tomato. *The Plant Journal*, **61**, 300-311.

Wagner, D., Przybyla, D., Op den Camp, R., Kim, C., Landgraf, F., Lee, K.P., Wursch, M., Laloi, C., Nater, M., Hideg, E. and Apel, K. (2004) The genetic basis of singlet oxygen-induced stress responses of *Arabidopsis thaliana*. *Science*, **306**, 1183-1185.

Walter, M., Floss, D. and Strack, D. (2010) Apocarotenoids: hormones, mycorrhizal metabolites and aroma volatiles. *Planta*, **232**, 1-17.

Walter, M.H. and Strack, D. (2011) Carotenoids and their cleavage products: Biosynthesis and functions. *Natural Product Reports*, **28**, 663-692.

Wei, S., Hannoufa, A., Soroka, J., Xu, N., Li, X., Zebarjadi, A. and Gruber, M. (2011) Enhanced β-ionone emission in arabidopsis over-expressing AtCCD1

reduces feeding damage in vivo by the crucifer flea beetle. *Environmental Entomology*, **40**, 1622-1630.

Wickham, H. (2009) *ggplot2: Elegant Graphics for Data Analysis* New York, United States: Springer-Verlag.

Wickham, H. (2011) The split-apply-combine strategy for data analysis. *Journal of Statistical Software*, **40**, 29.

Winterhalter, P. and Schreier, P. (1988) 4-Hydroxy-7,8-dihydro-β-ionol: natural precursor of theaspiranes in quince fruit (*Cydonia oblonga*, Mill.). *Journal of Agricultural and Food Chemistry*, **36**, 560-562.

Wong, Y.F., Uekane, T.M., Rezende, C.M., Bizzo, H.R. and Marriott, P.J. (2016) Qualitative analysis of *Copaifera* oleoresin using comprehensive two-dimensional gas chromatography and gas chromatography with classical and cold electron ionisation mass spectrometry. *Journal of Chromatography A*, **1477**, 91-99.

Xiao, L., Lee, J., Zhang, G., Ebeler, S.E., Wickramasinghe, N., Seiber, J. and Mitchell, A.E. (2014) HS-SPME GC/MS characterization of volatiles in raw and dry-roasted almonds (*Prunus dulcis*). *Food Chemistry*, **151**, 31-39.

Xie, X., Yoneyama, K. and Yoneyama, K. (2010) The Strigolactone Story. *Annual Review of Phytopathology*, **48**, 93-117.

Yahyaa, M., Berim, A., Isaacson, T., Marzouk, S., Bar, E., Davidovich-Rikanati, R., Lewinsohn, E. and Ibdah, M. (2015) Isolation and functional characterization of carotenoid cleavage dioxygenase-1 from *Laurus nobilis* L. (Bay Laurel) fruits. *Journal of Agricultural and Food Chemistry*, **63**, 8275-8282.

Ytterberg, A.J., Peltier, J.-B. and van Wijk, K.J. (2006) Protein profiling of plastoglobules in chloroplasts and chromoplasts. A surprising site for differential accumulation of metabolic enzymes. *Plant Physiology*, **140**, 984-997.

Yuan, J., Reed, A., Chen, F. and Stewart, C.N. (2006) Statistical analysis of real-time PCR data. *BMC Bioinformatics*, **7**, 85.

Zentgraf, U., Laun, T. and Miao, Y. (2010) The complex regulation of WRKY53 during leaf senescence of *Arabidopsis thaliana*. *European Journal of Cell Biology*, **89**, 133-137.

Zhou, X., Welsch, R., Yang, Y., Álvarez, D., Riediger, M., Yuan, H., Fish, T., Liu, J., Thannhauser, T.W. and Li, L. (2015) Arabidopsis OR proteins are the major posttranscriptional regulators of phytoene synthase in controlling carotenoid biosynthesis. *Proceedings of the National Academy of Sciences*.